UNIVERSITY OF LIVERPOOL

Investigating the role of Deleted in Liver Cancer 1 in cell migration and invasion

Thesis submitted in accordance with the requirements of the University of Liverpool for the degree of Doctor in Philosophy by

Rebecca Kelly

February 2023

Acknowledgements

This thesis has been a long time in preparation, and there are many people to thank for its completion. First, I would like to thank my supervisors, Dr Tobias Zech, Prof. Violaine See and Dr Igor Barsukov. Without your advice, knowledge and input this thesis wouldn't have been possible. Special thanks to Tobi for taking me on and getting me over the finish line, thank you for all your support and time, I am extremely grateful.

I would also like to thank all the wonderful staff at the CCI, past and present! Thank you to Dr Dave Mason, who introduced me to my first microscope, image analysis basics and showed me the correlation between biscuits and productivity. Thanks to Jen Adcott, Dr Marco Marcello and Dr Marie Held, for all the pilots, analysis help and swapping the BioAFM over to TIRF every week. To Dr Tom Waring – special thanks for your patience and helping with FRET and analysis. Thank you to Dr Lorna Young for help with the focal adhesion experiments.

To all of Lab B, thank you! Dr Anne Hermann for all the support and friendship over the years, Dr Leonard Daly for the cloning ups and downs, laughs and gel recipes. A special thanks for Dr Chris Clarke for TC karaoke and the "can I ask you a silly question?" answers. To Alex Rothwell for always providing MATLAB support, playlists and pep talks.

To Dr Kit Sampat and Dr Claire Louise Kelly, where do I even start? Thank you so much for all the support, positivity and friendship. I couldn't have asked for better friends to do this PhD journey with, through the highs and lows, I will always cherish the laughs and memories we made together. Thank you both for everything, you two will always be the favourite part of my PhD.

I would also like to thank my colleagues at MDC, who have supported me whilst writing this thesis, with a special mention to Dr Emily Offer, Dr Isabel Peset Martin and Dr Emma Jones.

Thank you to all my family and friends who have supported me throughout my studies, special thanks to Grandad Jack and my dog Shadow. To my Mum, I couldn't have done this without you and your constant support, thank you for teaching me 'nothing worth having comes easy'. To my daughter Darcey, thank you for always being so caring, offering to type for me when I was tired and believing in me even when I didn't believe in myself.

Finally, to my late grandparents, Nanny Eileen, Nanny Margie and Grandad Pat, I wish you could have seen this finished, thank you for your love and support throughout, I dedicate this thesis in your memory.

Abstract

Cell migration is crucial for processes such as development, wound healing and immune response. RhoGAP proteins are a family of proteins regulating cell migration. They act as a molecular switch, which limits the activity of Rho GTPases – key regulators of the actin and microtubule cytoskeleton. Deleted in Liver Cancer 1 (DLC1) is a RhoGAP protein that has been shown to be a suppressor of tumour progression and metastasis. Transcriptional silencing of DLC1 is evident in several cancers such as breast, lung and colon and low levels of DLC1 in brain tumours is associated with poor prognosis. The aim of this thesis was to elucidate the molecular mechanisms by which DLC1 affects cell migration and also cell invasion in a 3D environment.

Using TIRF microscopy and the expression of a GFP-DLC1 fusion protein, DLC1 was visualised within focal adhesions, and co-localised with other focal adhesion proteins, talin and paxillin. For full evaluation of the role of DLC1, overexpression and silencing experiments were performed. U-87 MG cells were used for overexpression models, since they have low endogenous DLC1. In contrast HepG2 cells were used for silencing experiments, since they have endogenous levels of DLC1. The role of DLC1 in cell migration and invasion was also investigated using 2D migration and 3D invasion assays. Using live microscopy, cells with overexpressed DLC1 or knocked down DLC1 were followed in culture and their tracks quantified using image analysis software, ImageJ and IMARIS. The effect of DLC1 domain structure was evaluated using novel FRET sensors for conformation of DLC1 on its activity status and RhoA FRET sensors were also used to investigate how DLC1 affects RhoA activity.

Focal adhesion analysis suggests DLC1 has a small but significant effect on assembly/disassembly kinetics in comparison to talin, a well described adhesion protein. When GFP-DLC1 was overexpressed, assembly was reduced. However, the disassembly rate was increased compared to GFP-talin. Silencing of DLC1 had no effect on focal adhesion assembly, however, disassembly was increased compared to scrambled controls. GFP-DLC1 overexpression reduced track mean speed and displacement in 2D migration and 3D circular invasion assays (CIA), however, there was no significant effect of overexpression of GFP-DLC1 on cells in 3D spheroid invasion assays. Interestingly, knockdown of DLC1 increased track mean speed, and reduced displacement in 3D assays. Furthermore, no significant difference in normalised FRET index between the different constructs evaluated. Interestingly exogenous mRuby-DLC1 expression increased RhoA activity, whilst siRNA targeting DLC1 had no significant effects.

In conclusion, this study has shown that DLC1 has an important function in focal adhesions and in cell migration and invasion, which could be important for understanding its role in cancer, however, the mechanism of action of DLC1 is still unclear. Further research is required to fully understand the role of DLC1, and whether this could be a therapeutic target.

Table of Contents

List of figures

List of tables

List of videos

All videos can be accessed at
https://www.dropbox.com/scl/fo/9hvz0y848903pe3oybcl3/h?dl=0&rlkey=kvvzvb0oatwhrs0odc1ndl32t

Video 1: Focal adhesion dynamics of mRuby-DLC1 - Timelapse videos of HeLa cells transfected with mRuby-DLC1. Imaged using TIRF microscopy, every minute.

Video 2: Focal adhesion dynamics of GFP-talin - Timelapse videos of HeLa cells transfected with GFP-talin. Imaged using TIRF microscopy, every minute.

Video 3: Focal adhesion dynamics of mRuby-DLC1 and GFP-talin - Timelapse videos of HeLa cells co transfected with mRuby-DLC1 and GFP-Talin. Imaged using TIRF microscopy, every minute.

Video 4: Focal adhesion dynamics of GFP-talin and siRNA scrambled control - Timelapse videos of HepG2 cells transfected with siRNA scrambled control and GFP-talin. Imaged using TIRF microscopy, every minute.

Video 5: Focal adhesion dynamics of GFP-talin and siRNA DLC1 - Timelapse videos of HepG2 cells transfected with siRNA DLC1 and GFP-talin. Imaged using TIRF microscopy, every minute.

Video 6: 2D cell migration GFP Control - Timelapse videos of U-87 MG cells transfected with GFP control. Imaged with epifluorescence microscopy, every 3 minutes for 24 hours.

Video 7: 2D cell migration GFP DLC1 - Timelapse videos of U-87 MG cells transfected with GFP-DLC1. Imaged with epifluorescence microscopy, every 3 minutes for 24 hours.

Video 8: 2D cell migration GFP control (GFP talin mRuby DLC1) - Timelapse videos of U-87 MG cells transfected with GFP control. Imaged with epifluorescence microscopy, every 3 minutes for 24 hours.

Video 9: 2D cell migration GFP talin mRuby DLC1 - Timelapse videos of U-87 MG cells transfected with GFP-talin and mRuby-DLC1. Imaged with epifluorescence microscopy, every 3 minutes for 24 hours.

Video 10: 2D cell migration untransfected H2B-RFP control - Timelapse videos of HepG2 H2B RFP cells. Imaged with epifluorescence microscopy, every 3 minutes for 24 hours.

Video 11: 2D cell migration siRNA scrambled control - Timelapse videos of HepG2 H2B RFP cells, transfected with siRNA scrambled control. Imaged with epifluorescence microscopy, every 3 minutes for 24 hours.

Video 12: 2D cell migration siRNA DLC1 - Timelapse videos of HepG2 H2B RFP cells, transfected with siRNA DLC1. Imaged with epifluorescence microscopy, every 3 minutes for 24 hours.

Video 13: CIA assay U87 H2B-RFP control - Timelapse videos of U-87 MG cells. Imaged with epifluorescence microscopy, every 3 minutes for 24 hours.

Video 14: CIA assay U87 GFP DLC1 - Timelapse videos of U-87 MG cells transfected with GFP-DLC1. Imaged with epifluorescence microscopy, every 3 minutes for 24 hours.

Video 15: CIA assay HepG2 H2B-RFP control - Timelapse videos of HepG2 H2B RFP cells. Imaged with epifluorescence microscopy, every 3 minutes for 24 hours.

Video 16: CIA assay HepG2 siRNA scrambled control - Timelapse videos of HepG2 H2B RFP cells, transfected with siRNA scrambled control. Imaged with epifluorescence microscopy, every 3 minutes for 24 hours.

Video 17: CIA assay HepG2 siRNA DLC1 - Timelapse videos of HepG2 H2B RFP cells, transfected with siRNA DLC1. Imaged with epifluorescence microscopy, every 3 minutes for 24 hours.

Video 18: U87 H2B-RFP Control 3D spheroid - Timelapse videos of U-87 MG H2B RFP spheroid. Imaged with lightsheet microscopy, every 3 minutes for 16 hours.

Video 19: U87 H2B-RFP GFP DLC1 3D spheroid - Timelapse videos of U-87 MG GFP DLC1 spheroid. Imaged with lightsheet microscopy, every 3 minutes for 16 hours.

Video 20: HepG2 H2B-RFP control 3D spheroid - Timelapse videos of HepG2 H2B RFP spheroid. Imaged with lightsheet microscopy, every 3 minutes for 16 hours.

Video 21: HepG2 H2B-RFP siRNA scrambled control 3D spheroid - Timelapse videos of HepG2 siRNA scrambled control spheroid. Imaged with lightsheet microscopy, every 3 minutes for 16 hours.

Video 22: HepG2 H2B-RFP siRNA DLC1 3D spheroid - Timelapse videos of HepG2 siRNA DLC1 spheroid. Imaged with lightsheet microscopy, every 3 minutes for 16 hours.

Abbreviations

2D: Two-dimensional

3D: Three-dimensional

ADF: Actin-depolymerizing factor

AFM: Atomic force microscopy

AKT: Protein Kinase B

ARP2/3: Actin-related protein 2/3

CAV-1: Cavelolin-1

CDK5: Cyclin-dependent kinase 5

CFP: Cyan fluorescent protein

CIA: Circular invasion assay

CO_2: Carbon dioxide

DAPI: 4’,6-diamidino-2-phenylindole

DLC1: Deleted in liver cancer 1

DLC2: Deleted in liver cancer 2

DLC3: Deleted in liver cancer 3

DMEM: Dulbecco's Modified Eagle Medium

DMFS: Distance metastatic-free survival

ECM: Extracellular matrix

ECO: Engineered cancer organoids

EMT: Epithelial-to-mesenchymal transition

ERM: Ezrin-radixin-moesin

FA: Focal adhesion

FAAS: Focal adhesion analysis server

FAK: Focal adhesion kinase

FAT: Focal adhesion targeting

FEP: Fluorinated ethylene propylene

FKBP51: FK506 binding protein 51

FRAP: Fluorescence recovery after photobleaching

FRET: Förster resonance energy transfer

GAP: GTPase-activating protein

GDI: Guanine nucleotide dissociation inhibitors

GEF: Guanine nucleotide exchange factor

GDP: Guanosine diphosphate

GFP: Green fluorescent protein

GTP: Guanosine triphosphate

HCC: Hepatocellular carcinoma

HDAC: Histone deacetylase

HRP: Horse radish peroxide

iPSCs: Induced pluripotent stem cells

IVM: Intravital microscopy

LIMK1: LIM kinase-1

LSFM: Light-sheet fluorescent microscopy

MAPK: Mitogen-activated protein kinase

MCTS: Multicellular tumour spheroids

MEF: Mouse embryonic fibroblast

MEM: Minimum Essential Media

miRNA: Micro RNAs

MIP: Maximum intensity projection

MLC: Myosin light chain

MSD: Mean squared displacement

NFP: Nucleation-promoting factors

OS: Overall survival

PBS: Phosphate buffer saline

PCR: Polymerase chain reaction

PEI: Polyethylenimine

PFA: Paraformaldehyde

PI3Ks: Phosphoinositide 3-kinases

PKA: Protein kinase A

PKC: Protein kinase C

PKD: Protein kinase D

PRDM13: PR domain containing 13

RBD: Rho-binding domain

RFP: Red fluorescent protein

ROCK: Rho-associated serine/threonine kinase

SAM: Sterile α motif

SDS: Sodium dodecyl sulfate

SR: Serine-rich region

START: Steroidogenic acute regulatory protein (StAR)-related lipid transfer

TAZ: PDZ binding motif protein

TBST: Tris buffered saline with Tween-20

TCF4: T-cell factor 4

TFM: Traction force microscopy

TFP: Teal fluorescent protein

TIRF: Total Internal Reflection Fluorescence

VASP: Vasidilator-stimulated phosphoprotein

WASP: Wiskott-Aldrich syndrome protein

YAP: Yes-associated protein

YFP: Yellow fluorescent protein

Chapter 1: Introduction

Cell migration is essential for all multicellular organisms and fundamental to biological processes such as embryonic development, tissue formation and immune response. Aberrant cell migration can lead to pathologies such as vascular disease, chronic inflammatory diseases, tumour formation and metastasis (Webb, 2005).

Cell migration is dependent on co-ordination of signalling pathways and spatial cues from the surrounding environment, the extracellular matrix (ECM). Intracellular regulatory mechanisms that control the mode and rates of cell migration can be directly influenced by ECM microenvironmental properties (Doyle et al., 2013). This requires co-ordination of cytoskeletal dynamics and reorganisation, cell adhesion and signal transduction (Devreotes and Horwitz, 2015). Cell migration is an energy demanding process that requires cells to maintain an adequate amount of energy to fuel motility, therefore metabolism is important for migration (Wu et al., 2021b).

The linkage of the ECM to the cell requires transmembrane cell adhesion proteins that act as matrix receptors and tie the matrix to the cell cytoskeleton. The principal receptors for binding most ECM proteins are integrins (Alberts, 2002). Integrins bind to extracellular ligands via their outer domains, whereas their internal, cytoplasmic domains are linked to a multitude of structural and signalling molecules as well as the actin cytoskeleton (Vicente-Manzanares et al.,

2009, Humphries and Newham, 1998, Hynes, 1992, Zaidel-Bar et al., 2007). Integrins and actin are coupled through a physical linkage, which provides traction for migration (Vicente-Manzanares et al., 2009).

The actin cytoskeleton, a collection of actin filaments with their accessory and regulatory proteins, is the primary force-generating machinery in the cell, important for cell migration (Svitkina, 2018). The morphological and physical behaviours of migrating cells are driven by a dynamic filamentous actin (F-actin) cytoskeleton, which is coupled to the ECM via dynamic assemblies of structural and signalling proteins known as focal adhesions (Gardel et al., 2010).

A variety of signalling molecules and downstream effectors provide spatiotemporal regulation of these physical structures, the most prominent being the Rho family GTPases (Raftopoulou and Hall, 2004). In addition to Rho GTPases, numerous mechanical and biochemical cues mediate the interplay between the F-actin cytoskeleton and integrin-mediated adhesion to regulate the co-ordination of migrating cells (Gardel et al., 2010).

1.1 Rho GTPases

Rho GTPases are involved in a wide range of cellular responses including cell cytoskeleton organisation, migration, transcription and proliferation (Parri and Chiarugi, 2010, Hodge and Ridley, 2016). They are a family of small signalling G proteins, characterised by a Rho insert domain located between a β-strand and a α-helix within the small GTPase domain (Parri and Chiarugi, 2010). They are described as key regulators of cell migration as they are involved in dynamic reorganisation of actin cytoskeleton, driving cell motility and invasion (O'Connor and Chen, 2013). The most characterised Rho GTPases are Rac, RhoA and Cdc42.

1.1.1 Regulation of Rho GTPases

Rho GTPases are molecular switches, cycling from an active GTP-bound state to inactive GDP-bound state (Figure 1.1). When Rho GTPases are in their GTP-bound active form they can interact with a diverse range of targets to induce cellular responses (Hodge and Ridley, 2016). The GDP-GTP cycle is highly regulated by guanine nucleotide exchange factors (GEFs) that catalyse the exchange of the bound GDP to GTP to turn on signalling, and by GTPase-activating proteins (GAPs) that terminate signalling by inducing GTP hydrolysis (Parri and Chiarugi, 2010).

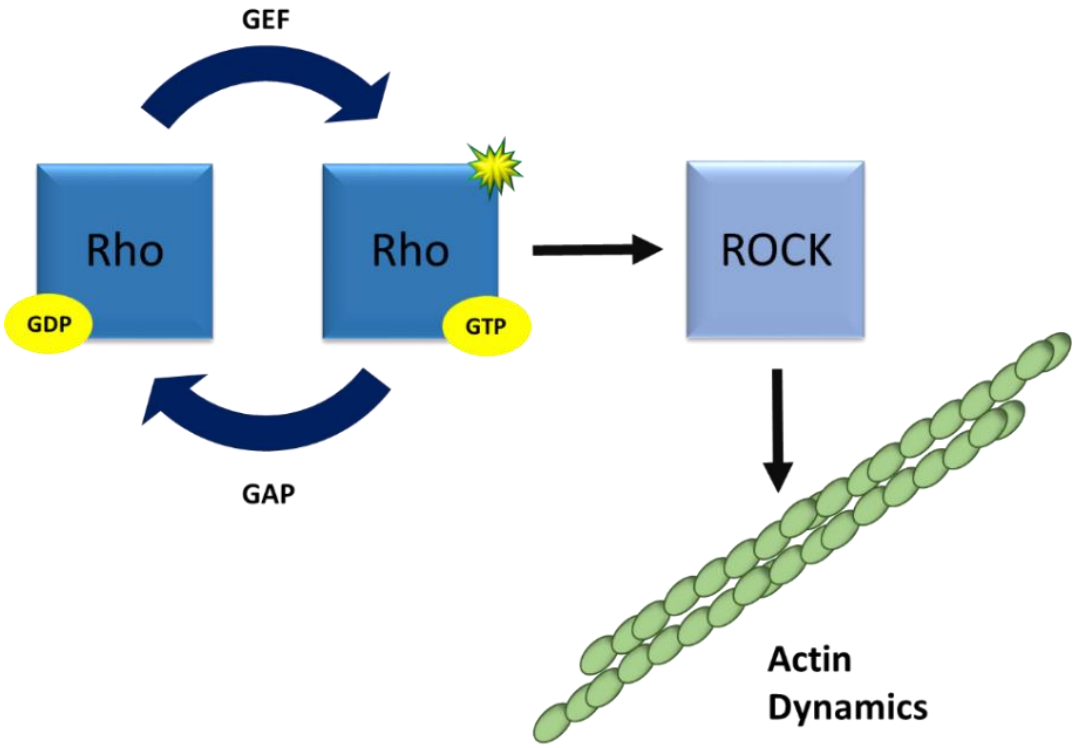

Figure 1.1: The RhoGTPase Cycle. Model showing how Rho-GTPases are regulated, GEFs promote GTP loading and activation of Rho-GTPases and GAPS stimulate inactivation of Rho-GTPases by promoting GTP hydrolysis to GDP. Modulation of RhoGTPase influences downstream signalling cascades involving Rho associated kinase (ROCK) and modulates actin dynamics. (Redrawn from Huveneers and Danen, 2009).

A further level of regulation for Rho GTPases are the guanine nucleotide dissociation inhibitors (GDIs). GDIs sequester the inactive GTPase in an inhibitory action, which prevents dissociation of GDP and inhibits interactions with regulatory and effector molecules, preventing the activation of the GTPase and implementation of their biological effect (DerMardirossian and Bokoch, 2005, Ueda et al., 1991). In addition to cycling between GTP- and GDP-bound conformations, Rho

GTPases are regulated by post-translational modifications, including lipid modifications, phosphorylation, ubiquitination and SUMOylation (Haga and Ridley, 2016).

1.1.2 Rho GTPases in cell migration

Rac, RhoA and Cdc42 are the most studied RhoGTPases involved in cell migration and each are required for different processes within cell migration (Figure 1.2). Lamellipodia extension is driven predominantly by Rac, which induces the extension through the WAVE complex, which activates the Arp2/3 complex (Ridley, 2015). In addition to Rac, RhoA and Cdc42 are active in lamellipodia region and contribute to lamellipodia extension (Ridley, 2015).

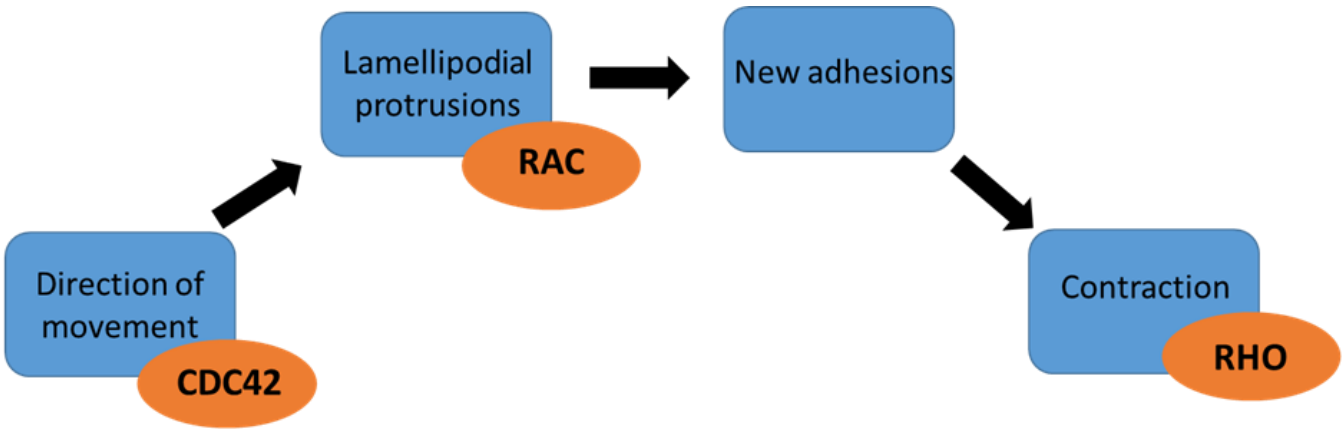

Figure 1.2: Effects of RhoGTPases Cdc42, Rac and Rho on cell migration cycle. Each RhoGTPase is associated with a different stage of cell migration. Whilst Cdc42 is involved in direction of movement through filopodia, Rac is responsible for lamellipodia and Rho is involved in the contraction of the cell body (Ridley, 2015).

Rho regulates actomyosin contractility, which can lead to the formation of actin stress fibers and focal adhesions (Clayton and Ridley, 2020). RhoA has been identified at the leading edge of the cell, and is associated with membrane ruffling, lamellae formation and membrane blebbing, suggesting an active role in membrane protrusions (O'Connor and Chen, 2013).

Rho modulates actin dynamics through Rho-associated serine/threonine kinase (ROCK). Activation of ROCK inhibits myosin light chain phosphatase leading to increased phosphorylation of myosin light chain (MLC). Accumulated levels of MLC causes actin bundling, contraction and formation of stress fibers (Barras and Widmann, 2013). ROCK can also influence cell migration by activating LIM kinase causing phosphorylation and inactivation of ADF/cofilin resulting in an increase of actin filaments (Riento and Ridley, 2003).

Cdc42 is known to be required for filopodium formation through N-WASP mediated activation of the Arp2/3 complex, as well as F-actin bundling proteins, fascin and formin (Nobes and Hall, 1995, de Beco et al., 2018). Cdc42 also plays an important role in establishing cell migratory polarity and migratory persistence, acting through Par polarity complex and other targets (Ridley, 2015).

The Rho GTPases co-ordinate cell migration and cells can switch between different modes of cell migration (Ridley, 2015). For example, cells switch from lamellipodium-driven migration to bleb migration when RhoA/ROCK activity increases (Sanz-Moreno et al., 2008). RhoGTase activity needs to be balanced, as high levels of RhoA/ROCK activity can induce actomyosin-mediated retraction of lamellipodia and inhibit this type of migration (Petrie et al., 2012).

Whilst each functions differently within cell migration, RhoGTPase activity is co-ordinated, Rac1 RhoA and Cdc42work together to control cytoskeletal dynamics and all three GTPases are activated at the front of migrating cells (Jaffe and Hall, 2005, Kraynov et al., 2000, Nalbant et al., 2004, Pertz et al., 2006). Rac1 and RhoA operate antagonistically through spatial separation and precise timing, RhoA plays a role in the initial events of protrusion, and Rac1 and Cdc42 activate pathways implicated in reinforcement and stabilization of newly expanded protrusions (Machacek et al., 2009).

1.2 Mechanisms of cell migration

Decades of research into cell migration mechanisms has identified that there are different forms of cell migration and a range of mechanisms which are utilised by cells in various environments.

The classic mode of cell migration was first described by Abercrombie in 1980, observing fibroblast migration as a canonical three step process: extension of the cell leading edge in a protrusion termed lamellipodium, attachment of the leading edge to the substrate and contraction of the rear with disassembly of adhesions (Paluch et al., 2016). These initial observations helped to establish key concepts about cell migration based on adhesion and interactions with a two-dimensional (2D) surface. Further research into signalling pathways involved in cell migration led to discovery that the outer environment and ECM can strongly modulate cell migration. This resulted in the generation and use of three-dimensional (3D) ECM models that mimic more-physiological *in vivo* conditions (Doyle et al., 2013). Comparison between 2D and 3D cell migration models has revealed substantial differences (Caswell and Zech, 2018).

Cell migration strategies differ across different cells; leukocytes display amoeba-like movement and morphology, keratocytes display a gliding motion and epithelial monolayers retain cell-cell contacts during motility for gastrulation and wound healing (Vicente-Manzanares et al., 2005).

Cells have different modes of cell migration, including single cell and collective cell migration (Figure 1.3). They can switch between states in a dynamic and adaptable manner (Stock and Pauli, 2021). Migrating cells share one main characteristic, front-rear polarity along the axis of migration (Mayor and Etienne-Manneville, 2016, De Pascalis and Etienne-Manneville, 2017).

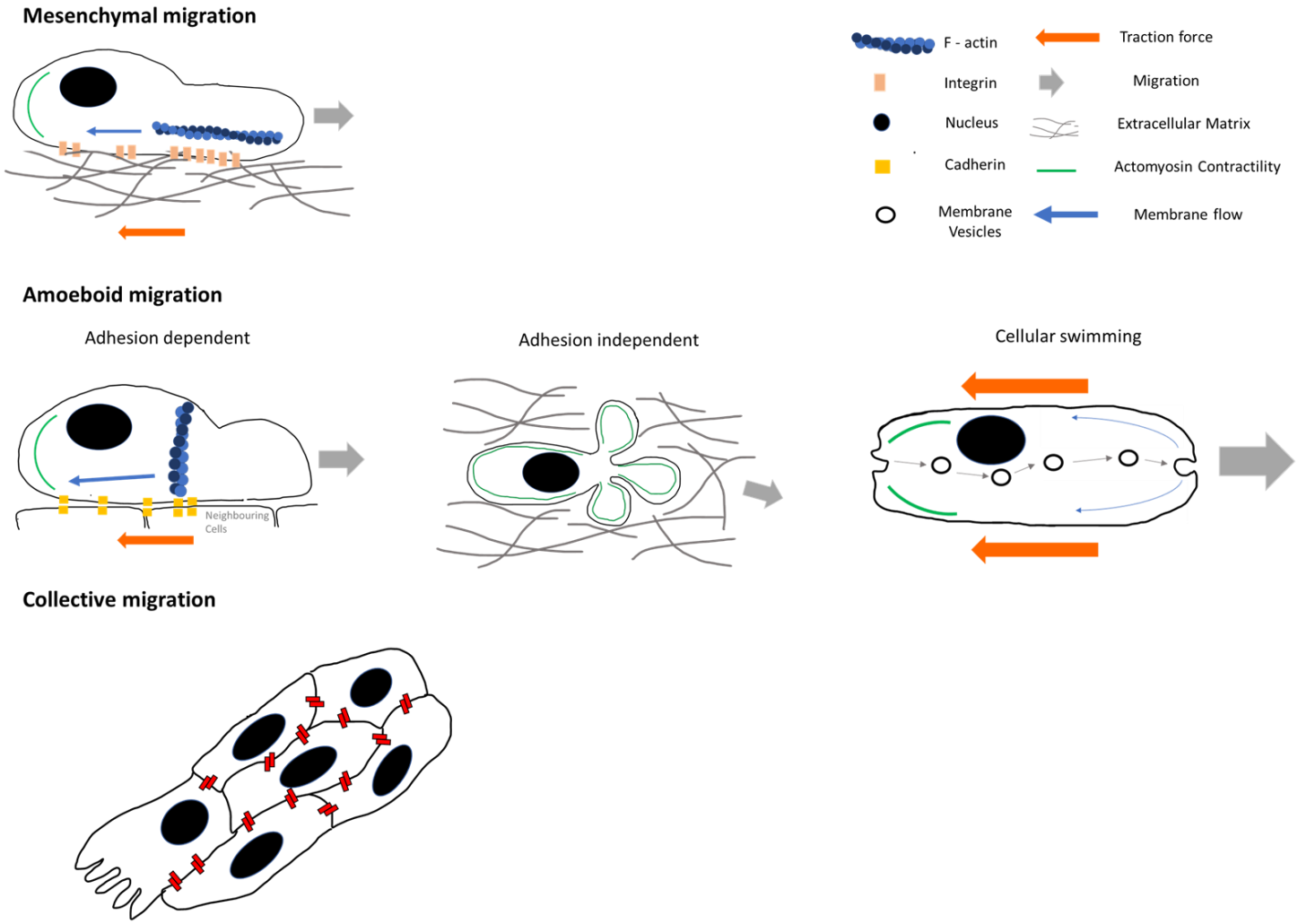

Figure 1.3: Different types of cell migration modes: Single cell migration can be classified into mesenchymal and ameboid. Mesenchymal is characterised by an elongated cell shape and actin of actin-rich protrusions. Ameboid can be classified further into adhesion dependent, adhesion independent and cellular swimming, and each of these are associated with a round cell shape and increased cellular contractility. Cells can also migrate collectively in a cluster, where they polarise together and migrate as a unit. (Redrawn from Stock and Pauli, 2021).

1.2.1 Single cell migration

Single cells can utilise two main modes of migration, amoeboid and mesenchymal. Mesenchymal is generally considered the most prevalent mode of migration and is characterised by an elongated cell shape and actin polymerisation at the leading edge, causing the extension of actin-rich protrusions (Stock and Pauli, 2021). Integrin-mediated focal adhesions tether the frontal actin cortex to the substrate, while adhesive contacts in the rear detach. Rear contraction causes a retrograde actin flow that causes a traction force, thereby pulling the cell forward (De Pascalis and Etienne-Manneville, 2017).

Amoeboid migration is characterised by a round cell shape and increased cellular contractility, which several types characterised including adhesion dependent (primordial germ cells), adhesion independent (leukocytes) and cellular swimming (macrophages) (Stock and Pauli, 2021). Adhesion dependent cells are characterised by high contractility, breaks in the cortex cause the extension of hydrostatic actin depleted blebs, with cadherin-mediated adhesion occurring through the actin cortex at the base of the bleb. The high contractility in the cell triggers a retrograde actin flow that generates sufficient traction force to pull the cell forwards (Paluch and Raz, 2013). In adhesion independent mode, amoeboid cells use their ability to easily change shape to move through a 3D environment, extending into surrounding structures (e.g. ECM) (Yamada and Sixt, 2019). Cells use a nucleus-first configuration to facilitate rapid navigation along the path of least resistance, this mode of migration depends on strongly rear polarised myosin II activity, which drives global retrograde flow of the actin cytoskeletal cortex (Renkawitz et al., 2019, Liu et al., 2015). Cellular swimming is seen in macrophages, high contractility at the rear of

a cell causes a rearward membrane flow. The membrane flow exhibits a rearward traction force against the surrounding medium that propels the cell forwards (O'Neill et al., 2018).

Cells can alternate their migration modes as they navigate the microenvironment. The migration mode of a cell is mediated by its adhesivity to the matrix. Adhesivity is controlled by the architecture, composition and mechanical properties of the ECM (Lintz et al., 2017). For example, intrinsic actomyosin activity generates key mechanical signals from the ECM to the cell, resulting in generation of contractile forces within the cytoskeleton. These forces transmit to adhesion complexes linking the cells to their surroundings, and facilitating movement along and within the matrix (Chi et al., 2014, Mak et al., 2016). These adhesion complexes are essential to mesenchymal migration and are less critical during amoeboid migration (Lintz et al., 2017). Three key parameters modulate the mode of migration of cells, protrusion, contractility and adhesion. Altering the balance between these parameters causes cells to adapt their motility to different migration environments, allowing migrating cells to negotiate the topologies of the different tissues they encounter (Lämmermann and Sixt, 2009).

1.2.2 Collective cell migration

Collective cell migration occurs during many developmental and pathological processes including morphogenesis, wound healing and cancer metastasis (Shellard and Mayor, 2019, Friedl and Gilmour, 2009, Mayor and Etienne-Manneville, 2016). Within an organism, cells often migrate in a more collective manner to shape tissues or populate new areas (Stock and Pauli, 2021, Scarpa and Mayor, 2016, Weijer, 2009).

There are two reported modes of collective cell migration. In one mode, cells within the collective polarize individually, but depend on communication with other cells in the cluster for efficient migration (Stock and Pauli, 2021). In the other mode, the cell collective moves as a supracellular unit characterised by an overarching polarity with clear leader and follower cells, the groups of cells are dependent on each other and not able to migrate on their own (Stock and Pauli, 2021). Most cases of collective migration combine the aspects of both individual and supracellular behaviour, suggesting that collective migration is more of a spectrum rather than defined (Stock and Pauli, 2021).

During collective migration, intercellular contacts are maintained as cells move with one another. Where individual migrating cells are not physically coupled to other cells, meaning they can move around freely, the cell-cell adhesions require that cells cooperate and coordinate their activities or migration can be hindered by their adhesions (Shellard and Mayor, 2019). Collective cells have a more coordinated response, migrating in response to the environment in the same direction at similar speeds. This results in more efficient movement than individual cells which would be stationary or migrate in different directions (Mayor and Etienne-Manneville, 2016, Malet-Engra et al., 2015, Theveneau et al., 2010).

Collective migration uses the same mechanism seen in single cell migration; however, this is modified slightly by the cellular contacts of cohesive cell groups (Vaughan and Trinkaus, 1966, Mayor and Etienne-Manneville, 2016). The cells located at the front of the group are called leader cells, which sense the microenvironment and dictate the direction and speed of migration of the entire cluster (Haga et al., 2005, Khalil and Friedl, 2010). Leader and follower cells are defined

due to their relative positions within the cell group, with leader at the front and follower cells behind. Leader cells are exposed to higher levels of external signals and play a major part in ECM remodelling (Omelchenko et al., 2003).

1.3 2D Cell Migration

1.3.1 Cell migration cycle

Classical mesenchymal cell migration is described as a cycle of polarisation, protrusion, adhesion, and contraction (Figure 1.4). The initial step is polarisation, followed by actin-based protrusions in the direction of migration, at the front of the cell. These protrusions are driven by actin polymerisation and stabilised by adhering to the ECM or adjacent cells (Ridley et al., 2003). The adhesions serve as traction sites for migration and myosin-driven contractile forces that lead to detachment are generated at the rear, causing the cell to move forward (Mak et al., 2016).

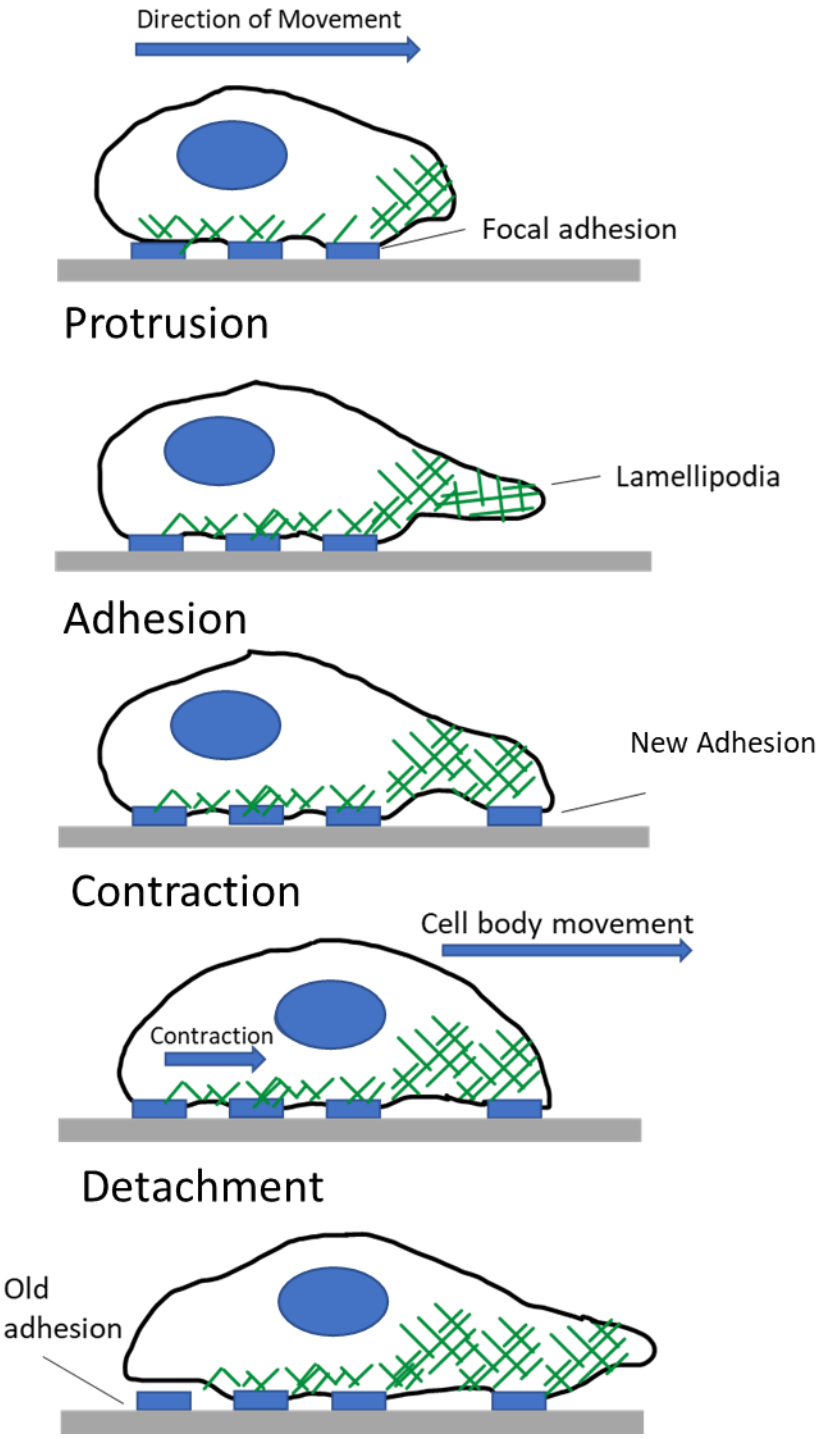

Figure 1.4: The mesenchymal mode of migration. The mesenchymal cell migration cycle is described as polarisation, protrusion adhesion and contraction. Actin-based protrusions initiate in the direction of migration, adhesion sites stables and act as traction sites for migration and myosin driven contractile forces drive the cell body forward, with detachment at the rear of the cell (Mak et al 2016, Tschumperlin, 2013).

1.3.2 Polarisation

Cell migration is fundamentally a polarised process, in both random cell migration and directed cell migration, cell polarity is required to generate a front-rear axis (Etienne-Manneville, 2008, Ridley et al., 2003). Migratory cells have a distinctive organisation between the leading edge and rear of the cell, including polarised cytoskeletal arrangements and organisation of membrane trafficking (Mayor and Etienne-Manneville, 2016). Whilst actin polymerisation is induced at the leading edge and actomyosin contraction at the rear, centrosomes, microtubules and secretory pathways (Golgi) are orientated toward the front of the cell (Nelson, 2009).

Cell polarity is established in response to extracellular stimuli and is mediated by a set of positive feedback loops including Rho GTPases, phosphoinositide 3-kinases (PI3Ks), integrins, microtubules, and vesicular transport (Ridley et al., 2003). The small G-proteins, Cdc42, Rac and Rho, are involved in the initial signals leading to the polarization (Kölsch et al., 2008). Cdc42 is a master regulator of cell polarity in eukaryotic organisms, and is active toward the front of migrating cells, and both inhibition and global activation of Cdc42 can disrupt the directionality of migration (Etienne-Manneville and Hall, 2002, Etienne-Manneville, 2008, Itoh et al., 2002).

1.3.3 Protrusive machinery

Cell migration relies on the dynamic reassembly of actin filaments. Coordinated polymerization of multiple actin filaments produce protrusive forces that drive the extension of the plasma membrane at the cell leading edge (Pollard and Borisy, 2003). However, the organisation of filaments depends on the type of protrusion: in lamellipodia, actin filaments form a branching

"dendritic" network, whereas in filopodia they are organized into long parallel bundles (Figure 1.5) (Ridley et al., 2003).

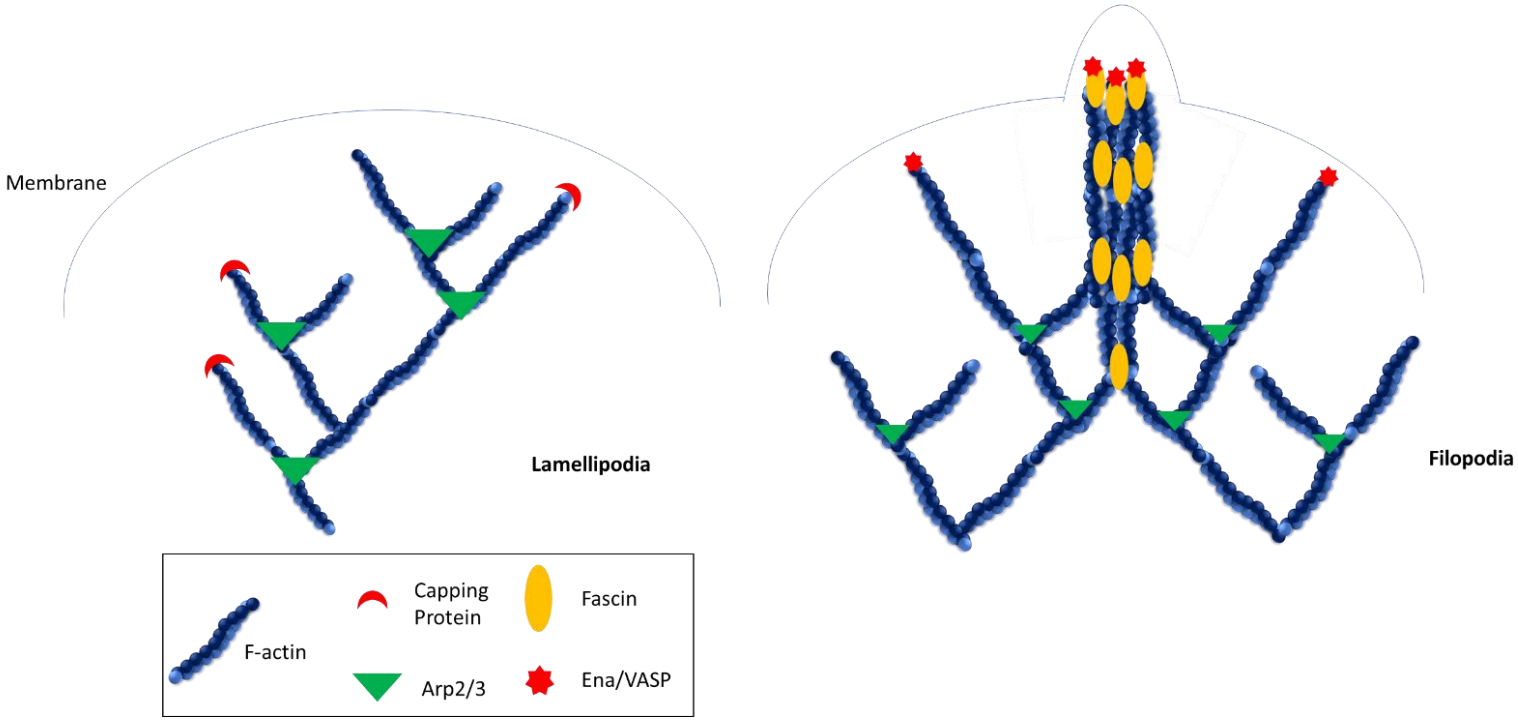

Figure 1.5: Actin structures in lamellipodia and filopodia. The organisation of actin filaments depends on the type of protrusion: in lamellipodia, actin filaments form a branching "dendritic" network, whereas in filopodia they are organized into long parallel bundles (Ridley et al., 2003). Adapted from Ayscough and Winder 2004.

1.3.4 Lamellipodia

Lamellipodia are broad, flat cellular protrusions at the leading edge of the cell. They are the major cellular engine to propel the leading edge forward and function as navigation for guiding cells around obstacles, sensing soluble guidance cues and probing the chemical and mechanical properties of the substratum (Svitkina, 2018). Lamellipodia are transient structures which protrude and retract, allowing adhesions to be established with the underlaying substratum, generating traction and driving cell migration (Krause and Gautreau, 2014).

Actin polymerisation is promoted by actin nucleators and actin elongators. The actin-related protein 2/3 (ARP2/3) complex is the main actin nucleator in lamellipodia and generates new actin filaments which branch off the side of pre-existing filaments (Ridley, 2011, Campellone and Welch, 2010). This is an autocatalytic reaction, where the new filament acts as a substrate of the next branching reaction and increases the mass of actin polymers.

Actin polymerisation produces a pushing force due to the structural polarity of actin filaments, which have a 'barbed' end that polymerises faster than the other 'pointed' end (Woodrum et al., 1975, Huxley, 1963). In cells, polymerising actin filaments are orientated with their barbed ends towards the load (usually the plasma membrane). The elongated barbed ends push on the load, creating the force of actin polymerisation (Svitkina, 2018). Depolymerisation occurs closer to the pointed ends to release monomers for recycling (Svitkina, 2018).

New polymerising actin filaments can become capped by heterodimeric capping protein, preventing their growth. However, elongators such as ENA/VASP and formins protect the

filament ends and increase the elongation rate and duration (Cooper and Sept, 2008, Romero et al., 2004, Breitsprecher et al., 2011, Pollard, 2016). Proteins of the ENA/VASP and formin families compete with capping proteins that could terminate barbed end elongation and keep elongating ends near to the membrane to increase efficiency of the pushing force (Pollard, 2016).

During actin polymerisation, the actin network and ARP2/3 complexes, forming branched junctions, undergo a retrograde flow with the plasma membrane (Lai et al., 2008). Retrograde flow is generated by the combination of the actin polymerisation at the leading edge of the cell and depolymerisation towards the rear of protrusion. Actin polymerisation at the front of the cell pushes the lamellipodial actin network backwards and the myosin contraction at the back of the lamellipodia, which pulls the lamellipodial actin network backwards (Krause and Gautreau, 2014, Lai et al., 2008, Yang et al., 2012). Adhesion to the ECM provides a link between the actin network and integrin adhesion receptor complexes, producing anchor points that act as traction to enable the force of actin polymerisation to be used for membrane protrusion (Krause and Gautreau, 2014, Giannone et al., 2009). The ARP2/3 complex is activated by nucleation-promoting factors (NFPs). There are four families of NFPs which activate branched nucleation at different cell locations where actin polymerisation is required (Rottner et al., 2010, Krause and Gautreau, 2014). The SCAR/WAVE NPF's recruit and activate the ARP2/3 complex at the lamellipodium edge. Both NPFs and elongators have to be recruited and activated at the plasma membrane to generate lamellipodial protrusions (Krause and Gautreau, 2014). Lamellipodia have mostly been studied on 2D flat surfaces, cells cultured in more physiological 3D environments have been observed using lamellipodia for protrusion, however this is uncommon (Caswell and Zech, 2018).

1.3.5 Filopodia

Filopodia are finger-like protrusions formed at the leading edge of migrating cells, such as fibroblasts, or cells extending long processes, such as neurons. Filopodia extend beyond the cell leading edge and reach or sense distant targets (Svitkina, 2018). Tips of leading edge filopodia are enriched with adhesion and signalling proteins, which triggers cellular responses when the filopodium come into contact with appropriate targets or contacts adhesive surfaces (Svitkina, 2018).

Individual actin filaments in filopodia span the whole structure and are orientated with their barbed ends towards the filopodial tip (Small and Celis, 1978). During protrusion actin subunits are added at the filopodium tip, move away from the tip during elongation and are released at the rear of filopodium (Wang, 1985, Mallavarapu and Mitchison, 1999). The major bundling protein in leading edge filopodia is fascin, a small monomeric protein that makes tight cross links between filaments (Jawhari et al., 2003, Vignjevic et al., 2006). Actin filaments are also laterally attached to the plasma membrane by ezrin-radixin-moesin (ERM) proteins to contribute to the stiffness of the filopodium (Niggli and Rossy, 2008). Formin and Ena/VASP proteins are enriched at the filopodial tips. Similar to their role with lamellipodia, they protect the barbed edges from capping and help elongation by recruiting actin-profilin complexes (Svitkina et al., 2003, Yang et al., 2007). Actin-depolymerizing factor (ADF)/cofilin and myosin II sever actin filaments at the filopodial base for actin depolymerisation and recycling (Breitsprecher et al., 2011, Medeiros et al., 2006, Svitkina, 2018).

Protrusion of the plasma membrane in cell migration can be achieved by different mechanisms involving actin filaments (Schaks et al., 2019). Lamellipodia hallmarks the cell's leading edge and is regarded as the major force driving mesenchymal cell migration in 2D and 3D environments (Svitkina and Borisy, 1999, Raftopoulou and Hall, 2004). Filopodia are enriched with several types of receptor including growth-factor receptors and sense chemical and mechanical cues (Mattila and Lappalainen, 2008). Co-ordinated polymerisation of multiple actin filaments produces forces that drive the protrusion that is needed for cell motility in the cell migration cycle.

1.3.6 Adhesion

Focal adhesions are dynamic integrin-based structures that link the cell to the ECM (Doyle et al., 2015). Adhesions are signalling hubs that sense biochemical and physical cues in the environment and serve as force transmission sites driving tissue morphogenesis, cell movement and ECM modelling (Case et al., 2015). Adhesions work as a molecular clutch, transferring force between the ECM and the cytoskeleton, this force application can promote cell adhesion growth, maturity and stability while bound to the ECM (Doyle et al., 2015).

The diverse functions of adhesions are represented by their biochemical complexity, containing hundreds of different proteins and compositions, making them important sites of mechanotransduction (Case et al., 2015, Byron, 2011, Schiller et al., 2011). However, although functionally and biochemical complex they have a conserved nanoscale protein organisation, suggesting that the position of proteins within focal adhesions regulate their activity and function (Case et al., 2015). In addition using proteomic quantification of adhesion dynamics, a consensus integrin adhesome has been identified which represents the core adhesion machinery (Horton

et al., 2015). It has been estimated that around 500 genes encode the glycoproteins and proteogylcans that combine to form ECM fibres and networks, despite the diverse range of ECM components, cellular recognition is mediated by a small number of receptor families – which integrins and syndecans are dominant (Byron et al., 2010).

During cell migration focal adhesions are constantly remodelled – new adhesions are born at the leading edge of the lamellipodia, they can then mature or be dissembled (Berginski et al., 2011). During protrusion, small nascent focal adhesions form containing clustered integrins, focal adhesion kinase (FAK) and paxillin (Choi et al., 2008). Nascent focal adhesions undergo a process of actomyosin-dependent maturation in which they grow in length and change molecular composition, if young adhesions do not engage with the actin flow, they are quickly turned over (Case et al., 2015, Choi et al., 2008). Mature focal adhesions exhibit variation in protein composition along their length, with phosphorylated paxillin concentrating at their distal tips and actin binding proteins such as vinculin, VASP and a-actinin at the proximal tips where they attach to actin stress fibers (Kanchanawong et al., 2010, Zamir et al., 1999, Wolfenson et al., 2009). Both talin and tensin are integrin related proteins that co-ordinate signals from the ECM to the cytoskeleton (Stylianou et al., 2019, Geiger et al., 2001). Tensins link the cytoskeleton to the integrin cytoplasmic tails, providing a crucial function in cell migration (Lo, 2004, Chen et al., 2002).

Talin is a large protein that can directly interact with both integrin and actin (Critchley, 2009). The talin head which binds β-integrin cytoplasmic tails, co localises with paxillin and FAK near the plasma membrane, whereas the talin tail which binds actin localises higher (Calderwood et al.,

1999, Kanchanawong et al., 2010, Case et al., 2015, Horwitz et al., 1986, Goldmann et al., 1997). Vinculin primarily co-localizes with the talin rod in the intermediary region, or 'force transduction layer', but is initially recruited near the plasma membrane and is redistributed upwards as the focal adhesion matures (Kanchanawong et al., 2010, Case et al., 2015). Mature adhesions remain attached to stress fibers throughout their lifetime and are regulated by F-actin bundles (Pellegrin and Mellor, 2007).

Super resolution microscopy of focal adhesions has identified three general nanodomains, the integrin signalling layer, the force transduction layer, and the actin regulatory layer (Figure 1. 6). The integrin signalling layer is nearest to the plasma membrane, containing FAK and talin's regulatory head domain whereas mechanosensing proteins such as talin and vinculin are contained in the force transduction layer, acting as an intermediate between mechanical signalling and cytoskeletal layers (Case et al., 2015, Shams et al., 2018). The actin regulatory layer is ∼50–60 nm from the membrane and extends upwards into the stress fiber, containing actin and actin binding proteins α-actinin, VASP and zyxin. The force transduction layer containing the rod domain of talin spans between the integrin signalling and actin regulatory layer. Although the structure of this focal adhesion has been visualised the function of these layers are yet to be understood, the organisation could sterically limit protein-protein interactions and dictate specific downstream functions (Case et al., 2015). This layered nanostructure has been demonstrated across a range of studies with different techniques suggesting that the layered nature is a result of a cell-type independent organising principle, and independent of matrix proteins (Legerstee and Houtsmuller, 2021).

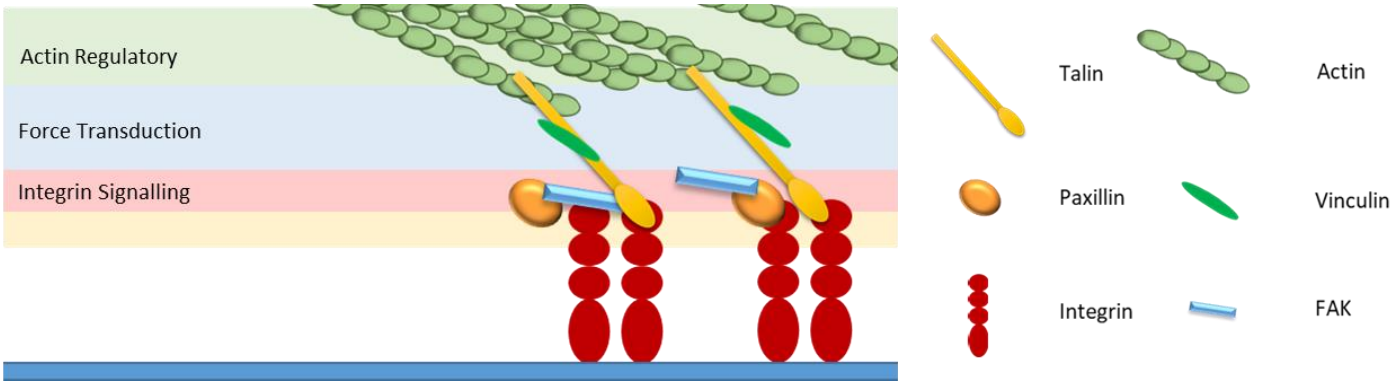

Figure 1.6: Focal adhesion architecture. Model showing layer structure of focal adhesions the integrin signalling layer contains regulatory proteins paxillin, focal adhesion kinase (FAK) and talin regulatory head domain. The force transduction layer contains mechanosensitive proteins talin and vinculin and the actin regulatory layer contains actin and actin regulatory proteins. Adapted from Case 2015.

Focal adhesions are mechanosensitive and form a mechanical link between the ECM and actin cytoskeleton. The primary site of force transmission to the cell is the cellular membrane, its direct contact with the ECM allows mechanical stimuli to be transmitted to cells through diverse mechanosensitive molecules such as integrins, stretch activated ion channels, G protein coupled receptors and growth factor receptors which activate different mechanotransduction pathways (Martino et al., 2018, Martinac, 2014, José Luis and Wolfgang, 2016). Focal adhesions are the main hub of cell-ECM interaction, sensitive to ECM composition and mechanics, they detect and transfer mechanical cues from the ECM (Martino et al., 2018, Schiller and Fässler, 2013). The main focal adhesion proteins involved in mechanotransduction are FAK, talin and vinculin. The forces generated by cell migration can induce force conformational changes which is required for regulating new binding events and can also significantly affect signalling cascades (Shams et al., 2018). Focal adhesion dynamics are highly regulated by structural and signalling molecules, including kinases and alterations in these factors play a role in adhesion turnover, signalling and

normal cell function (Berginski et al., 2011). Adhesion formation and maturation are well characterised on flat 2D surfaces however little is known about the dynamics of 3D ECM-cell adhesion sites (Doyle et al., 2013, Doyle et al., 2015). Several publications have visualised discrete adhesion structures in cells within a 3D matrix, and these 3D adhesions have been shown to have the same molecules as 2D, such as integrins, vinculin and paxillin in normal and cancerous cells (Harunaga and Yamada, 2011). However, the shape, size and localisation patterns of 3D focal adhesions are varied across studies, needing further evaluation. It is also thought that 3D adhesions can be sensitive to ECM architecture, and there is evidence that a force dependency exists for certain adhesion components in 3D (Doyle et al., 2015). More in-depth studies are needed to uncover the specific molecular composition of 3D matrix adhesions.

1.3.7 Contraction

The final step of cell migration is translocation of the cell body and rear of the cell, the adhesions at the rear must disassemble and the trailing edge retract (Ananthakrishnan and Ehrlicher, 2007, Vicente-Manzanares et al., 2005). Cell body contraction is dependent on actomyosin contractility, provided by non-muscle myosin II (Svitkina et al., 1997, Vicente-Manzanares et al., 2005). Stress fiber assembly and contraction is controlled by myosin II, and predominantly induced by the small G protein Rho, and its downstream effector, ROCK (Parri and Chiarugi, 2010). Rho acts via ROCKs to affect myosin light chain phosphorylation, by inhibiting MLC phosphatase and by phosphorylating MLC (Parri and Chiarugi, 2010, Fukata et al., 2001).

1.4 3D cell migration

All previous cell migration strategies discussed in this thesis have been observed using 2D techniques, with cells migrating across solid surfaces, which is not physiologically relevant *in vivo.* Although this research has gained insight into fundamental cell migration mechanisms, in the past decade there has been a shift into using 3D systems as they are considered a more physiologically relevant model. This is partly due to the ability to recapitulate the ECM, which has a crucial contribution to cell migration. Most cells migrating through tissues undergo 3D migration as they are continuously embedded in a cellular or ECM context (Yamada and Sixt, 2019). During embryonic development, 3D cell migration by individual cells, pairs and larger clusters is crucial for forming tissues and organs, and these processes become disrupted in cancer invasion (Yamada and Cukierman, 2007).

The modes of individual and collective 3D cell migration differ depending on the specific cell and tissue functional requirements, and the ECM environment the cells migrate through can also affect their 3D migratory mode (Yamada and Sixt, 2019). The major categories of 3D cell migration are mesenchymal, amoeboid and lobopodial. The two most extensively characterized modes of 3D cell migration are mesenchymal and amoeboid migration. Compared to the other modes, mesenchymal cell migration in 3D collagen rich microenvironments is most similar to the equivalent mode of migration in 2D (Yamada and Sixt, 2019). Cells migrate using actin polymerisation at the leading edge and during adhesion, they largely use the same molecular machinery composed of integrins and associated focal adhesions proteins in 2D and 3D (Doyle et al., 2009, Caswell and Zech, 2018, Newman et al., 2021). However, it is unknown whether the

subsequent steps of focal adhesion release and cell contraction are similar in the different environments.

Amoeboid and lobopodial migration differ considerably more from the classical 2D stepwise migration model (Petrie et al., 2012). As previously discussed, amoeboid is characterised by rounded morphology and low adhesion interactions. Lobopodial migration can be viewed as a hybrid between amoeboid and mesenchymal migration, and it uses asymmetric intracellular pressure to generate blunt cylindrical protrusions of the leading edge called 'lobopodia' (Petrie et al., 2012). At the same time, the cells adhere tightly to their substrate and exert pulling forces on the ECM, while the nucleus moves forward in a piston-like manner to generate anterior pressure (Yamada and Sixt, 2019).

Complex 3D environments provide challenging physical features to migrating cells, including composition and topology of the local environment which includes ECM and physical factors such as stiffness and size of pores or passageways for migration (te Boekhorst et al., 2016, Doyle et al., 2013).

One implication in 3D migration is being physically confined by ECM or tightly packed cells, cells can be stimulated to use protease activity to degrade the ECM allowing movement, alternatively they can permanently or transiently remodel the ECM, using adhesive and contractile forces to deform ECM fibres (Gaggioli et al., 2007). Active modification of the extracellular environment is a feature of mesenchymal cell types, ameboid cells such as leukocytes show limited proteolytic capacity and largely reduced adhesion that limits their ability to pull on and rearrange ECM fibres. These cells usually do not create passages by ECM degradation or deformation, but instead use

opportunistic strategies to adapt to the environment and navigate through tissues by selecting the path of least resistance, for example with appropriately sized ECM pores (Wolf et al., 2009, Renkawitz et al., 2019). Another strategy is to switch migration modes, and become proteolytic in environments where ameboid migration is not sustainable, however there is little consensus about the molecular mechanism by which cells achieve this (van den Berg et al., 2019). The detailed molecular mechanisms driving each of the different modes of 3D cell migration are considerably less explored than those involved in 2D migration.

Further insights into 3D migration are developing, with recent research suggesting that amoeboid is not only a migration mode, but a cell state detectable in pathological contexts and a mode which cancer cells apply to achieve survival and invasive advantages while overcoming certain environmental challenges (Graziani et al., 2022, Liu et al., 2015). The amoeboid status has been understudied as the majority of cancer biology was performed in 2D culture systems where detecting amoeboid features is challenging (Čermák et al., 2020).

This highlights that despite the research into 3D cell migration and invasion, there is much still unknown. Although new model systems have been developed to provide insight to regulation of 3D migration, further evaluation is needed to put these findings into context with the wider field. Direct in-depth comparisons between 3D and classical 2D migration is needed to determine the potentially altered roles of specific molecules (for example the ‘adhesome’ and signalling complexes) used in different 3D contexts (Yamada and Sixt, 2019).

1.5 Cell migration in cancer

Cell migration is dependent on co-ordinated and tightly regulated mechanisms; any mis-regulation can lead to pathological diseases such as vascular and chronic inflammatory diseases (Horwitz and Webb, 2003). Any unauthorised cell migration can also lead to tumour formation, invasion, and metastasis (Webb, 2005, Ritch et al., 2019). Metastasis is the term given when cells from the primary tumour disseminate and form secondary sites around the body. Cancer invasion and metastasis are landmark events that transform a locally growing tumour into a life threatening disease (Friedl and Alexander, 2011).

The terms migration and invasion are often used interchangeably, and although closely related, cell migration is defined as directed translocation of cells on a 2D substrate or through a 3D matrix. Cell invasion on the other hand, is defined as cell movement through a 3D matrix accompanied by restructuring the 3D environment (Thijssen-van Loosdregt, 2020, van Roosmalen et al., 2015, Ilina and Friedl, 2009). The process of cell invasion involves the adherence of cells to the ECM, where they can remodel their local environment by degradation of existing ECM components and deposition of new ECM components before being able to migrate through the ECM (van Roosmalen et al., 2015, Ilina and Friedl, 2009). Therefore the term invasion describes a specific mode of 3D migration including ECM degradation, where migration is used to describe non-destructive movement in both 2D and 3D environments (Thijssen-van Loosdregt, 2020).

Cancer metastasis and the burden of secondary tumours are the most common causes of mortality for most patients, responsible for 90% of cancer related deaths (Ritch et al., 2019).

Metastasis remains problematic due to clinical failures in treatment of metastases and poor understanding of the molecular mechanisms. The high mortality associated with metastasis further highlights the failure of managing the disease once it disseminates through the body (Fares et al., 2020, Paul et al., 2017, Seyfried et al., 2014).

1.5.1 Process of metastasis

The metastatic cascade is complex and contains multiple sequential related steps (Figure 1.7). Cancer cells must first detach and migrate away from the primary tumour, intravasate into the lymphatic and circulatory system, evade immune response, transit through secondary tissues, and invade and proliferate in distant organs (Paul et al., 2017, Seyfried et al., 2014, Welch, 2006, Gupta and Massagué, 2006). Metastatic cells must also establish a microenvironment that facilitates angiogenesis and proliferation resulting in a malignant secondary tumour (Seyfried et al., 2014).

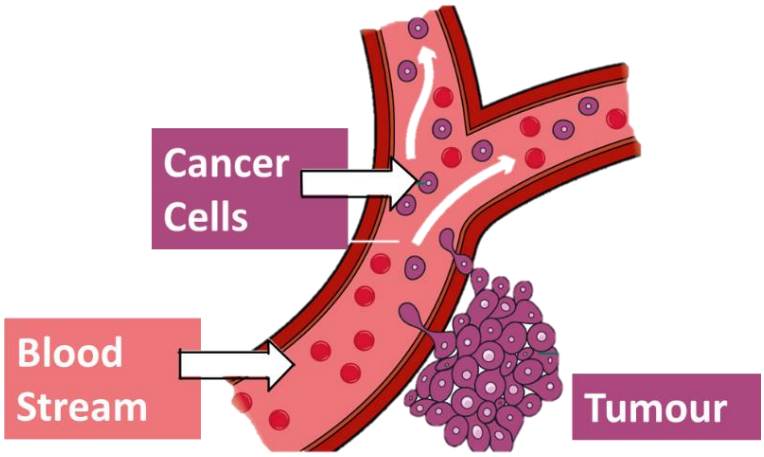

Figure 1.7: The process of metastasis. During the complex mechanism of metastasis, cancer cells must detatch and migrate away from the primary tumour, intravasate into the circulatory and lymphatic system, evade immune response, transit through secondary tissues, and invade and proliferate in distant organs (Paul et al., 2017, Seyfried et al., 2014, Welch, 2006, Gupta and Massagué, 2006).

Cancer cell migration and invasion is a cell and tissue driven process, where the physical, cellular and molecular factors adapt and react throughout the progression of the disease (Friedl and Alexander, 2011). Cancer cell motility is an important aspect of metastasis, as the invasive capacity of cells is mainly driven by motility (Le Dévédec et al., 2010).

1.5.2 Types of cancer cell migration

Cancer cell motility is dependent on changes in tumour cell morphology caused by actin modifications and rearrangements of the cytoskeleton (Vignjevic and Montagnac, 2008). The changes in cellular morphology and their impact on motility are associated with changes in epithelial and mesenchymal phenotypes, a process known as epithelial-to-mesenchymal transition (EMT). The transition from an epithelial to a more mesenchymal state is linked to morphological modifications, loss of tight junctions, remodelling of the cytoskeleton and gain of migratory and invasive capacities (Valastyan and Weinberg, 2011). EMT is a known driver in the pathogenesis of cancer, epithelial cells gain distinctly mesenchymal trails that give them the ability to invade adjacent tissues locally and then to disseminate to distant tissues (Yang et al., 2020). Much of this phenotypic progression towards increased invasiveness depends on the activation of EMT (Tsai and Yang, 2013, Chaffer et al., 2016). Although EMT is often presumed to be a key milestone for tumour cell invasion, increasing evidence indicates the presence of additional dissemination mechanisms of tumour cells (Kalluri and Weinberg, 2009). Altered mechanical cues in the tumour microenvironment can increase cellular tension, and alter cell morphology, cytoskeletal dynamics and metabolism during invasion (Wu et al., 2021b).

Several studies have confirmed the existence of two main patterns of cancer cell invasion, collective cell migration and individual cell migration. Tumour cells can disseminate as individual cells via mesenchymal or ameboid modes or move as collective groups (Wu et al., 2021a). Mesenchymal cells exhibiting elongated morphology can move forward by generating traction force via cytoskeletal contractility and integrin mediated ECM-adhesion (Pearson, 2019). Proteolysis-dependent ECM degradation is also required for mesenchymal tumour cells to generate paths for their migration (Wu et al., 2021a). Amoeboid cells with rounded and deformable morphology can squeeze through narrow spaces and smaller pores of the ECM in the absence of proteolysis-dependent ECM remodelling (Lorentzen et al., 2011). During this type of movement, the cells exhibit bleb like protrusions driven by actomyosin contractility and maintain weak and dynamic cell adhesion to the ECM, resulting in high speed movement (te Boekhorst et al., 2016). Distinct from single cell motility, collective cell migration is a movement pattern of multiple cells that retain cell-cell connections and migrate co-ordinately (Haeger et al., 2015) . This type of tumour cell movement depends on actin dynamics, integrin-based ECM adhesion and proteolytic cleavage of ECM (Wu et al., 2021a).

Cancer cells use many tools to migrate *in vivo*, including degrading their surrounding ECM to create their own tracks or by following 'leader' cancer cells or cancer associated stromal cells that open up migratory paths (Paul et al., 2017, Bremer et al., 2001, Fisher et al., 2009, Gaggioli et al., 2007, Patsialou et al., 2013). Another tool is to move through pre-existing channel-like tracks created by anatomical structures (Friedl and Alexander, 2011, Wolf and Friedl, 2011).

During cancer metastasis, cancer cells can use collective migration in response to some physical cues, such as collagen fibres, myofibrils, or basal lamina from muscles, nerves or blood vessels (Friedl and Gilmour, 2009). Recent studies have shown that collectively migrating tumour cells are more aggressive and have increased survival in response to chemotherapeutics (Lintz et al., 2017, Cheung et al., 2016, Aceto et al., 2014, Maddipati and Stanger, 2015). *In vivo*, collections of tumour cells outgrow depositing matrix, realigning the matrix fibres and secreting growth factors causing mechanical stress and enhanced cellular proliferation (Provenzano et al., 2006, Rizwan et al., 2015).

As the extracellular environment contains confining pores or fibre-like and channel-like tracks, matrix degradation is required for cancer cell migration to occur (Wolf et al., 2013). Evidence suggests that confinement is a physical cue that modulates intracellular signalling and thereby alters the tumour cell migration mechanism (Hung et al., 2016). In cancer metastasis, ECM remodelling is hijacked, leading to tumorigenesis (Fares et al., 2020, Sonnenschein and Soto, 2016). Disassembly of the ECM and its constituents is an important step in invasion, and enzymes such as matrix metalloproteinases (MMPs) play an important role in this. MMPs are essential for invasion and for cell proliferation, survival, immune response, angiogenesis (Kessenbrock et al., 2010, Shuman Moss et al., 2012). MMPs are elevated in most cancer types and associated with poor prognosis (Egeblad and Werb, 2002, Hadler-Olsen et al., 2013). Cancer cells adjust the metastatic niche to drive growth by remodelling the ECM (Fares et al., 2020).

1.5.3 Therapeutic targeting of metastasis

Treatment of cancer metastasis and growth at secondary sites remains the most challenging aspect of oncology, across all cancer types only 20% of patients with stage IV metastatic disease survive beyond 5 years of diagnosis (Edwards et al., 2021, Miller et al., 2019). Classical cancer therapy targets cell proliferation at the primary site without discriminating cancer cells from normal cycling cells (Chabner and Roberts, 2005, Ritch et al., 2019). More recent approaches have concentrated on targeted treatments and immunotherapy to improve specificity and reduce toxicity (Huang et al., 2014, Pardoll, 2012). Future approaches could concentrate on preventing metastases forming, however the heterogeneous microenvironments which cancer cells migrate *in vivo* and the diversity of migratory mechanisms available to cancer cells add complexity to anti-metastatic approaches (Friedl and Alexander, 2011, Wolf and Friedl, 2011). Furthermore, the plasticity of cancer invasion can make therapeutic targeting difficult, as cancer cells are able to adapt their metastatic dissemination programs by switching between collective and individual-cell migration programs (Ilina et al., 2018, Cheung et al., 2016).

While considerable progress has been made in studying the genetic and cellular aspects of metastasis with *in vitro* cell culture and *in vivo* animal models, the driving mechanisms of metastasis are still relatively unclear due to their complexity (Hapach et al., 2019). Models of metastasis are crucial to mimic human disease progression and find open therapeutic windows for successful intervention (Hapach et al., 2019, Fares et al., 2020).

1.6 Models of metastasis

Decades of research into metastasis in different organs and patients have depicted a landscape of genomic intra- and inter-patient heterogeneity (Masmudi-Martín et al., 2021, Hu et al., 2020, Priego et al., 2018, Robinson et al., 2017, Zehir et al., 2017). The complexity may arise from the multistep process of metastasis, which transforms a local tumour into a system disease which is more difficult to control therapeutically (Masmudi-Martín et al., 2021).

In historical research, animal models have been the gold standard for understanding the disease development and treatment response. Anti-cancer medicines require evaluation in animal models to ensure efficacy and safety before moving to human trials. Animal models allow whole-body distribution studies which then guide the transition of medicines from pre-clinical to clinical studies (Rohiwal, 2020). Use of animal models allows information such as tumour size, number of metastases and animal survival to be obtained. However, this must be used in combination with other studies such as drug-tumour accumulation, targeting efficiency, pharmacokinetics (e.g., circulating drug concentration over time, the volume of distribution, mean clearance time, bioavailability) and pharmacodynamics (absorption, biodistribution, drug metabolism and excretion) (Boix-Montesinos et al., 2021). Several animal models are available and are largely dependent on the specific research aims, the recapitulation of different phases of the disease, development of metastasis, immune system status and overall resemblance to the human disease (Ireson et al., 2019). The use of animal models incorporates the role of tumour microenvironment and angiogenesis in tumour response to therapy and can also sometimes include the immune response (Castro et al., 2021). The most used type of oncology animal

models are xenografts, which are easily established and can be used with most cell lines, however this model implicates an immunodeficient host as well as a homogenous tumour formation which does not represent tumour heterogeneity (Castro et al., 2021). Organoid and patient-derived xenografts (PDX) can overcome the tumour heterogeneity, but these methods also require the use of immunocompromised models, which compromises the impact of the drugs on the immune cells or the immunotherapies screening (Castro et al., 2021). PDXs have been used for many decades in cancer research and have many advantages including the choice of generation from primary tumours or metastatic legions (Golan et al., 2021). Preclinical studies test novel drugs in non-human subjects and are used in combination with *in vitro*, *ex vivo* and *in vivo* screenings, but the results are not always predicative of the *in vivo* outcome, identifying a clear need for more biometric and clinically relevant models of disease (Castro et al., 2021).

Current knowledge of cancer biology, signalling pathways and therapeutic targets have been provided by 2D systems with immortalised cancer cell lines (Castro et al., 2021). However, these systems do not always accurately represent *in vivo* tissues or tumours (Pozzi et al., 2021). The absence of ECM, oxygen and nutrient gradients or relevant cell-cell and cell-ECM interactions make these models insufficient in mirroring the complex biological features seen *in vivo* (Henrich 2021). While 2D models are simple, well established and low cost they also lack mechanical and natural structure of tumours, heterogeneity of tumour population and are a poor representation of cell proliferation, differentiation, cell hierarchy, gene and protein expression, response to perturbations, stimuli and drugs, migration, invasion, and other cellular functions (Pozzi et al., 2021, Duval et al., 2017, Melissaridou et al., 2019).

A metastatic disease model is necessary to establish the field of metastatic research and provide foundational concepts, however this is difficult to recapitulate in a model due to the integrated and complex nature of its processes (Suhail et al., 2019). Therefore, in order to overcome the limitations of *in vitro* studies and bridge the gap between oversimplified 2D and unrepresentative animal models, advanced 3D cancer models have been developed (Castro et al., 2021).

1.6.1 3D *in vitro* models

A variety of 3D cancer models have been developed to create a more physiological system that better resembles the tumour microenvironment. Where genetic cues, as well as physical and mechanical properties, can contribute to disease development, metastatic spread and response to therapy (Castro et al., 2021, Quail and Joyce, 2013, Correia and Bissell, 2012). Most 3D systems share the key characteristics of generation of gradients, the presence of ECM and the presence of cell-cell/cell-matrix interactions (Lu and Stenzel, 2018, Boix-Montesinos et al., 2021). Furthermore, their biological relevance has been demonstrated in several studies showing their gene expression profiles and response to treatment resemble more closely the *in vivo* situation (Riedl et al., 2017, Koch et al., 2021, Luca et al., 2013). *In vitro* 3D cultures of tumour and stromal cells have been demonstrated to better resemble the architecture and phenotypical features found in solid tumours (Hickman et al., 2014).

Although 3D systems have many advantages there is pressure to fulfil certain criteria. The 3D model must fully mimic the cancer in a biologically relevant way, presenting a platform suitable for drug screening and development as well as investigation of cellular and acellular processes (Heinrich et al., 2019). Whilst most 3D models, such as spheroids, can be developed from any

cancer cell type, it is more complex to produce a 3D invasive model. In addition, the 3D models must not only overcome the limitations of previous 2D assays, but match the ability to be high throughput, easily reproducible, a simple readout and cost reductive compared to animal models (Heinrich et al., 2021). The choice of a fit-for-purpose model, that is as simple as possible but complex enough to answer a scientific question is a challenging concept, therefore some 3D *in vitro* models come with caveats (Riss and Trask, 2021).

In general, two different approaches to create *in vitro* models have emerged, cell-based approaches (3D spheroids and organoids) and engineered-based approaches (scaffold-based, 3D bio printed models and tumour-on-a-chip) (Rodrigues et al., 2018, Brancato et al., 2020, Drost and Clevers, 2018, Fetah et al., 2019, Heinrich et al., 2021). Whereas cell based rely on the natural ability of cells to organise themselves into 3D structures, engineered-based approaches are mainly driven by a specific goal, which defines the structure and composition of the model (Heinrich et al., 2021). Each of the models differ in terms of cancer cell sources, protocols, equipment resources and specific sets of conditions. And the use of the models is dependent on the research question. For example, organoids are useful for reproducing tumour cell architecture and used to recapitulate historical features and cellular heterogeneity of tumours. However, multicellular tumour spheroids are usually grown from cancer cell lines, and while they poorly resemble the *in vivo* biology of cancers, they maintain the metabolic and proliferative gradients of *in vivo* tumours, along with cell signalling mechanisms (e.g. adhesion and motility) (Pozzi et al., 2021).

1.6.2 3D spheroid models

3D spheroid models are one of the main representatives of cell based *in vitro* models. There are several techniques to generate spheroids. However, the general principle is based on the cell's own capacity to form 3D cell aggregations that are held together by cell-cell contacts and the presence of the ECM that is produced by cells themselves (Heinrich et al., 2021). Based on the dense environment that is generated spheroids often shown nutrient and oxygen gradients similar as observed *in vivo* (Nunes et al., 2019).

Multicellular tumour spheroids (MCTS) have been widely used to study several biological processes and interactions of cancer cells. MCTS display an intermediate complexity between *in vivo* solid tumours and *in vitro* cells grown in monolayers. This can reproduce features found in solid tumours such as cellular heterogeneity, cell interactions and signalling pathways, migration and invasion and tumour organisation (Pozzi et al., 2021). The spheroids can also be embedded into hydrogel scaffolds to mimic the *in vivo* physical interactions of ECM-cell adhesion and cell-cell contact points (Nunes et al., 2019, Costa et al., 2016). Furthermore, MCTS can also recapitulate the kinetics of cell growth and gene expression profiles, making them suitable 3D models for studying tumour biology and anti-cancer treatment approaches (Nunes et al., 2019).

MCTS are considered very effective and low cost *in vitro* 3D models (Costa et al., 2016). Further advantages for the spheroids over other 3D models are the ease of maintenance and simplicity of genetic manipulation (Ishiguro et al., 2017). However, although it is simple to generate spheroids and there is potential to include stomal components, spheroids face some limitations

with reproducibility. A major challenge is the lack of overall control on the spheroid architecture (Heinrich et al., 2021).

1.6.3 3D organoid models

3D organoids are emerging as promising models for modelling cancer development and treatment. Organoids are 3D tissues that mimic organ-like structures and functions, they contain key biological features and relevant tissue development (Drost and Clevers, 2018). Organoids are usually developed from pluripotent stem cells (iPSCs) or tumour cells, encapsulated into a hydrogel environment and left to develop. In this way, 3D organ-like structures are generated which follow development steps like natural tissues, representing tissue-specific morphology and architecture (Heinrich et al., 2021). The ability of the organoid to organise itself based on its own genetic information is much more representative of tumorigenesis, making it more of a physiological model (Castro et al., 2021).

There are two types of organoids, engineered cancer organoids (ECO) and patient derived cancer organoids (PDO). While the engineered cancer organoids are based on iPSC cells forming a healthy tissue organoid before genetic editing towards a tumour organoid, patient derived cancer organoids are developed with tumour cells obtained from patients (Heinrich et al., 2021). The use of the patients own cells recreates intra and interpatient heterogeneity, which makes them desirable for a personalised medicine approach (Bruun et al., 2020). Patient derived cancer organoids form a suitable platform for rapid screening of personalised medicine due to their tumour origin and relatively low culture efforts which can lead to new prognostic biomarkers and personalised anti-cancer therapies (Drost and Clevers, 2018, Fan et al., 2019). 3D organoids have

been suggested as a better alternative to expensive and labour-intensive patient-derived tumour xenografts (Castro et al., 2021). The use of patient derived cancer organoids can be complimentary to PDX models as they are more cost efficient and quicker and may also reduce the use of animal models (Golan et al., 2021).

3D models can bridge the gap between traditional 2D assays, animal models and human clinical trials. Not only do 3D models improve predictions of invasion and migration, but they can also model immunotherapy, which is a major strategy in oncology (Pozzi et al., 2021). Metastatic death remains the main cause of cancer related death, therefore developing models that fully capture the metastatic cascade are of major interest to not only discover novel drug targets, but to assess efficacy of drugs on the metastatic niche (Castro et al., 2021). Recent efforts to achieve this include a multi-site metastasis-on-a-chip model, composed of multiple bioengineered 3D organoids using 3D photopatterning (Aleman and Skardal, 2019).

The major challenge with all 3D *in vitro* models is the lack of standardised protocols for imaging, quantification, and analysis (Nunes et al., 2019, Costa et al., 2016). Further, the correlation between response to therapy in 3D, *in vitro, in vivo* and clinical studies still remains to be consolidated (Nunes et al., 2019).

1.6.4 Imaging techniques for metastasis

The rise of more physiologically relevant 3D models has added pressure for development of novel methods to visualise and measure events in more complex structures in comparison to cell monolayers (Riss and Trask, 2021). To study the structure and function of cells in 3D, light

microscopy is frequently used with important insights into the metastatic process gained specifically through the use of imaging technology (Edwards et al., 2020, Fein and Egeblad, 2013).

The three most common optical sectioning microscope systems used for imaging 3D cell models include confocal, high resolution microscopy (including light-sheet based instruments) and wide-field microscopy (Figure 1.8) (Riss and Trask, 2021). Confocal imaging systems remain the most common instrument for higher throughput 3D microscopy, more readily-available compared to other specialist systems they offer optical sectioning of 3D cell models (Riss and Trask, 2021). One of the limiting factors of confocal and wide-field microscope systems is the depth of focus penetration of light into the sample, which depends on the sample preparation and the optical configuration of the microscope system (Riss and Trask, 2021).

Multiphoton microscopy is another technique beneficial for imaging 3D samples, as it achieves deeper penetration and minimal phototoxicity and photobleaching. Multiphoton microscopy uses short pulses of infrared laser light to excite fluorophores and under optimal circumstances, excited and emitted light penetrates tissues up to 1000 µm, although 200–300 µm is a common limit (Fein and Egeblad, 2013).

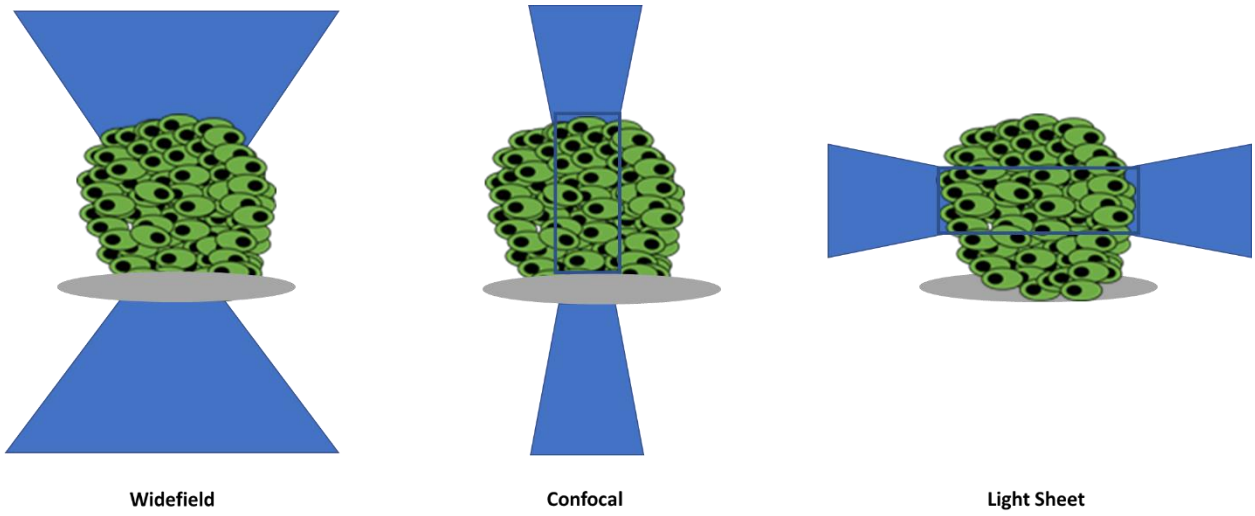

Figure 1.8: Illumination from different microscopy. Broad illumination from widefield microscopy, pinpoint vertical illumination from confocal microscopy and narrow horizontal illumination from light-sheet microscopy (Riss and Trask, 2021).

Live microscopy with expression of fluorescent proteins has provided insight into what types of behaviour and cell-cell interactions differentiate metastatic and non-metastatic cancer cells (Fein and Egeblad, 2013). Labelling cells for confocal or multiphoton microscopy is accomplished by expression of fluorescent proteins or injectable imaging agents, e.g. fluorescent dextran (Condeelis and Weissleder, 2010). Live microscopy allows high resolution analysis of cell activities including migration and signalling responses spanning over days, but requires an excitation source and can suffer from poor light penetration and tissue autofluorescence (Prescher and Contag, 2010). However, live microscopy techniques have been particularly useful for imaging cellular behaviours in tumours, such as migration, intravasation, extravasation, and cell-cell or cell-ECM interactions (Fein and Egeblad, 2013).

The main challenges of imaging organoids and spheroids are the light scattering nature of their 3D architecture and, preparation of 3D cell cultures for light microscopy can be destructive, including physical sectioning of the samples, which results in loss of 3D information (Edwards et al., 2020). Fast volumetric imaging is often preferred, with reduced light exposure to reduce phototoxicity and photobleaching (Edwards et al., 2020). To this extent, light sheet fluorescence microscopy has been the method of choice to study organoid and spheroid development over longer time scales (Pampaloni et al., 2015, Serra et al., 2019).

Light-sheet fluorescent microscopy (LSFM) was first described as ultramicroscopy in 1902, refined with the development of orthogonal-plane fluorescent optical section in 1993, to its current name first described as LSFM in 2004 (Voie et al., 1993, Huisken et al., 2004). LSFM is a method that uses a sheet of light to illuminate a whole plane of the sample, much more gentle and faster than traditional microscopy methods. Light sheet microscopy has undergone rapid expansion and grown in popularity over the last decade with 3D volumetric images and improved temporal and lateral resolution (Riss and Trask, 2021). More recently, lattice light-sheet microscopy developed by Eric Betzig's lab has improved sample preparation requirements and reaching spatiotemporal resolution close to 20 µm (Chen et al., 2014). Appropriate sample preparation is still required for LSFM, but is often simpler compared to other high resolution techniques, however, image acquisition can be complicated and not suitable for automated high throughput of multiple samples (Riss and Trask, 2021).

Intravital microscopy (IVM) is an imaging method that has identified early steps and molecular drivers of metastasis *in vivo*. IVM involves imaging of a live animal through an imaging window

implanted into the animal, enabling assessment of tumour pathophysiology at a higher resolution, and in an intact host (Malandrino et al., 2018). IVM can measure anatomical and functional parameters linked to the mechanics of metastatic events and assess the general mechanisms of cell migration during invasion and intravasation (Jain et al., 2002, Condeelis and Segall, 2003, Friedl and Alexander, 2011). With the capability to image deeper within a sample than other light microscopy techniques, IVM can prove effective to study cancer metastasis despite the inability to control key parameters during *in vivo* imaging (Malandrino et al., 2018). Recently, spheroids were microimplanted in an intravital microscopy approach, allowing observation of the critical early steps of collective invasion and cytoskeletal plasticity in breast cancer tumours (Ilina et al., 2018).

Resolution within intact tissues at the subcellular scale is hard to achieve, though optical super-resolution imaging has given insights at the molecular scale, for example imaging clustering and localisation of single molecules (Oleksiuk et al., 2015). Super resolution is currently limited to specific applications, and not used commonly in visualising dynamic metastatic events.

Microscopy is a powerful tool for visualisation and analysis of 3D cell models especially when combined with methods such as second harmonic generation for collagen imaging and specialist reporter constructs (Campagnola, 2011).

As tissue culture methods advance, sample preparation as well as microscopy techniques must be improved and adapted. For example, the use of tissue clearing approaches which mitigate light scattering and enable high-resolution imaging of 3D samples without the need of physical sectioning, but does require fixation (Edwards et al., 2020). End-point fluorescent imaging of fixed

organoids and spheroids is typically limited to the outermost cell layers, due to light scatter and the poor penetrance of labels into the samples. The recent development of tissue clearing techniques has enabled 3D intact imaging by reducing light scatter and improving the penetrance of labels through harsh permeabilization steps (Unnersjö-Jess et al., 2016).

Furthermore, imaging of 3D samples are often low throughput and further developments would allow for spheroids and organoids grown in glass-bottomed multi-well plates to be imaged in the well. This would also allow the spheroids or organoids to be screened in a high-throughput manner, potentially in combination with small molecule compounds and imaged without the requirement for transfers and associated losses. Open top light sheet microscopes designed for fast 3D imaging of cleared biopsies could be adapted to provide fast volumetric imaging for a variety of samples (Edwards et al., 2020).

1.7 Rho GTPases in cancer

Rho GTPases are important signal transducers in regulation of cell migration, proliferation, survival and death (Haga and Ridley, 2016, Toksoz and Merdek, 2002). These processes are crucial for maintenance of normal tissues, but also contribute to cancer progression (Sahai and Marshall, 2002, Toksoz and Merdek, 2002). Rho GTPases were first proposed to support cancer formation and progression as activated forms of Rho GTPases were found to promote fibroblast transformation and dominant-negative mutants (which inhibit Rho GTPase specific GEFs) prevent transformation (Svensmark and Brakebusch, 2019, Prendergast et al., 1995, Lin et al., 1997). Further, RhoA, Rac1 and Cdc42 were shown to be essential for cell migration as they are involved in controlling cell contraction, membrane protrusion and directionality, indicating an important role for these Rho GTPases in cancer cell invasion and metastasis (Svensmark and Brakebusch, 2019).

While several Rho GTPases were reported to be overexpressed in human cancers, activating mutations of Rho GTPases appear to be rare, and deletion of specific Rho GTPase genes in mice do not support a tumour promoting role of Rho GTPases (Karlsson et al., 2012). Although these rare mutations are likely to be important in tumour development, in most cases, Rho GTPases are found to be upregulated or have their activity increased by changes in the expression of GAPs, GEFs and or GDIs (Porter et al., 2016). Several Rho GTPases are often upregulated in human tumours including RhoA, RhoC, Rac1, Rac2, Rac3, Cdc42, RhoV and RhoF (Porter et al., 2016, Pajic et al., 2015).

RhoA is involved in almost all stages of tumour progression, one example is hyperactivity in gastric cell lines, with suppression leading to partial inhibition of the proliferative phenotype (Zhang et al., 2009). Furthermore, several studies *in vitro* and *in vivo* suggest that RhoA is involved in tumour angiogenesis, and mutations in RhoA that lead to loss of GTPase activity are important to drive cancer progression (Haga and Ridley, 2016, Chiba et al., 2015).

Rac1 is another Rho GTPase that is found modified in several stages of tumour progression. Deregulation of Rac signalling can be caused by changes in the upstream signalling, including tyrosine kinase receptors, PI3Ks, GEFs and GAPs (Haga and Ridley, 2016). One example of this is the activation of Rac1 in breast cancer, where the Rac GEF P-Rex1 causes activation of Rac1 after stimulation of tyrosine kinase receptors and GPCR's (Wertheimer et al., 2012).

The role of Rho GTPases in cancer is complex, their contributions are dependent on cell type, extracellular stimuli and signalling pathways involved in the particular cancer and not all data obtained from cell models, animal models and patients easily fit together (Haga and Ridley, 2016, Svensmark and Brakebusch, 2019, Karlsson et al., 2012, Porter et al., 2016).

1.8 Deleted in Liver Cancer 1 (DLC1)

Deleted in Liver Cancer 1 is a RhoGAP protein with tumour and metastatic suppressor activities which is frequently mutated in aggressive cancers (Durkin et al., 2007a, Barras and Widmann, 2013). DLC1 acts as a switch by promoting conversion of the active GTP bound Rho into the inactive RhoGDP to affect cytoskeleton, focal adhesion and cell migration (Zhang and Li, 2020, Barras and Widmann, 2013). First discovered as a tumour suppressor that was lost in hepatocarcinomas, DLC1 was later found to be lost in several other malignancies including haematological, lung, breast, prostate, kidney, colon, uterus, ovary, and stomach cancers (Yuan et al., 2003b, Durkin et al., 2007b). DLC1 has been extensively investigated for its role as a tumour suppressor. It is now known that DLC1 expression prevents cell migration, invasion and metastatic progression in various cancer types (Durkin et al., 2007b, Liao and Lo, 2008, Lukasik et al., 2011, El-Sitt and El-Sibai, 2013, Kim et al., 2009, Feng et al., 2013, Wu et al., 2009, Heering et al., 2009b, Kim et al., 2008, Wong et al., 2005, Ullmannova-Benson et al., 2009, Steve Goodison, 2005, Healy et al., 2008, Zhou et al., 2008).

DLC1 belongs to the DLC family which contains two other members DLC2 and DLC3. DLCs are structurally and functionally similar (Wolosz et al., 2014, Leung et al., 2005, Kawai et al., 2007). They all possess three functional domains, sterile α motif (SAM) domain, catalytic RhoGAP domain and steroidogenic acute regulatory protein (StAR)-related lipid transfer (START) domain, and a serine-rich region (SR region) or a linker region located between the SAM and RhoGAP domains (Durkin et al., 2007b). All DLC members localise at focal adhesions and have similar RhoGAP domain inhibition of RhoA activity and actin stress fibers formation (Zhang and Li, 2020).

All DLCs are downregulated in most cancer cells and tumour tissues, but DLC1 is thought to be the most biologically relevant downregulated family member. The tumour inhibition mechanisms of the other members of the DLC family are still relatively unknown (Wang et al., 2016).

DLC1 has five isoforms; DLC1 isoform 1 and DLC1 isoform 2 are present at focal adhesions, DLC1 isoform 3 is present in the cytoplasm, and DLC1 isoform 4 is a presumed mitochondrial protein (Figure 1.9) (Ren and Li, 2021, Ko and Ping Yam, 2014). Most studies have focused on the widely distributed and predominant DLC1 isoform 2 (Bujko et al., 2016). Four of the isoforms are found in tumour cell lines, isoform 1 and 3 are silent in almost all immortalised and cancer cell lines and isoform 2 and 4 are frequently downregulated in a variety of carcinoma cell lines (Zhang and Li, 2020, Ko et al., 2010a). All DLC1 isoforms are expressed at different levels and have overlapping ubiquitous expression pattern in a panel of normal adult and fetal tissues (including heart, liver, kidney and brain) (Low et al., 2011). DLC1 isoform 1 and 2 were shown to suppress stress fiber formation and HCC cell growth, however DLC1 isoform 3 was not (Ko et al., 2010b). Different DLC1 isoforms may have different functional specialisation in cellular homeostasis and oncogenesis, however, this needs further exploration.

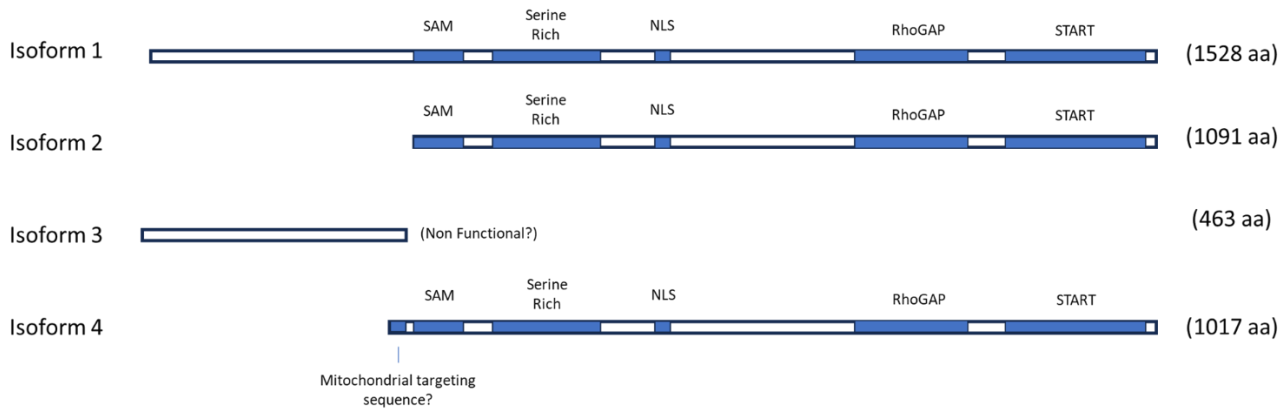

Figure 1.9: Isoforms of DLC1. There are 5 isoforms of DLC1, however only 4 are known in detail. While their structures are similar, they have different functions, both isoform 1 and 2 have tumour suppressor function while isoform 4 is a presumed mitochondrial protein. Most studies have focused on the widely distributed and predominant DLC1 isoform 2. (Low et al., 2011, Ren and Li, 2021, Ko et al., 2010b)

DLC1 is essential for embryonic development, and DLC1 -/- mice embryos are defective in the neural tube, brain, heart and placenta (Sabbir et al., 2010). DLC1 is associated with neural tube defects in eight NTD families and peripheral nervous system development (Lemay et al., 2019, Liu et al., 2017).

1.8.1 Epigenetic modification of DLC1

The dlc1 gene is mapped to chromosome 8p22-p21.3, a region that frequently undergoes deletion by either genomic deletion or epigenetic silencing mechanisms in several types of solid cancers (Durkin et al., 2007a, Guan et al., 2006a). Deletion of the short arm of chromosome 8, containing the dlc1 gene is a frequent event associated with cancer development (Xue et al., 2008, Matsuyama et al., 2001). Copy number loss contributed to the gene loss of DLC1 in lung adenocarcinoma, lung squamous cell carcinoma and HCC tissue and cell lines (Wang et al., 2016, Bao-Zhu Yuan, 1998).

Transcriptional silencing of DLC1 is primarily associated with DNA hypermethylation (Zhang and Li, 2020). DLC1 promoter methylations mostly occur in the CpG islands of the gene promoter regions, observed in lung, medulloblastoma, multiple myeloma, cutaneous melanoma, angiosarcoma, colorectal cancer, prostate cancer, gall bladder cancer, triple negative breast cancer, pancreatic ductal adenocarcinoma, extramammary Paget's disease tumours, acute leukaemia, non-Hodgkins lymphoma and nasopharyngeal, oesophageal and cervical carcinomas (Castro et al., 2010, Feng et al., 2013, Yin et al., 2002, Song et al., 2006, Sjoestroem et al., 2014, Ullmannova-Benson et al., 2009, Bujko et al., 2016, Sánchez-Martín et al., 2018, Peng et al., 2013,

Wu et al., 2011, Xue et al., 2013, Guan et al., 2006b, Singh et al., 2022, Zhou et al., 2020, Kang et al., 2012, Fu et al., 2014, Rahmani et al., 2018, Seng et al., 2007).

Histone deacetylation is another epigenetic mechanism of DLC1 loss in cancer cells. Histone deacetylation of the dlc1 promoter is partly responsible for the low levels of DLC1 in three prostate carcinoma cell lines, DLC1 is re-expressed when treated with a an histone deacetylase (HDAC) inhibitor, resulting in RhoA inactivation, apoptosis is induced and cell growth is inhibited (Zhou et al., 2012). Deletion of DLC1 was also observed in pancreatic carcinoma cell lines and patient samples, caused by DNA methylation and deacetylation (Guan et al., 2006b). Treatment of histone deacetylase inhibitor TSA and DNA methylation inhibitor 5-Aza-CdR significantly increased the expression of DLC1, cell growth inhibition and apoptosis induction compared to treatment with the inhibitors alone (Guo et al., 2014). Acetylation and deacetylation play important roles in the epigenetic modification of DLC1, however there are few studies on the acetylation and deacetylation of the DLC1 promoter, therefore more study is needed (Ren and Li, 2021).

Several microRNAs (miRNA) have demonstrated the ability to regulate DLC1, expression of miRNA is upregulated in cancer tissues and cell lines and they inhibit DLC1 expression (Ren and Li, 2021). For example, miR-106b targeted DLC1 promoting cell migration and invasion in colorectal cancer (Zhang et al., 2015, Liu et al., 2015, Liu et al., 2020). Similar results have been seen in other miRNAs, miR-141 and MiR-301a-3p with reintroduction of DLC1 decreasing growth rate and reversing the induced cell proliferation, migration, invasion and apoptosis inhibition in colorectal clinical tissues and cell lines (Wu et al., 2015, Zhang et al., 2019).

Additionally, three circRNAs (hsacirc-0083373, hsa-circ-0083374, and hsa-circ-0083375) were identified to regulate DLC1 by bioinformatic analysis, mediated via hsa-mir-511 the circRNAs are involved in the pathogenesis and development of breast cancer (Ma et al., 2020). Another circRNA, circZKSCAN1 (has-circ-0001727), promotes expression of DLC1 by targeting miR-873-5p and eventually blocks the proliferation, migration, and invasion of HCC cells (Li et al., 2021).

1.8.2 Post transcriptional modifications

Ubiquitin dependent proteosome degradation can also be responsible for the downregulation of DLC1 in lung adenocarcinoma and lung squamous cell carcinoma tissues (Kim et al., 2013). The altered activity of several phosphopeptides may be associated with low expression of DLC1 in oestrogen receptor positive breast cancer patients (Gökmen-Polar et al., 2018). In gastric cancer tissue, microsatellite instability may account for the significant downregulation of DLC1 (Verma et al., 2019).

DLC1 carries many potential phosphorylation sites within its serine-rich region and DLC1 is a target of protein kinase A (PKA), PKB/AKT, PKC and PKD (Figure 1.10) (Scholz et al., 2011, Ko et al., 2010a, Ko et al., 2013). Protein kinase B (AKT) phosphorylates three serines in DLC1 (S298, S329, and S567), which inhibits tumour inhibitory activity of DLC1 and the colocalization of DLC1 within focal adhesions (Tripathi et al., 2017). Activated PKC and PKD phosphorylate DLC1 on S327, S431 and S807 inhibiting cellular DLC1 GAP activity via binding to 14-3-3 (Scholz et al., 2011).

CDK5 can form a complex with DLC1 and phosphorylates four serine sites (Ser120, Ser205, Ser422 and Ser509) (Figure 1.10). This reduces the autoinhibitory binding of DLC1 causing activation of

DLC1 and coordination of FA localisation, RhoGAP activity and ability to other partners (Tripathi et al., 2014b). CDK5 regulates DLC1 by downregulating the binding of tensin and talin promoting cell migration (Tripathi et al., 2014a).

1.8.3 Structure

DLC1 interacts with its partners through conserved domains, a sterile alpha motif (SAM) domain, a GAP domain, a START domain and a serine-rich (SR) region (Figure 1.10). The SAM domain is involved in protein-protein interactions and also interacts with RNA and DNA (Lukasik et al., 2011, Qiao, 2005). The C-terminal part of DLC1 is occupied by a START domain, a conserved ~210 amino acid sequence forming a hydrophobic pocket that can bind lipids (Clark, 2012).

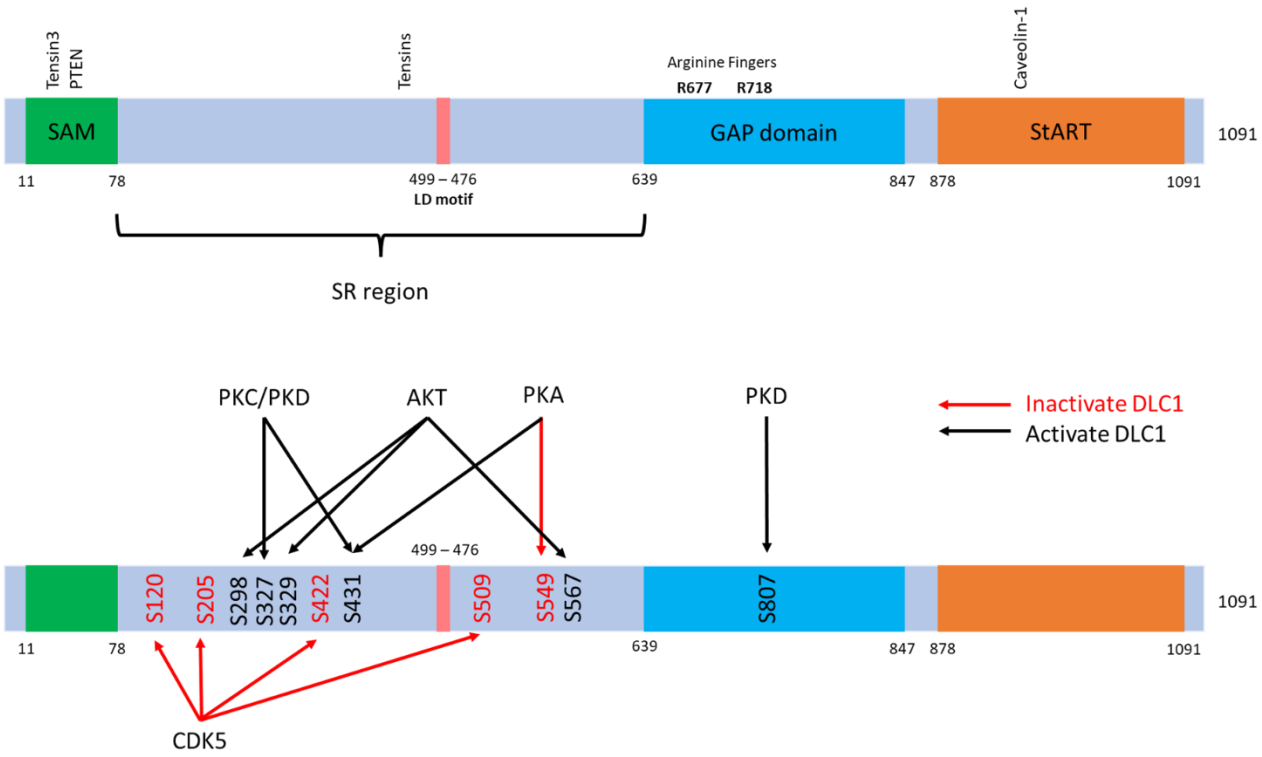

Figure 1.10: Domain structure of DLC1. Structural organisation of the different domains within the DLC1 gene and binding sites of partner proteins. DLC1 contains a sterile alpha motif (SAM), a focal adhesion targeting (FAT) domain, a polybasic region, a RhoGAP domain and a START domain. (Barras and Widmann, 2013). Also shown are the different phosphorylation sites by kinases (Scholz et al., 2011, Ko et al., 2013, Ko et al., 2010a, Tripathi et al., 2014b, Ren and Li, 2021)

The GAP domain is highly conserved between the three DLC family members and displays strong GAP activity for RhoA, weak activity for Cdc42, but no activity for Rac (Holeiter et al., 2012, Citi et al., 2014). Two arginine residues within the GAP domain, R677 and R718 are crucial for DLC1 GAP activity, most likely acting as arginine fingers (Du et al., 2012, Wang et al., 2020). The RhoGAP domain supresses RhoA activity and RhoA further mediates cell adhesion, shape, and migration by modulating the cytoskeleton networks and FA turnover (Zhang et al., 2016a, Khatibi et al., 2018).

Sandwiched between the SAM and RhoGAP domain is a long unstructured hinge region, rich in serine residues. This region determines focal adhesion localisation of DLC1 mainly through phosphorylation and interaction with other substances, so is referenced as the focal adhesion targeting (FAT) region (Durkin et al., 2007a, Liao et al., 2007). There is a LD-like motif, a 8-aa sequence which is essential for the binding of DLC1 to talin and focal adhesion kinase (FAK), regulating the tumour-suppressive activity of DLC1 and promoting DLC1 to contact with focal adhesions (Li et al., 2011). This relatively unstructured region is mainly responsible for co-localisation with proteins that interact with FAs, so can be referred to as focal adhesion targeting (Liao et al., 2007, Liao and Lo, 2008, Qian et al., 2007). Interaction partners have been identified for each region of DLC1 and each domain of DLC1 plays a different role in cancer suppression, supporting that each sequence plays an important role in DLC1's functions (Ren and Li, 2021).

1.8.4 The function and signalling pathways of DLC1

DLC1 mediates its tumour suppressive function through different signalling pathways which in turn affects biological processes such as proliferation, apoptosis and migration. The full tumour suppressor activity of DLC1 requires a functional GAP domain, however GAP independent mechanisms have also been linked to tumour cell phenotype, showing that the function of DLC1 in malignancy is complex (Durkin et al., 2007a, Wong et al., 2005, Kim et al., 2007, Healy et al., 2008, Qian et al., 2007, Yang et al., 2009).

1.8.4.1 Focal Adhesions

It is hypothesised that the tumour suppressor activity of DLC1 at focal adhesion sites is due to the presence of an LD motif contained within its structure (Li et al., 2011). This motif directs localisation to focal adhesions and allows co-localisation with several other proteins including integrin related proteins talin and tensin and also focal adhesions proteins FAK and paxillin (Qian et al., 2007, Liao and Lo, 2008, Li et al., 2011, Zacharchenko et al., 2016, Kaushik et al., 2014, van der Stoel et al., 2020). It is hypothesised that localisation of DLC1 to focal adhesions regulates cell migration, suggesting a tumour suppressor role of DLC1 (Li et al., 2011).

Localisation at the FA complex is required for full DLC1 activity. Mutants incapable of binding to FA's showed reduced ability to supress cell migration, anchorage independent growth *in vitro* and xenograft tumour formation *in vivo*, although the RhoGAP activity was comparable to WT DLC1 (Li et al., 2011). DLC1 negatively regulates paxillin dynamics in a GAP-independent but FAK-dependent manner and it has been proposed that DLC1 and FAK act in combination to ensure paxillin regulation (Kaushik et al., 2014).

Tensin is an important binding partner of DLC1, with reports of DLC1 interacting with all tensin family members (Yam et al., 2006, Qian et al., 2007, Liao et al., 2007, Cao et al., 2012). Binding of DLC1 to tensin is complex as it varies between isoforms, they generally bind in the linker region of DLC1 through the SH2 region of tensin (Qian et al., 2007, Liao et al., 2007, Yam et al., 2006). Mutational driven distribution of this binding prevents DLC1 FA localization and inhibits colony growth formation without negatively impacting its GAP activity (Liao et al., 2007).

Talin plays a key role in coupling integrin receptors to actomyosin contractile machinery, and is known to bind to DLC1. Talin binds to the LD motif of DLC1 forming a helix which binds to the four-helix bundle of talin's R8 domain (Zacharchenko et al., 2016). A R8 mutant favouring DLC1 binding, had a decreased pMLC-2/MLC-2 ratio compared to the WT talin, the R8 mutant was associated with downstream reductions in MLC-2 activation, force generation, and cell migration (Haining et al., 2018).

Cell matrix adhesions are hotspots for mechanotransduction, the cellular processes that translates mechanical tension or forces into a chemical or electrical signal, DLC1 has been linked with mechanotransduction proteins talin and vinculin (Rahikainen et al., 2017). In addition to mechanical force, cell-matrix adhesions transmit biochemical signals across the plasma membrane (Rahikainen et al., 2017).

Interactions between vinculin and talin are sensitive to mechanical loading, applying force to talin exposes vinculin binding sites (Rothenberg et al., 2018). In talin mediated focal adhesion activation, as force is applied to talin, vinculin binding sites become exposed allowing vinculin to bind (Carisey et al., 2013, Zacharchenko et al., 2016). Recently, it has been suggested that the force disrupts binding of DLC1, reducing its effect on RhoA activity, increasing the forces at growing adhesions (Haining et al., 2018). In early adhesions, DLC1 binds and regulates talin activity. As more force is applied in the maturing adhesions, vinculin's ability to bind increases which leads to more force generation, allowing adhesion maturity and recruitment of talin and vinculin (Haining et al., 2018, Rahikainen et al., 2017).

Although the specific molecular mechanisms of DLC1 function at the focal adhesions are unclear, it is certain that the localization of DLC1 at FA's is crucial for its tumor suppressor activity, indicating that DLC1 has a regulatory role within the focal adhesion complex.

1.8.4.2 Cell Migration

DLC1 inhibits migration by downregulating Rho signalling (Schaks et al., 2019). DLC1 uses its RhoGAP domain to inhibit Rho GTPases such as RhoA, RhoB, RhoC and Cdc42 causing downstream effectors such as ROCK to inhibit cell migration (Figure 1.11) (Barras and Widmann, 2013). DLC1 can also regulate migration through Rho effector protein Dia1 independent of Rho kinase activity (Holeiter et al., 2008).

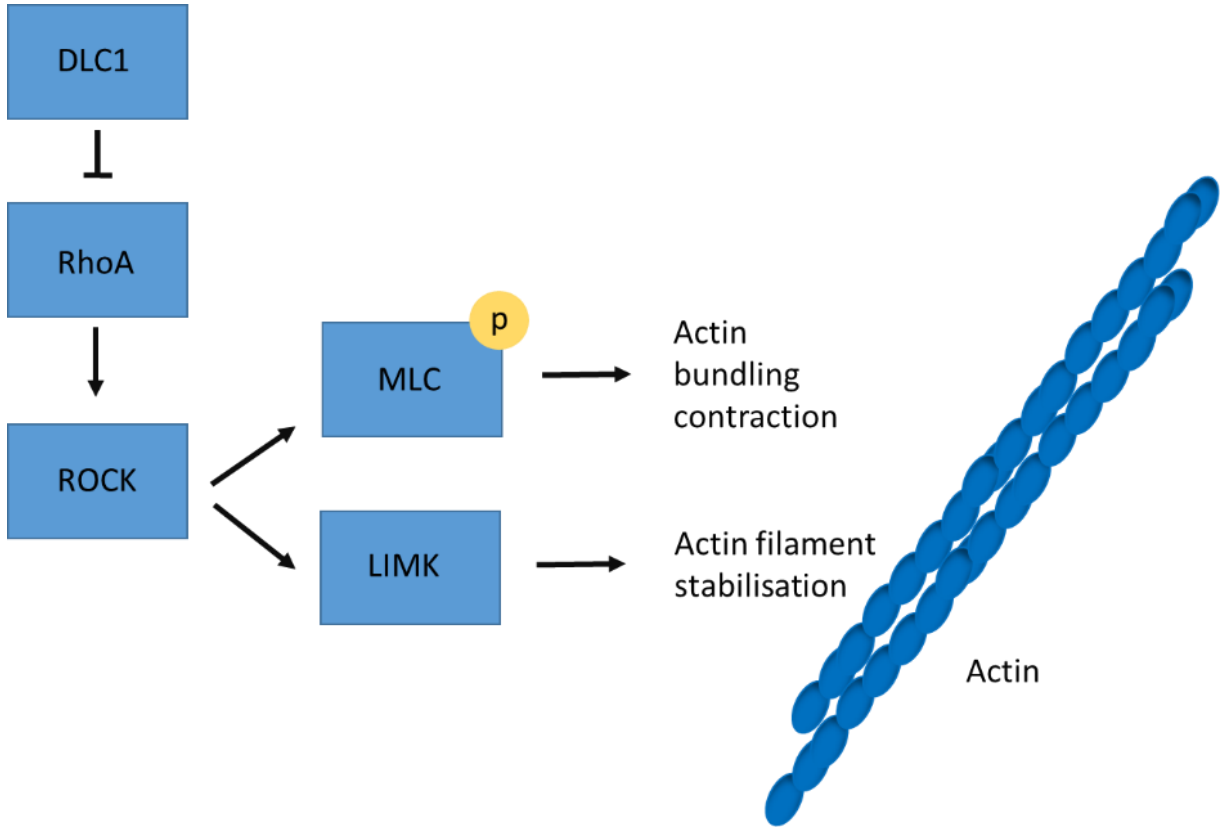

Figure 1.11: Effect of DLC1 on Rho signalling pathways. DLC1 negatively regulates RhoA which causes inhibition of ROCK and therefore limits actin dynamics (Barras and Widmann, 2013).

Re-expression of DLC1 inhibits the migration and invasion of tumour cells through the RhoA pathway in multiple myeloma cells, nasopharyngeal cancer cells, breast cancer cells and hepatocellular carcinoma cells (Ullmannova-Benson et al., 2009, Feng et al., 2013, Zhu et al., 2016, Yam et al., 2009). DLC1 regulates cancer cell migration through two main pathways, the DLC1/RhoA pathway and the Wnt/β- catenin pathway (Zhang et al., 2019). The Wnt/β- catenin pathway was observed in HCC cells where DLC1 decreased TCF4 expression, as well as β- catenin and TCF4 interaction and inactivated Wnt/β- catenin signal to supress migration and invasion (Wu et al., 2018).

In addition to the main signalling pathways, DLC1 is associated with a range of proteins which results in regulation of cell migration. For example, DLC1 interacts with CAV-1, FK506 binding protein 51 (FKBP51), EF1A1 and S100A1, which mediates RhoA and ROCK activation and therefore controls cell migration and invasion (Yang et al., 2017, Takaoka et al., 2017, Zhong et al., 2009, Yang et al., 2011).

1.8.4.3 Proliferation

DLC1 is frequently deficient in human cancer and re-expression of DLC1 inhibits cell proliferation in a range of cancer cell lines (Zhang et al., 2019, Zhou et al., 2004, Healy et al., 2008, Feng et al., 2013, Liu et al., 2012, Wang et al., 2014). Furthermore, DLC1 can affect proliferation through downstream signalling, modulating other pathways which results in reduced proliferation. For example, the overexpression of PRDM13 upregulates DLC1 and then inhibits proliferation and invasion of U87 cells (Zhang et al., 2018).

DLC1's ability to mediate proliferation has been linked to two different signaling pathways, the Wnt/β-catenin signaling pathway and the RhoA-ROCK-cofilin pathway (Wang et al., 2014, Kim et al., 2013). *In vivo*, DLC1 is a critical regulator of proliferation in endothelial cells of angiosarcoma, an endothelial cell-derived invasive malignancy (Sánchez-Martín et al., 2018).

1.8.4.4 Apoptosis

DLC1 has also demonstrated the ability to promote programmed cell death (apoptosis) in cancer cells. Apoptotic signaling protects the integrity of the genome, which can be manipulated during cancer, promoting tumorigenesis and making cancer cells resistant to treatment (Fulda, 2010).

Restoration of DLC1 expression results in caspase3-mediated apoptosis, and inhibits proliferation and invasiveness in Burkitt's lymphoma, renal cell carcinoma, prostate carcinoma, liver cancer, HT29, OVCAR-3, NPC and gallbladder cancer cells, as well as reduces the ability of tumour formation in athymic nude mice (Qin et al., 2014, Liu et al., 2012).

A further observation of DLC1 expression is that different localizations of DLC1 can have differing effects, DLC1 functions as an inhibitor of tumour cell proliferation and migration in the cytoplasm, but acts as an inducer of caspase3-dependent apoptosis in the nucleus (Yuan et al., 2007).

It can be concluded that DLC1 expression affects several pathways in combination, as adenovirus-mediated DLC1 transfer into cells inhibited cell proliferation and anchorage independent growth *in vitro* and induced apoptosis. It also induced cell cycle arrest, inhibited RhoA activation and formation of actin stress fibers in prostrate cancer (Guan et al., 2008).

1.8.4.5 DLC1 as a transcription target

DLC1 has been identified as a novel transcriptional target of the activated YAP/TAZ–TEAD complex. Yes-associated protein (YAP) and PDZ binding motif protein (TAZ) are co-transcriptional activators and are involved in several different mechanisms such as proliferation, cell plasticity, and metastasis (Zanconato et al., 2019). YAP and TAZ are induced in most human solid tumours and are instrumental for tumour initiation and progression in multiple tissue types, as shown in several experimental model systems (Zanconato et al., 2019, Zanconato et al., 2016, Wang et al., 2018). YAP and TAZ are activated by mechanical cues, such as ECM stiffness and shear stress. They are further regulated by RhoGTPase signalling and cytoskeletal contractility (Dupont, 2016, Dupont et al., 2011, Elosegui-Artola et al., 2017).

YAP/TAZ are important mechanotransducers that translocate to the nucleus upon cell–ECM adhesion-induced actomyosin tension (van der Stoel et al., 2020, Dupont et al., 2011). YAP/TAZ activation has been shown to control focal adhesions in various cell types and shown to provide feedback signals of YAP/TAZ activity limiting adhesion maturation (Nardone et al., 2017, Mason et al., 2019). DLC1 was found to be a direct transcriptional target of YAP/TAZ and involved in related YAP/TAZ-driven mechanotransduction processes, such as flow sensing, contact inhibition and the development of stiffness-related vascular disease (van der Stoel et al., 2020).

1.8.4.6 Association with other proteins

DLC1 has been linked to other biological functions which supports its tumour suppressor role. It has been linked to promotion of senescence in cancer cell lines and inhibition of autophagy in cell lines (Zhang and Li, 2020, Pluquet et al., 2015, Hampl et al., 2013, Ji et al., 2018).

Further observations provide evidence of DLC1's protective role such as suppressing S100A10 (a proinflammatory protein and cell surface receptor that promotes tumour cell invasion) in lung cancer, and interaction with Caveolin-1 (CAV-1) to inhibit migratory and tumorigenic phenotypes in NSCLC (Popescu and Goodison, 2014, Du et al., 2012). DLC1 has been implicated in several different pathways within cancer, however the most investigated are the role of DLC1 in cancer cell adhesions, migration and invasion (Zhang and Li, 2020).

1.8.5 DLC1 as a therapeutic target of Cancer

DLC1 is a crucial tumour suppressor gene and clinical data has confirmed that loss of DLC1 frequently occurs in tumour tissues. Restoration of DLC1 expression or function plays an essential role in inhibiting tumour growth, metastasis and tumour microenviroment (Ren and Li, 2021). Both *in vitro* and *in vivo* studies have shown DLC1 exerts its tumour suppressive role through RhoGAP dependent and independent mechanisms (Barras and Widmann, 2013). Many molecules can interact with DLC1 at the gene and protein levels to regulate its expression, activity, and localisation, suggesting that DLC1 could be a feasible therapeutic target. Targeting the interaction of DLC1 with binding partners may offer therapeutic and diagnostic strategies for cancer (Ren and Li, 2021).

Epigenetic drugs such as thymoquinone (TQ) and azacitidine (AZA)and some compounds such as flavone and resveratrol have reportedly restored the expression of DLC1 and shown some anticancer effects in several cancer lines (Zhang and Li, 2020, Ren and Li, 2021, Martín et al., 2020, Qadi et al., 2019). Targeting the RhoA pathway and Rho kinase could also offer promising options for therapeutic interventions of the DLC1 regulated pathway (Xue et al., 2008, Popescu

and Goodison, 2014, Lahoz and Hall, 2008). Several ROCK inhibitors are already available and have shown anti-metastatic activity in cancer cell lines and *in vivo* models (Lee et al., 2019). Another strategy could be to target prooncogenic pathways downregulated by DLC1, this could be effective for supressing metastatic cancer spread (Du et al., 2012).

DLC1 was found to be essentially required for TAT-RasGAP317–326, a peptide corresponding to the 317-326 sequence of p120 RasGAP coupled with a cell-permeable TAT-derived peptide that sensitizes the death response of various tumour cells to several anticancer treatments (Michod et al., 2004). Recent investigations show that this peptide can also hamper cell migration and invasion, and DLC1 was found to be essentially required to promote cell adhesion and inhibit migration (Barras et al., 2014). Combination strategies that couple therapeutics with manipulation of the DLC1 gene could provide a powerful application to tackle cancers.

DLC1 is negatively correlated with poor prognosis, susceptibility and recurrence in many cancers such as gall bladder cancer, urothelial carcinoma, endometrial cancer, lung adenocarcinoma cancer, breast cancer, ovarian cancer, colorectal cancer, pancreatic ductal adenocarcinoma, gastric cancer, hepatocellular cancer and penile carcinoma (Singh et al., 2022, Chen et al., 2013, Okayama et al., 2014, Sun et al., 2019, Gökmen-Polar et al., 2018, Ma et al., 2020, Zhou et al., 2020, Zhang et al., 2015, Xue et al., 2013, Su et al., 2015, Song et al., 2016, Busso-Lopes et al., 2015).

The expression of DLC1 is positively correlated with several survival indicators, such as mean survival, distance metastatic-free survival (DMFS), overall survival (OS), relapse-free survival (RFS), progression free survival (PFS) (Ren and Li, 2021). DLC1 is negatively associated with overall

survival and DMSF survival in patients with urothelial carcinoma, multivariate data showed that DLC1 expression was a significant independent predictor of DMSF, but not OS (Castro et al., 2010). The combination of loss of DLC1 and gain of GRHL2 is predictive of worse survival in estrogen receptor-positive breast cancer (Chi et al., 2019). DLC1 is also a negative biomarker for 5-year survival rates and OS in melanoma and pancreatic ductal adenocarcinoma (Xue et al., 2013, Sjoestroem et al., 2014). In addition, downregulated DLC1 was associated with poor survival in glioblastoma tumours (Czernicki et al., 2007).

Although evident that DLC1 is a metastatic suppressor, further investigation is needed into DLC1's molecular mechanisms to fully understand its potential as a therapeutic target. The added complexity of DLC1's involvement in different pathways and its dynamic range of binding partners can make it challenging to identify a clear role within cancer (Figure 1.12).

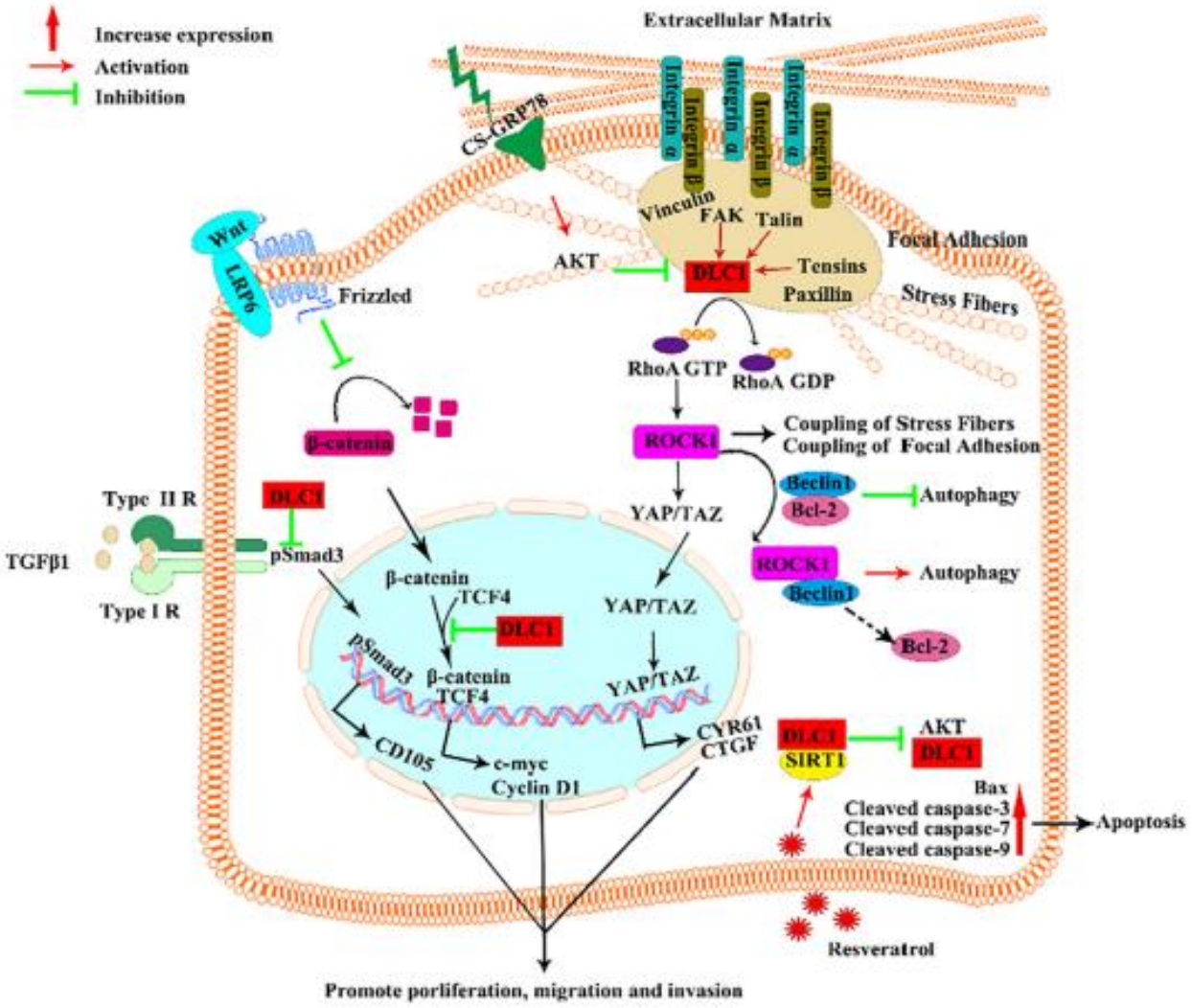

Figure 1.12 Schematic representation of DLC1 signalling pathways. The figure illustrates key signalling pathways which involve in the activators and inhibitors of DLC1, localization of DLC1, possible downstream effectors and induced effects (Ren and Li, 2021).

1.9 Project aims & objectives

The overall aim of this project was to investigate the role of DLC1 in focal adhesions, cell migration and invasion using live imaging. To help elucidate the role of DLC1, overexpression and silencing models were used. The first aim was to examine DLC1 and its binding partner talin using live focal adhesion dynamics.

The next aim was to observe how manipulating DLC1 level affects the migratory behaviour of cells in 2D cell migration and 3D invasion assays. Most of the previous DLC1 literature has focused on 2D migration or end point invasion assays, here live cell tracking of DLC1 in a 3D spheroid model was evaluated.

The final aims of this project were to use FRET sensors to study DLC1's effect on RhoA activity and also use novel FRET sensors to investigate how the different domains of DLC1 structure affect its activity.

Chapter 2 : Materials & Methods

2.1 Chemicals and reagents

All tissue culture reagents were purchased from Gibco. Chemicals were purchased from Sigma-Aldrich, unless stated otherwise.

2.2 Cell culture

2.2.1 Cell passaging

Cells were maintained in the medium displayed in Table 2.1. Cells were cultured in 75cm^2 tissue culture flasks (Corning) and passaged when they had reached approximately 80% confluence. The media was aspirated from the flask, washed with phosphate buffer saline (PBS) and the adhesion cells were detached by addition of 3ml of 1x Trypsin-EDTA (Sigma). The cells were incubated with trypsin at 37°C for 5 minutes. 9ml of growth media was added to the flask to stop the trypsin reaction. Cells were counted using a TC20 cell counter (BioRad). 1 x 10^6 cells were seeded into a new 75cm^2 flask. All cells were maintained at 37°C with 5% CO_2.

Table 2.1: Composition of medium for cell lines used.

Cell line	Culture Medium
U-87 MG	MEM supplemented with 10% FCS, 1% Pyruvate.
U-87 MG-H2BmRFP	
U-251 MG	
D566	
HeLa	MEM supplemented with 10% FCS, 1% non-essential amino acids.
HepG2	DMEM supplemented with10% FCS, 1% L-glutamine
HepG2-H2BmRFP	
MDA-MB-231	DMEM supplemented with 10% FCS

2.2.2 Transient transfection

U-87 MG and HeLa cells were transfected 24 hours prior to experimental use. HepG2 cells were transfected when plated for better transfection efficiency. Different transfection reagents were used for different cell lines as described in Table 2.2. All transfections were performed using manufacturer's guidelines. For co-transfections plasmid DNA was transfected in equal amounts. Details of the plasmids used in transient transfections are below (Table 2.3).

Table 2.2: Details of transfection agents for each cell line

Cell Type	Transfection Reagent	Manufacturer	Recommended ratio (Reagent: DNA)	Quantity DNA / 8.8cm^2 dish (µg)
U-87 MG	Viromer	ORIGENE	0.4:1	1
HeLa	Fugene6 HD	Promega	2:1	1
HepG2	Lipofectamine 3000	Invitrogen	3:1	1

Table 2.3: Plasmids used in transfections

Plasmid	
GFP-DLC1	Sequence in appendix
GFP-Talin	
mRuby-DLC1 (Cloned using GFP-DLC1 as a template)	

2.2.3 siRNA transfection

For silencing of DLC1, stealth siRNA's were purchased from Invitrogen (Set of 3) HSS173600, HSS173601, HSS173602). The set of siRNA's were mixed together in a 1:1:1 ratio. These were then transfected into cells according to the lipofectamine 3000 siRNA protocol.

2.3 Western Blotting

2.3.1 Sample extraction and preparation

Cells were seeded in 6cm tissue culture dishes. Samples were transfected with GFP-DLC1 24 hours before lysis. After incubation cells were washed with PBS before addition of 150µl lysis buffer (50mM Tris-HCL pH 7.5, 1mM EDTA, 1mM EGTA, 0.5 mM Na_3VO_4, 1% Triton X-100, 50mM Sodium Fluoride, 5mM Sodium Pyrophosphate, 10mM Sodium β-glycerophosphate, 0.1mM PMSF, 1 in 100 Protease Cocktail inhibitor (Sigma). Cells were collected using a cell scraper and frozen at -20°C. Lysates were thawed at 4°C, centrifuged for 15 minutes at 15000xg and the supernatant collected in a 1.5ml Eppendorf. The protein was quantified using Pierce BCA Protein Assay Kit (ThermoFisher Scientific) according to the manufacture's instruction. Samples were mixed with 5x Laemmli buffer (250mM Tris HCL pH 6.8, 10% SDS, 30% Glycerol, 5% β-mercaptoethanol, 0.02% Bromophenol blue) and boiled at 95°C for 5 minutes.

2.3.2 SDS-PAGE

30µg of protein was loaded onto 10% acrylamide gels (see Table 2.4). 6µl of Precision Plus Protein All Blue Standards ladder (Bio-Rad) was also loaded onto the gel. The electrophoresis was at 200V for 40 minutes in running buffer (25mM Tris base, 192mM Glycine, 1% SDS).

Table 2.4: Composition of Acrylamide Gels

Acrylamide Gels	Reagents and concentration
4% Stacking gel	0.4M Tris base pH 6.8, 0.1% SDS, 4% acrylamide, 0.65ng/µl APS and 0.325% TEMED
7.5% Running Gel	0.4M Tris base pH 8.8, 0.1% SDS, 7.5% acrylamide, 0.25ng/µl APS and 0.125% TEMED

2.3.3 Protein transfer and detection

The polypeptides were transferred onto nitrocellulose membranes (0.2µm, Bio-Rad) at 4°C for 1.5 hours (300mA) in transfer buffer (25mM Tris base, 192mM glycine, 20% ethanol). Membranes were blocked in 5% milk powder for 1 hour and then washed in TBST (20mM Tris, 140mM NaCl, adjusted to pH 7.6, 0.1% Tween-20). Membranes were incubated overnight in primary antibodies diluted in 5% (Table 2.5). Membranes were then washed 3 times in TBST and incubated in secondary antibody for 1 hour at room temperature (Table 2.5). After incubation with secondary antibody membranes were washed 3 times in TBST and immunoreactivity was

visualised using Amersham ECL western blotting detection kit (GE Healthcare). Membranes were incubated with 1ml for 2 minutes before development using a Syngene gel imaging G-Box. Images were collected using GeneSnap image acquisition software.

Table 2.5: Antibodies used for western blot

Antibody	Dilution	Species	Source	Cat. No
DLC1	1:200	Mouse	BD Biosciences	612020
Beta-Actin	1:5000	Mouse	Abcam	ab8226
Anti-mouse HRP	1:5000	Sheep	Abcam	ab6808

2.4 Cloning techniques

2.4.1 Plasmids

A plasmid encoding full length pEGFP-DLC1 (a gift from I. Baruskov) was used as a PCR template to produce an N-terminal construct (Ruby-DLC1).

2.4.2 Plasmid amplification

2.4.2.1 Transformation

50µl of competent DH5α competent bacteria were added to round bottomed tubes (prechilled on ice). 1µg/µl of PEGFP-DLC1 construct was added to the DH5α bacteria and incubated on ice for 30 minutes. The mixture was then heat shocked at 42°C for 45 seconds before being incubated on ice for a further 2 minutes. 450µl of SOC medium was then added to the transformation

mixture before incubation in in the shaking incubator at 37°C 225rpm for 1hour. 100µl transformation mixture was plated on pre-warmed kanamycin plates (50µg/mL^{-1}) and left to grow overnight in a 37°C incubator**.**

2.4.2.2 Miniprep

Under aseptic technique, a single colony was picked from the incubated agar plate and added to 5ml LB broth containing 50µg/mL^{-1} kanamycin antibiotic. The mini-culture was incubated at 37°C 225rpm for 6-8 hours. The plasmid was then purified from 2mL of the mini-culture using the GeneJET Plasmid Miniprep Kit and protocol (Thermo Scientific, Ma, USA).

2.4.2.3 Maxiprep

Under aseptic technique, 2mL of culture (Section 2.4.2.2) was inserted into a 200ml maxi-culture containing 50µg/mL^{-1} kanamycin antibiotic. The maxi-culture was incubated at 37°C 225rpm overnight. Cells were harvested using a Sorvall centrifuge, they were centrifuged at 4 °C, 6800 × g for 1 hour. Plasmids were then purified using Purelink TM HiPure Plasmid Filter Purification Kit using the associated protocol (Invitrogen, CA, USA). The purified plasmid DNA was diluted to 1 µg/µL^{-1}.

2.4.3 Polymerase Chain Reaction (PCR)

PCR was used to amplify the PEGFP-DLC1 gene and the vectors for cloning of the N-terminal constructs. KOD Hot Start DNA polymerase (Novagen, Germany) was used in combination with the components seen in Table 2.6, using the primers in Table 2.7. All products were amplified in a Px2 Thermal Cycler (Thermo Scientific, MA, USA). PCR programme is described in Table 2.8.

Table 2.6: PCR set up for amplification of N- and C- terminal DLC1/Ruby constructs

Component	Amount
$MgS0_4$	3µl
2mM dNTPs	5µl
10x PCR Buffer	5µl
10µM Forward Primer	1.5µl
10µM Reverse Primer	1.5µl
Template DNA	20ng
KOD Hot Start Polymerase	1µl
DdH_20	Up to final volume of 50µl

Table 2.7: Primers used for Plasmid Cloning

Plasmid	**Primer**	**Sequence 5" to 3"**
pG-mRuby-DLC1	Forward	TACAAGAGATCTCGAGATGTGCAGAAAGAAGCCGGA
pG-mRuby-DLC1	Reverse	GCAGAATTCTCGAAGCTTTCACCTAGATTTGGTGTCTTTGG

Table 2.8: PCR programme for amplification of N- and C- terminal DLC1/Ruby constructs

Stage	Temp	Time	Cycles
1	94°C	5 min	x 1
2	94°C	20 seconds	x 30
	65°C	3 min	
	72°C	3 min	
3	72°C	10 min	x 1

2.4.4 In-Fusion Cloning

The DLC1 gene was inserted into the destination vector (the plasmid backbone containing mRuby), using the Clonetech Infusion HD cloning kit (Clontech, Canada). First, the destination vector was cleaved using Xho1 and HindIII restriction enzymes. The PCR product and the cleaved vector were separated on a 1% agarose gel at 100V for 1 hour before the PCR/vector bands were cut from the gel. The DNA from the bands was purified using the E.Z.N.A. gel extraction kit and accompanying protocol (Omega Biotek, GA, USA). The DLC1 gene was then inserted into the appropriate vector using the Clontech infusion reaction protocol (Figure 2.1, Table 2.9). For the reaction, the concentration of the vector and PCR end product was measured on the nanodrop before using the In-Fusion® Molar Ratio Calculator to calculate the amounts needed in the reaction (http://bioinfo.clontech.com/infusion/molarRatio.do; insert: vector ratio = 2). The total volume of the infusion reaction was 10 µL, with 2 µL of 5X In-Fusion HD Enzyme included. The

infusion reaction was incubated at 50°C for 15 minutes. 1uL of Proteinase K (Invitrogen, CA, USA) was added to the infusion reaction followed by incubation for 10 minutes at 37°C to improve transfection efficiency. The reaction mixture was then transformed into Stellar competent cells (Clontech, Canada) using the same protocol as before. After transformation a miniprep was performed to purify DNA. The products were analysed using restriction digests and transfection before being sequenced (GATC, Germany).

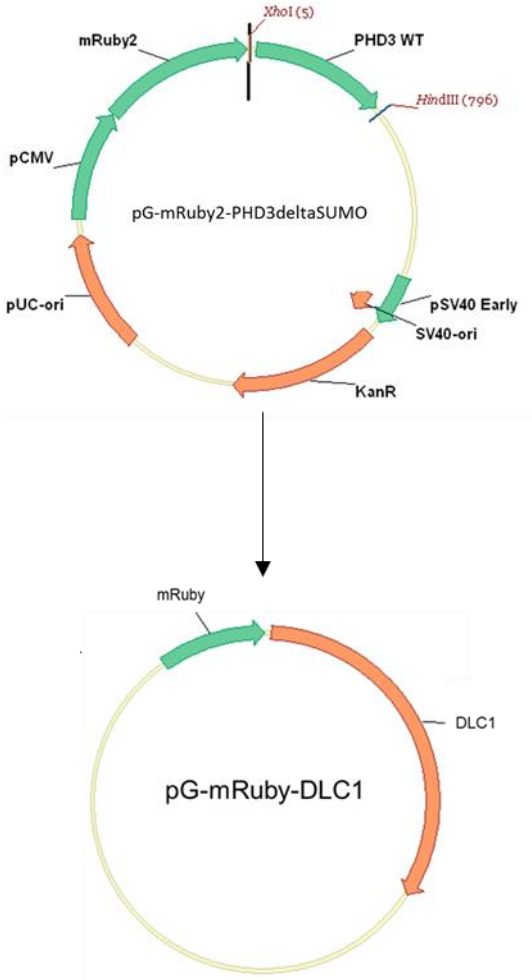

Figure 2.1: Cloning Strategy for mRuby2-DLC1 construct. The HAF gene was cut out of the pG-mRuby2-PHDdeltaSUMO plasmid using Xho1 and HindIII restriction sites, the amplified DLC1 gene was then inserted into this plasmid by infusion cloning to produce pG-mRuby-DLC1 (N-terminal construct).

Table 2.9: Components used to create DLC1/mRuby N- and C-terminal constructs using Infusion cloning

Plasmid	Destination Vector	Restriction Enzymes	Insert	Insert amplified from
pG-mRuby-DLC1	pG-mRuby2-PHD3deltaSUMO	Xho1 and HindIII	DLC1	pEGFP-DLC1

2.5 Stable cell line generation

For 2D cell migration and 3D cell invasion assays U-87 MG and HepG2 histone H2B monomeric red fluorescent protein (H2BmRFP) stable cell lines were produced for easy tracking during analysis. Cells were transduced in a lentiviral transduction method which inserted the pHIV-H2BmRFP plasmid (addgene plasmid number #18982). This plasmid includes the eukaryotic translation elongation factor 1 α (EF1α) promoter for reporter expression.

HEK293T cells were seeded at a density of $1.5x10^6$ in twelve 10cm cell culture dishes and incubated overnight at 37°C. Cells were transfected with the lentiviral reagent, made up in a 4:2:1 ratio of vector:packaging:envelope. The plasmids were then transfected in polyethylenimine (PEI) at a ratio of 2:1 PEI:DNA in serum-free DMEM and incubated at 37°C for 16 hours. The medium was then changed on all dishes. 72 hours after transfection, the condition medium was collected, centrifuged at 1000xg for 5 minutes and filtered through a 0.45µM PES filter. The medium was transferred to ultracentrifugation tubes and a 20% sucrose cushion was also added.

Ultracentrifugation was performed at 4°C for 2 hours at 21000 rpm and viral particles were resuspended in 600µl PBS. For transduction in cells, $1.4x10^5$ HepG2 and U-87 MG cells were seeded into a T25 flask and all 600µl of concentrated virus was applied and a medium change performed after 72 hours.

2.6 Immunostaining

HeLa and HepG2 cells were seeded into 3cm glass bottom dishes (Greiner) and incubated for 24 hours. For U-87 MG glass dishes were coated with poly-l-lysine. 1ml of 100 µg/ml Poly-Lysine (Sigma) was added to 3cm glass bottom dishes (Greiner) and left to incubate for 15 minutes. The dishes were rinsed with sterile H_20 and left to dry overnight with the lid slightly loose in a sterile dish within a 37°C 5% CO_2 incubator. U-87 MG cells were then seeded into the dish and incubated for 24 hours. For overexpression experiments, samples were transfected 24 hours before fixing. After incubation cells were washed three times with PBS. Cells were then fixed with 4% Paraformaldehyde (in PBS) for 10 minutes at room temperature and then rinsed three times with PBS after fixation. Cells were blocked with blocking buffer for 1 hour (1% BSA, 0.1% Triton X-100, and 0.4% Tween 20 in PBS). Cells were incubated overnight in primary antibody (see Table 2.10). After overnight incubation plates were washed with blocking buffer three times and incubated in secondary antibody for 1 hour (see Table 2.10). Dishes were washed with PBS 3 times before addition of 1:1000 DAPI. After a 15 minute incubation, the dish was washed 3 more times before imaging.

Table 2.10: Antibodies used for Immunostaining

	Antibody	Dilution	Species	Source	Cat. No
Primary	DLC1	1:500	Mouse	BD Biosciences	612020
	Paxillin	1:500	Mouse	BD Biosciences	610619
	Talin	1:500	Mouse	Sigma Aldrich	T3287
Secondary	Anti-mouse Alexa 488	1:1000	Goat	Thermofisher	11001

The glass dishes were imaged in ICC blocking buffer using confocal and Total Internal Reflection Fluorescence (TIRF) microscopy described in section 2.10.2.

2.7 Cell migration assays

2.7.1 Cell migration assay

For overexpression, 15,000 U-87 MG cells were seeded into a 4 well plate (Greiner). Samples were transfected 24 hours prior to imaging. Cells were imaged for 48 hours with an epifluorescent microscope (Axio ObserverZ1: Zeiss) equipped with an AndoriXon 897 Ultra camera for fast image acquisition. Time-lapse videos were taken with a 10x objective and acquired every 3 minutes using appropriate optics for transmitted light, GFP (Zeiss Filter set 38HE) and mCherry (Zeiss Filter set 43HE). During the time series samples were incubated at 37°C with 5% CO_2. The cell tracks were then analysed using Fiji Trackmate software.

2.7.2 3D circular assay

A 2 well culture insert (Ibidi) was inserted into a 3cm imaging dish and 600 000 of either HepG2-H2BmRFP or U-87 MG-H2BmRFP cells were seeded around the outside of the insert. For overexpression cells were transfected 24 hours after seeding. For knockdown experiments HepG2 cells were transfected with siRNA as they were seeded. 48 hours later the insert was removed and a mixture of Matrigel:medium:HEPES was added onto the top the cells (50:50:10 ratio). This was left to set at 37°C for 2 hours. Fresh medium was gently added on top before imaging. Cells were imaged for 24 hours with an epifluorescent microscope (Axio ObserverZ1: Zeiss) equipped with an AndoriXon 897 Ultra camera for fast image acquisition. Time-lapse videos were taken at multiple positions with a 10x objective and acquired every 3 minutes using appropriate optics for transmitted light, GFP (Zeiss Filter set 38HE) and mCherry (Zeiss Filter set

43HE). During the time series samples were incubated at 37°C with 5% CO_2. The cell tracks were then analysed using Fiji Trackmate software.

2.7.3 Cell migration track analysis

Cell migration tracks were tracked using ImageJ TrackMate plug in. The software applies automated single-particle tracking and applies a tracking algorithm LoG detector, the best detector for Gaussian-like particles in the presence of noise. Spots were identified with a 25µm diameter and threshold of 4. Cells were tracked using the simple LAP tracker. The linking max distance and gap-closing max distance were set to 25 and the gap-closing max frame was set to 2. A filter was applied to remove tracks with spots less than 20 to exclude any background noise of spot detection. For co-transfections TrackMate Extras were used and an additional spot filter of GFP mean intensity was selected to ensure that only cells that were co-transfected were included in the tracking. Track information was exported which provided mean track speed and length. To calculate track displacement and straightness, the TrackMate TrackLength-and-Straightness R script was used, which was provided by Dr Marie Held at the CCI Liverpool. The R script calculated the Track Displacement, total Track Length and Track Straightness from TrackMate data.

2.7.4 Mean square displacement

For further mean square displacement analysis, TrackMate trajectories were exported to MATLAB and analysed using the class @msdanalyzer (https://tinevez.github.io/msdanalyzer/) (Tarantino et al., 2014). This allowed the diffusion co-efficient to be calculated for the MSD measurement.

2.8 Spheroid culture

Spheroids were formed by seeding $1x10^7$ U-87 MG-H2BmRFP cells into a 5D Spherical Plate (Kugelmeiers). Cells were maintained at 37°C with 5% CO_2 and harvested after 24 hours. For overexpressed samples cells were transfected when plated.

2.8.1 Spheroid mounting

Table 2.11 Spheroid mounting media

Mounting Media	Composition
Standard mounting media	50% ice cold Matrigel (Corning), 50% Medium and 25mM Hepes
FITC-Dextran mounting media	1:1000 5mg/ml FITC-Dextran () dissolved in 50% medium and 25mM Hepes before mixing with 50% ice cold Matrigel (Corning).

Harvested spheroids were placed into a 35mm tissue culture dish, the media was aspirated and 50µl of the specific mounting media was pipetted on top of the spheroids (see Table 2.11). A P10 pipette was used to suck the spheroid and mounting media up into a fluorinated ethylene

propylene (FEP) tube (S 1815-04, BOLA, Germany). The end was sealed using parafilm. The FEP tube was then inserted into a glass capillary (inner diameter 1.5mm) ready for mounting on the Lightsheet microscope.

2.8.2 Spheroid imaging

The glass capillary was then inserted into the lightsheet holder and mounted into the Lightsheet Z.1 (Zeiss) sample chamber. The sample was immersed in water and maintained at 37°C with 5% CO_2.

2.8.3 FITC-Dextran imaging

For the FITC-dextran imaging spheriods were mounted and imaged at time 0. They were then imaged at 24 and 48 hour time points.

2.8.4 Invasion assay

After mounting Spheriods were left for approximately 3 hours to settle before time-lapse imaging. Spheriods were illuminated with 561nm and 488nm laser line and imaged using a 20x W Plan-Apochromat objective every 3 minutes with a z-step of 5µm for 320 cycles, 16 hours. Lightsheet Z.1 Zen software (Zeiss) was used to aquire images using online dual side fusion with pivot scan. Images were detected using a pco.edge scientific complementary metal-oxide-semiconductor (sCMOS) camera.

2.8.5 Spheroid tracking analysis

IMARIS v9.6 software (Oxford Instruments) was used to visualise, process and track the spheroids. First a reference frame was placed in the centre of the spheroid, mainly to correct for

sample drift. As the sample drifted over time, the reference frame was repositioned manually to follow the drift. This was then used to counteract the movement of the sample on the tracking measurements.

To track each cell, the IMARIS feature 'spots' was used, this segments out cells using the fluorescence channel of interest. The spots were identified as 10µm diameter in the RFP channel. Cells were tracked using the 'Autogressive Motion' option with the following parameters: max gap of 0 and max distance of 10µM. A basic quality filter was applied to the spots to filter out any with low intensity. Once the tracks had been calculated, any tracks less than 1 hour were filtered out.

In the cases of transfected cells, the tracks were then filtered on intensity to separate out control and GFP-DLC1 cells. For control cells, a filter was applied to just select RFP cells. For GFP-DLC1 cells a filter was applied to select cells with high GFP intensity. Track mean speed, track displacement length, track straightness and mean square displacement were all calculated for each spheroid.

For analysis of inner and outer spots, the reference frame was used as a point of origin, which could then be used to classify spots close to this (inner) and spots further away (outer) using the distance from origin parameter. This value slightly differed as the reference frame was placed manually so, therefore, was variable between spheroids (Table 2.12). Each spheroid was checked by eye to ensure that the inside and outside areas were similar across all spheroids.

Table 2.12 Range for IMARIS 'Distance from Origin' filter

Condition	Distance from Origin, Reference Frame (µm)
U-87 MG GFP-DLC1 spheroid	64.3-81.3
U-87 MG H2B-RFP control spheroid	48.1-66.8
HepG2-H2B RFP control spheroid	54.9-85
HepG2 siRNA scrambled control	51.2-59.7
HepG2 siRNA DLC1	44-65

2.9 Focal adhesion dynamics

2.9.1 Cell seeding

100,000 HeLa and 150,000 U-87 MG cells were seeded into 3cm dishes (Greiner). After 24 hours of incubation cells were transfected with mRuby DLC1, GFP-Talin or both. 24 hours after transfection dishes were imaged using the TIRF microscopy as described below. Cells were imaged every minute for 3 hours. For siRNA experiments, cells were pre-transfected as described in 2.2.3.

2.9.2 Immunostaining

siRNA DLC1 treated HepG2 cells were grown on fibronectin coated coverslips and fixed with 4% PFA (in PBS) after 24 hours. Cells were permeabilised with 0.3% Triton X-100 for 15 minutes and incubated with 10% blocking buffer for 60 minutes. Primary antibodies in 1% blocking buffer (1% BSA, 0.1% Triton X-100, and 0.4% Tween 20 in PBS)were added for 1-2 hours, followed by 3 washes in 1x PBS. Cells were incubated with secondary antibody diluted in 1% blocking buffer for 1-2 hours. Coverslips were washed 3 times with 1 x PBS and mounted onto glass slides. Images were acquired on a Marianas spinning disk confocal microscope (3i) using a 63x 1.4NA on FLASH4 Scmos (Hamamatsu) camera. Experiments were performed by Dr. Lorna Young (Zech Lab).

Table 2.13: Antibodies used for focal adhesion specific immunostaining

	Antibody	Dilution	Species	Source	Cat. No
Primary	VASP	1:100	Rabbit	Cell signalling	3131
	Actin phalloidin 670	1:500	N/A	Cytoskeleton, inc	PHDN1-A
	Tubulin	1:200	Mouse	Sigma	T5168
Secondary	Anti-rabbit Alexa 488	1:500	Goat	Thermofisher	11008

Focal adhesions were analysed using a custom script Dr Tom Waring at the CCI Liverpool.

2.9.3 Focal adhesion dynamics image analysis

Microscope files were uploaded to the Focal Adhesion Analysis Server (FAAS) (Berginski and Gomez, 2013). Focal adhesions were identified by segmentation and tracked over time frames. The time between frames was entered into the server and all the standard parameters were used. The server than supplies an output with different focal adhesion measurements such as assembly, disassembly and focal adhesion area. For assembly and disassembly rates of the focal adhesion, the platform quantifies the normalised intensity of each adhesion over its lifespan and uses a log-linear assembly and disassembly phase, fit to a log-linear model, generating rates of assembly and disassembly.

Only single channel data can be uploaded to the server, therefore single channel data could be uploaded un-manipulated. Data with two channels needed to be converted to single channel data. The original two channel data was initially saved as a TIFF file using ImageJ software. This data was then manipulated into one channel by creating a maximum intensity projection (MIP). The MIP was created by using image properties to change two channels into 2 slices and then these slices were combined using Z projection (max setting). The maximum intensity projection was then uploaded to the FAAS server and the outputs were produced. A MATLAB script designed by D.Mason, image analysis at the University of Liverpool, Centre for Cell Imaging was then used to combine the intensities of the original channel data and the tracking data from the FAAS. Therefore, the adhesion kinetics of assembly and disassembly could be calculated for the two-channel data.

2.10 Imaging

2.10.1 Spinning disk confocal microscopy

U-87 MG and HeLa cells were seeded into glass bottom 30mm imaging dishes. Overexpressed samples were transfected 24 hours before fixing. Dishes were imaged using a 63x Alpha Plan-Apo oil immersion objective lens (NA = 1.46) on Andor Dragonfly spinning disk confocal. The sample was illuminated with the 488nm and 561nm laser line and transmitted light was detected.

2.10.2 TIRF microscopy

Total Internal Reflection Fluorescence Microscopy was performed on a Andor Dragonfly spinning disk confocal using a 63x Alpha Plan-Apo oil immersion objective lens (NA=1.46). Samples were illuminated with 488nm and 561nm laser lines and the TIRF depth was adjusted to 116nm until TIR illumination was achieved. The system was controlled and images were acquired through Fusion software (Andor, Oxford, UK). For time lapse experiments cells were imaged every 3 minutes for 3 hours.

2.10.3 RhoA FRET experiments

U-87 MG and HepG2 cells were plated into 3cm dishes at a confluent density. Cells were transfected with WT, negative control or positive control RhoA FRET sensor plasmids as described in Table 2.12. Cells were transfected with Lipofectamine 3000 according to manufacturers instructions. After 24 hours cells were imaged in OPTI-MEM media. For overexpression experiments, U-87 MG cells were transfected with GFP-DLC1 as previously described with co-transfection of RhoA sensor. For siRNA DLC1 silencing experiments, HepG2 cells were transfected

with siRNA DLC1/siRNA scrambled control as previously described, 24 hours prior to transfection of RhoA sensor.

Table 2.14 RhoA Fret sensor plasmids

Plasmid	Addgene plasmid number
pTriEx-RhoA FLARE.sc Biosensor WT	#12150
pTriEx-RhoA FLARE.sc Biosensor T19N	#12152
pTriEx-RhoA FLARE.sc Biosensor Q63L	#12151

2.10.4 RhoA FRET imaging and analysis

Images were acquired using the Zeiss 880 with a 40X 1.3NA detection objective. Experimental designer was used to create 3 different blocks for imaging. For block 1, channels were created for CFP, YFP and FRET, with FRET being excited with CFP (458 nm) and emission in the donor range (YFP). The range for emission for the different channels was taken from the (Pertz et al., 2006) paper to minimize cross talk. Block 2 was used to bleach the cells, with the bleaching protocol of 100 iterations embedded in a timelapse of the 512 nm laser line at 100% in a ROI (square 20x20). Finally block 3 reimaged the CFP channel only, as set up in block 1.

To ensure FRET was occurring, normalisation curves were produced. Each timepoint was normalised to the prebleached average (first 10 acquired pre-bleaching images). The YFP/CFP ratio was calculated for each condition.

2.10.5 DLC1 FRET

2.10.5.1 Cell seeding, transfection and imaging

HepG2 cells were plated into ibidi 8 chamber u-slides at a confluent density. Cells were transfected with the different FRET constructs shown in Table 2.13, (Full DLC1 sensor, mTFP DLC1 alone sensor, Venus DLC1 sensor, GAP-deficient or SAM-deficient FRET sensor plasmids) Cells were transfected with Lipofectamine 3000 according to manufacturers instructions. After 24 hours cells were imaged in OPTI-MEM media. Images were acquired as previously described in section 2.10.4.

Table 2.15 DLC1 FRET sensor plasmids

Plasmid	Details
TFP DLC1 1 - 846 Venus	Full DLC1 protein
TFP DLC1 1-846	mTFP fluorophore only control
DLC1 1-846 Venus	Venus fluorophore only control
TFP DLC1 80 - 846 Venus	SAM-deficient protein
TFP DLC1 1-550 Venus	GAP-deficient protein

2.10.5.2 Image analysis

Images were analysed using ImageJ plug in PixFRET, the TFP DLC1 1-846 was used a donor bleed through control to calculate crosstalk. The background was calculated for each individual image before FRET calculation. Normalized FRET index was calculated (FRET/Acceptor).

2.11 Statistics

All statistics were calculated using Prism Graphpad software. For comparison between two conditions, a two-tailed t-test was performed. For experiments with more than two conditions, a one-way ANOVA test was used. Statistical tests are stated in figure legends.

Chapter 3 : Characterisation of DLC1

A meta-analysis of DLC1 expression has shown that it is usually reduced in late-stage metastatic cancers, and when DLC1 is re-introduced, can induce apoptosis and inhibit cell growth, migration and invasion (Wang et al., 2016). Introduction of DLC1 in *in vitro* cancer cells and *in vivo* models, where it is typically absent, such as breast, lung, ovarian and HHC cancer, has shown to inhibit cell migration and invasion, however, the mechanistic basis for DLC1's tumour suppressive properties is currently not known. (Yuan et al., 2003a, Yuan et al., 2004, Durkin et al., 2007a, Zhang et al., 2005, Wong et al., 2005).

The quest to find the functional basis for DLC1's frequent inactivation in cancer led to investigation of DLC1 in focal adhesions. The interaction of DLC1 and talin was first reported in 2011, with the discovery that talin could bind to the LD motif of DLC1, and this could impact its tumor suppressor activity by reducing the DLC1-mediated inhibition of colony growth and cell migration (Li et al., 2011). Further investigation revealed that the DLC 1 interaction was through the four-helix bundle of talins R8 domain and a helix of the LD motif of DLC1 (Zacharchenko et al., 2016). However, although it is clear that DLC1 and talin interaction is important in focal adhesion biology, it is unknown how the interaction of these two proteins affects focal adhesion dynamics.

3.1 Aims

The aim of this chapter is to investigate the role of DLC1 in focal adhesions. The first objective was to generate molecular tools to enable DLC1 visualisation. The next objective was to determine the levels of endogenous DLC1 expression in a range of cancer cell lines and to validate the exogenously expressed fluorescent construct. Following this, the aim was to visualise DLC1 localisation using TIRF microscopy. The final objective of the chapter was to assess the role of DLC1 in focal adhesion dynamics and to investigate the relationship between DLC1 and binding partner talin on focal adhesion dynamics.

3.2 Results

3.2.1 Endogenous levels of DLC1

The first objective was to determine the level of endogenous DLC1 across a range of cell types. DLC1 is reported as lost in different cancers, yet this might not be true in the cell lines generated from the tumours. A selection of metastatic and invasive cell lines was probed, with a focus on brain tumours, (glioblastoma: U-87 MG, U-251 MG and D566), cervical (HeLa), breast (MDA-MB231) and liver (HepG2). Loss of DLC1 is associated with poor prognosis in the highly invasive cancer glioblastoma, however, little is reported about this relationship, therefore these cell lines were the focus with the other cell lines as a comparison (Czernicki et al., 2007). Using western blotting, DLC1 was detectable in the HepG2 cells, faint traces of a DLC1 band could be seen in U87 and MDAMB-231. (Figure 3.1). GFP-DLC1 was expressed in HeLa cells as a comparison between endogenous and exogenous DLC1 expression (far right lane). Exogenously expressed EGFP-DLC1 was detected, as an additional upper band in the HeLa GFP DLC1 sample. Interestingly, two bands were identified around 123kD, the size of endogenous DLC1, suggesting the presence of two different isoforms of DLC1. DLC1 has five different isoforms, with isoforms 1 through 4 expressed in cancer cells. Isoforms 1 and 3 silenced in all cancers and immortalised cells, whereas 2 and 4 are frequently downregulated (Low et al., 2011). Isoform 2 is considered the canonical form with 1091 amino acids, whereas isoform 4 has 1017 amino acids. Therefore, it is likely that these are the isoforms detected.

Different molecular weight bands were present within different cell types, suggesting expression of different isoforms of DLC1. For example, U-87 MG and MDA-MB231 had a very faint expression

of the lower weight band whereas HepG2 had a detectable band of the higher molecular weight. DLC1 is expressed across normal tissues, therefore it would have been advantageous to use a normal cell line as a positive control.

From these expression levels, we decided to use HepG2 cells for DLC1 silencing experiments. U-87 MG cells were selected for an overexpression model, as they are a glioblastoma cell line with low DLC1 levels, in addition U-87 MG cells were identified as more motile and invasive than U-251 MG. HeLa cells were used for initial optimisation of staining and transfection as they are quick growing and easy to manipulate and maintain.

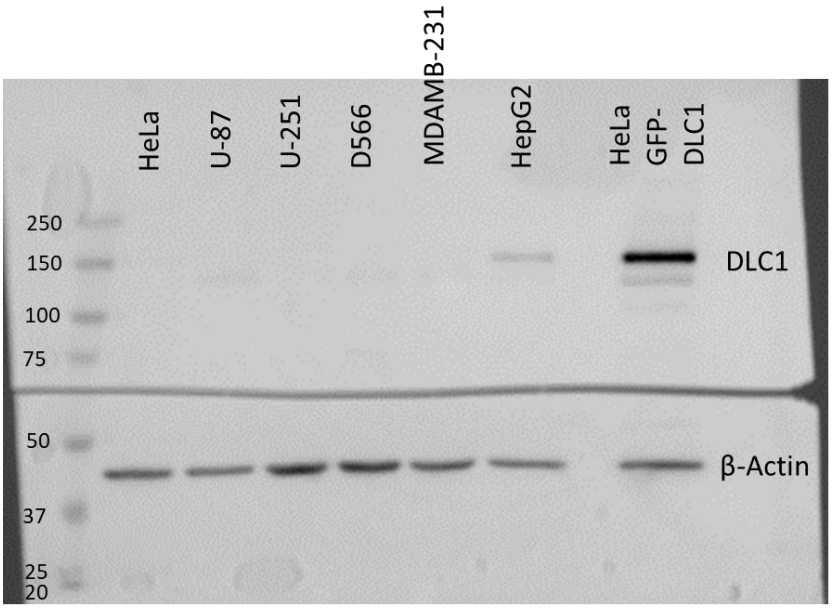

Figure 3.1: Endogenous and ectopic protein expression of DLC1 across cancer cell lines. Endogenous levels of DLC1 were measured in cell lysates of different cell lines by western blotting (anti-DLC1, BD Biosciences, 1:500). Anti-DLC1 was probed in cervical (HeLa), glioblastoma (U-87 MG, U-251 MG, D566), breast (MDA-MB-231) and liver (HepG2) cell lines. One cell line (HeLa) was transfected with EGFP-DLC1 for comparison between endogenous and ectopic expression.

3.2.2 Endogenous localisation of DLC1

DLC1 has previously been reported to localise at focal adhesions, to confirm literature and reproducibility, as well as to validate the antibody for immunofluorescence, endogenous levels were probed using immunostaining. As DLC1 levels could be detected in HepG2 cell line by western blotting, this cell line was used initially for endogenous DLC1 detection and localisation by immunofluorescence. DLC1 was shown to be localised in small foci structures (Figure 3.2), confirming localisation in focal adhesion structures.

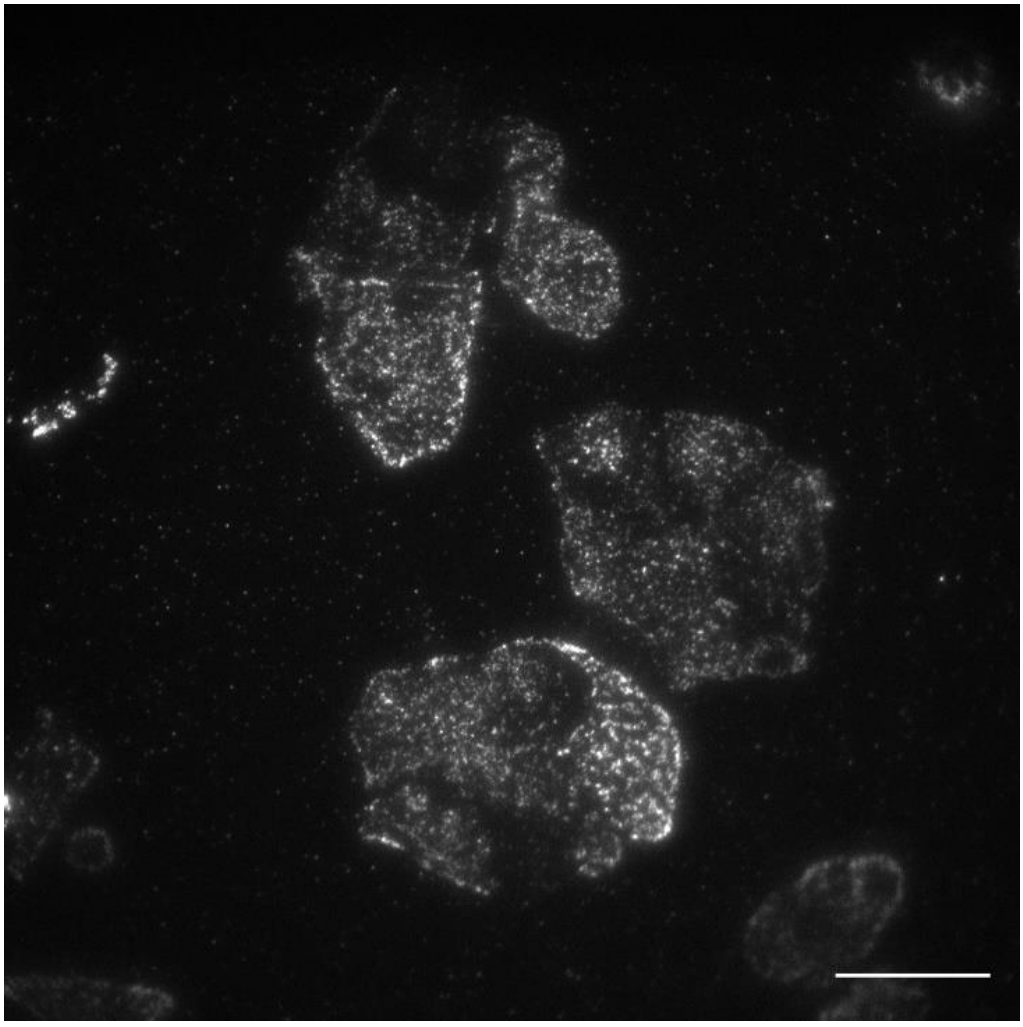

Figure 3.2: Endogenous localisation of DLC1. Endogenous levels of DLC1 were visualised by immunocytochemistry. HepG2 cells were fixed and stained with Anti DLC1 (1:500, BD biosciences).and labelled with Alexa 488 (1:5000). Scale bar 30um. Images acquired using TIRF microscopy on a Leica DMi8 with Andor Dragonfly using a 63x objective.

3.2.3 Localisation of exogenous EGFP-DLC1

To ensure adequate localisation of the fused DLC1 with EGFP, EGFP-DLC1 was transfected into HeLa cells, these cells were chosen due to ease of transfection to initially check the construct. EGFP-DLC1 was observed in foci structures, typical of focal adhesions, confirming literature and endogenous staining (Figure 3.3). EGFP-DLC1 focal adhesions did differ in localisation compared to Hepg2 endogenous focal adhesions, but this could be due to overexpression, differing cell types and live vs fixed samples.

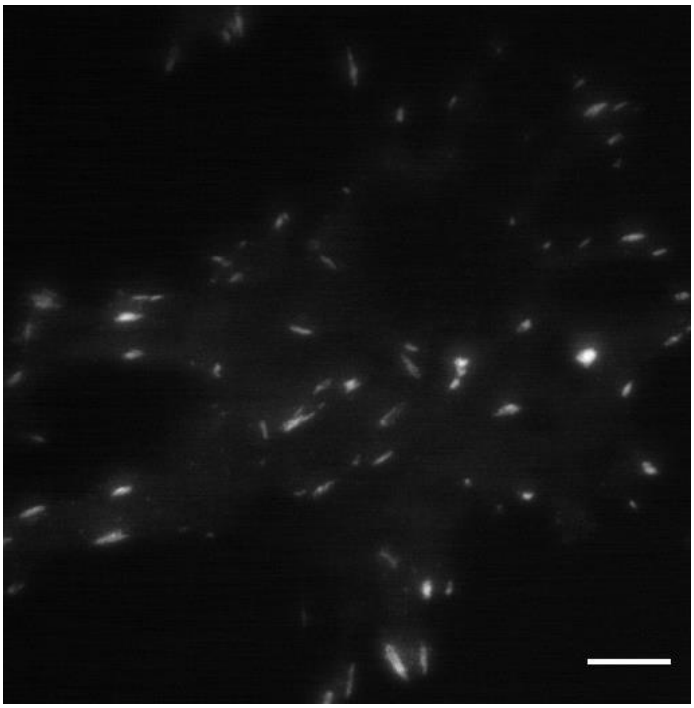

Figure 3.3: Localisation of exogenous DLC1. HeLa cells were transfected with EGFP-DLC1 and imaged using TIRF microscopy on a Zeiss LSM 880, using a 100x objective. Scale bar 10um.

To provide fluorophore flexibility and ability to co-express DLC1 with fluorescently labelled partners, it is advantageous to have constructs available with different fluorophores. Both GFP and mRuby-DLC1 constructs were transfected into HeLa cells as a comparison and showed identical localisation (Figure 3.4).

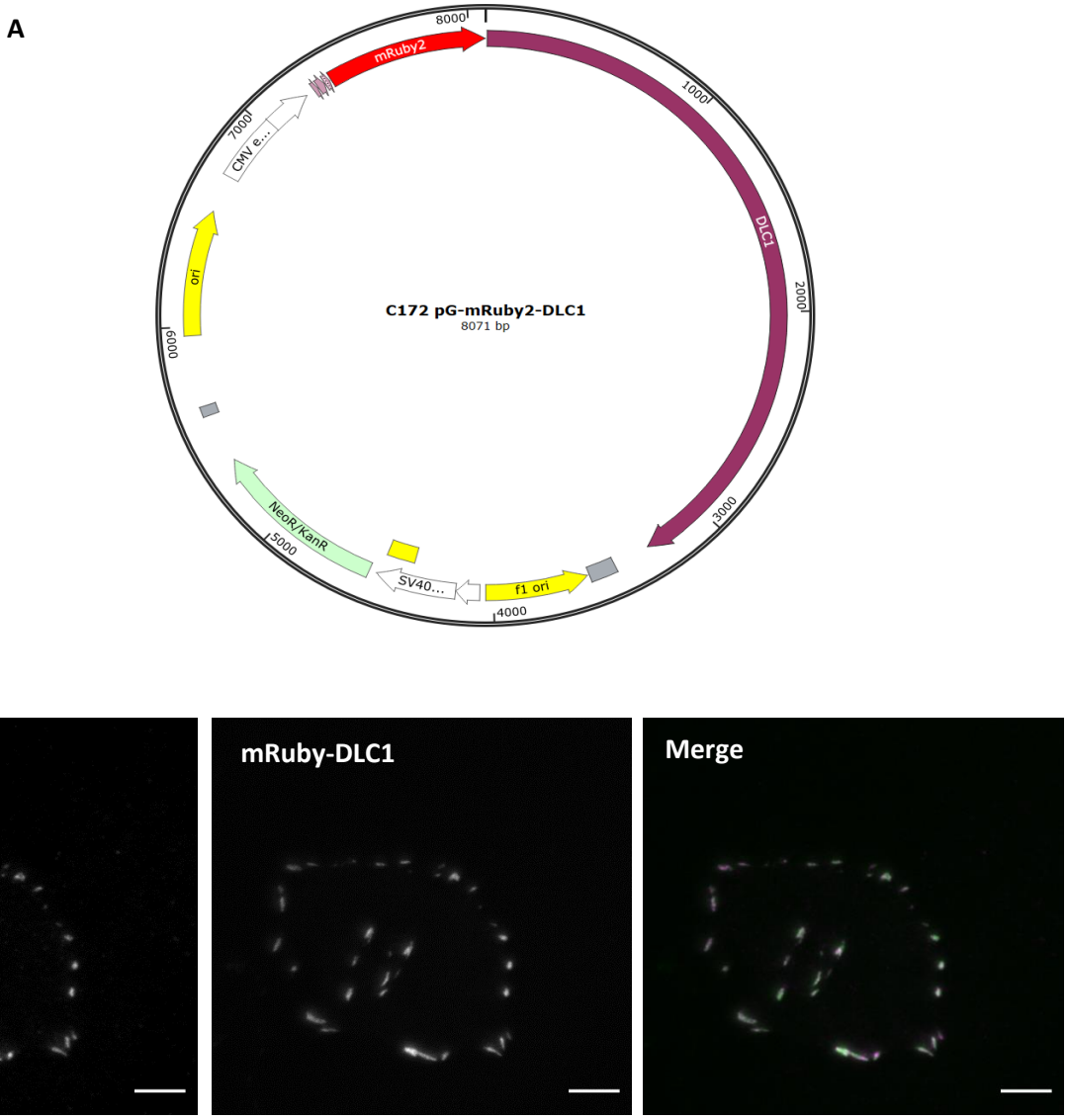

Figure 3.4: Generation and imaging of mRuby-DLC1 plasmid. mRuby DLC1 construct was cloned from the original GFP-DLC1 using infusion cloning. **A** pG-mRuby-DLC1 plasmid map showing cloning orientation of DLC1 gene. **B** EGFP-DLC1 and mRuby-DLC1 were co-transfected into HeLa cells. Images acquired using TIRF microscopy on a Zeiss LSM 880, using a 100x objective. Scale bar 10um.

3.2.4 Co-localisation of DLC1 with focal adhesion proteins

Endogenous and exogenously expressed DLC1 were visualised in focal adhesion-like structures. To confirm that DLC1 is actually localised within a focal adhesion complex, co-localisation experiments of DLC1 with paxillin, a characterised focal adhesion protein, were performed. There are numerous reports of DLC1 localising to focal adhesions, therefore only one FA marker was stained for to ensure the DLC1 construct we were using had the correct localisation. Multiplexing of both DLC1 and paxillin was not possible due to antibodies species. Therefore, mRuby-DLC1 was overexpressed and endogenous paxillin was detected in U-87 MG, HepG2 and HeLa cells.

Cells were imaged using TIRF microscopy and the distinct foci pattern of paxillin seen in the literature was identified in both cell lines (Figure 3.5). Paxillin co-localised with DLC1 in the transfected cells, which was expected as Paxillin and DLC1 are known to co-localise and DLC1 down-regulates paxillin turnover (Kaushik et al., 2014). Since paxillin is a recognised focal adhesion protein, the co-localisation confirms DLC1 is localisation in focal adhesions.

As discussed, talin is another focal adhesion protein known to bind to DLC1, yet the effect of this interaction is not reported (Li et al., 2011, Zacharchenko et al., 2016). To investigate the impact of talin on DLC1 dynamics in focal adhesions, and as a first step, talin-DLC1 co-localisation were imaged on fixed cells using TIRF microscopy. As expected, talin was visualised in focal adhesion structures, co-localising with mRuby-DLC1 (Figure 3.6).

The co-localisation experiments confirmed DLC1 localisation with focal adhesion proteins and in focal adhesion complexes, and further validates the use of the fluorescent fusion construct of DLC1. HepG2 cells had noticeably less adhesions compared to the other cell lines.

3.2.5 Exogenous Expression of DLC1 and talin

Investigation of the dynamic relationship between DLC1 and talin in living cells, requires exogenous expression of fluorescent fusion of both proteins. A GFP-talin construct was co-expressed with the mRuby-DLC1 construct in HeLa cells (Figure 3.7). The constructs displayed a similar localisation to the endogenous proteins, validating this approach for live imaging experiments.

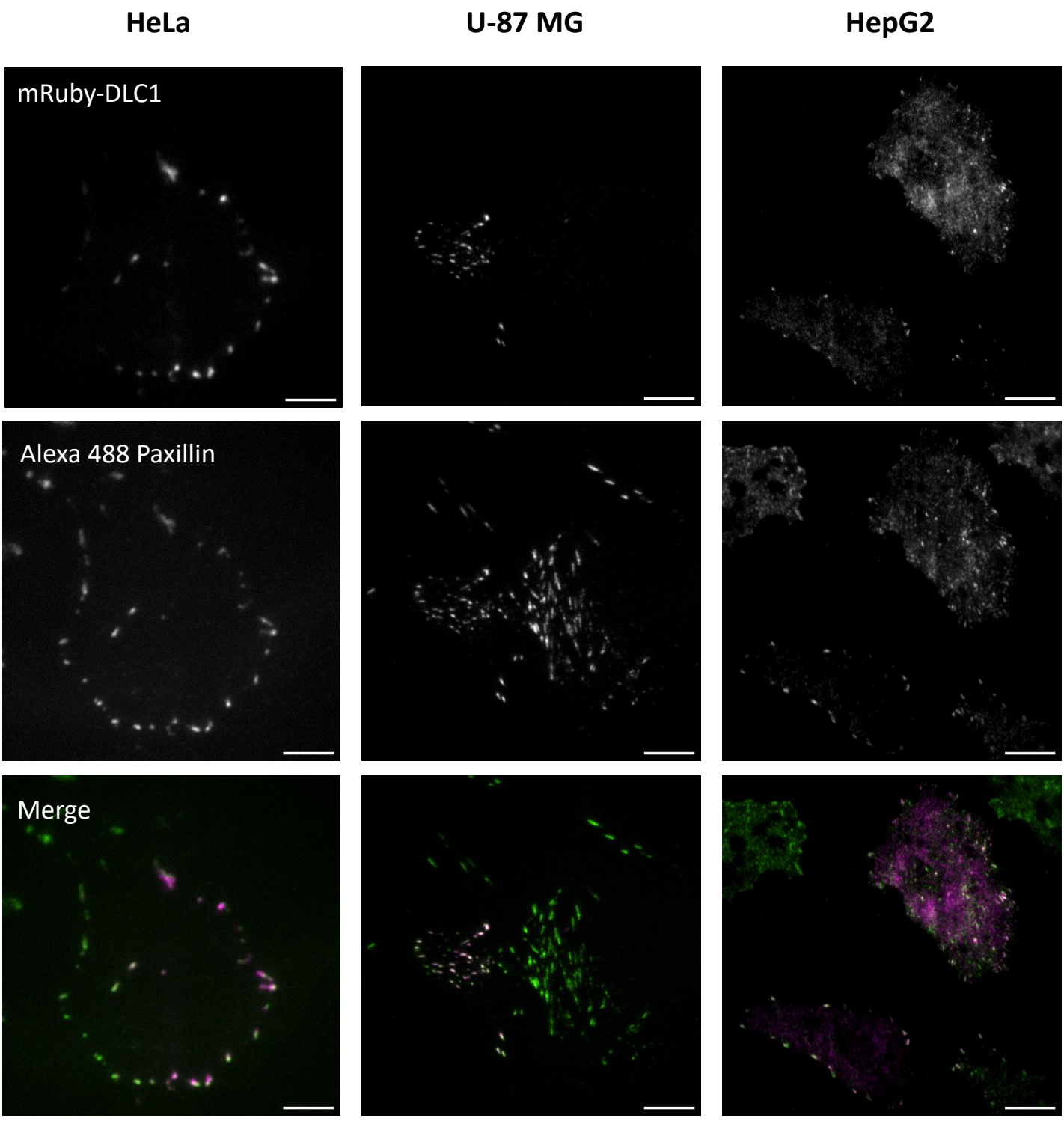

Figure 3.5: Localisation of mRuby-DLC1 and endogenous Paxillin. HeLa, U-87 MG and HepG2 cells were transfected with mRuby DLC1 plasmid and stained for anti-Paxillin using secondary antibody Alexa 488. Images acquired using TIRF microscopy on a Leica DMi8 with Andor Dragonfly using a 63x objective. Scale bar 15µm

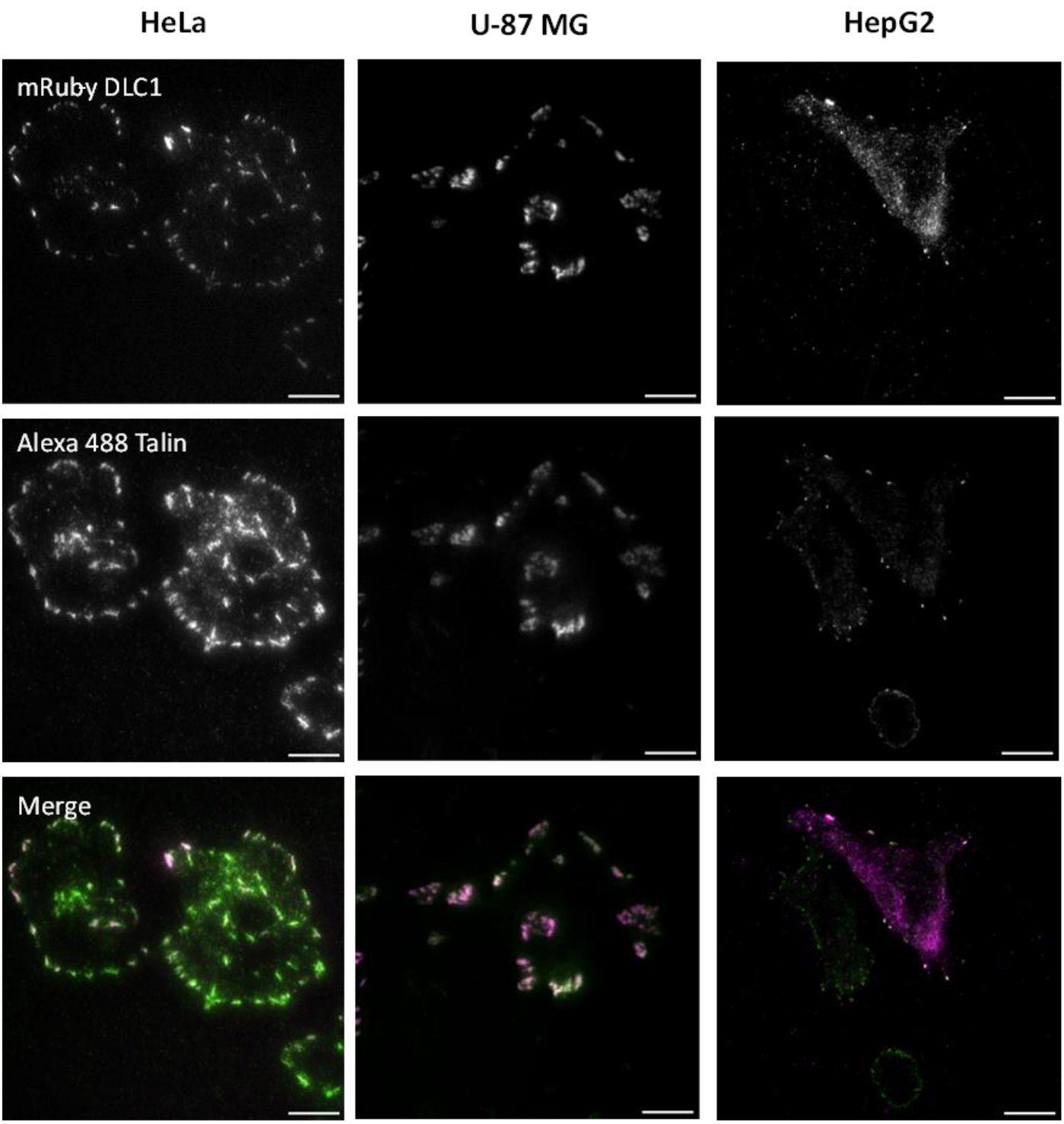

Figure 3.6: Localisation of mRuby-DLC1 and endogenous talin. HeLa U-87 MG and HepG2 cells were transfected with mRuby DLC1 plasmid and stained for anti-talin using secondary antibody Alexa 488. Images acquired using TIRF microscopy on a Leica DMi8 with Andor Dragonfly using a 63x objective. Scale bar 15µm.

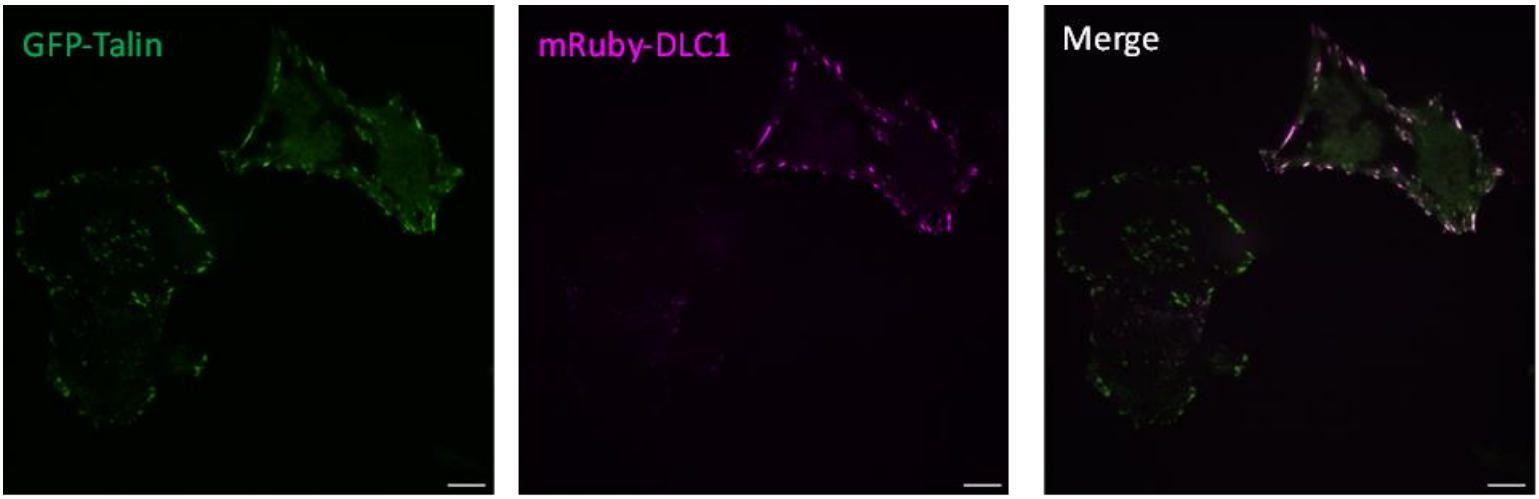

Figure 3.7: Co-localisation of mRuby-DLC1 and GFP-Talin. HeLa cells were transfected with mRuby DLC1 and GFP Talin plasmids. TIRF microscopy was used to visualise both mRuby DLC1 and GFP talin. Images acquired using TIRF microscopy on a Leica DMi8 with Andor Dragonfly using a 63x objective. Scale bar 15µm.

3.2.6 Focal adhesion dynamics of DLC1

3.2.6.1 Focal adhesion assembly and disassembly in mRuby DLC1 and GFP talin expressing cells

Previous literature has shown that DLC1 can bind to talin through a LD motif (Li et al., 2011), yet the function of this interaction is yet to be characterised. We, therefore, decided to visualise and quantify focal adhesion dynamics using time-lapse microscopy and investigate the impact of the ratio between DLC1 and talin on these dynamics. Exogenous DLC1 was detected in the focal adhesions and the cell protrusions migrating across the field of view (Figure 3.8 – A). Using a focal adhesion analysis server (Berginski and Gomez, 2013), the assembly and disassembly rates of focal adhesions were calculated (Figure 3.8 B–D). The expression of DLC1 and talin individually or together were compared (Figure 3.9, Video 1–3). After transfection mRuby-DLC1 focal adhesions had a reduced assembly rate (**M** = 0.033 ± 0.022 (min^{-1})) compared to GFP-talin (**M** = 0.041 ± 0.033 (min^{-1})). Overexpression of both mRuby-DLC1 and GFP-talin together had an assembly rate of 0.035 ± 0.027 (min^{-1}), closer to the value seen of mRuby-DLC1 alone. The assembly rates between the three conditions were significantly different when analysed by one-way ANOVA ($F(2,5434) = 31.83$, $p = <0.0001$). Despite the statistical difference, the biological difference is likely to be limited given the small differences between the conditions.

Likewise, the disassembly kinetics of focal adhesions were compared between the 3 conditions, mRuby-DLC1 disassembly (**M** = 0.034 ± 0.022 (min^{-1})) was increased compared to GFP-talin disassembly (**M** = 0.029 ± 0.023 (min^{-1})). When the two constructs were co-expressing the disassembly rate was reduced (**M** = 0.028 ± 0.021 (min^{1})) compared to GFP-talin alone. The

disassembly rates between the three conditions were statistically significant when analysed by one-way ANOVA, ($F(2, 3722) = 18.08$, $p = <0.0001$).

Taken together, this shows that focal adhesions with overexpressed DLC1 have a faster assembly rate and a slower disassembly rate compared to focal adhesions with overexpression of talin. Interestingly, in focal adhesions were DLC1 and talin were co-expressed, both the assembly and disassembly rate were faster compared to talin alone focal adhesions. The co-expressed focal adhesion disassembly rate was quicker than both mRuby-DLC1 and GFP-talin alone.

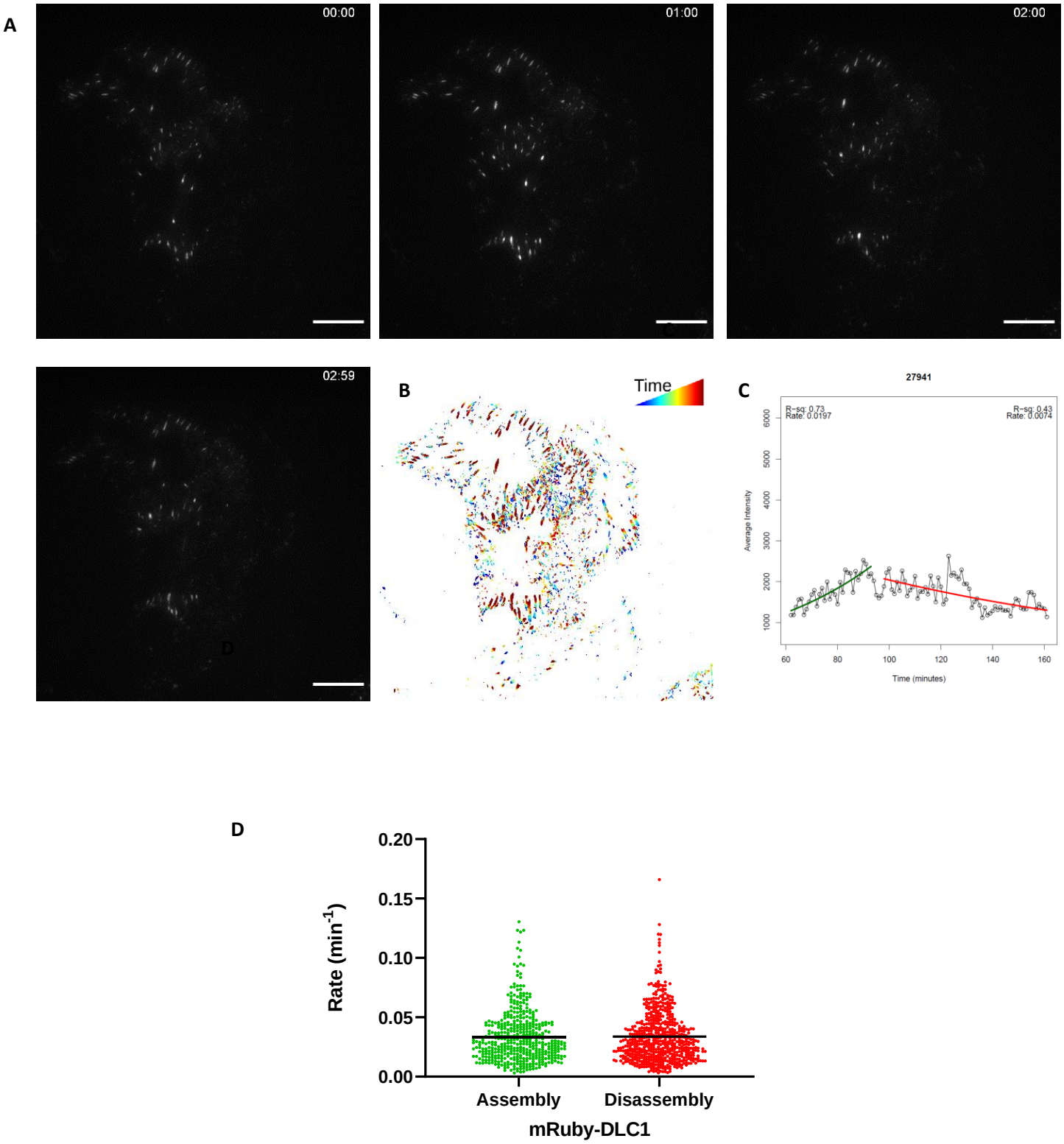

Figure 3.8: Focal adhesion dynamics of DLC1 overexpression. **A** HeLa cells were transfected with mRuby DLC1 plasmid and imaged every minute for 3 hours. Images acquired using TIRF microscopy on a Leica DMi8 with Andor Dragonfly using a 63x objective. **B** Acquisition files were uploaded to Focal Adhesion Analysis Server (Berginski, 2013). Each adhesion is tracked and can be visualised. **C** The rate of assembly and disassembly of each adhesion is plotted. **D** All assembly and disassembly rates of adhesions from one field of view plotted together (n = 12).

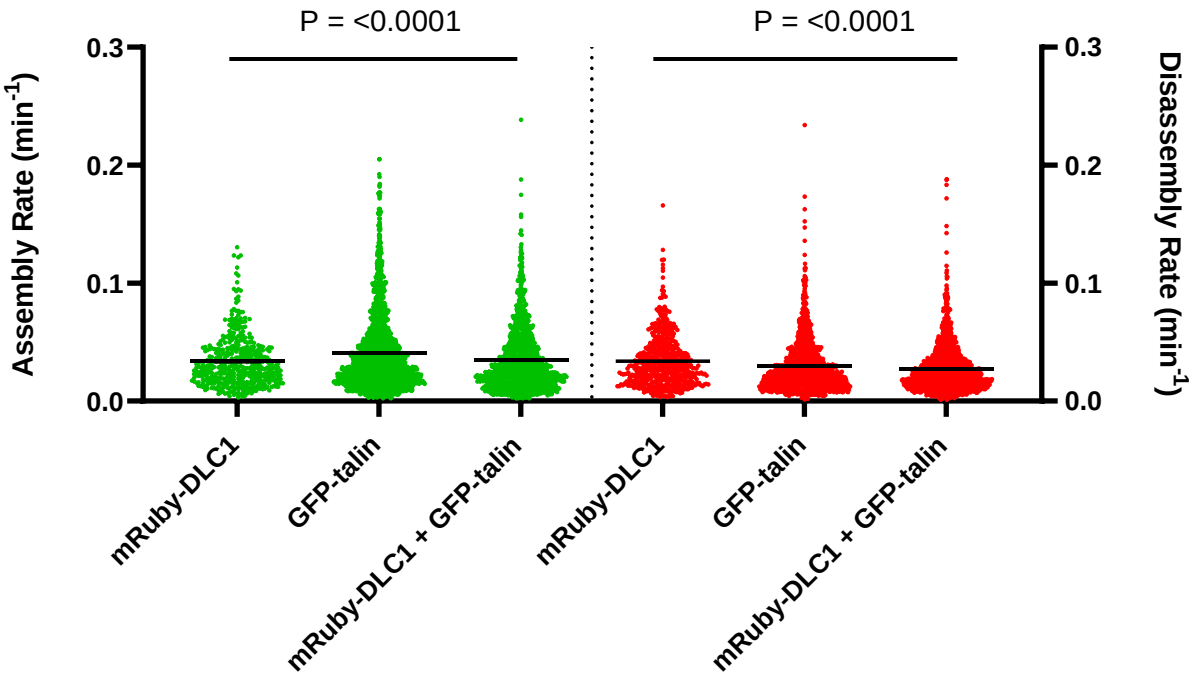

Figure 3.9: Focal adhesion rate is affected by DLC1 and talin co-overexpression. HeLa cells were transfected with mRuby DLC1, GFP Talin or both plasmids together and imaged every minute for 3 hours. Acquisition files were uploaded to Focal Adhesion Analysis Server (Berginski, 2013). The rate of assembly of each condition was plotted, mRuby DLC1 (n=12), GFP talin (n=12) and mRuby DLC1 and GFP talin (n=16). The assembly rate was determined significantly different by one-way ANOVA, ($F(2,5434) = 31.83$, $p = <0.0001$). The disassembly rate was also significantly different, by one-way ANOVA, ($F(2, 3722) = 18.08$, $p = <0.0001$).

3.2.6.2 Focal Adhesion Ratio of mRuby-DLC1 and GFP-talin

The consequence of the transient transfection used for the focal adhesion dynamic experiment was the differing intensities of each protein in different cells. This could affect focal adhesion turnover. To investigate this, the assembly and disassembly rate of each focal adhesion was plotted over the intensity ratio of the two fluorescent channels, (log2(channel1/channel2). If the intensity ratio was positive, there was a higher intensity in channel 1 (DLC1) than channel 2 (talin), and if reversed, and the intensity ratio was negative, there was more talin than DLC1. No correlation between the focal adhesion assembly and disassembly rates and the ratio of mRuby-DLC1 and GFP-talin was found (example in Figure 3.10).

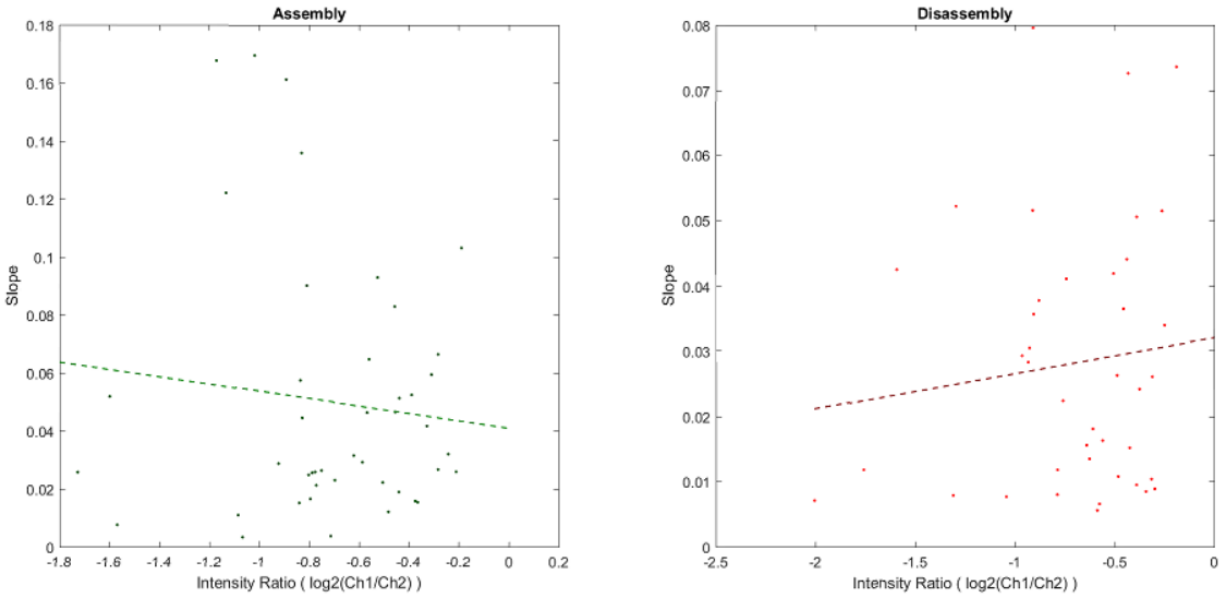

Figure 3.10: Focal adhesion assembly and disassembly rate is not affected by mRuby-DLC1: GFP-talin ratio. The assembly and disassembly rates of focal adhesions were plotted over the fluorescent intensity of mRuby DLC1 and GFP talin transfected cells (log2(channel1/channel2)). There was no correlation between the ratio of the two proteins when looking at assembly and disassembly across the focal adhesions.

3.2.6.3 Focal adhesion dynamics in absence of DLC1

To assess if the loss of DLC1 could affect the focal adhesion turnover, DLC1 was silenced using RNA interference. To this end, the HepG2 cell line, with detectable endogenous levels of DLC1, was used. DLC1 silencing was validated by western blotting and immunostaining in comparison to a siRNA scrambled control. (Figure 3.11). For investigation of how DLC1 knockdown affects focal adhesions, siRNA DLC1 HepG2 cells were fixed, stained with multiple cell markers, (tubulin, VASP and phalloidin) and imaged using spinning disk confocal microscopy. The focal adhesions for each condition (control and siRNA DLC1) were analysed using a bespoke ImageJ analysis script.

SiRNA DLC1 focal adhesions had a significantly smaller area (**M** = 1.362) compared to the control (**M** = 1.516), two tailed t-test (1127) = 3.711, p = <0.001). There was no significant difference between roundness or number of focal adhesions between the two conditions. This could suggest a role within focal adhesions as when DLC1 level is reduced, the focal adhesion area is reduced.

For live focal adhesion visualisation and analysis, a focal adhesion marker was needed, therefore GFP-talin was co-transfected with siRNA DLC1. GFP-talin levels were not affected by DLC1 silencing (Figure 3.11 A).

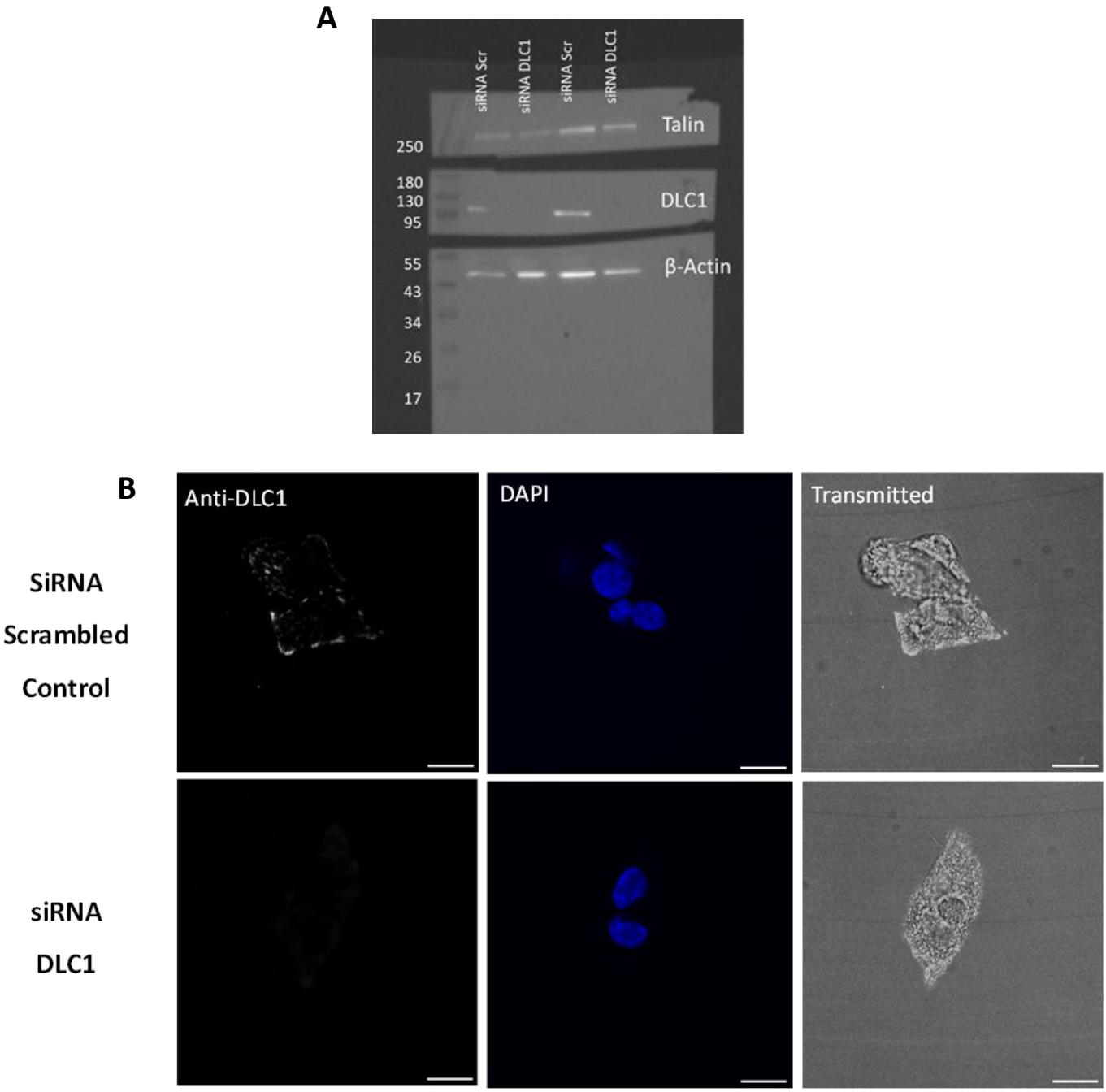

Figure 3.11: Silencing of DLC1 using siRNA DLC1. **A** HepG2 cells were transfected with either 10µM siRNA DLC1 or siRNA scrambled control, after 24 hours they were transfected with GFP-talin. Samples were collected and probed for with anti-DLC1 (1:500, BD biosciences) and anti-talin antibodies (1:500, sigma). DLC1 level could be detected in the siRNA scrambled control sample but not siRNA DLC1 (two repeats are shown). **B** Immunofluorescence was performed to confirm silencing of DLC1, HepG2 cells were transfected with siRNA DLC1, or siRNA control scrambled. After 24 hours cells were fixed, stained with anti-DLC1 and images acquired using TIRF microscopy on a Leica DMi8 with Andor Dragonfly using a 63x objective. DLC1 could be visualised in the siRNA control but only very faint signal could be detected in the siRNA DLC1 sample.

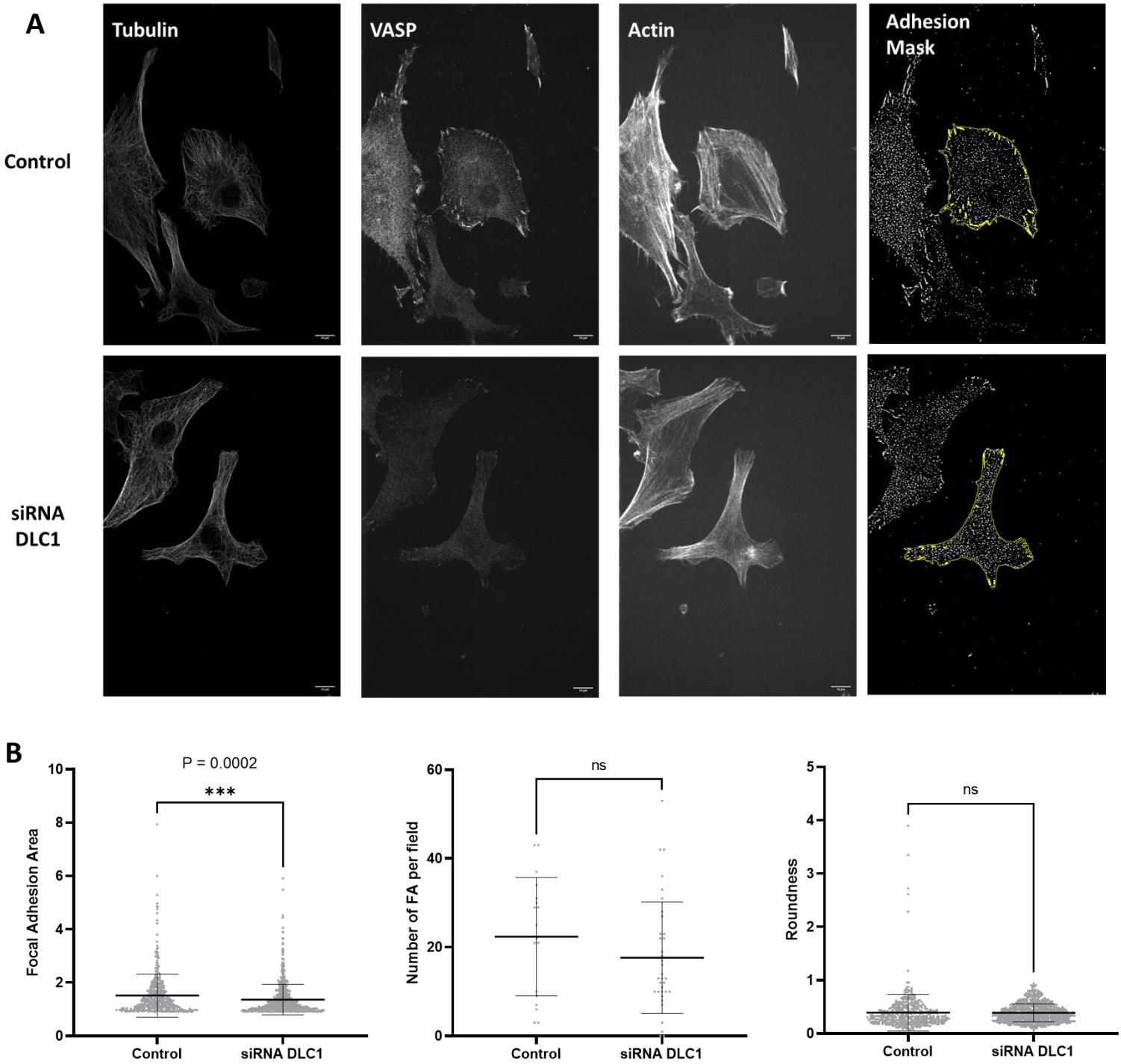

Figure 3.12: Effect of siRNA DLC1 knockdown on focal adhesions. **A** HepG2 cells were transfected with either 10µM siRNA DLC1. Samples were fixed and stained with anti-tubulin, anti-VASP and phalloidin. Cells were acquired on a Marianas spinning disk confocal microscope (3i) using a 63x 1.4NA. Experiment was performed by Dr Lorna Young. Focal adhesions were measured using a bespoke Fiji script, which identified a adhesion mask.. **B** siRNA DLC1 adhesions had a significantly smaller area, two tailed t test (1127) = 3.711, p = <0.001), however there was no significant effect on focal adhesion number or roundness.

There was no significant difference in assembly rate between the GFP-talin + siRNA DLC1 (**M** = 0.021 ± 0.018 (min^{-1})) and GFP-talin + scrambled siRNA conditions (**M** = 0.021 ± 0.017 (min^{-1})) (Figure 3.13, Video 4-5). The disassembly rate of GFP-talin + siRNA DLC1 was slower (**M** = 0.031 ± 0.030 (min^{-1})) compared to GFP-talin + siRNA scrambled control (**M** = 0.018 ± 0.015 (min^{-1})) (Fig 3.12). The disassembly rates were significantly different according to two tailed t test, (416) = 5.772 p = <0.0001), suggesting that loss of DLC1 affects focal adhesion disassembly.

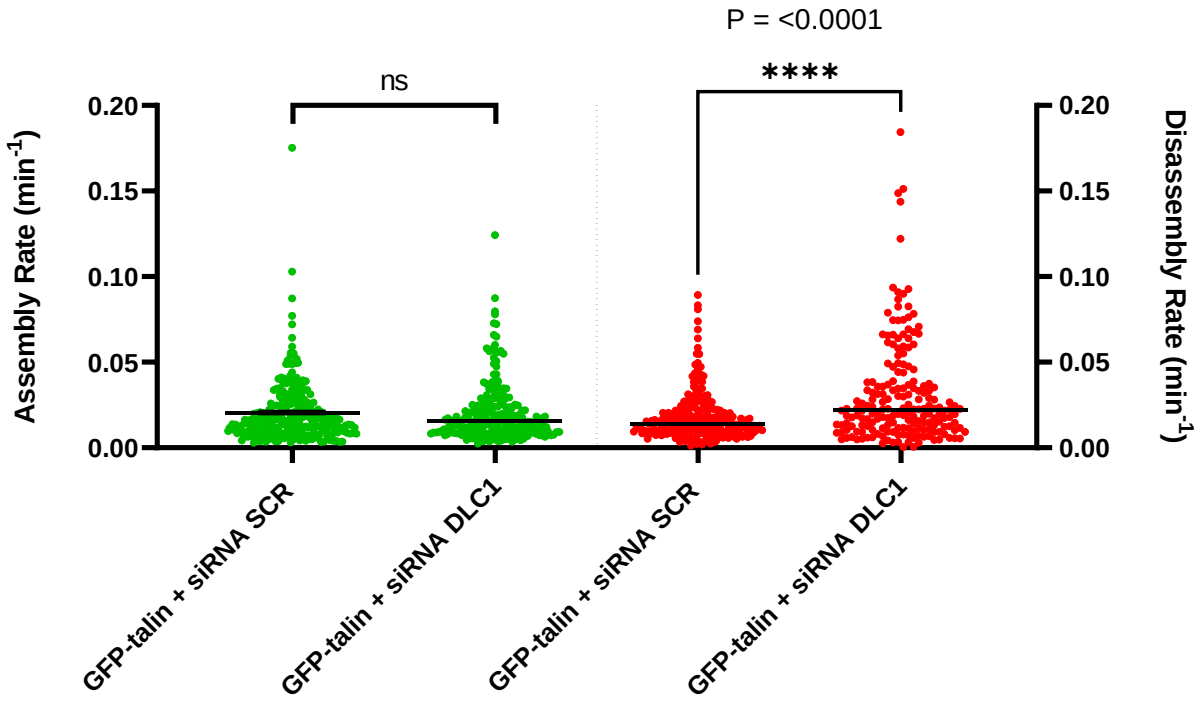

Figure 3.13: Focal adhesion disassembly rate is affected by DLC1 silencing. To silence DLC1 HepG2 cells were transfected with siRNA DLC1 or a negative scrambled control. 24 hours later cells were transfected with focal adhesion marker GFP Talin and imaged every minute for 3 hours. Acquisition files were uploaded to Focal Adhesion Analysis Server (Berginski, 2013). The rate of assembly and disassembly of each condition was plotted GFP talin siRNA scrambled (n=6) and GFP talin siRNA DLC1 (n=8). There was no significant difference between the assembly rates of both conditions. The disassembly rates of GFP-Talin and siRNA DLC1 were significantly slower according to two tailed t test, (416) = 5.772 p = <0.0001).

3.3 Discussion

3.3.1 Focal Adhesion dynamics

The aim of the project described in this chapter was to investigate the role of DLC1 in focal adhesion dynamics. First, DLC1 was confirmed to localise in focal adhesions and to co-localise with the well-characterised focal adhesion proteins paxillin and talin, as previously reported in the literature (Kaushik et al., 2014, Li et al., 2011). Despite several studies confirming that DLC1 is localised to focal adhesions and with other focal adhesions proteins, the impact of DLC1 on focal adhesion dynamics was yet to be investigated.

Here cells with overexpression of DLC1 had faster assembly rates compared to overexpressed talin. When DLC1 and talin were expressed together, the assembly rate was comparable to DLC1 expression alone; and it was reduced in comparison to GFP-talin. This provides further support that DLC1 overexpression could regulate talin at focal adhesions. Further experiments observing focal adhesion dynamics with an independent marker such as paxillin could determine whether DLC1 is truly affecting focal adhesion turnover.

During disassembly, overexpressed DLC1 slightly decreased disassembly speed compared to both overexpressed talin alone and talin + DLC1 expression. Mechanical force has been shown to promote the growth and maturation of focal adhesions, which could affect assembly and turnover of focal adhesions (Lawson and Burridge, 2014). Talin is involved in mechanosensing at focal adhesions, which could explain the increased disassembly rate. A literature search could not determine any previously published talin focal adhesion turnover rates. Interestingly, a study by Lele in 2008 discussed how turnover of focal adhesion proteins depends on the number of

interactive partners, slower turnover rates are observed if proteins (such as talin) bind integrins compared to critical signaling proteins with a higher turnover (Lele et al., 2008). Talin had the slowest turnover rate compared to the other proteins in this study, noting they were evaluated using a different technique, FRAP. However, this study did highlight the lack of studies evaluating focal adhesion dynamics.

Surprisingly when DLC1 was silenced, there was no significant effect on focal adhesion assembly rate (Figure 3.11 A). However, as the silencing was combined with GFP-talin as a focal adhesion marker, this could influence the dynamics, and mask the effect of silenced DLC1.

GFP-talin expression and combined DLC1 silencing increased disassembly rate compared to siRNA knock out control. DLC1 silencing has been reported to reduce disassembly (van der Stoel et al., 2020). The same server was used to analyze the focal adhesion turnover and it was found that silenced DLC1 reduced focal adhesion disassembly compared to control, suggesting impaired function without DLC1. However, this was reported in a different cell line, and without the influence of overexpressed talin, with the focal adhesions measured using a transduced paxillin-mCherry marker. Interestingly the opposite effect was observed here with silencing DLC1 and overexpressed talin, suggesting overexpression of talin could reverse the effects of DLC1 knockdown. As mentioned previously, use of an independent label such as paxillin may provide more clarity into DLC1's dynamics, a follow up experiment could be to knockdown DLC1 with and without talin overexpression to further investigate this.

The focal adhesion turnover rates of paxillin and FAK have also been observed using the FAAS. Paxillin focal adhesions were found to have an assembly rate of 0.031+/-0.023 (min^{-1}) and a

disassembly of (0.020+/-0.014 min^{-1}) (Berginski and Gomez, 2013). It was also reported that there was a statistically indistinguishable difference between paxillin and FAK focal adhesions, suggesting that the reported rate was common among focal adhesion proteins.

Here overexpressed DLC1 was found to have an assembly rate of 0.033 +/-0.022 (min^{-1}) and GFP talin 0.041 +/- 0.033 (min^{-1}). Paxillin is a well characterised focal adhesion protein and one of the initial proteins recruited to focal adhesion complexes. Interestingly overexpression of DLC1 has comparable rates to this protein, suggesting that the increased level of DLC1 at focal adhesion does not have any effect on focal adhesion assembly.

For disassembly, paxillin has been reported as 0.020 +/- 0.014 (min^{-1}), here mRuby DLC1 had a disassembly rate of 0.034 +/- 0.022 (min^{-1}) and GFP talin disassembly was 0.029 +/- 0.023 (min^{-1}). Therefore, overexpressed DLC1 disassembly rate is higher than reported for paxillin. This could suggest a role of DLC1 regulating focal adhesion turnover, to reduce traction and prevent maturation and migration. This could be supported by reported previous reporting that DLC1 knockdown decreases focal adhesion disassembly (van der Stoel et al., 2020).

Past research into focal adhesions have utilised a variety of techniques to investigate functions of focal adhesions. Focal adhesion movement was first studied using GFP fusion proteins and microscopy in 1999, as the field and technology has evolved, several different techniques have been established (Smilenov et al., 1999). Development of microscopy applications such as TIRF offer increased resolution of focal adhesion proteins, reducing the background noise, allowing higher resolution and tracking of focal adhesion proteins. Several studies have focused on fluorescently tagged focal adhesion proteins and tracking the fluorescence over time to establish

rate of dynamics. In a landmark study by Webb, this allowed tracking of paxillin and several other mutants to establish assembly and disassembly rates. Webb showed the turnover of paxillin in MEF fibroblasts with assembly rate calculated at $(8.8 \pm 0.4) \times 10^{-2}$ (min^{-1}) and disassembly rate $(1.2 \pm 0.4) \times 10^{-1}$ (min^{-1}). However, only 10-20 adhesions across 4-5 cells were analyzed. These results show quicker dynamics compared to the focal adhesion in this study which were quantified using the FAAS, however, this uses an automated detection and analyses a larger number of adhesions compared to the Webb study (Berginski and Gomez, 2013). The study compared paxillin dynamics when different components related to focal adhesion biology was manipulated, for example mutations in FAK, SRC, Rho and Tiam2, and found that these mutations all severely decreased disassembly rates (Webb et al., 2004). The fold decrease relative to wild-type paxillin in MEF was used to measure the differences in disassembly rate. The disassembly of the ΔLD4 mutant (lacking the LD motif in paxillin) was calculated at $(1.3 \pm 0.1) \times 10^{-2}$, a 11-fold decrease compared to wild-type paxillin. Another serine mutant, (S188A,S190A) reported a 2-fold decrease. In this study, there was a 1.7 fold increase in disassembly rate of siRNA DLC1 compared to siRNA scrambled control.

3.3.2 Differing DLC1 levels

In this chapter several cell lines investigated were found to have differing levels of DLC1 expression, with invasive cell types such as glioblastoma (U-87 MG and U-251 MG), breast (MDAMB231) and cervical (HeLa) found to have low DLC1 level and a liver cell line (HepG2) was identified as having higher detectable DLC1 expression.

As previously described, DLC1 is lost in metastatic cancers and literature has reported a range of cancers and cell lines with differing DLC1 levels. Transcriptional silencing is the main reason DLC1 is lost within cancer cell lines and tumour samples. DLC1 was reported to be silenced in different tumour types including lung, multiple myeloma, cutaneous melanoma, angiosarcoma, colorectal, prostate, extramammary Paget's tumours, acute leukaemia, nasopharyngeal, oesophageal and cervical carcinomas (Castro et al., 2010, Song et al., 2006, Sjoestroem et al., 2014, Sánchez-Martín et al., 2018, Peng et al., 2013, Guan et al., 2006a, Kang et al., 2012, Fu et al., 2014, Seng et al., 2007). A further study of DLC1 expression compared breast, cervical and oesophageal cancer cell lines to representative patient tumours and concluded that loss of DLC1 by methylation was tumour specific and comparable between cell lines and tumours (Seng et al., 2007). DLC1 has long been hypothesized as a metastatic suppressor gene, and reintroduction of DLC1 into tissues reduces metastatic effects. This effect is demonstrated both *in vivo* and *in vitro* using several different methods, reviewed in (Barras and Widmann, 2013) .

Previous literature has observed the effect of DLC1 on focal adhesions, and reported that altering DLC1 expression has an impact on focal adhesions, actin dynamics and migratory capacity of the cells (Barras and Widmann, 2013). DLC1 mutant studies demonstrated that DLC1 affects cell morphology and cytoskeletal organisation with the loss of actin stress fibers and reduction of focal adhesions (Kim et al., 2008, Sekimata et al., 1999). Furthermore, DLC1 deficient cells had fewer actin stress fibers and a reduced number of focal adhesion like structures (Durkin et al., 2005). Here, siRNA DLC1 treated cells had a smaller focal adhesion area compared to the control cells (Figure 3.12) supporting the evidence that reducing DLC1 level does affect focal adhesions.

Re-expression of DLC1 in deficient cells causes significant morphological changes, such as decreased cell spreading, decrease in actin bundles and a reduction in the number of mature focal cell-substrate contacts (Zhou et al., 2008). Similarly, experimental overexpression of DLC1 in cells significantly suppressed the formation of stress fibers but caused extensive cell rounding and cortical retraction (Wong et al., 2005). Here, with DLC1 overexpression, some of the mRuby-DLC1 cells were bright and very rounded when looking down the microscope, indicating that overexpression of DLC1 can dramatically change the cell morphology, in line with what Is reported in the literature. Optimisation was initiated to investigate how DLC1 affects actin dynamics, using live actin dye SIR-actin. However, this work could not be finalised due to time restraints of the project.

From these studies, it is evident that DLC1 is involved with focal adhesion dynamics, however both overexpression and total absence of DLC1 may both compromise proper cytoskeleton dynamics and migration (Barras and Widmann, 2013). Furthermore, there are contradictory reports that silencing of DLC1 favours migration in prostrate cells, which adds more complexity to the role of DLC1 (Shih et al., 2012).

3.3.3 The effect of focal adhesion dynamics on cell migration

Adhesion is an important part of the cell migration cycle as focal adhesion turnover is involved in driving cell migration, which raises the question of whether changes in adhesion dynamics can affect cell migration. Many studies have evaluated whether the focal adhesion morphology, number and size can affect cell migration rate. It has been observed that fast moving cells, such as *Dictyostelium discoideum* and neutrophils, display disappearing small focal adhesions, while

slowly moving cells such as fibroblasts show prominent focal adhesions (Nagasaki et al., 2009, Kim and Wirtz, 2013b). The results in this chapter show that altering the levels of DLC1 by either overexpression or siRNA knockdown affects focal adhesion turnover, which may affect the cells ability to migrate.

Kim and Wirtz, using high throughput live-cell microscopy, suggested that the mean size of focal adhesions and mean cell migration speed were biphasically related, and focal adhesions are larger and more elongated in fast moving cells (Kim and Wirtz, 2013a, Kim and Wirtz, 2013b). However, it was concluded that neither the shape of focal adhesions, nor their number or the relative cell surface occupied by focal adhesions, nor the molecular composition of focal adhesions seems to predict cell migration (Kim and Wirtz, 2013b). Focal adhesion biology varies across cell types. The morphology and dynamics of focal adhesions such as size, shape, molecular density and activity, turnover rate, and spatial distribution, strongly depend on the cell type and matrix properties such as dimensionality, topology, and compliance (Kim and Wirtz, 2013a, Kim and Wirtz, 2013b, Berginski and Gomez, 2013, Fraley et al., 2010, Walcott et al., 2011, Kim and Wirtz, 2011). It has also been demonstrated that focal adhesion size and composition contribute to cellular functions such as migration and mechanosensing (Maziveyi and Alahari, 2017, Shemesh et al., 2005). Alternatively, the presence of focal adhesions can hinder cell migration due to excessive adhesion, and cells can migrate without the presence of focal adhesions (Burridge and Guilluy, 2016).

Alterations in the formation and composition can affect the cell migration process. For example, migration defects are observed in FAK and Src-null cells (Webb et al., 2004). Mutations in focal

adhesion proteins can also affect focal adhesion numbers and formation (Webb et al., 2002). Mutations have shown to affect focal assembly and disassembly rates, but have not demonstrated a direct effect on cell migration (Berginski and Gomez, 2013). Alterations in the adhesion mechanics of cells may play a role in the development and progression of cancer, with research focused on identifying key proteins involved in adhesion signalling, linking these incidents with oncogenic events (Maziveyi and Alahari, 2017, Nagano et al., 2012). Therefore, it can be concluded that focal adhesion dynamics do affect cell migration, however, not enough is known to conclude whether small fluctuations in assembly or disassembly rate directly affect cell migration.

3.4 Conclusions

In conclusion, the data from this chapter show that DLC1 expression varies across different cell lines and suitable cell lines for overexpression and silencing models have been identified.

Focal adhesion analysis has shown that DLC1 overexpression affects focal adhesion dynamics. When DLC1 and talin are co-expressed, the assembly rate is comparable to mRuby-DLC1 expressed alone, which could imply that the mRuby-DLC1 overexpression has more impact than the GFP-talin. siRNA DLC1 was shown to affect focal adhesion area. Further experiments are required to fully investigate the effect of DLC1 on focal adhesion dynamics, and there is little literature available on the turnover rates of focal adhesion dynamics for comparison. A study measuring the focal adhesion dynamics of classical focal adhesions (paxillin, FAK, talin) in comparison to different DLC1 manipulations (overexpressed, silenced, mutants) would be advantageous in clarifying DLC1's role.

Chapter 4 : Effect of DLC1 on cell migration and invasion

4.1 Introduction

Previously, it was shown that DLC1 overexpression affects focal adhesion dynamics, which are known to impact cell motility and migration. DLC1 expression was varied across the cell lines examined, enabling identification of suitable cell lines for overexpression and silencing experiments; despite the well-described role of DLC1 in metastasis, previous reports provide a conflicted view on the effect of differing DLC1 levels on migration. Investigation of overexpression and silencing of DLC1 in 2D and 3D cell migration assays could provide further understanding to the role of DLC1 in cell migration and invasion.

The effect of DLC1 expression on cell migration and invasion has previously been investigated using 2D wound healing assays and transwell invasion assays where the cells must invade through Matrigel. However, no studies have assessed DLC1 invasion using a more physiologically relevant 3D spheroid model which better recapitulates a solid tumour.

4.2 Aims

The aim of this chapter was to investigate the role of DLC1 in cell migration and invasion. This was achieved by observing overexpression and silencing of DLC1 in 2D cell migration assays and investigating how overexpression and silencing of DLC1 affects invasion in 3D migration models.

4.3 Results

4.3.1 Effect of GFP-DLC1 on cell migration

DLC1 is a Rho GAP protein known to inhibit cell migration. The loss of DLC1 has been identified in several tumour types and cancer cell lines. The effect of DLC1 overexpression in cancer cell lines was investigated to evaluate the effect on migration. Wild-type (WT) parental U-87 MG cells have endogenously low DLC1, therefore these cells were used for the overexpression studies (Figure 3.1). GFP and GFP-DLC1 were transfected into the parental U-87 MG cells to assess whether overexpression affected cell migration (Video 6-7). Cells overexpressed with GFP-DLC1 were noticeably rounder compared to GFP control (Figure 4.1).

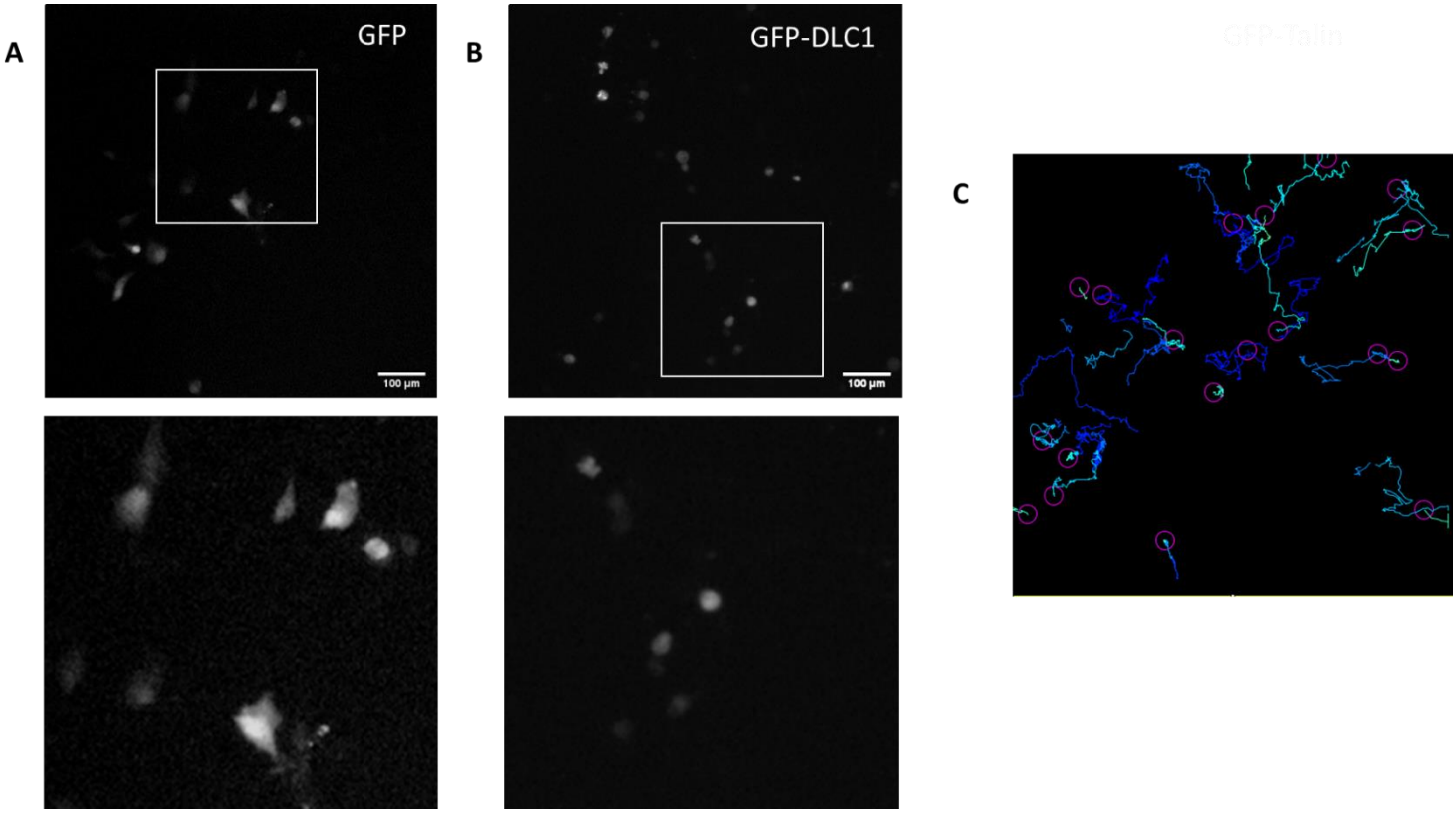

Figure 4.1: Tracking single cell migration of cells expressing GFP-DLC1. U-87 MG cells were transfected with **A** GFP control **B** GFP-DLC1 constructs**.** Images were acquired every 3 minutes for a 24 hour period using a Zeiss Axio Observer Z.1, 10x objective and 488nm fluorescence intensity. Scale bar 100µm. **C** Cells were tracked using ImageJ Trackmate plug in. N = 3.

Analysis of cell trajectories provides quantification of a variety of parameters, as a single parameter is not enough to fully describe the migration dynamics (Svensson 2018). Characteristics such as cell migration speed and the directedness of its migration path can be quantified to provide metrics that determine which biochemical and biomechanical factors affect cell migration (Loosely 2015). To investigate the effect of DLC1 on cell migration, the 'track mean speed', 'track displacement' and 'track straightness' were analysed by segmentation of the GFP-positive cells. 'Track displacement' describes the length of the shortest path between the first and final point (Figure 4.2). In isolation, this parameter can be misleading, for example in Figure 4.2, track 3 would have the shortest displacement length, but actually have a much longer track length and less straight path. Track 1 would have the furthest and most direct migration but this would be lost if only concentrating on track length. Migration could be compromised by affecting directionality (straightness) and causing the cell to migrate randomly instead of directed, increasing the track length and displacement of the tracks but not migrating as far as other cells. Therefore, using parameters in combination will allow observation of cell migration behaviour.

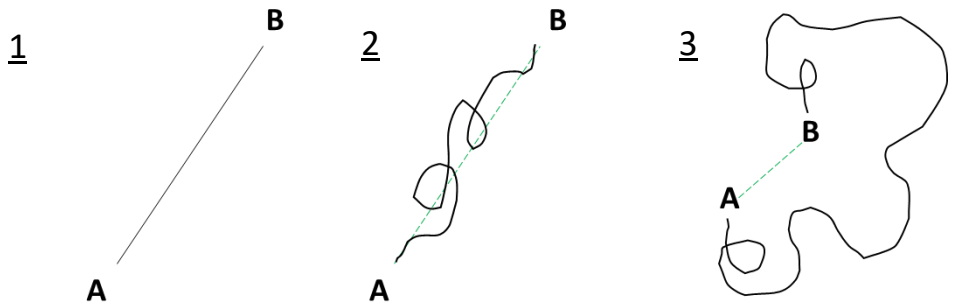

Figure 4.2: Analysing cell migration tracks allows characterisation of cell movement. Track displacement describes the length of the shortest path between the first and final point (A and B). This is shown as the green line between the second and third tracks, although this describes some movement of the cells, it does not give information about the track itself (for example straightness), therefore several other tracking parameters are needed in combination to characterise cell migration.

GFP-DLC1 overexpression significantly reduced track mean speed ($P<0.0001$, **M** = 0.616 ± 0.3 µm/min) compared to GFP control (**M** = 0.744 ± 0.3 µm/min) (Figure 4.3). Track displacement (distance between the first and last spot position) was also calculated for each condition. GFP-DLC1 significantly reduced track displacement (**M** = 32.60 ± 31.35 µm) compared to GFP control ($P<0.0001$, **M** = 52.60 ± 50.69 µm) (Figure 4.3).

To investigate the pattern of the tracks, track straightness was also calculated, the track displacement divided by the track length. There was no significant difference in track straightness between GFP-DLC1 (**M** = $4.616 \times 10^{-5} \pm 0.0001063$) and GFP control (**M** = $5.913 \times 10^{-5} \pm 9.548 \times 10^{-5}$) (Figure 4.3).

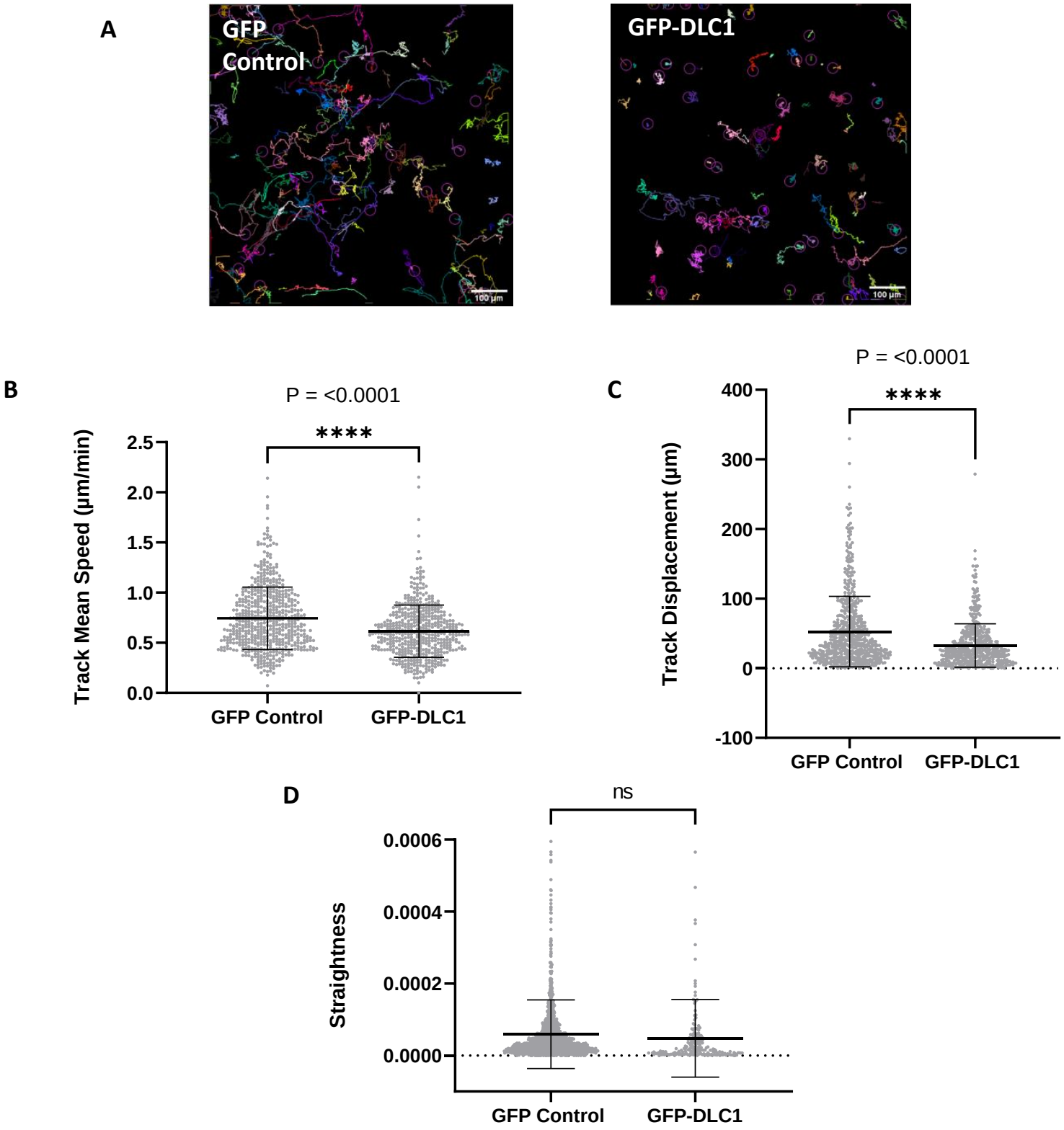

Figure 4.3: GFP-DLC1 overexpression reduces track mean speed and track displacement. U-87 MG cells were transfected with GFP control GFP-DLC1 and tracked using ImageJ Trackmate plug in. A GFP-DLC1 significantly reduces track mean speed (µm/s) compared to GFP control t (1118) = 7.434, P < 0.0001). B GFP-DLC1 significantly reduces track displacement t (1118) = 7.816, P < 0.0001). C Track straightness, the track displacement divided by the track length, was calculated for each condition. There was no significant difference between the straightness of GFP control and GFP-DLC1. N = 3.

For further insight into the different condition tracks, mean square displacement (MSD) was calculated. Mean squared displacement (MSD) is a common metric for measuring migration speed and distance travelled because it is easily interpretable and readily derived from mathematical models of motion (Loosley et al., 2015). MSD is a measure of the deviation of the position of a particle with respect to a reference position over time (Saxton and Jacobson, 1997). MSD is the sum displacement squared for each time point, and can determine more information about modes of movement. Several modes of motion have been observed: immobile, directed, confined, tethered, normal diffusion, and anomalous diffusion. The time dependence of the MSD for pure modes of motion is much different so the motion can be classified readily (Figure 4.4) (Saxton and Jacobson, 1997). The type of diffusion can be calculated from the pattern of the MSD plot, if the diffusion coefficient is equal to 1, this indicates the cells are moving randomly without direction. If the plot shows an increasing slope ($D > 1$), this indicates a more directed 'super diffusion' motion, whereas $D < 1$ shows sub-diffusion. A plateaued MSD plot indicates confined diffusion, where a particle is restricted/tethered as indicated in Figure 4.4. Whilst track displacement only provides information about the beginning and the end of the track, MSD measures how particles move over time and whether the particles are moving due to diffusion or other forces (Michalet, 2010).

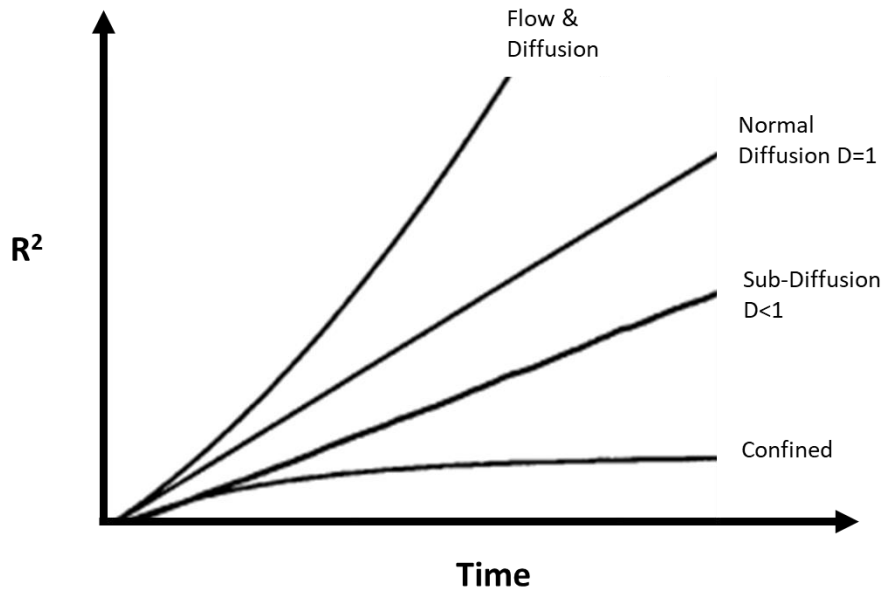

Figure 4.4: MSD plots to classify cell trajectories. Schematic showing the MSD (r^2) versus time for different particle movements, flow and diffusion, normal diffusion, sub diffusion and confined. The MSD can be analysed for each cell trajectory and self-diffusion coefficient (D) can be calculated to describe cell tracks. Figure adapted from (Saxton and Jacobson, 1997).

The MSD was plotted for both GFP and GFP-DLC1 tracks using an opensource tool, msdanalyser. This tool can calculate the MSD of multiple trajectories and calculates the average MSD for each condition (black linear line), the grey area depicts the range of MSD in the sample. A representative sample was plotted for GFP and GFP-DLC1, the trajectories of the samples are also shown (Figure 4.5). The diffusion-like coefficients were also calculated for each replicate, with GFP-DLC1 having a statistically decreased diffusion coefficient ($P > 0.05$, **M** = 1.81 ± 2.2 µm/min) compared to GFP (**M** = 7.22 ± 1.4 µm/min). As the diffusion coefficient of each condition was over 1, this suggests super diffusion motion, with GFP-DLC1 having reduced motion compared to GFP control.

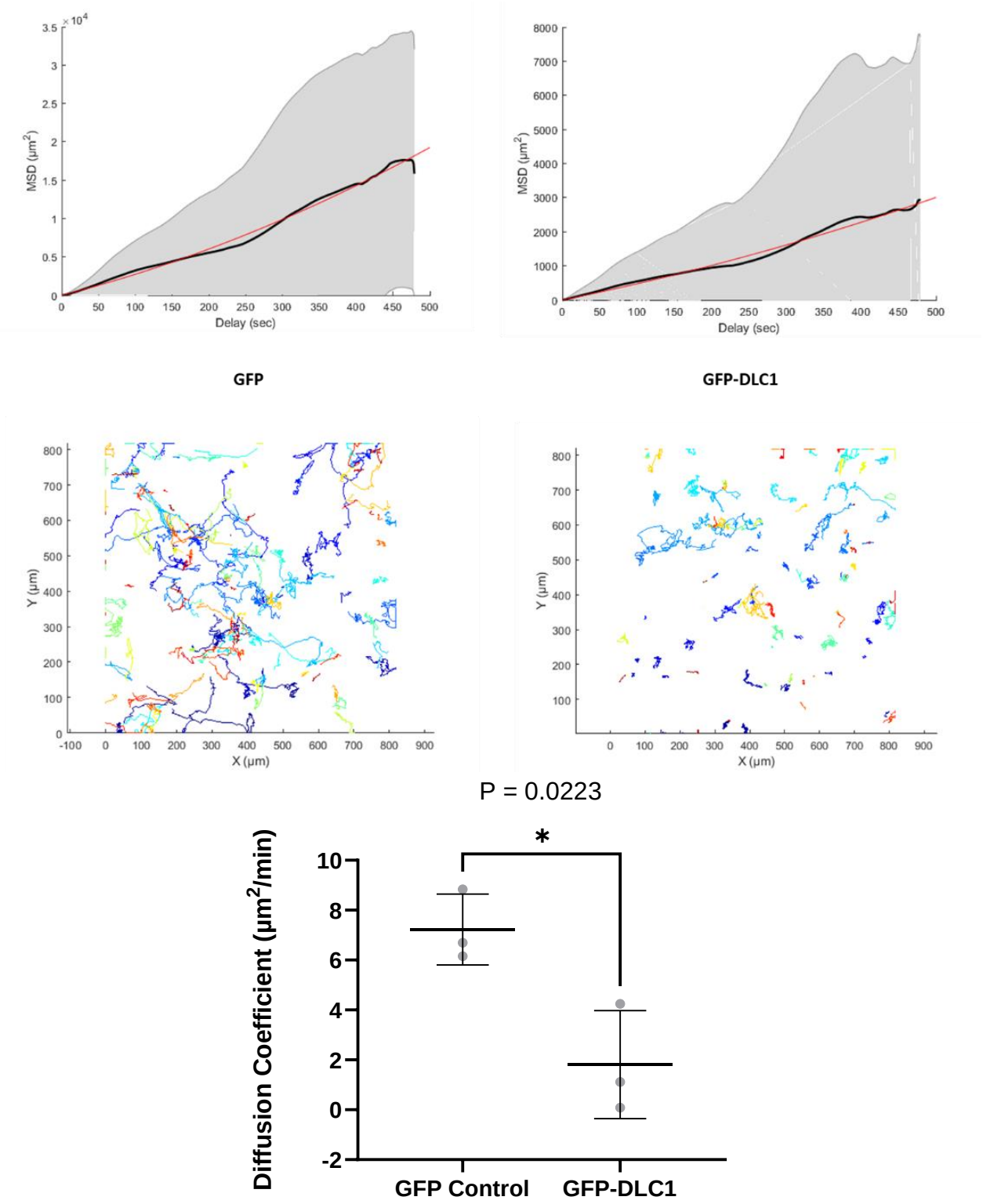

Figure 4.5: GFP-DLC1 reduces track mean square displacement. U-87 MG cells were transfected with GFP control GFP-DLC1 and GFP-talin constructs and tracked using ImageJ Trackmate plug in. Mean square displacement was calculated for each condition, and an example graph from each replicate is shown. The diffusion coefficient (D) (um^2/sec) was calculated for each rate, GFP-DLC1 tracks had an increased diffusion coefficient compared to GFP control, $t(4) = 3.622$, $P < 0.05$. A trajectory plot is also shown for the representative plot. N = 3.

4.3.2 Effect of DLC1 and talin co-expression on cell migration

As both DLC1 and talin had both an individual effect on cell migration, we next investigated the impact of co-expression of both proteins on cell migration (Figure 4.6, Video 8-9).

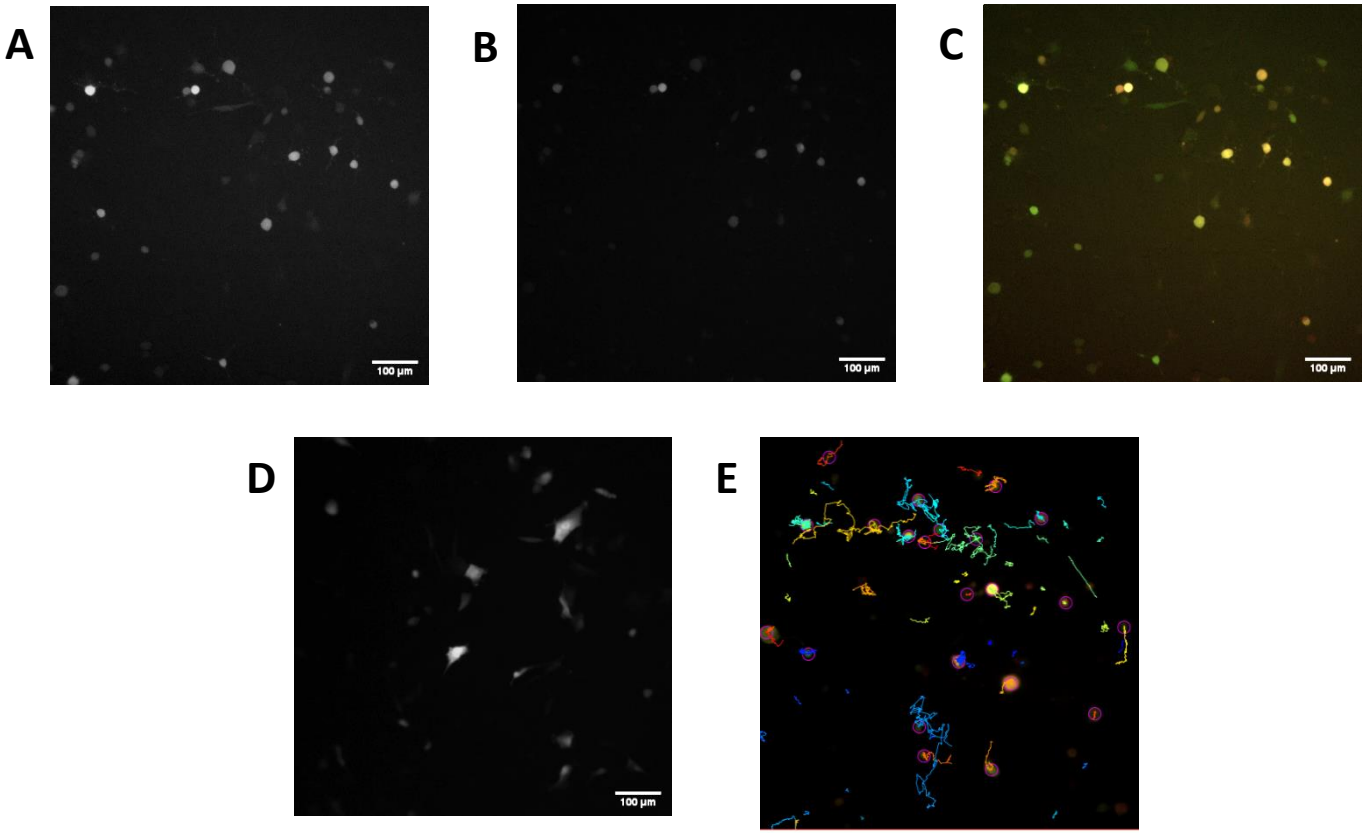

Figure 4.6: Co-expression of GFP-talin and mRuby-DLC1 and effect on cell migration. U-87 MG cells were co-transfected with **A** GFP-talin and **B** mRuby-DLC1 **C** Merge. **D** A GFP control was also transfected into cells. Images were acquired every 3 minutes for a 24-hour period using a Zeiss Axio Observer Z.1, 10x objective with 488nm and 561nm fluorescence intensity. Scale bar 100µm. **E** Cells were tracked using ImageJ Trackmate plug in. For co-expressed cells, cells were filtered to include fluorescence intensity of both 488nm and 561nm channels. N = 3.

A GFP construct was also transfected as a control. Track mean speed was calculated for both conditions, and there was no significant difference between the GFP control (**M** = 0.664 ± 0.3

μm/s) and co-expressed GFP-talin and mRuby-DLC1 (**M** = 0.665 ± 0.3 μm/s) (Figure 4.7). The presence of GFP-talin and mRuby-DLC1 significantly reduced track displacement (**M** = 44.81 ± 51.88 μm) compared to GFP control ($P < 0.05$, **M** =51.67 ± 58.15 μm) (Figure 4.7).

Straightness was also calculated for co-expressed GFP-talin and mRuby-DLC1 and GFP control. There was a significant difference between co-expressed GFP-talin and mRuby-DLC1 ($P = 0.0001$, **M** = 7.804 $x10^{-5}$ ± 0.0001057) and GFP control (**M** = 9.549 $x10^{-5}$ ± 0.0001560) (Figure 4.7). The tracks of co-expressed talin and DLC1 were less straight.

MSD was also calculated for GFP-talin and mRuby-DLC1 and representative plots are shown in Figure 4.8, the diffusion coefficient of GFP-talin and mRuby-DLC1 was significantly reduced ($P > 0.05$, **M** = 0.201 ± 0.2 μm^2/min) compared to GFP alone (**M =** 4.63 ± 2 μm^2/min). This implies that GFP-talin and mRuby-DLC1 tracks had sub-diffusion motion compared to GFP control.

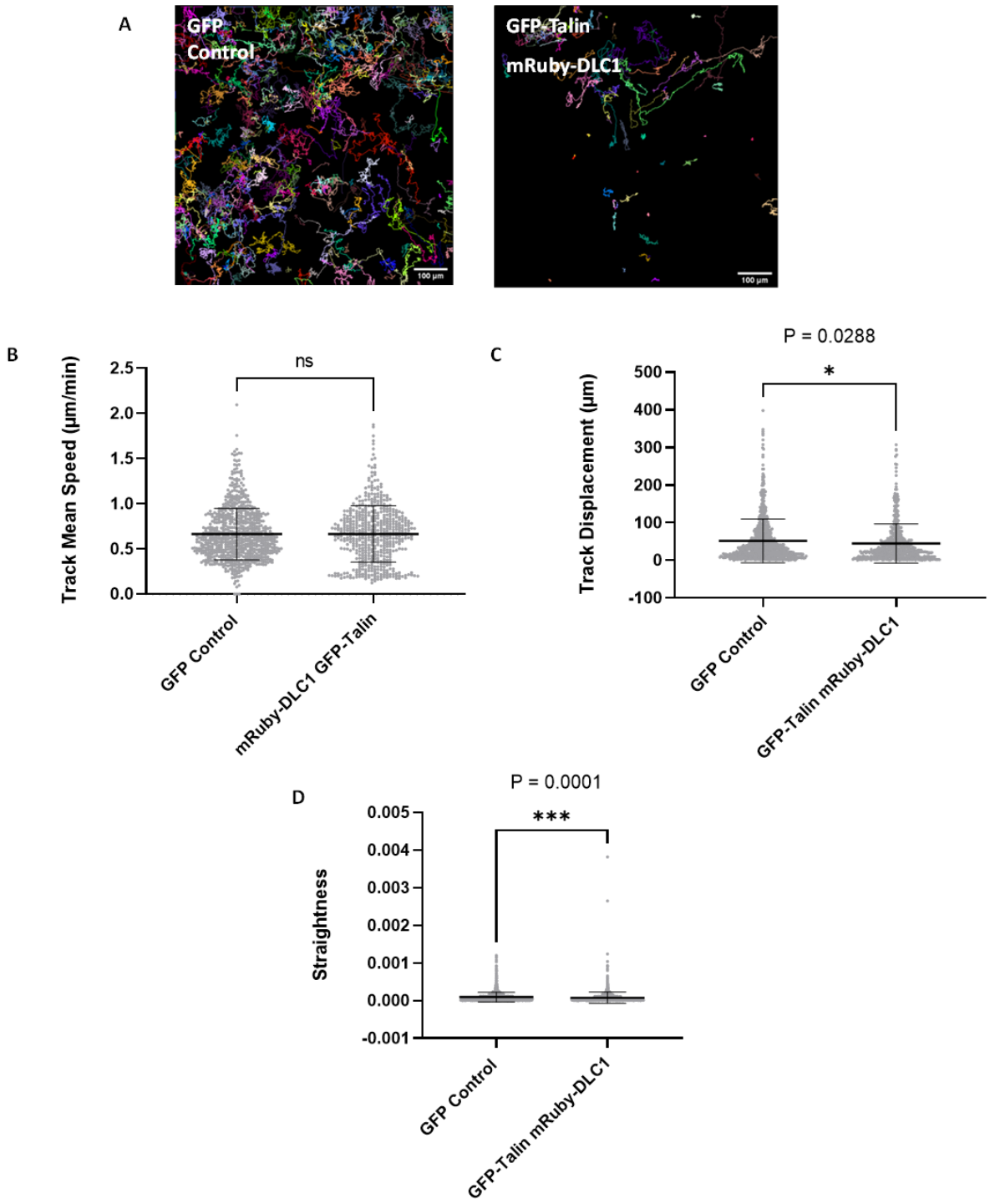

Figure 4.7: GFP-talin and mRuby-DLC1 co-expression reduces track displacement and straightness but does not affect track speed. U-87 MG cells were transfected with GFP control or combined GFP-talin and mRuby-DLC1. Cells were tracked using ImageJ Trackmate plug in. A There was no significant difference between GFP control and GFP-talin and mRuby-DLC1 co expression on track speed. B GFP-talin and mRuby-DLC1 co expression significantly reduced track displacement compared to GFP control t (1290) = 2.189, $P < 0.05$ C Straightness was significantly reduced by GFP-talin and mRuby-DLC1 co expression, t (3913) = 3.879, $P < 0.0001$). N = 3.

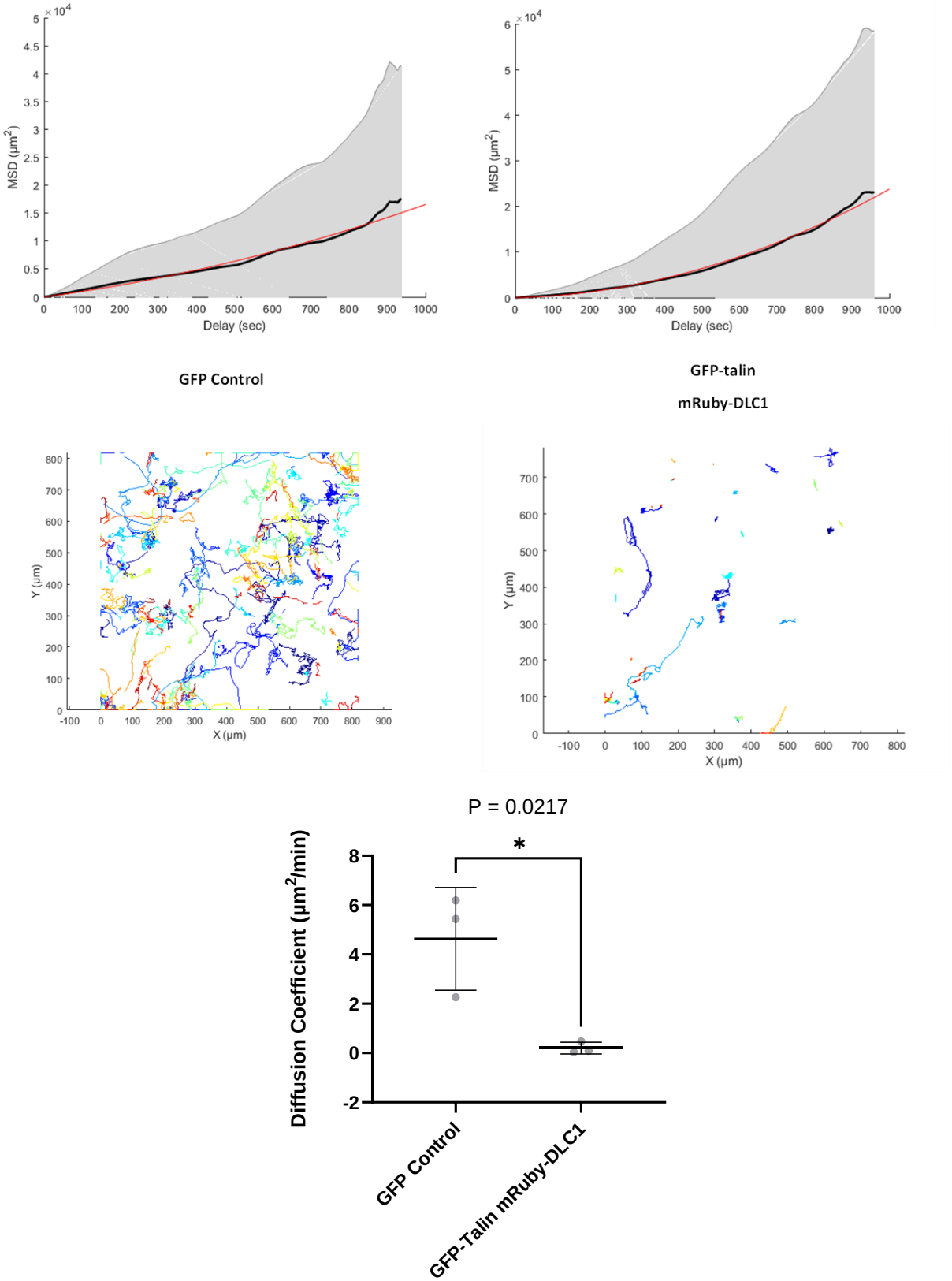

Figure 4.8: GFP-talin and mRuby-DLC1 reduces MSD of tracks. U-87 MG cells were transfected with GFP control or combined GFP talin and mRuby DLC1. Cells were tracked using ImageJ Trackmate plug in. Mean square displacement was calculated for each condition, and an example graph from each replicate is shown. The diffusion coefficient (um^2/sec) was calculated for each condition, GFP-Talin mRuby DLC1 was significantly reduced compared to GFP control, $t(4) = 3.653$, $P < 0.05$). A trajectory plot is also shown for the representative plot. N = 3.

4.3.3 Effect of DLC1 silencing on cell migration

To continue investigation into DLC1's effect on cell migration, DLC1 was silenced in HepG2 cells. In the previous chapter, WT HepG2 cells were shown to have the highest DLC1 levels, amongst the lines tested, making them suitable for knockdown experiments. siRNA DLC1 and siRNA scrambled control were transfected into HepG2 cells and the cells were then lysed at 24, 48 and 72 hours. An untransfected control was also included. DLC1 expression level was probed using western blotting and DLC1 was detectable at all timepoints in both the control and scrambled siRNA samples, but no band was observed in any of the cells transfected with siRNA targeting DLC1 at any of the timepoints, making it suitable for a 24 hour knockdown cell migration experiments (Figure 4.9).

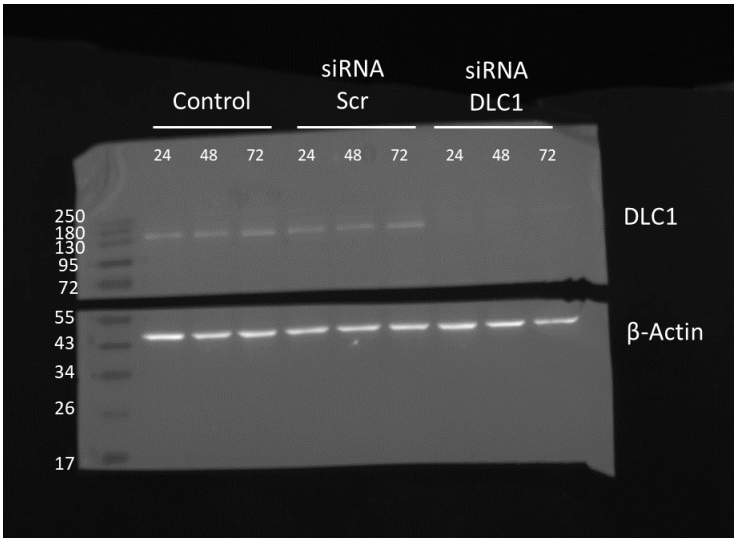

Figure 4.9 siRNA knockdown of DLC1. HepG2 cells were transfected with 10µM siRNA scrambled control and 10µM siRNA DLC1 constructs. An untransfected control was also included. Each condition was collected at 24, 48 and 72 hours and probed for DLC1 using western blotting (anti-DLC1, BD Biosciences, 1:500). DLC1 was detectable at all timepoints in both control and scrambled siRNA samples, but not detectable in all siRNA DLC1 timepoints.

HepG2-H2B-RFP cells were transfected with siRNA DLC1, siRNA scrambled control or left untransfected as a control (Video 10 – 12). Nuclear marker H2B was used as a tracking control in all conditions. Track mean speed, track displacement, straightness and MSD were calculated.

There was no difference in track mean speed between siRNA DLC1 (**M** = 0.304, ± 0.2 µm/min) and siRNA scrambled control (**M** = 0.294 ± 0.2 µm/min) (Figure 4.10).

Surprisingly, siRNA DLC1 had significantly reduced track displacement ($P<0.001$, **M** = 8.115 ± 8.877 µm) compared to siRNA scrambled control (**M** = 9.477 ± 16.80 µm) (Figure 4.10). The HepG2 cells within the silencing model had less displacement than the U-87 MG cells in the overexpression model, highlighting how variable migration is between two different cell types.

Track straightness was also calculated, siRNA DLC1 tracks (**M** = $1.17x10^{-5}$ ± $3x10^{-5}$) were significantly less straight than siRNA control tracks ($P<0.0001$), **M** = $2.5x10^{-3}$ ± $4x10^{-3}$) (Figure 4.10).

MSD was also calculated, with representative MSD and trajectory plots (Figure 4.11). The diffusion coefficient was calculated, and whilst siRNA DLC1 had the lowest displacement (**M** = 0.113 ± 0.04 μm^2/min) compared to siRNA scrambled control (**M** = 0.233 ± 0.08 μm^2/min) and H2B control (**M** = 0.576 ± 0.5 μm^2/min), there was no significant difference.

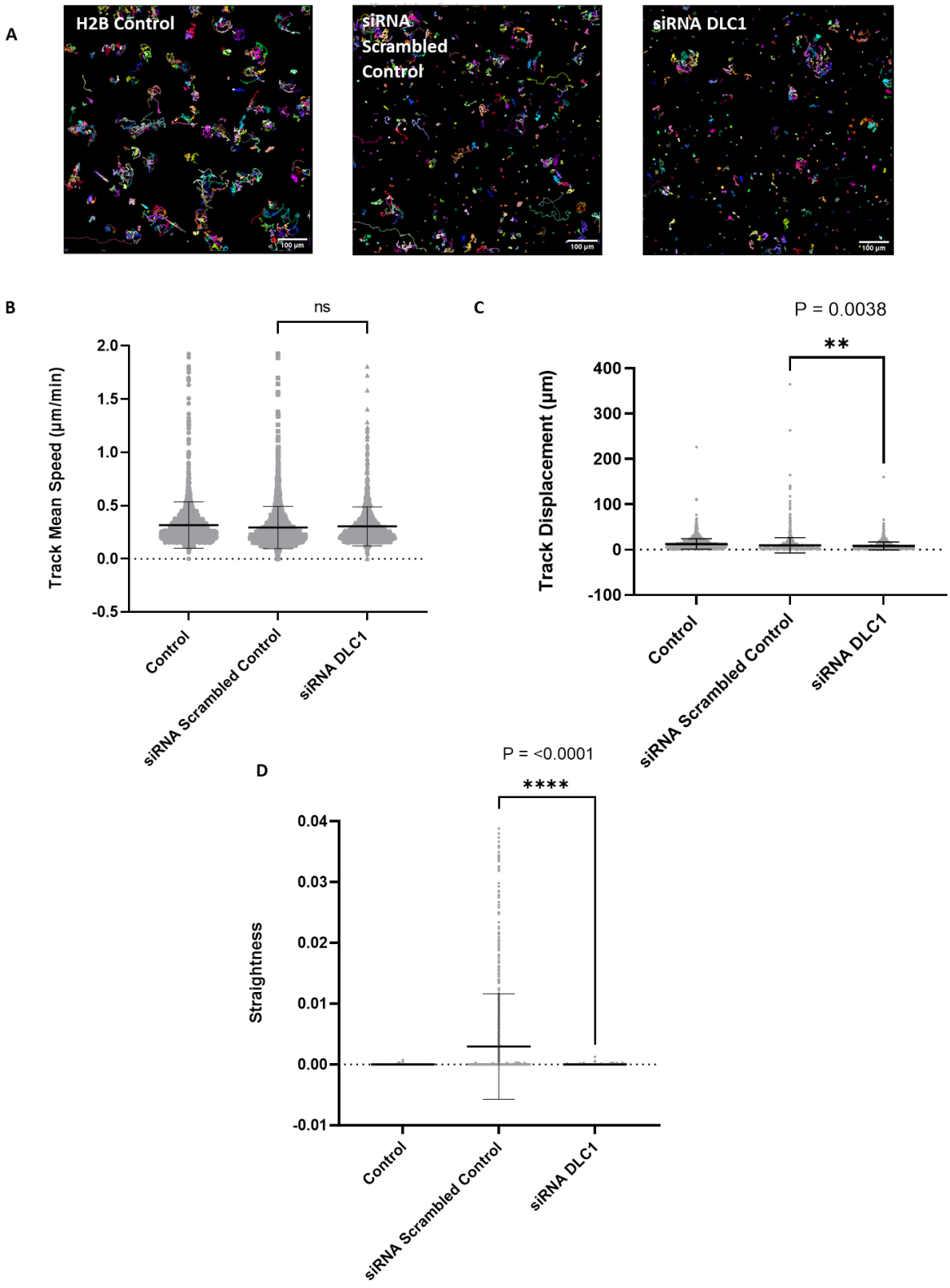

Figure 4.10: siRNA DLC1 reduces displacement and straightness. HepG2-H2B-RFP cells were transfected with siRNA DLC1 or siRNA scrambled control and tracked using ImageJ Trackmate plug in. Untransfected cells were also used as a control. **A** There was no significant difference in mean track speed between siRNA DLC1 and scrambled control. **B** siRNA DLC1 significantly reduced track displacement compared to siRNA scrambled control $t(6013) = 21.24$, $P < 0.0001$. **C** siRNA DLC1 tracks were less straight than siRNA scrambled control, $t(3338) = 2.9$, $P < 0.01$. $N = 3$.

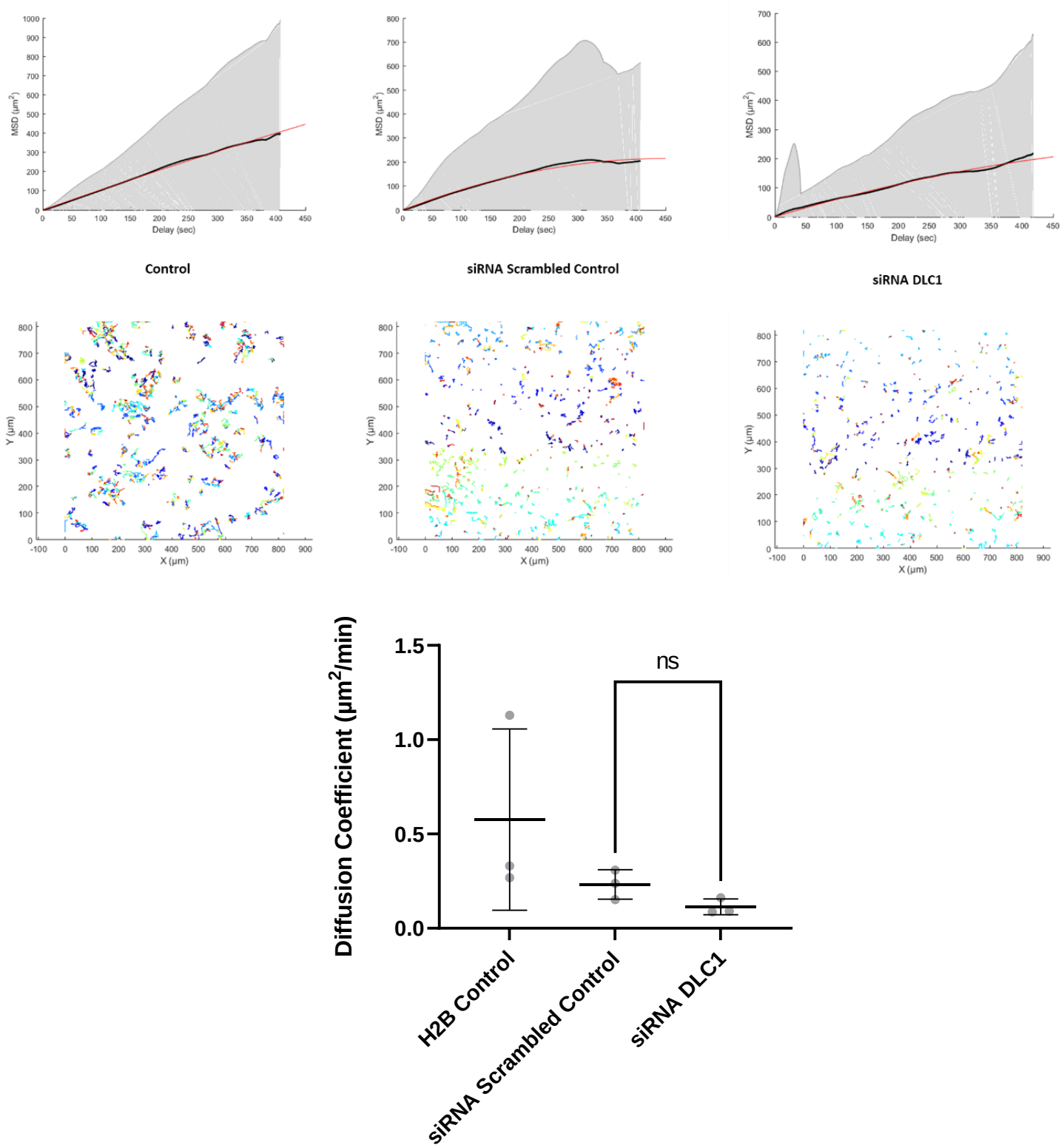

Figure 4.11: siRNA DLC1 had no effect on track mean square displacement. HepG2-H2B-RFP cells were transfected with siRNA DLC1 or siRNA scrambled control and tracked using ImageJ Trackmate plug in. Untransfected cells were also used as a control. Mean square displacement was calculated for each condition, and an example graph from each replicate is shown. The diffusion coefficient (um^2/sec) was calculated for each condition but there was no significant difference between siRNA DLC1 AND scrambled siRNA control. N = 3.

4.3.4 Using 3D migration assays to assess DLC1's role within migration

2D assays can be problematic when investigating cell migration as they have limited physiological relevance due to migration over a plastic/glass surface and the absence of an ECM, an important influencer of cell migration (Frantz et al., 2010, Heinrich et al., 2019). Recently cell migration assays have moved to 3D to better mimic conditions seen *in vivo*, however, this can be extremely complicated due to increased complexity of the model. As the 3D models become more complex, they can be harder to produce, replicate and analyse (Jensen and Teng, 2020, Jensen et al., 2022).

To investigate the effect of DLC1 in 3D cell migration a circular invasion assay (CIA) was used (Yu and Machesky, 2012). The circular invasion assay allows cells to be plated on glass similar to 2D, but the addition of Matrigel on top and around the cells allows interaction with the components of the ECM (Figure 4.12 - A). A ibidi insert is placed into the middle of the dish, with cells plated around it. This creates space, and when the insert is removed matrigel is added to the whole dish, creating a layer within the central empty space and on top and around the plated cells. This allows cells to invade into the empty space filled with matrigel. The CIA is a more physiological and straightforward assay, which allows more of a 2D/3D hybrid before moving to models fully embedded in matrigel (Yu and Machesky, 2012). The rationale was that introducing the ECM to the current assay would allow a gradual build-up of complexity, and the ability to assess how adding an ECM would affect DLC1'S role within cell migration.

U-87 MG cells stably expressing H2B-RFP were plated in glass dishes and transfected with GFP-DLC1. Untransfected cells were used as a control as the nucleus was already labelled for analysis.

Cells were imaged over a period of 24 hours, and invasion of the cells into the empty space was visualised (Figure 4.12 B – C, Video 13 - 14).

As before, the track displacement and track mean speed were calculated by ImageJ plugin Trackmate. GFP-DLC1 overexpression significantly reduced mean track speed (**M** = 0.61 ± 0.2 µm/min) compared to the control ($P < 0.0001$, **M** = 0.97 ± 0.4 µm/min) (Figure 4.13). Similarly, GFP-DLC1 significantly reduced track displacement (**M** = 45.03 ± 46.57 µm) compared to the H2B control ($P < 0.0001$, **M** = 68.82 ± 68.34 µm) (Figure 4.13).

Straightness was also calculated for each condition. GFP-DLC1 significantly increased track straightness (**M** = 9.891×10^{-5} ± 0.0005) compared to H2B control (P = <0.0001, **M** = 4.080×10^{-5} ± 5.787×10^{-5}). For further investigation of the tracks, **M**SD was calculated for GFP-DLC1 and GFP control, with representative plots and trajectories shown (Figure 4.14). The diffusion coefficient (µm^2/sec) was significantly reduced for GFP-DLC1 ($P < 0.01$, **M** = 4.226 ± 1.05 µm^2/min) compared to GFP control (**M** = 20.82 ± 15.13 µm²/min), suggesting GFP-DLC1 decreases cell movement over time.

Taken together, these results mimic the 2D assay observations, excluding the straightness, which is increased in the CIA assay. DLC1 expression reduces track displacement, MSD and track mean speed.

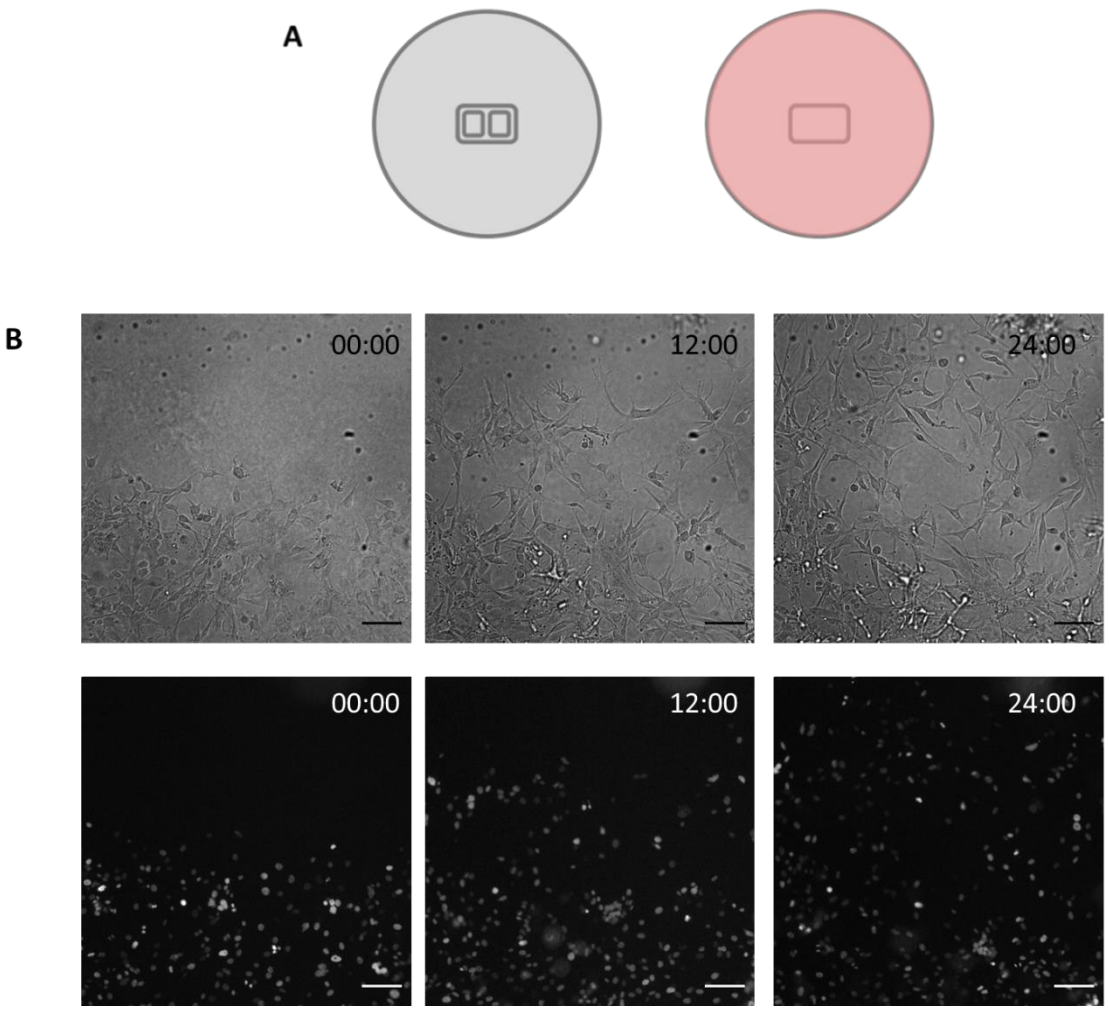

Figure 4.12: Set up of the circular invasion assay to measure DLC1's affect on migration. A U-87 MG -H2B-RFP cells were plated in glass dishes around ibidi dish insert and left overnight. The insert was removed, leaving empty space in the middle of the dish. A layer of media and Matrigel mix was then added on top of cells. This was left to set for 2 hours with additional media added. Cells were imaged every 3 minutes over 24 hours as they invaded into the space using a Zeiss Axio Observer Z.1, 10x objective with brightfield and 561nm fluorescence intensity. **B** Brightfield image of cells invading **C** 561nm channel showing U-87 MG -H2B-RFP cell invading.

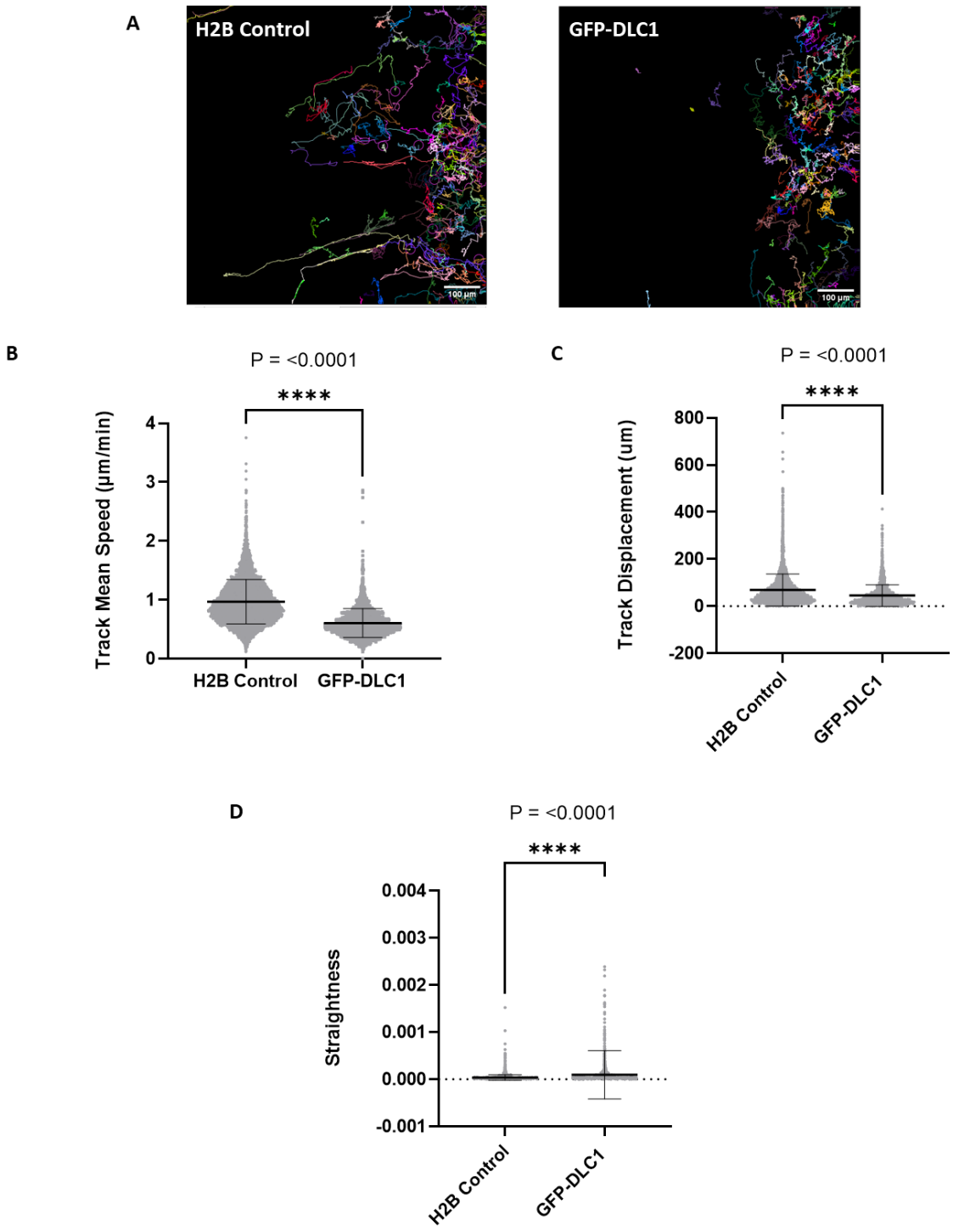

Figure 4.13: GFP-DLC1 reduces track displacement and speed in CIA assay, but increases track straightness. U-87 MG -H2B-RFP cells were plated in the CIA assay and transfected with GFP-DLC1 or left untransfected as a control. Cells were tracked using ImageJ Trackmate plug in. **A** GFP-DLC1 significantly reduced track mean speed compared to the GFP control two-tailed t-test, t (6641) = 37.66, P < 0.0001). **B** GFP-DLC1 significantly reduced track displacement compared to the GFP control, two-tailed t-test, t (6641) = 13.55, P < 0.0001. **C** GFP-DLC1 significantly increased track straightness compared to the GFP control, two-tailed t-test, t (9319) = 8.353, P = <0.0001. N = 3.

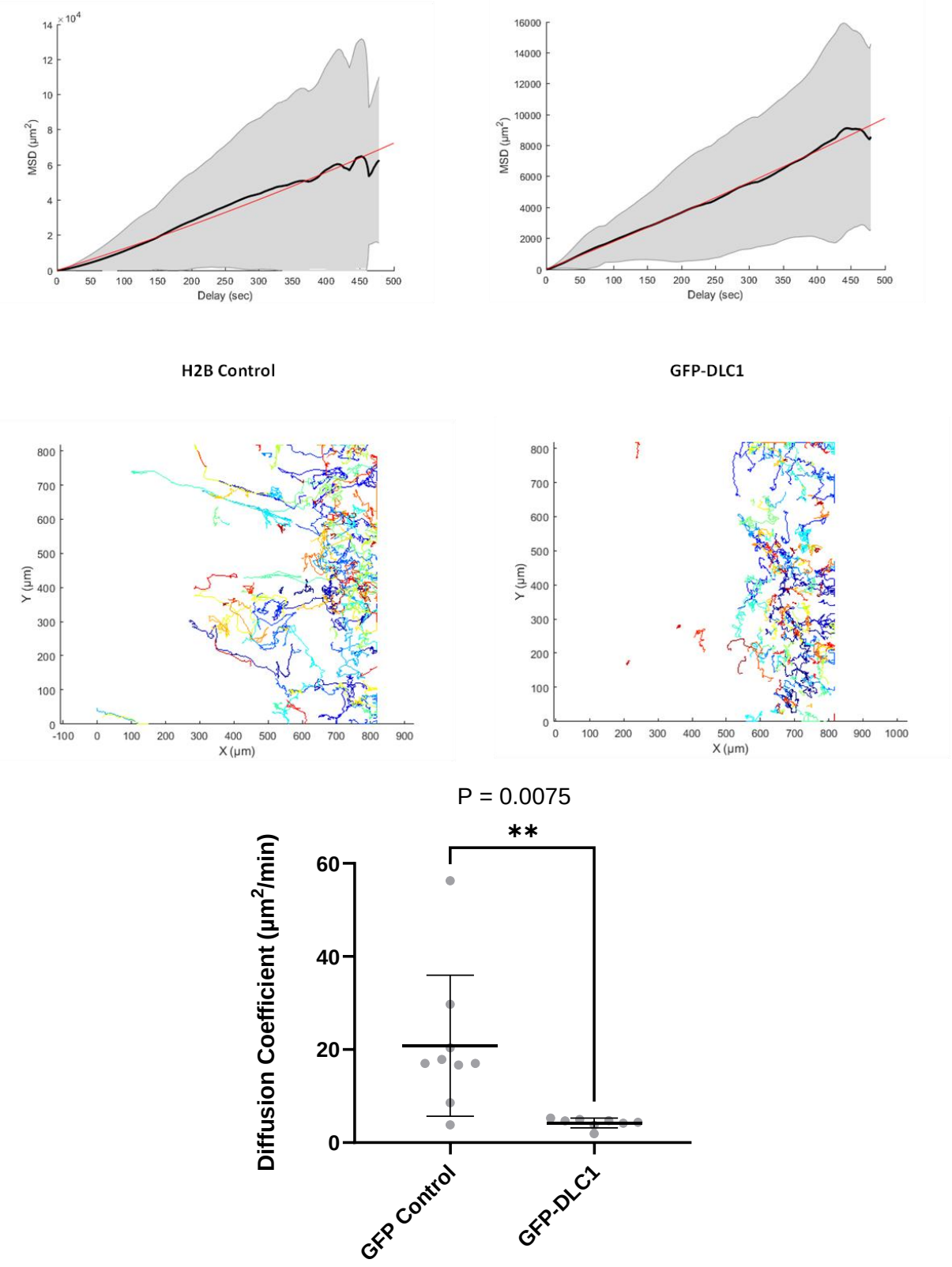

Figure 4.14: GFP-DLC1 reduces MSD in CIA assay. U-87 MG -H2B-RFP cells were plated in the CIA assay and transfected with GFP-DLC1 or left untransfected as a control. Cells were tracked using ImageJ Trackmate plug in. The diffusion coefficient (um^2/sec) was calculated for each condition, and an example graph and trajectory from each replicate is shown. GFP-DLC1 significantly decreased the diffusion coefficient compared to the GFP control, two-tailed t-test, t (15) = 3.085, P = < 0.01. N = 3.

Next, DLC1 knockdown experiments were performed to evaluate how loss of DLC1 affects cell invasion. A CIA assay was performed with siRNA targeting DLC1 transfected into HepG2-H2B-RFP cells and compared to untransfected and scrambled siRNA controls (Video 15 – 17).

DLC1 siRNA significantly increased track mean speed ($P<0.0001$, **M** = 0.228 ± 0.2 μm/min) compared to the scrambled siRNA control (**M** = 0.203 ± 0.08 μm/min) (Figure 4.15). There was a small but significant difference between the two conditions.

DLC1 siRNA significantly reduced track displacement ($P<0.0001$, **M** = 9.933 ± 8.581 μm), compared to the scrambled siRNA (**M** = 11.68 ± 10.19 μm) (Figure 4.15). This result is consistent with what was seen in the 2D cell migration experiments, where siRNA DLC1 also had a small reduction in track displacement (Figure 4.10).

Straightness was also calculated and siRNA DLC1 tracks were significantly straighter ($P<0.0001$ **M** = $3.965\times10^{-5} \pm 6.507\times10^{-3}$) than the siRNA scrambled control tracks (**M** = $4.3060^{-6} \pm 1.328\times10^{-5}$) (Figure 4.15). This suggests when DLC1 is lost, the migratory paths are straighter, which could be interpreted as more directed migration.

For more information on the track displacement, MSD was calculated for the siRNA experiments, with representative MSD and trajectories plotted (Figure 4.16). The diffusion coefficient (μm^2/min) was significantly reduced in siRNA DLC1 ($P<0.01$, **M** = 0.170 ± 0.03 μm^2/min) compared to siRNA scrambled control (**M** = 0.209 ± 0.02 μm^2/min). As the diffusion coefficients were less than 1, which suggests sub-diffusion.

In conclusion, in the CIA assay, siRNA DLC1 increases track speed and straightness but reduces displacement and MSD. The reduced displacement is surprising as the hypothesis was that without DLC1, migration would be increased. However this same phenomenon was also observed in the 2D assays. In the 2D assays siRNA DLC1 showed no effect on cell speed but reduced straightness.

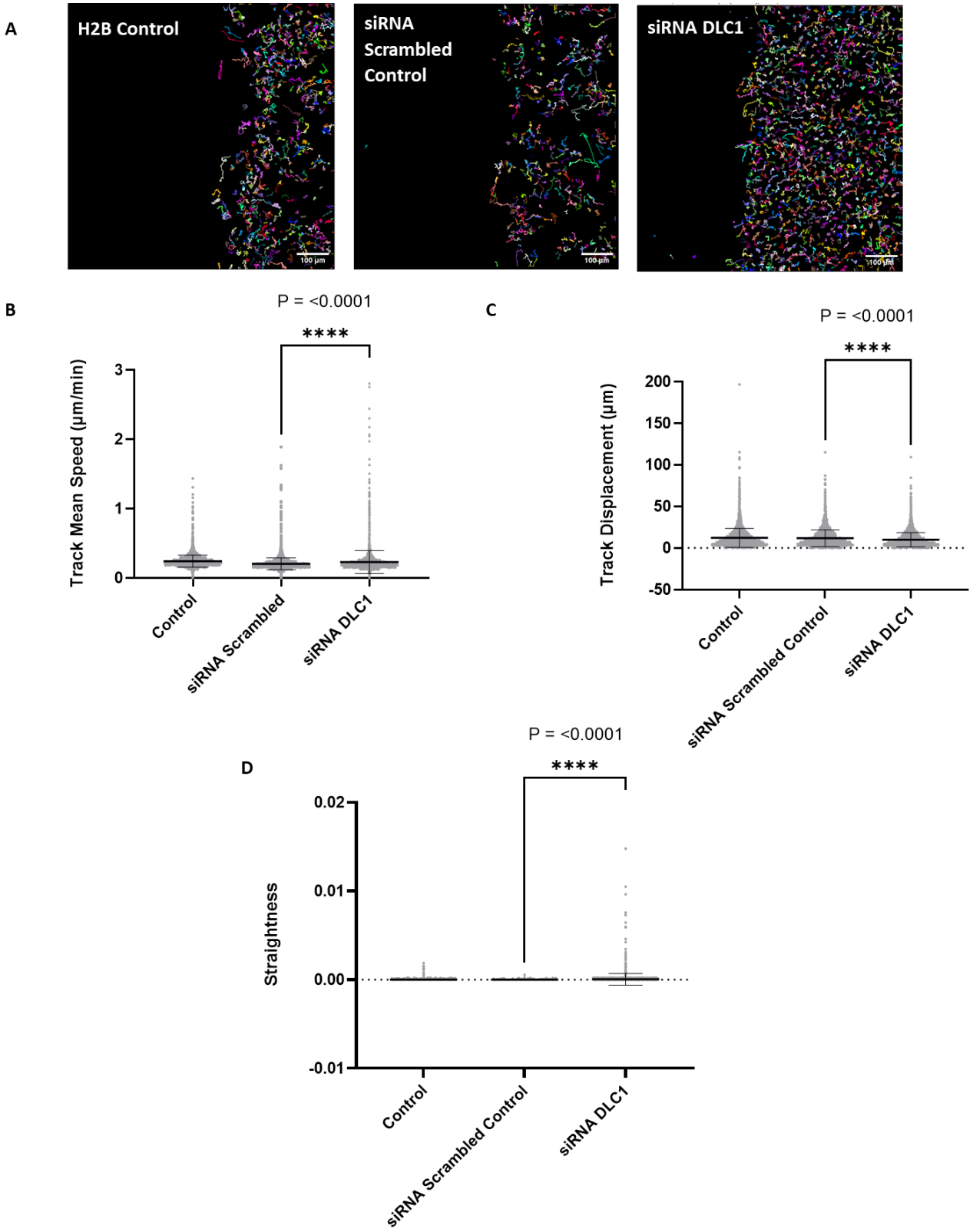

Figure 4.15: siRNA DLC1 increases track cell speed and straightness but reduces track displacement in CIA assay. HepG2-H2B-RFP cells were plated in the CIA assay and transfected with siRNA DLC1 or siRNA scrambled control. Cells were tracked using ImageJ Trackmate plug in. **A** siRNA DLC1 significantly increased track mean speed compared to the siRNA scrambled control, $t(13500) = 10.61$, $P < 0.0001$. **B** siRNA DLC1 significantly reduced track displacement compared to siRNA scrambled control, $t(13500) = 10.82$, $P < 0.0001$. **C** siRNA DLC1 increased track straightness compared to siRNA scrambled control $t(33572) = 4.662$, $P < 0.0001$. N = 3.

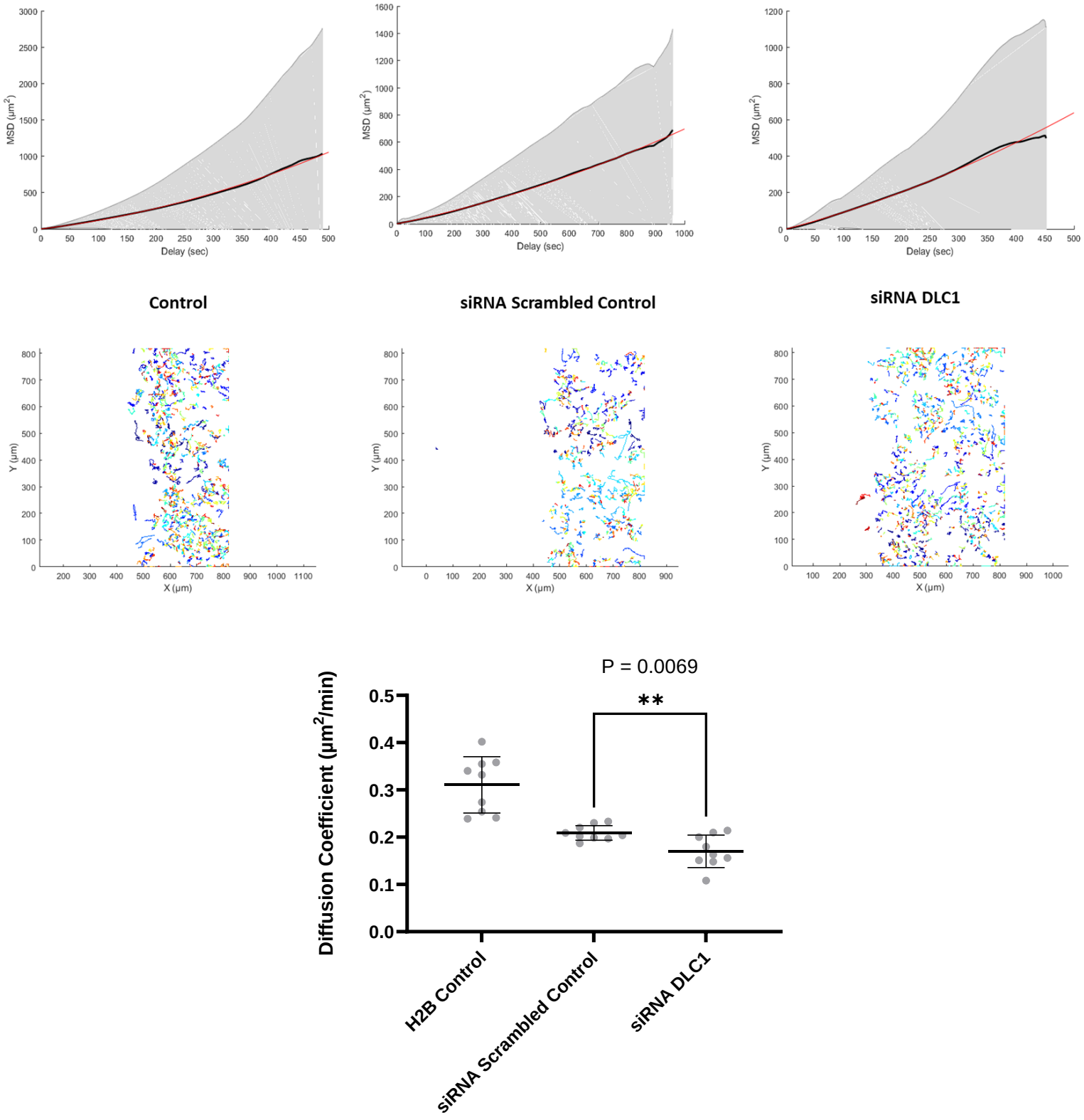

Figure 4.16: siRNA DLC1 significantly reduces MSD in CIA assay. U-87 MG -H2B-RFP cells were plated in the CIA assay and transfected with GFP DLC1 or left untransfected as a control. Cells were tracked using ImageJ Trackmate plug in. Mean square displacement was calculated for each condition, and an example graph and trajectory from each replicate is shown. The diffusion coefficient was significantly reduced in DLC1 siRNA compared to scrambled siRNA control and control cells two-tailed t-test, t (16) = 3.098, P = < 0.01. N = 3.

4.3.5 Effect of GFP-DLC1 overexpression in 3D spheroid cell invasion

After investigating the role of DLC1 in cell migration using 2D and CIA assays, the next step was to progress to the use of 3D spheroid invasion assays. Although the CIA assay included the presence of the ECM, cells were still grown on 2D surfaces. Spheroid assays are one of the most widely used 3D models, where cells are in a more physiological environment. Using the spheroid model allows the cells to invade into a 3D matrix. It is widely reported that 3D cell migration differs compared to 2D, and the effect of DLC1 within live 3D invasion is still unknown. U-87 MG-H2B cells were cultured as spheroids, embedded in matrigel and mounted onto a lightsheet microscope for live 3D imaging (Figure 4.17).

To investigate the effect of DLC1 overexpression on invasion, cells were transfected with GFP-DLC1 as they formed spheroids. GFP-DLC1 -transfected cells were visible in the spheroid, and they were imaged for 16 hours as they were migrating into the surrounding matrigel (Figure 4.18, Video 18 - 19). Track displacement, straightness and speed was calculated for each condition and GFP-DLC1 expressing cells were compared to untransfected cells within the same spheroid (Figure 4.17). All the tracks of the spheroid were analysed, including cells on the edge and inside. The data files produced by lightsheet microscopy are very large, therefore the spheroid data was analysed using IMARIS software, which is designed for large 3D datasets.

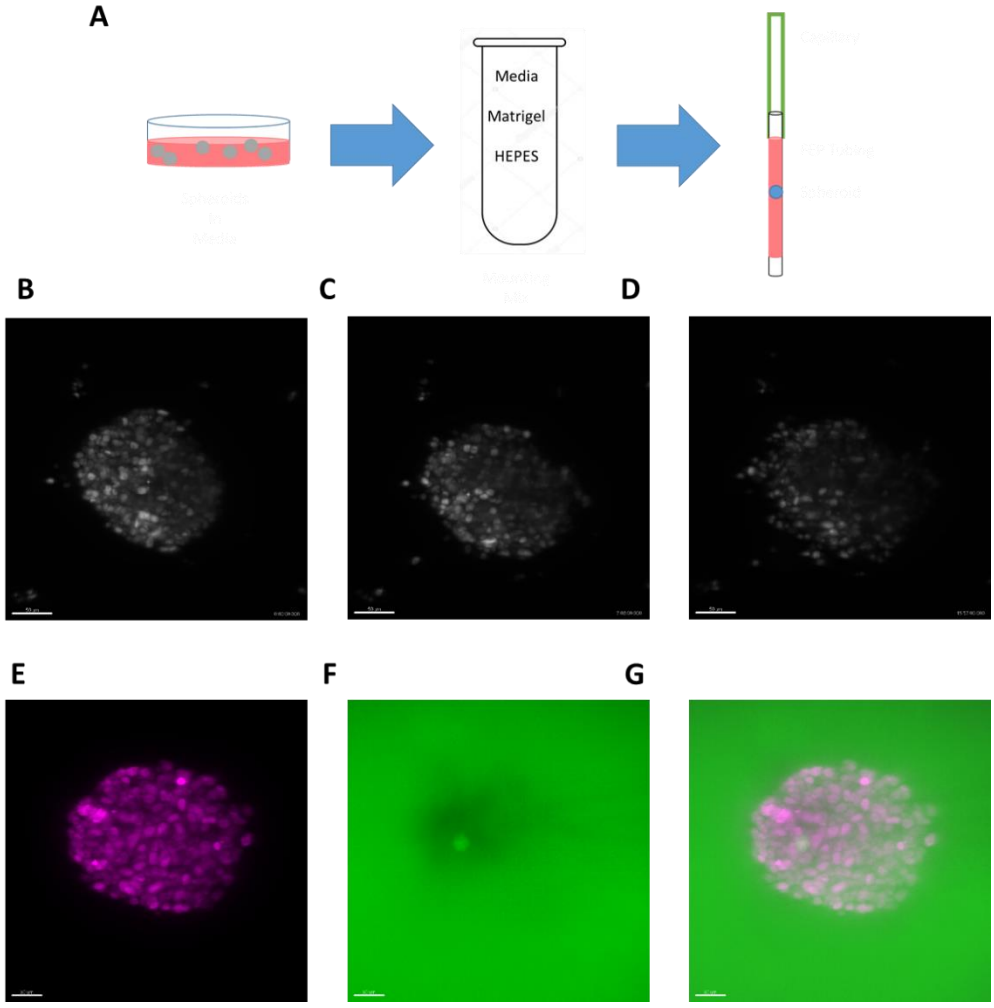

Figure 4.17: U-87 MG -H2B-RFP spheroid generation. **A** U-87 MG -H2B-RFP cells were plated in a Sphericalplate5D and formed spheroids after 24 hours. Spheroids were collected and then mounted into a capillary containing a mix of media, matrigel and HEPES. The capillary was then mounted onto a Zeiss Z.1 lightsheet microscope . **B** After mounting, spheroids were imaged at 20x using 568nm laser every 3 minutes. **C** Spheroid after 7 hours of imaging. **D** Spheroid after 16 hours. **E** U-87 MG -H2B-RFP spheroid embedded in matrigel at T0. **F** Matrigel identified with Dextran 488 dye, shadow showing position of spheroid. **G** Merge image of mounted spheroid in matrigel stained with Dextran. Scale bar 50µM.

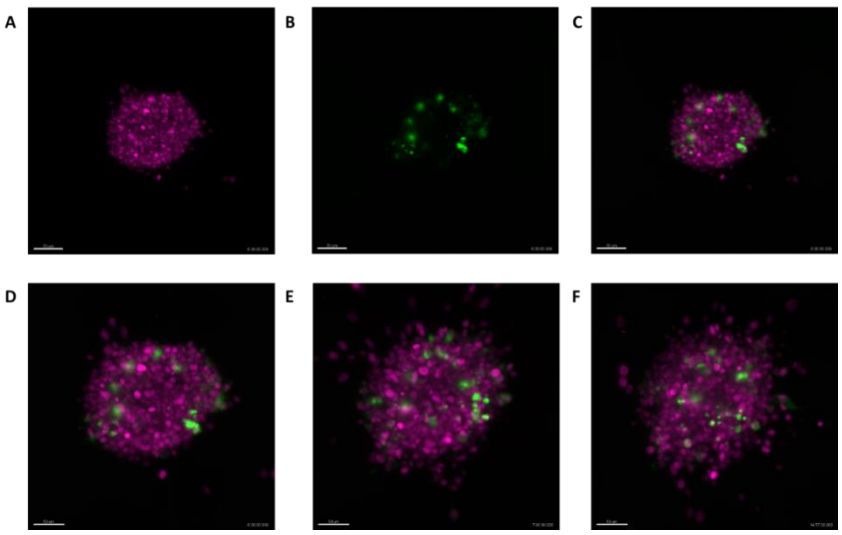

Figure 4.18: Transfection of GFP DLC1 into spheroids. As U-87 MG -H2B-RFP cells were plated in a Sphericalplate5D, they were transfected with GFP-DLC1. Spheroids were mounted onto a Zeiss Z.1 lightsheet microscope and imaged at 20x and illuminated with 488nm and 561nm lasers. **A** H2B-RFP **B** GFP-DLC1 **C** Merge of channels. Spheroids were imaged every 3 minutes for 16 hours. **D** Spheroid at 3 hours **E** 7 hours **F** 15 hours. Scale bar 50µM.

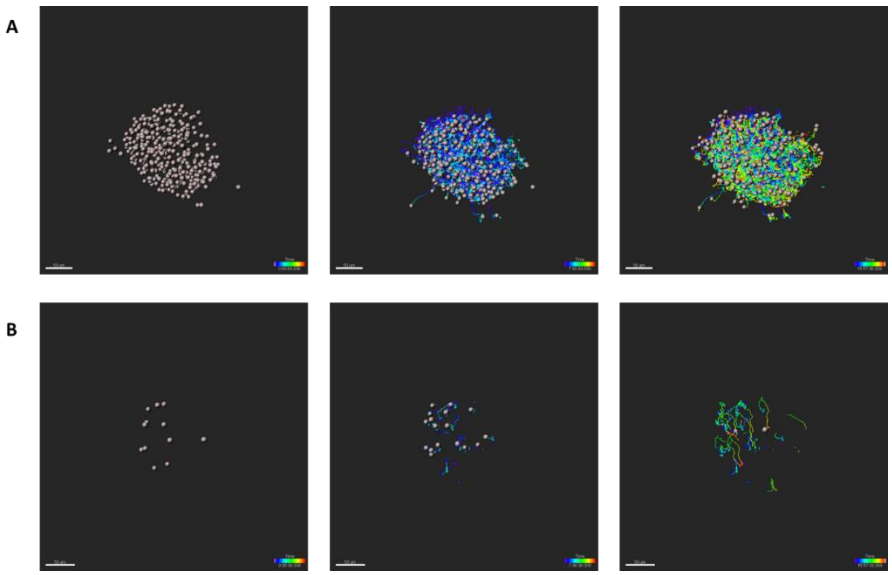

Figure 4.19: Spheroid tracking of GFP-DLC1. **A** Individual cells were tracked using IMARIS imaging analysis software. Individual cells were identified by the H2B-RFP nuclear marker. Using the 'spots' feature cells could be tracked over the 16 hours. **B** For GFP-DLC1 transfected cells, a filter was added to select a population of cells that had GFP intensity, these cells were then tracked separately over time. Scale bar 50µM.

GFP-DLC1 expression had no significant effect on track displacement length (**M** = 27.71 ± 22.81 µm) compared to the control (**M** = 24.42 ± 47.37 µm) (Figure 4.20). GFP-DLC1 slightly increased track speed (**M** = 0.436 ± 0.1µm/min) in comparison to control (**M** = 0.406 ± 0.2µm/min) however this was not significant (Figure 4.20). GFP-DLC1 cell tracks had slightly increased straightness (P = <0.01, **M** = 0.3142 ± 0.1476) in contrast to control tracks, however this was also not significant (**M** = 0.2607 ± 0.1564) (Figure 4.20).

MSD was calculated for GFP-DLC1 and H2B control tracks, however there was no significant difference in the diffusion coefficient between the two (Figure 4.21). The MSD was plotted for each spheroid, which highlighted the spheroid-spheroid variation. The plot also shows the best linear and square fit for the MSD curve. A precise linear fit would suggest that the objects move randomly (Brownian motion), while a good square fit would indicate a constant/linear trajectory (autoregressive motion).

Overexpression of DLC1 did not cause any significant differences in track mean speed, displacement or straightness. While GFP-DLC1 expression decreased track mean speed and displacement in the 2D and CIA assay there was no significant difference in the 3D spheroid model indicating that DLC1 has a different role in 3D.

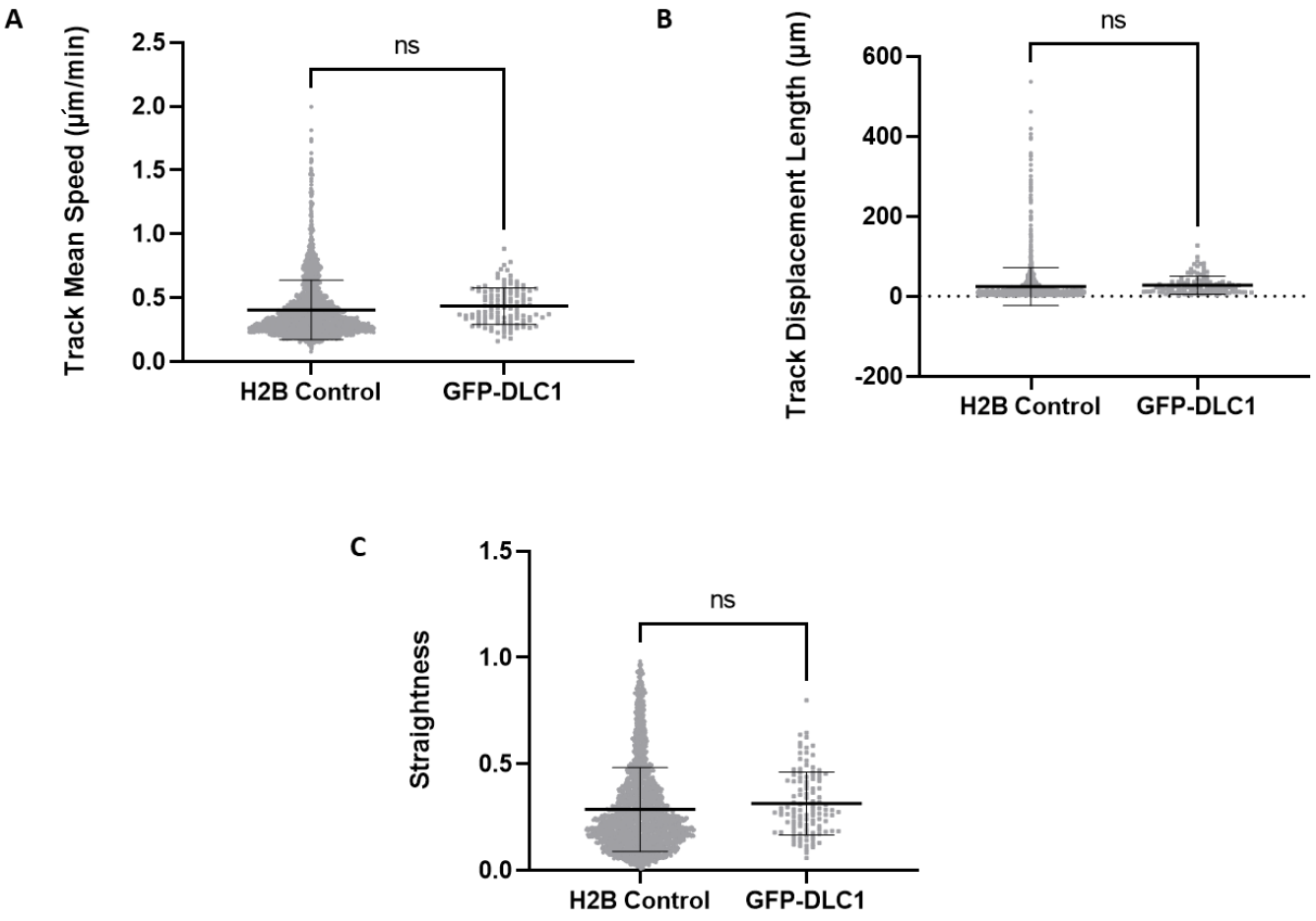

Figure 4.20: GFP DLC1 has no effect on track displacement length, speed and straightness. U-87 MG -H2B-RFP cells were transfected with GFP-DLC1 before spheroid formation. Spheroids were tracked for 16 hours and tracks were calculated using IMARIS software. **A** GFP-DLC1 has no effect on track mean speed. **B** GFP-DLC1 slightly increases track displacement length but this is non significant **C** GFP-DLC1 significantly increases straightness, however there is no statistical significance. N = 3.

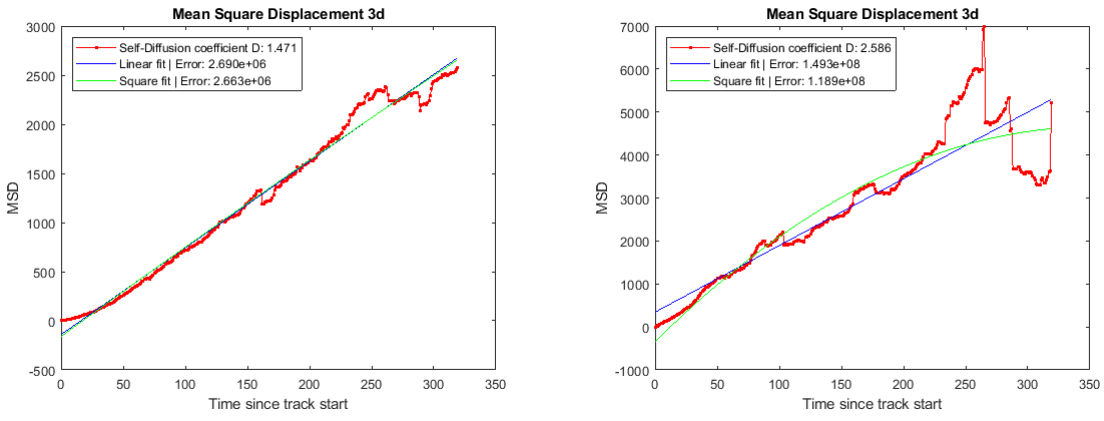

H2B control **GFP DLC1**

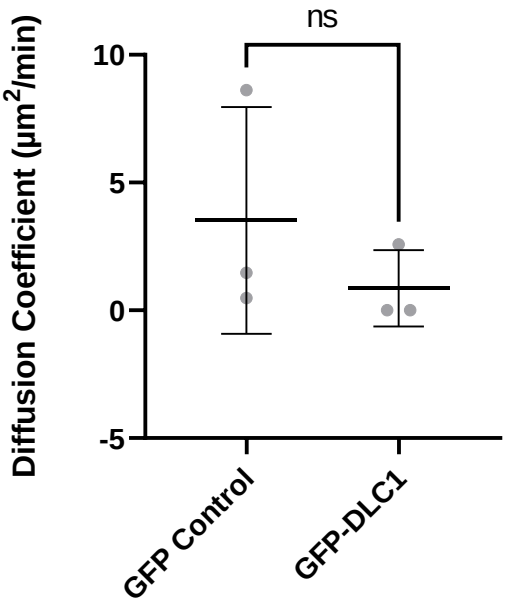

Figure 4.21: GFP DLC1 does not affect mean square displacement of tracks. U-87 MG -H2B-RFP cells were transfected with GFP-DLC1 before spheroid formation. Spheroids were tracked for 16 hours and tracks were calculated using IMARIS software. A MSD plot is shown for a representative spheroid of each condition. The diffusion coefficient was calculated for H2B control and GFP DLC1 conditions however there was no significant difference. Each point in the scatter plot dictates a spheroid, identifying variation between spheroids. N = 3.

4.3.6 DLC1 silencing in 3D invasion

For more insight into DLC1's role within invasion, the effect of DLC1 silencing on 3D invasion was investigated. DLC1 was silenced using siRNA before HepG2-H2B-RFP spheroids were formed. To confirm silencing of DLC1, spheroids with DLC1 siRNA and scrambled control siRNA were collected, sonicated and lysed to be probed by western blot. DLC1 was detected in the scrambled siRNA control, but not the DLC1 siRNA sample confirming knockdown (Figure 4.22). For further confirmation, BLOCK-iT™ Alexa Fluor® Red Fluorescent Control was transfected before spheroid formation to allow visualisation of siRNA transfection efficiency within the spheroid. The signal could be seen within the spheroid, confirming effective siRNA transfection.

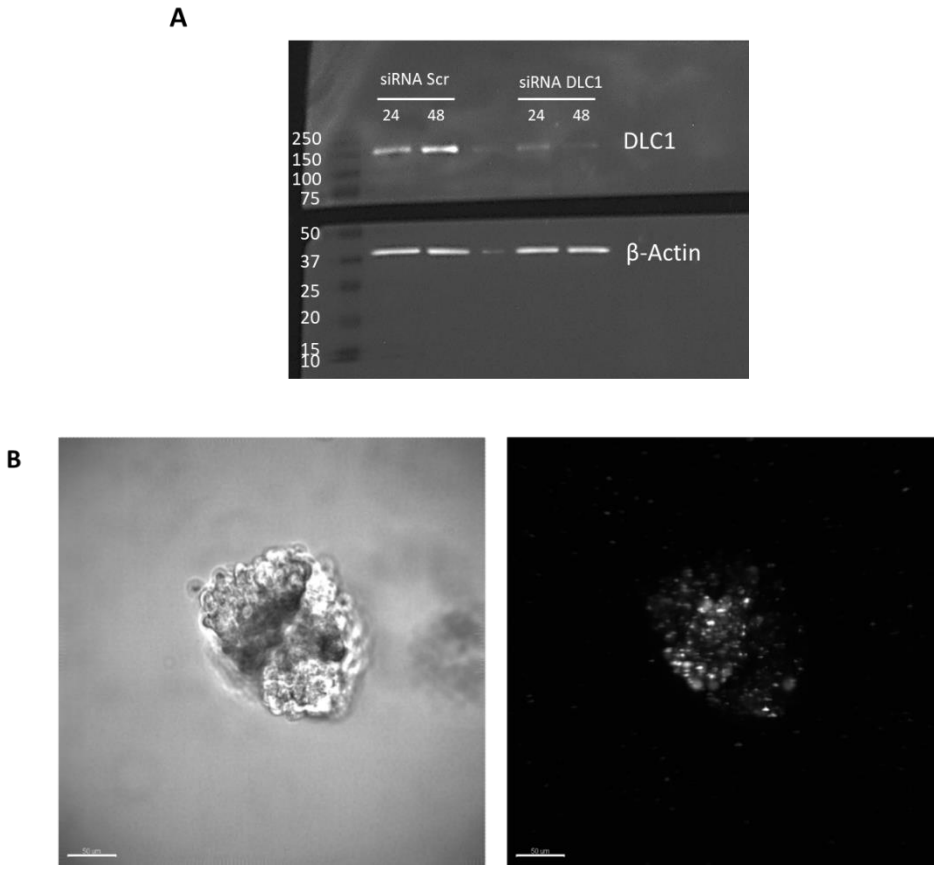

Figure 4.22: siRNA DLC1 silencing in HepG2-H2B-RFP spheroids. HepG2-H2B-RFP cells were transfected with 10µM scrambled siRNA scrambled control and 10µM siRNA DLC1 constructs before spheroid formation. **A** Spheroids were collected at 24 and 48 hours and probed for DLC1 using western blotting (anti-DLC1, BD Biosciences, 1:500). DLC1 was detectable at all timepoints in the scrambled siRNA control sample, but not in siRNA DLC1 timepoints**. B** To confirm siRNA transfection efficiency within the spheroid, BLOCK-iT™ Alexa Fluor® Red Fluorescent Control was transfected before spheroid formation. The spheroid was mounted in matrigel and imaged on the Zeiss Z.1 lightsheet microscope using 20x objective and brightfield and 561nm laser lines. Signal could be seen within the spheroid, confirming effective siRNA transfection. Scale bar 50µM.

Control and siRNA transfected cells were mounted as previously described for imaging using lightsheet microscopy (Figure 4.23). Spheroids were imaged every 3 minutes for 16 hours and tracked using IMARIS imaging software (Figure 4.24, Video 20 - 22). Track displacement length, straightness and speed were calculated for each condition.

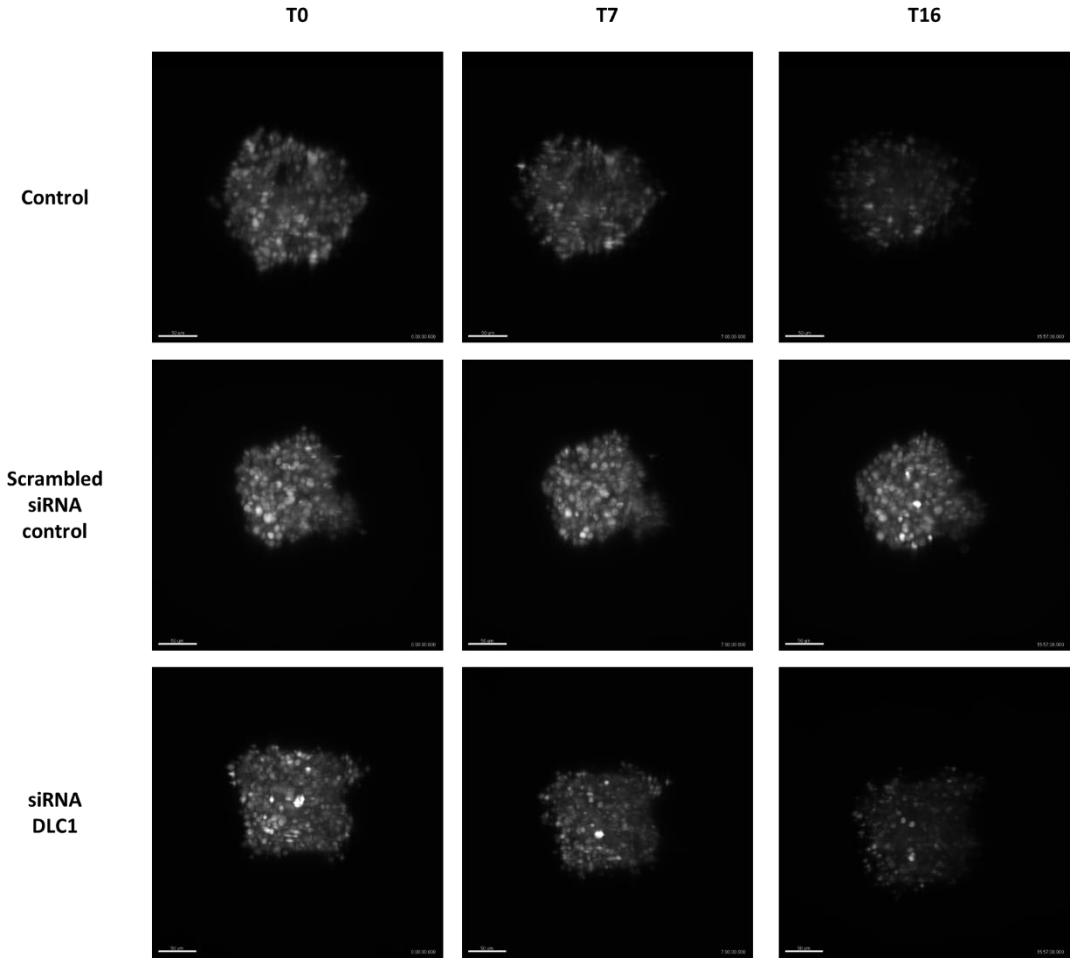

Figure 4.23: HepG2-H2B-RFP siRNA DLC1 spheroid image acquisition. HepG2-H2B-RFP cells were transfected with 10µM siRNA scrambled control and 10µM siRNA DLC1 constructs before spheroid formation. Control spheroids were left untransfected. Each condition was embedded in a matrigel, media, HEPES mix and mounted onto a Zeiss Z.1 lightsheet microscope. Spheroids were imaged every 3 minutes using a 561nm laser line and a 20x objective. Over the 16 hours cells invaded into the matrigel. Scale bar 50µM.

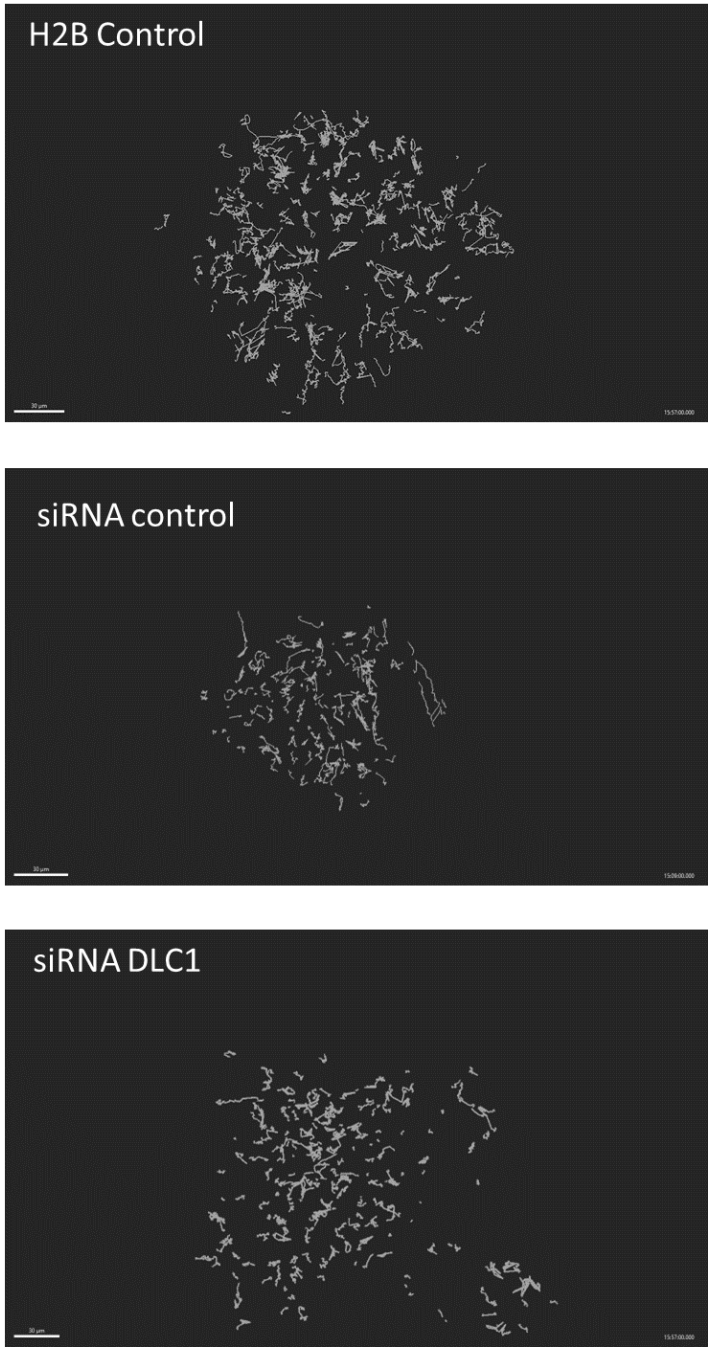

Figure 4.24: HepG2-H2B-RFP siRNA DLC1 spheroid tracking. siRNA control, DLC1 siRNA and controls spheroids were imaged for 16 hours using lightsheet microscopy. Each spheroid was analysed using IMARIS image analysis software. Cells were tracked over the 16 hours using the H2B nuclear marker. Tracks can be seen following cell invasion.

Cells transfected with siRNA DLC1 (**M** = 0.249 ± 0.1 µm/min) had a significantly increased track mean speed compared to scrambled control (P<0.0001, **M** = 0.237 ± 0.1 µm/min) (Figure 4.25).

There was no difference in track displacement length between siRNA DLC1 (**M** = 10.59 ± 7.9 µm) and siRNA scrambled control (**M** = 10.96 ± 9.1 µm) (Figure 4.25). Again, HepG2 cells had less displacement than U-87 MG cells, as seen in the 2D models. siRNA DLC1 treated cells were significantly straighter (**M** = 0.236 ± 0.1) than siRNA scrambled control tracks (P<0.0001, **M** = 0.190 ± 0.1) (Figure 4.25).

Mean square displacement was calculated for each track, however there was also no significant difference between siRNA DLC1 and siRNA scrambled control transfected cells (Figure 4.26). The MSD plot highlights the variability between each of the spheroids, and the challenge faced with these types of cultures.

When DLC1 was silenced in the 3D spheroid model, track mean speed and straightness increased, however there was no difference in track displacement. This could imply cells move quicker and more direct, but did not move further than siRNA scrambled control cells. This could support the hypothesis that loss of DLC1 affects cell invasion.

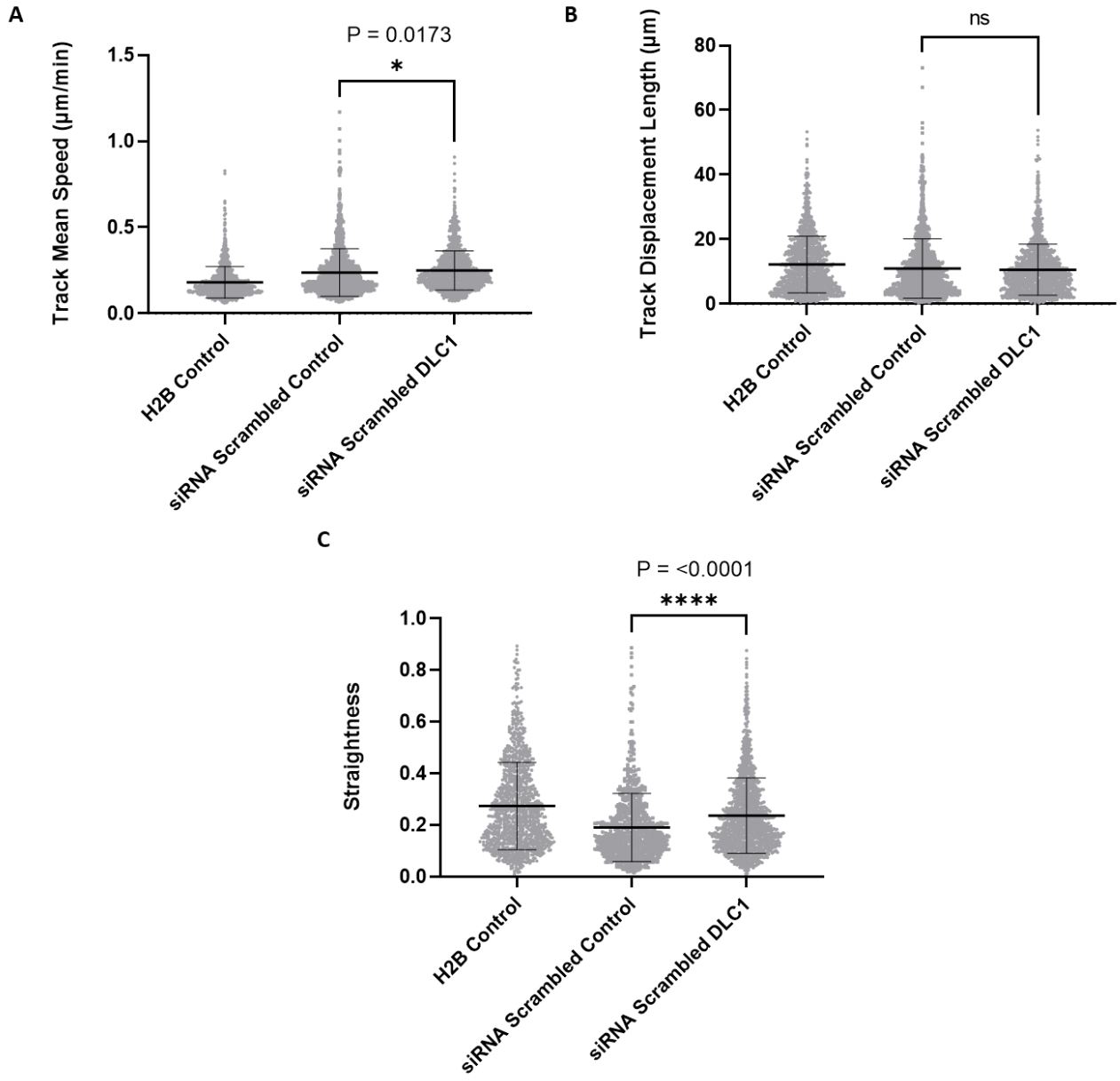

Figure 4.25: siRNA DLC1 significantly increases track speed and track straightness. HepG2-H2B-RFP cells were transfected with siRNA DLC1 or scrambled siRNA control before spheroid formation. Spheroids were tracked for 16 hours and tracks were calculated using IMARIS software. **A** siRNA DLC1 significantly increased track speed compared to siRNA scrambled control, $t(2492) = 2.381$, $P < 0.05$. **B** siRNA DLC1 had no effect on track displacement length **C** siRNA DLC1 significantly increased track straightness compared to siRNA scrambled tracks $t(2072) = 7.223$, $P < 0.0001$. N = 3.

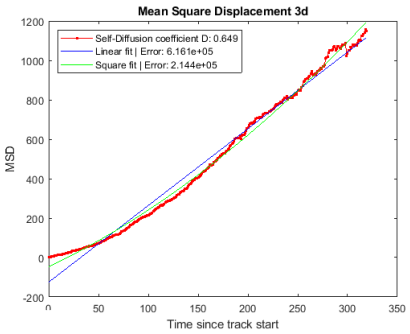

HepG2 Control

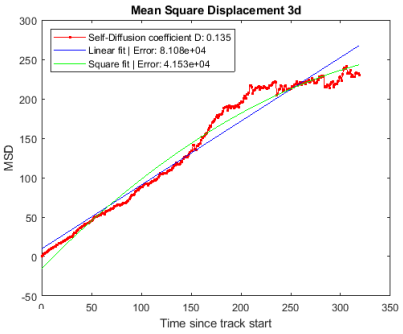

siRNA Scrambled Control

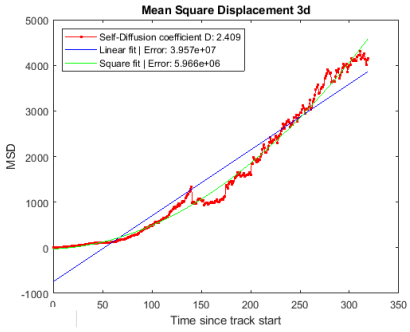

siRNA DLC1

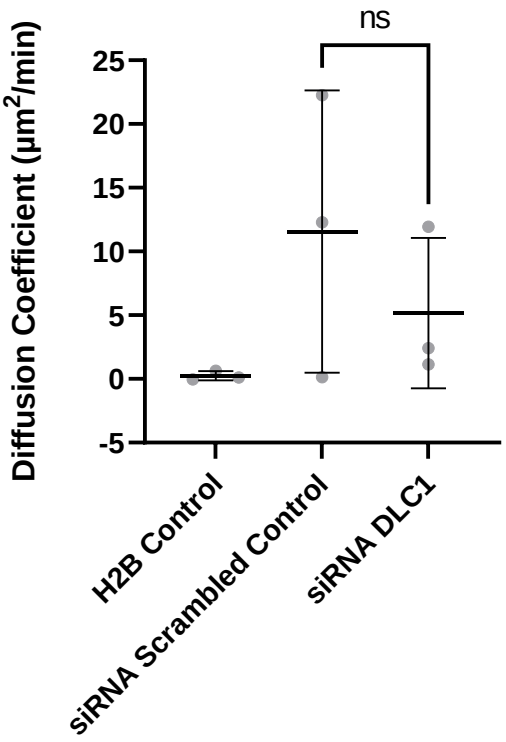

Figure 4.26: siRNA DLC1 does not affect track mean square displacement. HepG2-H2B-RFP cells were transfected with siRNA DLC1 or scrambled siRNA control before spheroid formation. Spheroids were tracked for 16 hours and tracks were calculated using IMARIS software. A MSD plot is shown for a representative spheroid of each condition. There was no significant difference in the diffusion coefficient between siRNA DLC1 and siRNA scrambled control. N = 3.

4.3.7 Analysis of inner and outer tracks within the spheroid

Previous analysis has looked at the spheroid model as a whole, analysing all of the spheroid tracks, however it could be hypothesised that cells act differently depending on where they are in the spheroid. Cells in the centre of the spheroid may not have the ability to invade as much as the cells on the edge, therefore looking at the spheroid as a whole may mask any effects of DLC1 invasion. For further investigation into the 3D spheroid model, spots were filtered into two classes; spots inside the spheroid and spots on the outer edge of the spheroid. Analysis was performed for the two different classes to see if the spots behave differently depending on where they are located within the spheroid. Using IMARIS software, a reference frame was placed in the centre of the spheroid, spots were then classified as inner when they were within close diameter to the reference frame, and outer when they were a further distance (Figure 4.27). To ensure reproducibility, a filter was applied to distinguish the "distance from origin" of the reference frame. The exact number varied between the spheroid conditions, as each spheroid varies slightly in size and shape, with the reference frame manually placed in the middle of the spheroid (Table 2.12). However, each spheroid was qualitatively checked by eye to ensure the inner/outer areas were uniform across the spheroids, with the inner area the inside of the spheroid (blue) and the outer area the edge if the spheroid (magenta).

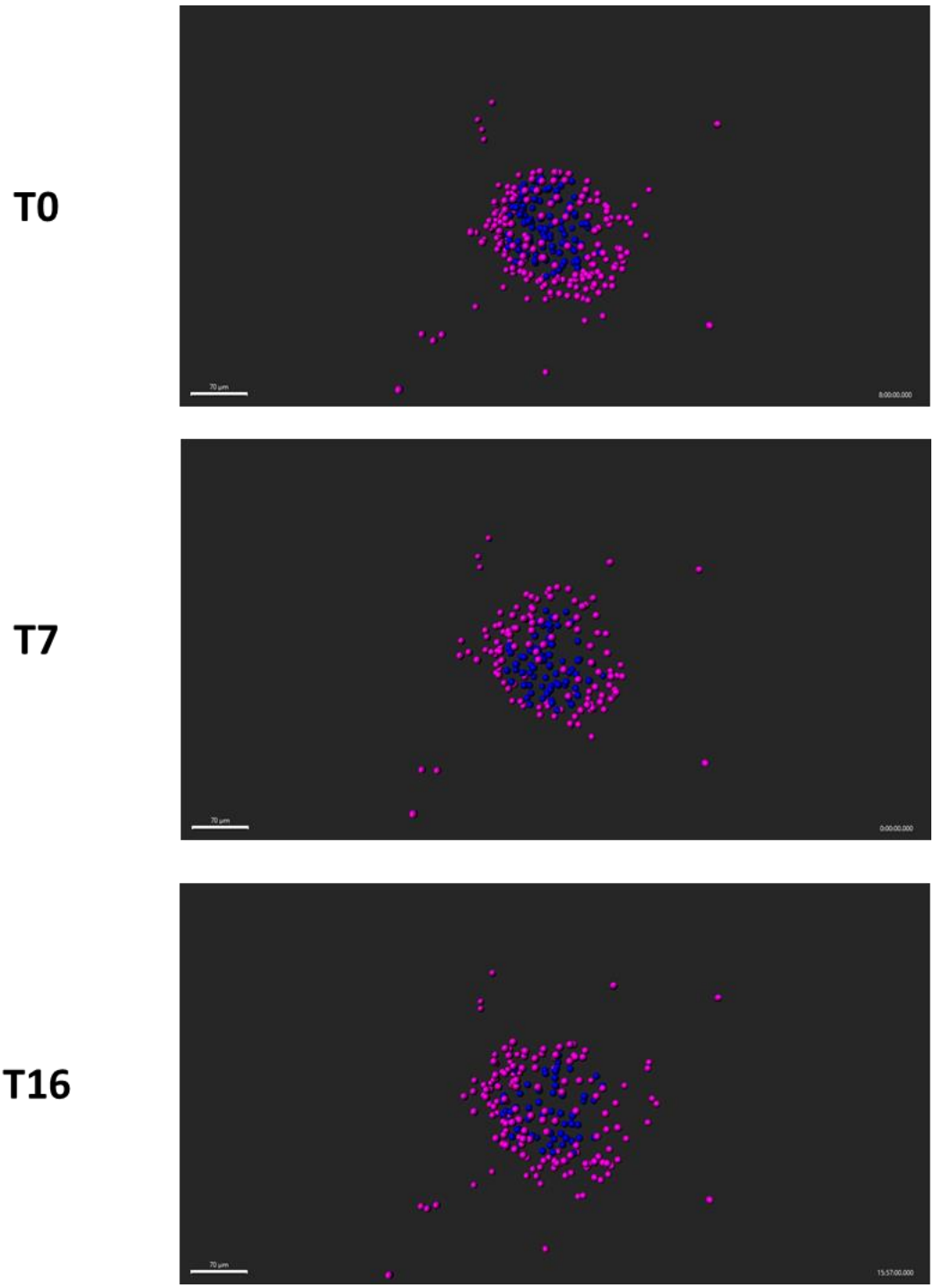

Figure 4.27: Spheroid spots were classified into inner and outer spots. To evaluate whether spot location affects invasion behaviour, cells within a U87 RFP-H2B spheroid were classified into inner (blue) and outer spots (magenta) using IMARIS software. As a 3D max projection, although some magenta spots appear inside, they are on the outer edge. Spot displacement and speed could then be calculated for each class. Scale bar 50µM.

4.3.8 Inner and outer spot effect on GFP DLC1

Spot displacement was compared between the inner and outer classes of spots for GFP-DLC1 and H2B Control. There was a significant difference between the inner and outer spots in both GFP DLC1 and H2B control conditions (Figure 4.28). In the GFP-DLC1 cells, displacement was significantly increased in outer spots (P = <0.0001, **M** = 27.28 ± 30.28 µm) compared to inner spots (**M** = 15.68 ± 17.01 µm). Similarly, H2B control cells displacement was increased in outer spots (P = <0.0001, **M** = 22.14 ± 41.02 µm) compared to inner spots (**M** = 19.44 ± 29.21 µm). There was more displacement in the outer spots, suggesting cells on the outer edge of the spheroid move more, which could be due to them invading into the matrix. The inner cells are more confined with other cells therefore do not have the ability to migrate/invade as much.

The GFP-DLC1 spheroid inner spots had significantly less displacement (P = <0.0001, **M** = 15.68 ± 17.01 µm) compared to the H2B control inner spots (**M** = 19.44 ± 29.21 µm). This supports the hypothesis that overexpression of GFP-DLC1 reduces migration, however it could be due to the inner cells not having the space to migrate out. GFP-DLC1 spheroid outer spots had significantly more displacement (P = <0.0001, **M** = 27.28 ± 30.28 µm), compared to the H2B control outer spots, (**M** = 22.14 ± 41.02 µm). Interestingly, despite the outer GFP DLC1 spots having increased displacement, there was no significant difference in the displacement of spheroid tracks as a whole. This confirmed the hypothesis that when average of the whole spheroid is used the differences can be masked.

Spot speed was also calculated for inner and outer spots (Figure 4.29). GFP-DLC1 spheroid outer spots were significantly faster (**M** = 0.349 ± 0.3 µm/min) compared to inner spots (P = <0.0001,

M = 0.3015 ± 0.2 μm/min). Interestingly, H2B control inner spots were significantly faster (P <0.0001, **M** = 0.302 ± 0.3 μm/min) compared to H2B control outer spots (**M** = 0.256 ± 0.2 μm/min). There was no significant difference between GFP DLC1 inner spots an H2B control inner spots, however there was significant difference between the outer spots of GFP-DLC1 (P <0.0001, **M** = 0.349 ± 0.3 μm/min) and H2B control, (**M** = 0.256 ± 0.2 μm/min), with GFP-DLC1 spots significantly faster.

These results confirm that cells on the edge of the spheroid have increased displacement and speed, suggesting they can move quicker and further into the matrix. Furthermore, the same trends were observed as the whole spheroid 3D analysis.

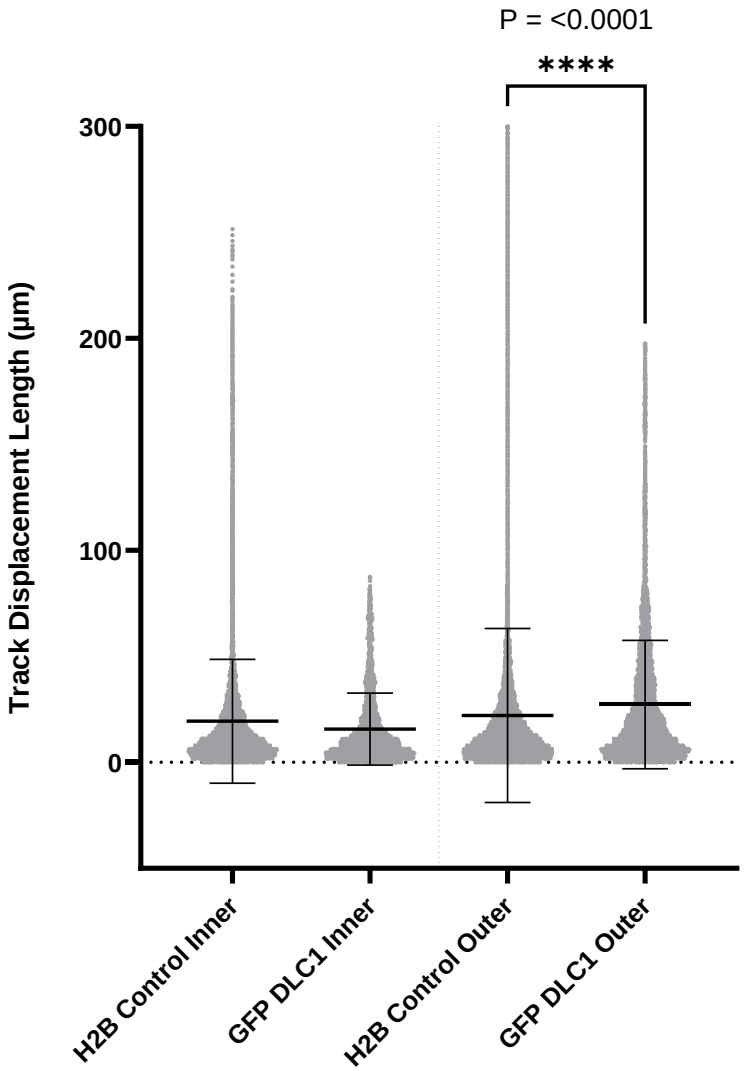

Figure 4.28: There are significant differences between the inner and outer spots of both GFP DLC1 and H2B control spot displacement. GFP DLC1 spot displacement was significantly increased in outer spots compared to inner spots, two tailed t-test t (30456) = 33.91 P = <0.0001. Similarly, spot displacement was significantly increased in H2B control outer spots compared to inner spots, two tailed t-test t (157649) = 13.05 , P = <0.0001. GFP DLC1 inner spots had less displacement compared to H2B control inner spots, two tailed t-test, t (56941) = 11.74 P = <0.0001 . GFP DLC1 spot displacement was significantly increased in outer spots compared to H2B control spots, two tailed t-test t (131164) = 17.50, P = <0.0001. N = 3.

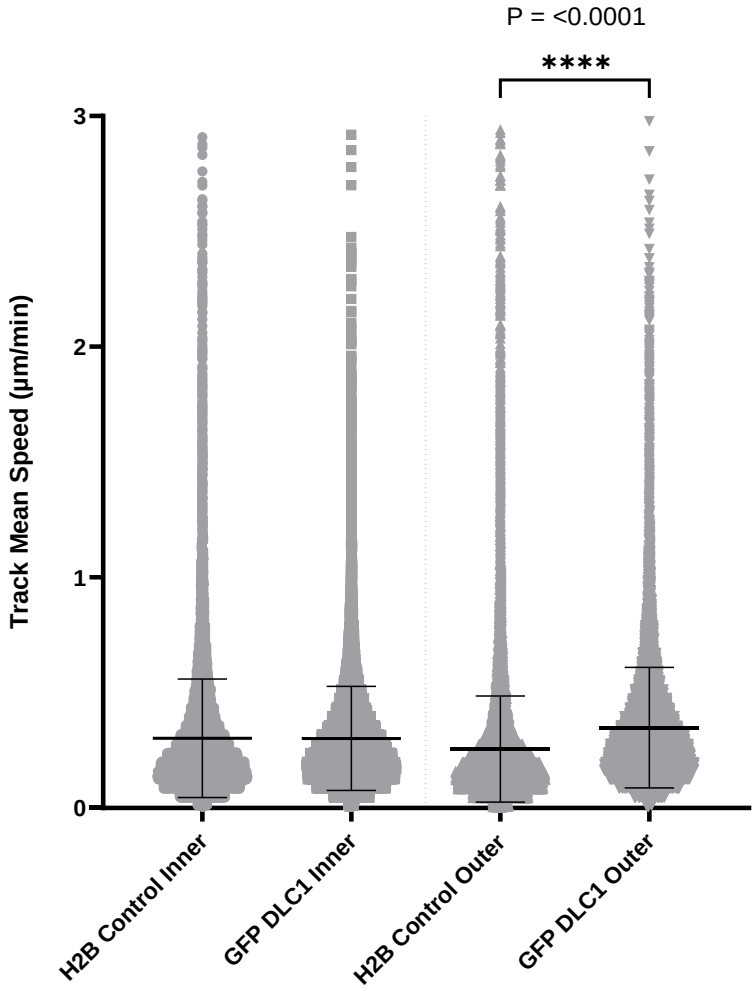

Figure 4.29: Spot speed was significantly different between GFP DLC1 and H2B control. GFP DLC1 spot speed was significantly increased in outer spots compared to inner spots, two tailed t-test t (57547) = 23.18, P = <0.0001. Interestingly, spot speed was significantly increased in H2B control inner spots compared to outer spots, two tailed t-test, t (157649) = 35.52, P <0.0001. There was no significant difference between the GFP DLC1 inner and H2B control inner spots. GFP DLC1 spot speed was significantly increased in outer spots compared to H2B control outer spots, two tailed t-test t(13783) = 58.81, P <0.0001. N = 3.

4.3.9 Inner and outer spot effect on siRNA DLC1

Spot displacement was also calculated for knockdown of DLC1 using siRNA, to see if the location of spots in the spheroid (inner or outer) affected the displacement. For all conditions (H2B control, scrambled siRNA control and DLC1 siRNA) the spot displacement was significantly increased in the outer spots compared to the inner spots, which support the hypothesis that cells on the edge of the spheroid can invade further than the inner spots (Figure 4.30).

The spot displacement of cells transfected with DLC1 siRNA, inner spots ($P < 0.0001$, **M** = 9.229 ± 6.744 µm) were significantly increased compared to scrambled siRNA control (**M** = 7.752 ± 6.294 µm) and untransfected control (**M** = 6.915 ± 8.893 µm). Similarly, the same trend was observed in the outer spots, siRNA DLC1 outer spots ($P < 0.0001$, **M** = 12.69 ± 9.980 µm) were significantly increased compared to siRNA scrambled control (**M** = 10.33 ± 8.946 µm) and control outer spots (**M** = 7.550 ± 8.614 µm). This suggests that silencing of DLC1 increases invasion by increasing displacement in siRNA DLC1 spots. All outer spots of each condition had a larger displacement than the inner spots, which supports the idea that the cells on the edge can migrate more than the cells confined with the spheroid. However, it is noted that the displacement numbers in the HepG2 spheroids were lower overall compared to the U-87 MG spheroids. Although HepG2 cells are migrating, the migration is reduced compared to the U-87 MG cells.

Spot speed was also calculated for all siRNA conditions (Figure 4.31). Interestingly, for all conditions (H2B control, siRNA scrambled control and siRNA DLC1) the inner spots had significantly increased spot speed compared to the outer spots. siRNA DLC1 inner spots were significantly faster ($P < 0.0001$, **M** = 0.249 ± 0.2 µm/min) compared to siRNA scrambled inner spots

(**M** = 0.163 ± 0.2 µm/min) and control (**M** = 0.139 ± 0.2 µm/min). Similarly, siRNA DLC1 outer spots were also significantly faster (P <0.0001, **M** = 0.225 ± 0.2 µm/min), compared to siRNA scrambled control outer spots (**M** = 0.187 ± 0.2 µm/min) and control outer spots (**M** = 0.125 ± 0.2 µm/min). The cells inside the spheroid moved quicker and but had less displacement, which could suggest they could not invade out into the matrix, but were migrating around the inside of the spheroid faster than the cells invading the matrix on the edge. siRNA DLC1 outer spots had the quickest migrating cells and the most displacement, which could suggest that loss of DLC1 allows cells to migrate quicker and to invade further, which supports the overall hypothesis of DLC1's role to supress cell migration and invasion.

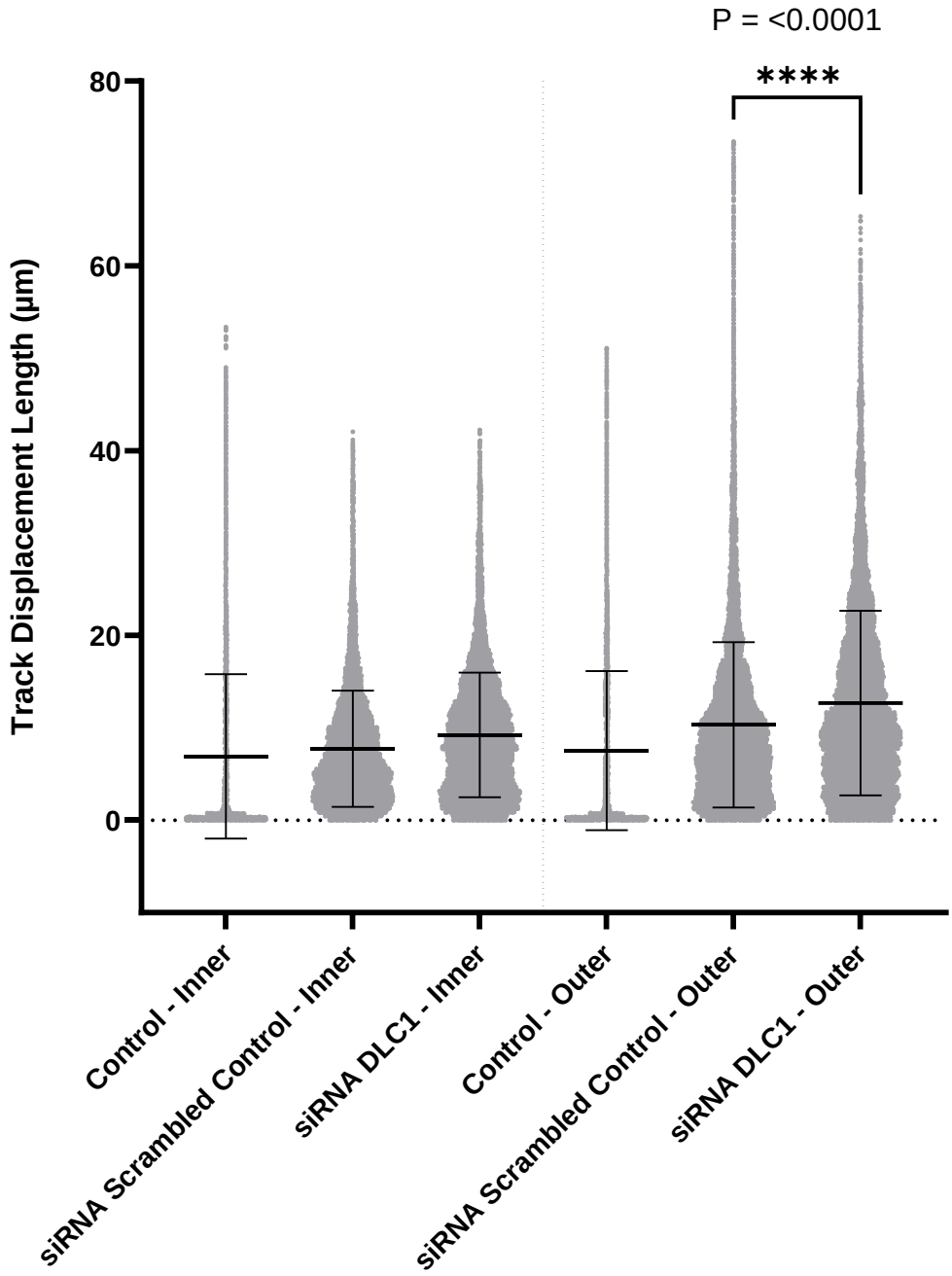

Figure 4.30: Spot displacement is significantly increased in outer spots compared to inner spots in both siRNA control and siRNA DLC1. The spot displacement of DLC1 siRNA inner spots were significantly increased compared to scrambled siRNA control and untransfected control, one-way ANOVA, $F(2, 138996) = 1078$, $P < 0.0001$. siRNA DLC1 outer spots were significantly increased compared to siRNA scrambled control and control outer spots, one-way ANOVA, $F(173811) = 4497$, $P < 0.0001$. N = 3.

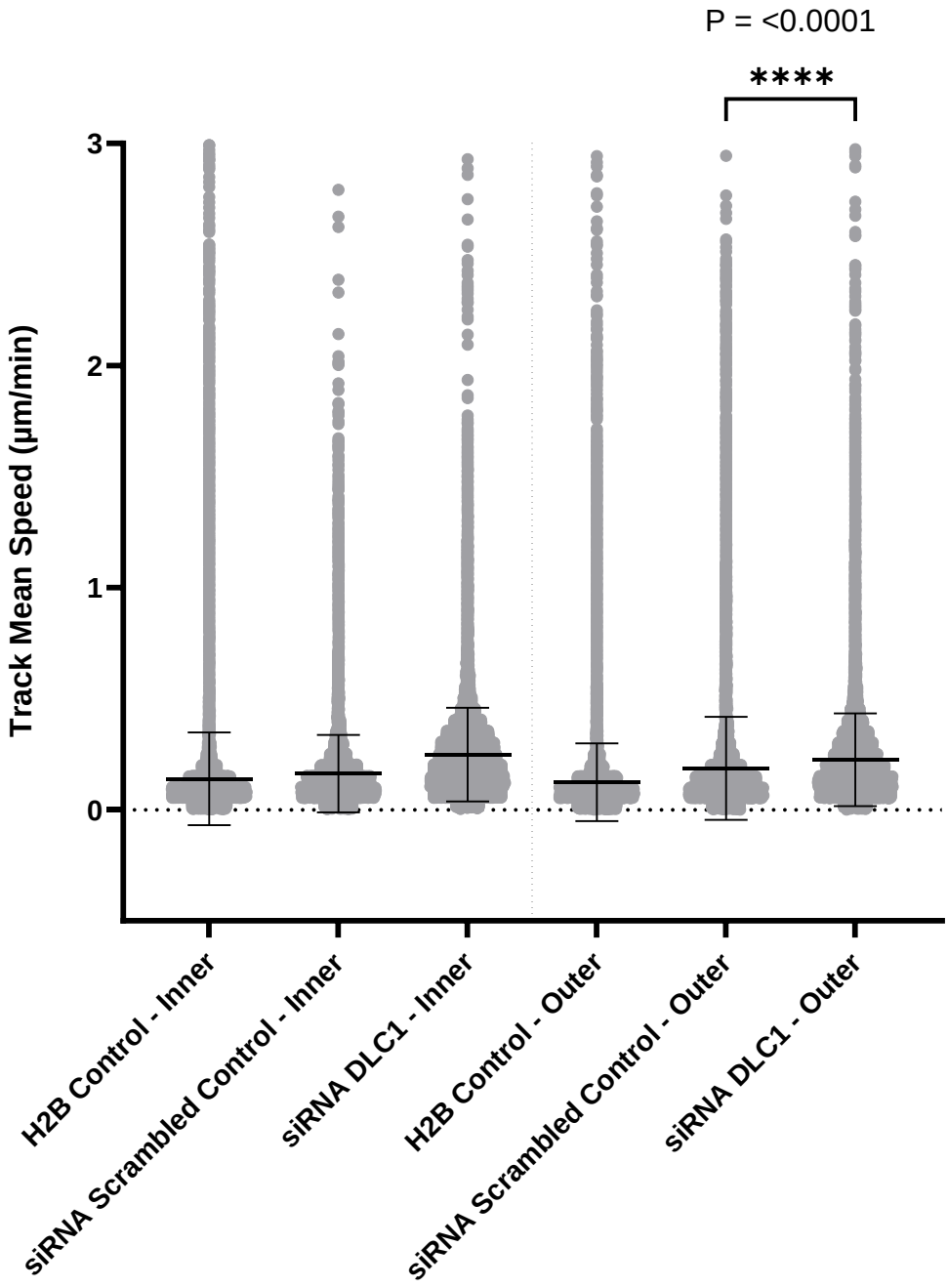

Figure 4.31: Spot speed is significantly increased in inner spots compared to outer spots in siRNA control and siRNA DLC1. siRNA DLC1 inner spots were significantly faster compared to siRNA scrambled inner spots and control inner spots, one-way ANOVA, F (2, 156895) = 408.2, P <0.0001. Similarly, siRNA DLC1 outer spots were also faster compared to siRNA scrambled and control outer spots, one-way ANOVA, F (2, 147156) = 1007 , P <0.0001. N = 3.

In conclusion, the impact of DLC1 was investigated across 2D, CIA and 3D spheroid assays, the effect of DLC1 overexpression and silencing are summarised in Table 4.2 and Table 4.3 respectively. Overexpression of DLC1 showed predicable observations within the 2D and 2D/3D assays, however in the 3D spheroid model, overexpression of DLC1 showed no significant effect. Seeing differences between the 2D and 3D assays indicates that the impact of DLC1 is complex and its role could differ in 2D to 3D.

Table 4.1: Effect of GFP-DLC1 overexpression on 2D, CIA and 3D spheroid assays.

Overexpressed DLC1	2D	CIA	3D
Track Speed	-	-	NSD
Track Displacement Length	-	-	NSD
Straightness	NSD	+	NSD
MSD	-	-	NSD

Table 4.2 Effect of siRNA DLC1 on 2D, CIA and 3D spheroid assays.

KO DLC1	2D	2D/3D	3D
Track Speed	NSD	+	+
Track Displacement Length	-	-	NSD
Straightness	+	+	+
MSD	NSD	-	NSD

When silencing DLC1 with siRNA, different effects were also observed across the 2D, CIA and 3D spheroid assays, which adds further evidence that the addition of a 3D matrix affects cell migration. In 2D, siRNA DLC1 was shown to and reduce displacement and straightness, it was

hypothesised that loss of DLC1 would increase cell migration however this effect was not observed on track displacement length. In both 3D assays, track mean speed of siRNA DLC1 was increased. The 3D spheroid assay did also not show an increased track displacement. However, siRNA DLC1 increases speed and straightness which could affect migration in the long term.

The difference in the results between 2D and 3D cell migration assays, are not surprising as it has been well reported that cells behave differently in 2D versus 3D. Whilst some of the hypothesised effects of DLC1 were not observed in these studies there were significant effects of the modulation of DLC1, indicating the expression of this protein has a role in cell migration and invasion.

4.4 Discussion

In this chapter, manipulating levels of DLC1 was shown to affect cell migration and invasion. Different invasion and migration assays were used with differing level of ECM influence and increasing complexity, with some contradictory results. Not only did the results vary between the assays, but intra-assay variability was also highlighted. This could be an effect of stiffness and crowding, the 2D assay had a thin 2D assay laid down by cells with space, whereas the 3D CIA matrix had an overlay of matrigel. Cells within the spheroid model were crowded, with the whole spheroid embedded in matrigel. U-87 MG cells were used in the overexpression model, and these cells were highly migratory showing displacement of tracks, however HepG2 cells which were used in the silencing model showed very little displacement, showing the variability in cell movement between cell lines. In addition, variability was also highlighted in the 3D spheroid

model, 3 spheroids per condition were analysed and when looking at the MSD of each of the spheroids, it did show a wide range.

4.4.1 Challenges with 3D spheroid model

U-87 MG and HepG2 spheroids were easily grown, each cell line was transduced with a lentiviral H2B-RFP nuclear marker, to allow for segmentation and easier tracking analysis and also to counteract the difficulties with staining penetration (Olofsson et al., 2021). Similarly, when spheroids were reverse transfected, they were transfected before formation to allow uptake into spheroid formation. Spheroids and mounting them was robust and reproducible, however image acquisition introduced more challenges.

When acquiring images over 16 hours there was a large amount of drift, where the spheroid would completely disappear from field of view. This was problematic and unpredictable, some spheroids would drift completely within a few minutes and others within hours. Troubleshooting included leaving the microscope to incubate for longer, leaving the sample on the microscope for hours prior to imaging to equilibrate, and increasing duration of embedding time to ensure that the matrigel had set. However, the drift was still experienced.

The next step in troubleshooting was to attempt to correct the drift post acquisition, which lead to different problems. The data acquired by the light sheet microscope are huge in size, which lead to difficulties when post-processing. Using ImageJ software, an attempt was made to open the dataset (16 hours, two channels, several z stacks) to try and fuse together the different

channels and correct the drift, however this was unsuccessful, as the dataset was too large, therefore concluding that analysis via ImageJ was not an option.

IMARIS software is specially designed for 3D imaging, ideal for analysis of the spheroids. This software performs 3D tracking and post-acquisition drift acquisition. However, although some of the drift could be corrected, it was still problematic. To try and improve the acquisition, more optimisation of the spheroid mounting protocol was required. During mounting the spheroid is embedded into FEP tubing, this tubing is then cut at the top to insert into the capillary and inserted onto the light sheet microscope. However this process could introduce an air bubble. This then rose and slowly caused the matrigel/media mix to rise up the tubing, causing the sample to drift upwards. This needed to be carefully considered, when inserting the tube, it was important to ensure no air bubbles were generated. Furthermore, as the tubing was simply inserted into the capillary, it was unstable and prone to slipping down, which would also disrupt the sample and cause the sample to move out of field. Another step was added to the protocol where the tubing would be supported by the addition of parafilm, which would add stability and prevent movement. These small modifications had a notable effect, and less drift was then seen during the invasion.

However, the samples still displayed drift which had to be addressed in the post-processing of the images. Using IMARIS software a reference frame was introduced into the middle of the spheroid, and as the spheroid drifted the reference frame was repositioned to mimic the direction of the drift. This is then applied to the statistics to correct the drift, which will make it

easier to differentiate between real cell movement and the effect of sample drift. If there was a large movement, this resulted in a reduction of the measured movement.

Sample drift can occur due to movement or growth in the sample or flexibility in sample media where even embedded samples can move, therefore it is common practice to correct for drift within acquisition (Parslow et al., 2014). Despite best efforts to limit the drift with sample preparation, the drift could be reduced but not completely removed. Applying a drift correction method made the measurements more precise, however it must be taken into account that it may have a small effect on the results. The IMARIS method involves the user manually placing the reference frame, which could introduce some errors. There are several other ways to correct drift, with the most precise method adding markers that are impartial to the sample, such as fluorescent beads in a separate imaging channel. Then this channel can be used as registration, to apply precise drift correction to the rest of the acquisition channels (Parslow et al., 2014).

Taking into account all these problems, it took longer than anticipated to collect and analyse the basic spheroid data. This meant that with the time restrictions of a PhD and also COVID-19 implications the spheroid model did not progress into being multicellular or multi-angle. The purpose of using lightsheet microscopy was to generate dynamic global information about DLC1's role in invasion, unfortunately for several reasons this was not fully accomplished.

Using the lightsheet allowed live time lapse imaging of spheroid invasion compared to the static end point invasion assays. However, it takes a longer time period to collect single spheroid data compared to high throughput imaging systems such as the Incuyte, where spheroids can be measured at higher throughput and basic invasion measured by brightfield microscopy. With

this particular microscopy set up, only one spheroid could be imaged at a time, meaning a 16 hour turn around for image acquisition alone. For this reason, only 3 spheroids were collected for each condition. As previously mentioned in this chapter, reproducibility of spheroid culture is a challenge. These spheroids were collected using the using spheroid microplate method and although all spheroids were measured and estimated similar sizes, perhaps a different method to generate spheroids would create more consistent results or more spheroids would need to be assayed.

Whilst the Incucyte is higher throughput and can perform live imaging, it only performs basic invasion analysis. In hindsight, as limited spheroid invasion could be performed in this thesis, it might have been more advantageous to use a system like the Incucyte system to generate more data for each DLC1 condition. On the other hand, using the lightsheet microscopy generated few data sets however, these were far richer in content, providing dynamic information such as speed, which could be used as a foundation for further experiments, with more replicates and longer time courses. In addition, the spheroid model and lightsheet microscopy could be used for static time point experiments, collecting data after long time lapses. Furthermore, lightsheet microscopy allows the best penetration for imaging of 3D spheroid models, allowing full acquisition of the spheroid which would be difficult using other microscopy techniques such as confocal or microscopy.

4.4.2 Effect of DLC1 on cell migration

In standard 2D cell migration experiments overexpression of DLC1 reduced track speed and displacement (Figure 4.3). In CIA experiments, a classic wound healing set up with the addition

of ECM (Matrigel) on top of cells and into the prepared empty space, similar effects were observed, in terms of reduced track speed, displacement and MSD, however straightness was increased in presence of DLC1 (Figure 4.13). As previously mentioned, DLC1 is reported as a potential metastatic suppressor, therefore reducing speed of cells and also track displacement supports this role.

The effect of co-expression of DLC1 and talin were also assessed in 2D migration assays, the track displacement and MSD were all reduced compared to GFP control, which is similar to what was observed with GFP-DLC1 expression alone. However, there was no difference between the mean track speed of GFP control and GFP-talin and mRuby-DLC1 expressed cells. This was unexpected, however the actual speed values across the two assays were very similar, GFP-DLC1 (0.616 µm/min) and GFP-talin mRuby DLC1 (0.665 µm/min). This could be due to several reasons such as variability within the assay (cell seeding, transfection efficiency, co-expression). To fully investigate this, further experiments would be required such as transfection of GFP-talin and mRuby DLC1 alone within the same 4 compartment dish.

To further understand the importance of DLC1 for cell migration and invasion, silencing experiments were performed. In the 2D and CIA assay, DLC1 siRNA reduced displacement (Figure 4.10, 4.15). This was surprising as previous reports have shown that silencing DLC1 increases invasion, which leads to the hypothesis that cells would have increased track displacement in the CIA and 3D spheroid assays (Wong et al., 2005, Feng et al., 2013, Ullmannova-Benson et al., 2009). Both knockdown and overexpression of DLC1 resulted in reduced displacement of tracks compared to control, which could imply that manipulation of DLC1 has an effect on cell tracks.

These results need to be carefully considered as the differences were small and although significant may not carry biological relevance. Also as a different cell line was used for each study there could be differences in dependence on DLC1 depending on the cell type.

Silencing DLC1 in both the 3D spheroid model and CIA resulted in increased track speed and straightness, however there was no effect on displacement in the 3D spheroid model (Figure 4.23). This could suggest cells moved fast, but did not have direct tracks. It would be hypothesised that loss of DLC1 would increase track displacement as it would favour invasion, however siRNA DLC1 reduced track displacement in 2D and CIA assays, and had no effect in the 3D spheroid model. These differences are minimal, which may not have biological relevance.

4.4.3 Effect of DLC1 on cell invasion

As described previously in this thesis, it is well known that 2D and 3D models show differing results (Doyle et al., 2013). Whilst the 2D and CIA assays showed the same trends, this was not seen when advancing to the 3D spheroid model, were cells were able to invade into the matrix in a 3D fashion. Overexpression of DLC1 in the spheroid model showed no significant difference in track speed, displacement or straightness compared to control (Figure 4.20). It could be hypothesised that with overexpression of DLC1 there would be a reduction in the invasion, however there was no difference between overexpression and control tracks.

DLC1 has been seen to reduce cell invasion in the transwell assay with melanoma, human nasopharyngeal and HCC cells (Ullmannova-Benson et al., 2009, Wong et al., 2005, Zhou et al., 2004). The number of cells that invaded through the assay were counted and compared to a control, in all three instances DLC1 expressing cells had less cells invasion. In the study by Feng

et el 2013, in the invasion assay, 190 DLC1 expressing cells invaded compared to 278 control cells, showing DLC1 significantly reduced the invasion. However, this type of assay does not measure how far each of the cells invade, just the number of cells in the field of view.

In a study by Kim et al 2008, DLC1 expression did not affect velocity of the cells in 2D, however different mutants lacking the SAM region (protein interaction domain) did reduce the velocity. This study also measured the directional persistence (D/T) of the cells, determined by dividing the net displacement by total length of the migration path, similar to the straightness measurement. The D/T of the full length DLC1 construct was increased compared to DLC1 mutants and GFP control. In this thesis, the straightness of GFP-DLC1 overexpressed cells was increased in CIA assay compared to GFP control, however there was no significant effect in 2D or 3D spheroid assays. This suggests that DLC1 can increase directionality/straightness of cell tracks in CIA 3D single cell assay, but not in the 3D spheroid assay. Of note, the Kim study used cells plated on fibronectin, which compares to observations in the CIA assay where straightness was increased in the influence of ECM.

A recent study published analysis of DLC1 in a spheroid model, focused on angiogenesis in HUVEC cells. Whilst the study had spheroids, there was no investigation into invasion and migration parameters, instead it was looking sprouting of the spheroid, counting the length and number of sprouts (van der Stoel et al., 2020).

Whilst there is no direct spheroid invasion model to compare to, there are previous DLC1 invasion results (Wong et al., 2005, Feng et al., 2013, Ullmannova-Benson et al., 2009). Although they are both invasion assays they measure different parameters. The transwell assay shows end point

data, where it counts the number of single cells invading into the gel, and showed significantly reduced numbers of DLC1-expressing migratory cells in different cell types. The aim of using the 3D spheroid model in this thesis was to look at live parameters of DLC1 invasion, how fast cells were traveling and how far they travelled. The invasion time for the 3D spheroid model was 16 hours, whereas the transwell assays varied from 16-60 hour invasion time, and although the assays differ, the reduced number of cells in the transwell assay could potentially be compared to reduced displacement in the spheroid model. Overexpression of DLC1 in the 3D spheroid model used here showed no significant changes in displacement, but this cannot easily be compared to the previous invasion assays published. However, in the spheroid model the cells can interact with other cells, which could affect their behaviour compared to the single cell migration in the transwell assay. Furthermore, maybe increasing the assay time would show more difference in invasion.

There are several differences with the assays including different cell types and different matrices that they are invading through. The work in this thesis has highlighted the difference in displacement between two different cell types, with HepG2 cells having less displacement compared to U-87 MG. Whilst the published transwell assay shows single cell invasion, the 3D spheroid model has cell-cell interactions combined with cell-ECM interactions, which could change the cell invasion behaviour. It can be concluded that more 3D invasion data is needed to fully understand the mechanism of DLC1 invasion, perhaps performing transwell invasion assays with these cell types in combination with 3D spheroid model would have provided more information about DLC1's role within 3D invasion. Furthermore, using a metalloprotease inhibitor

such as GM6001 would be a additional control to confirm that these assays are measuring invasion.

It is known that migratory modes can switch depending on different pathways and whether cells are in 2D or 3D. The RhoA–ROCK– myosin-II signalling axis has a key role in dictating the mode of 3D cell migration (Petrie and Yamada, 2012). Many cancer cell lines are able to change their mode of migration switching from lamellipodia based mesenchymal mode to ameboid form, and this plasticity highlights the need of cells to adapt their migratory strategy when encountering new micro environmental conditions (Petrie and Yamada, 2012, Yamada and Sixt, 2019). Amoeboid cancer cell migration is strongly dependent on RhoA and ROCK signalling along with actomyosin contractility, reducing RhoA, ROCK or myosin II signalling by direct inhibition or indirectly through Rho-Rac cross talk can lead to a switch where cancer cells use the elongated lamellipodial mode of 3D migration (Petrie and Yamada, 2012, Sanz-Moreno et al., 2008, Sahai and Marshall, 2002, Wilkinson et al., 2005, Yamazaki et al., 2009). The balance between Rho and Rac signalling as mediated by crosstalk governs the shift between llamelipodial and round bleb based migration of cancer cells and increasing Rac1 activity can suppress RhoA and ameboid activity (Yamazaki et al., 2009, Sanz-Moreno et al., 2008). Furthermore, knockdown of RhoA protein and activity switched the mode of 3D migration to lamellipodia based (Petrie et al., 2012).

DLC1 is a RhoGAP protein, and has been reported to inhibit RhoA, which could effect the migration behaviour. Therefore another invasion pathway maybe responsible for the invasion in the 3D spheroid model. Both Rac1 and RhoA pathways have been identified as 3D invasion drivers in glioblastoma, which could be applied to the U-87 MG overexpression model (Al-Koussa et al.,

2020). Further investigation into how DLC1 affects RhoA could elucidate information about the 3D migration mechanism.

Although the overall consensus has been that loss of DLC1 promotes invasion and overexpression of DLC1 inhibits invasion, there has been occasional reports of contradicting results. Silencing of DLC1 in prostrate cancer increased migration in a wound healing assay (Shih et al., 2012). Furthermore, silencing of DLC1 altered cytoskeletal organisation by reducing actin stress fibers and reduced the focal adhesion number (Durkin et al., 2005). Overexpression of DLC1 resulted in reduced number of focal adhesions and loss of cell fibres in breast cancer cells which could affect the migratory ability (Kim et al., 2008) . In DLC1 overexpressing HCC cancer cell line SMMC-7721, the formation of actin stress fibers were significantly suppressed, and extensive cell rounding was observed, these morphological changes are similar to ones initiated by a Rho inhibitor, C3 exoenzyme, suggesting inhibition of Rho proteins (Wong et al., 2005). Therefore, it could be concluded that both overexpression and total absence of DLC1 may both compromise cytoskeletal dynamics and migration and this is very dependent on cell type.

4.5 Conclusions

In summary, the effect of DLC1 on 2D, CIA and 3D spheroid invasion assays have been observed. It was shown that DLC1 reduced cell speed and displacement in 2D and CIA overexpression models but had no effect in 3D. Silencing of DLC1 resulted in increased track speed and straightness in 3D assays, and whilst track displacement was reduced in 2D and CIA there was no effect in 3D spheroid model. This suggests cells moved faster and straighter. Overall, this shows that manipulating DLC1 does affect cell migration, but further investigation is required for clarity of DLC1's role in 3D.

Chapter 5 : Investigating the effect of DLC1 on RhoA activity

5.1 Introduction

The previous work in this thesis has evaluated the effect of DLC1 overexpression and knockdown on focal adhesions, cell migration and invasion. This chapter concentrates on DLC1's activity using novel Förster resonance energy transfer (FRET) sensors and investigates the effect of DLC1 on RhoA activity using a RhoA FRET sensor.

5.1.1 DLC1 activation

The structure of DLC1 allows interaction with its many partners. DLC1 contains a N-terminal SAM domain, separated from a RhoGAP domain by a serine rich (SR) region (Braun and Olayioye, 2015) (Figure 1.9). The SR region is a hotspot for protein-protein interactions that play important roles in regulating DLC1's function, and has been shown to bind tensins, FAK, talin and 14-3-3 adaptor protein (Scholz RP, 2009, Li et al., 2011, Chan et al., 2009). The SR region undergoes phosphorylation mediated by CDK5 (Tripathi et al., 2014b). DLC1's regulation of cell migration is primarily dependent on its RhoGAP domain, which is regulated by phosphorylation of the SR region (Tripathi et al., 2017, Kim et al., 2009). It has also been shown that interaction between the SAM and RhoGAP domain keeps DLC1 in an autoinhibited state (Joshi et al., 2020, Tripathi et al., 2014b). The DLC1 SAM domain can bind EF1A1, TNS3 and PTEN in addition to the DLC1 RhoGAP domain (Cao et al., 2015, Heering et al., 2009a, Kim et al., 2008).

To investigate DLC1 activation, novel FRET sensors were developed. A full length DLC1 (Mtfp-DLC1-1-846-Venus) sensor was designed using the RhoA sensor as a template (Pertz and Hahn, 2004). This sensor was developed to investigate the hypothesis that DLC1 has active/inactive conformations. In a study published by Tripathi 2014, they hypothesised that when DLC1 was activated it was in an open conformation with high RhoGAP activity, and when DLC1 was inactivated it was in a closed, autoinhibitory conformation (Tripathi et al., 2014b). It is hypothesised that the intrinsic disordered region (IDR residues 80-846) is partially folded, bringing the SAM domain (residues 1-80) into the proximity of GAP domain (550-846), which inhibits the GAP activity. Upon activation, such as phosphorylation, the GAP domain is released, making the protein fully active (Tripathi et al., 2014b).

These novel DLC1 FRET sensors aimed to elucidate whether DLC1 is active by probing whether the N- and C-termini are close together. If the construct is partially folded, in a closed formation, the SAM and GAP domains should be in close proximity, meaning high levels of FRET. If the DLC1 is active and in a open formation, the two fluorophores will be apart and there will be low levels of FRET. If interaction between the SAM and GAP domains keeps DLC1 in a autoinhibited state, altering the structure may affect the DLC1 activity, and this can be measured with FRET. Several sensors were developed to investigate how the different domains of the protein affect its confirmation (Figure 5.1, Table 5.1).

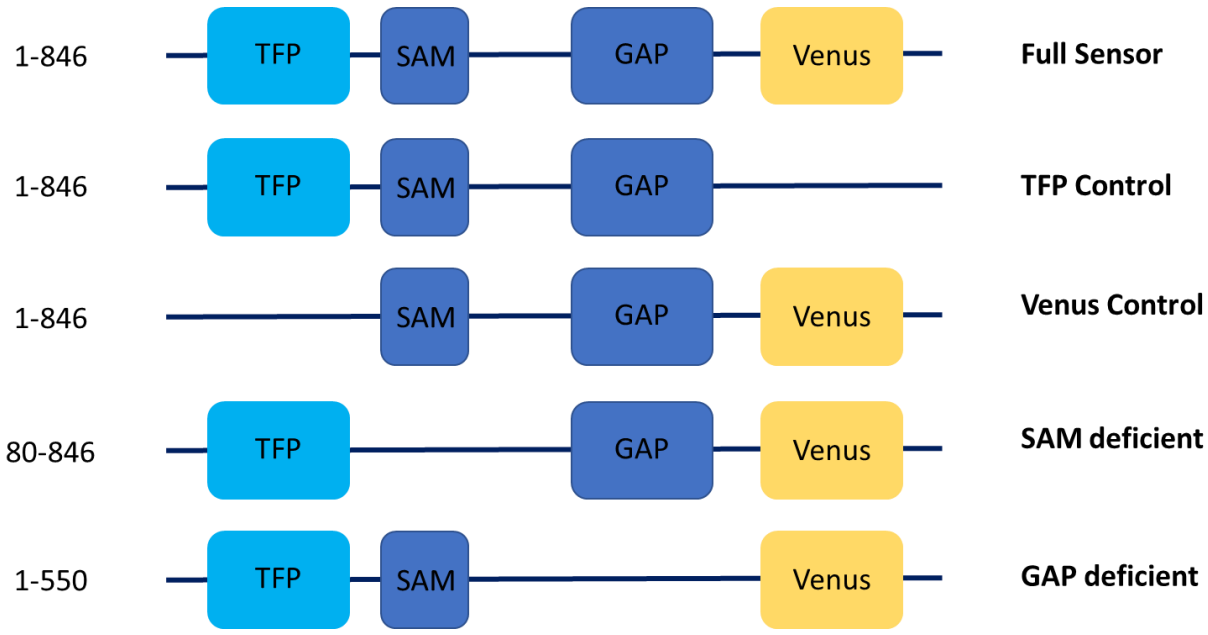

Figure 5.1: DLC1 FRET sensor structure. A range of constructs were developed to assess how domains affect DLC1 activation. It is hypothesised that DLC1 is partially folded and activity is inhibited by close proximity of the GAP and SAM domain therefore FRET sensors containing different domains were developed. These are full sensor TFP-DLC1-1-846-Venus, TFP and Venus single controls, SAM deficient TFP-DLC1-80-846-Venus and GAP deficient TFP-DLC1-1-550-Venus.

Table 5.1 DLC1 FRET sensor plasmids

Plasmid	Details
TFP DLC1 1 - 846 Venus	Full DLC1 protein
TFP DLC1 1-846	mTFP fluorophore only control
DLC1 1-846 Venus	Venus fluorophore only control
TFP DLC1 80 - 846 Venus	SAM-deficient protein
TFP DLC1 1-550 Venus	GAP-deficient protein

5.1.2 DLC1 and RhoA

DLC1 has GAP activity towards RhoA, B and C and Cdc42 (Figure 1.9) (Healy et al., 2008). DLC1 is known to affect RhoA activity through different signalling pathways, and it is hypothesised that ROCK inhibition by DLC1 contributes to its tumour growth suppressive function, while inhibition of mDia formins by DLC1 leads to a migration suppressor activity. DLC1 utilises its GAP domain to negatively regulate RhoA, B, C and Cdc42, to contribute to inhibition of cell migration and invasion (Barras and Widmann, 2013, Pollard and Borisy, 2003). Rho GTPases are prenylated and act at membranes, however there is a cytoplasmic pool of inactive Rho GTPases, which may account for 90-95% of the Rho proteins in the cell (Boulter et al., 2010, Garcia-Mata, 2011 #316). It is hypothesised that the cytoplasmic pool acts as a reservoir allowing the inactive Rho GTPases to be rapidly translocated to the plasma membrane for activation in response to specific signals. (Garcia-Mata et al., 2011).

Rho GTPase signalling is spatially and temporally controlled, although biochemical assays are well established and sensitive, they only show the average of a population (Mahlandt et al., 2021, Pertz, 2010). Genetically encoded fluorescent biosensors enable visualisation of protein dynamics in single living cells with micrometre spatial and sub-second temporal resolution (Mahlandt et al., 2021, Greenwald et al., 2018, Mehta and Zhang, 2011, Miyawaki and Niino, 2015). There are several biosensors available to visualise active Rho GTPase and these are classified into two groups, FRET based biosensors and localisation-based biosensors (Pertz and Hahn, 2004, Mahlandt et al., 2021).

Rho GTPase FRET-based biosensors consist of the Rho GTPase itself, a binding domain and a FRET pair (commonly CFP and YFP). Upon Rho GTPase activation the binding domain binds the GTP-bound Rho GTPase and this conformational change leads to a FRET ratio change with a relatively small dynamic range (Mahlandt et al., 2021). These FRET sensors report on the balance between GEFs and GAPs and report activity. In contrast, localisation sensors consist of a fluorescent protein fused to a binding domain, which has a high affinity for active GTP bound state, and these sensors visualise endogenous Rho-GTP. For example, when Rho GTPase activation occurs locally at the membrane the sensor will accumulate at this location, however one limitation is the background signal of the unbound biosensor in the cytosol, which may reduce the dynamic range (Mahlandt et al., 2021).

5.1.3 FRET sensors

FRET assays and sensors offer real-time, *in situ* detection of protein interaction (Algar et al., 2019). FRET is the transfer of excitation energy of a donor fluorophore to a nearby acceptor fluorophore. In protein studies the acceptor and donor fluorophores are each attached to the respective interacting proteins. The occurrence of FRET can be measured by the quenching of donor fluorescence or a reduction of the fluorescence lifetime, complemented by an increase in acceptor fluorescence emission (Conway et al., 2017). However, different FRET techniques are not applied consistently and there is no standard way to report results, which can make implementing and reproducing FRET experiments challenging (Algar et al., 2019). Further complexities to FRET experiments include selecting acceptor-donor pairing and imaging

efficiency (Mahlandt et al., 2021, Algar et al., 2019). To overcome limitations of FRET, sensors have been modified to increase sensitivity, for example genetically engineering sensors with fluorescent proteins structured internally, allowing native sensing of endogenous regulators such as Rho GTPases (Fritz et al., 2013, Pertz et al., 2006). Furthermore, the development of tools to simplify analysis of FRET assays may allow the technique to become more accessible in the future, as the availability of FRET sensors continues to increase.

The FRET sensor first published in Pertz 2006 allows study of spatiotemporal dynamics of RhoA activation in living cells. This sensor is a single-chain biosensor with intramolecular FRET responding to RhoA activation. The biosensor consists of a Rho-binding domain (RBD) of the effector rhotekin, which specifically binds to GTP RhoA, followed by CFP, an unstructured linker, a pH-insensitive variant of YFP and full-length RhoA (Pertz et al., 2006). When activated by GTP loading, the RBD binds to Rho, changing the relative orientation of the two fluorophores and increasing FRET (Figure 5.1 - A). As the two fluorescent proteins are attached to one another, RhoA activation can be approximated as being proportional to the FRET/CFP emission ratio (Pertz et al., 2006, Miyawaki and Tsien, 2000).

It has been proposed that DLC1 inhibits cellular dynamics through the RhoA signalling pathway. This chapter will investigate how DLC1 affects RhoA activity, using specific biosensors which will illuminate how DLC1 affects spatiotemporal dynamics of RhoA in living cells.

5.2 Aims

The aim of this chapter is to investigate DLC1 activity using a range of FRET constructs, to help elucidate how DLC1 structural domains affect it's activity. Furthermore, this chapter will assess how overexpression and silencing of DLC1 affects RhoA activity using a RhoA FRET sensor.

5.3 Results

5.3.1 DLC1 FRET constructs to assess activity

All FRET DLC1 constructs, full sensor (1-846 DLC1), SAM deficient (80-846 DLC1) and GAP deficient (1-550 DLC1) (Figure 5.1) were transfected into HepG2 cells to assess how different domains affect DLC1 activity. A TFP alone construct (mTFP-DLC1-1-846) was also transfected to be used as a bleed through control in the analysis. Lastly, co-transfection of TFP alone and Venus alone control constructs were included to calculate intermolecular FRET within the cell. All FRET constructs could be visualised in the Venus, TFP and FRET channels (Figure 5.2). To assess spatiotemporal activity of the DLC1 sensors, YFP/CFP ratiometric images were calculated. The DLC1 sensors localised around the cell periphery, however there was no difference in intensity between the three conditions. The TFP alone control showed no fluorescence (Figure 5.3).

As FRET signal changes are subtle with a small dynamic range, the experiment focused on imaging the base of single cells where focal adhesions are located. There was no difference in the mean normalised FRET index between the three FRET constructs, (full (**M** = 67.32) , SAM deficient (**M** = 65.5) and GAP deficient constructs (**M** = 65.06)) (Figure 5.3). Intramolecular FRET was calculated at 55% of full length DLC1 FRET efficiency. Higher FRET suggests that DLC1 is inactivated and in a closed conformation, however all of the constructs have variable measurements, with a similar

average FRET measurement. Due to COVID-19/time restraints further characterisation of the probes could not be completed.

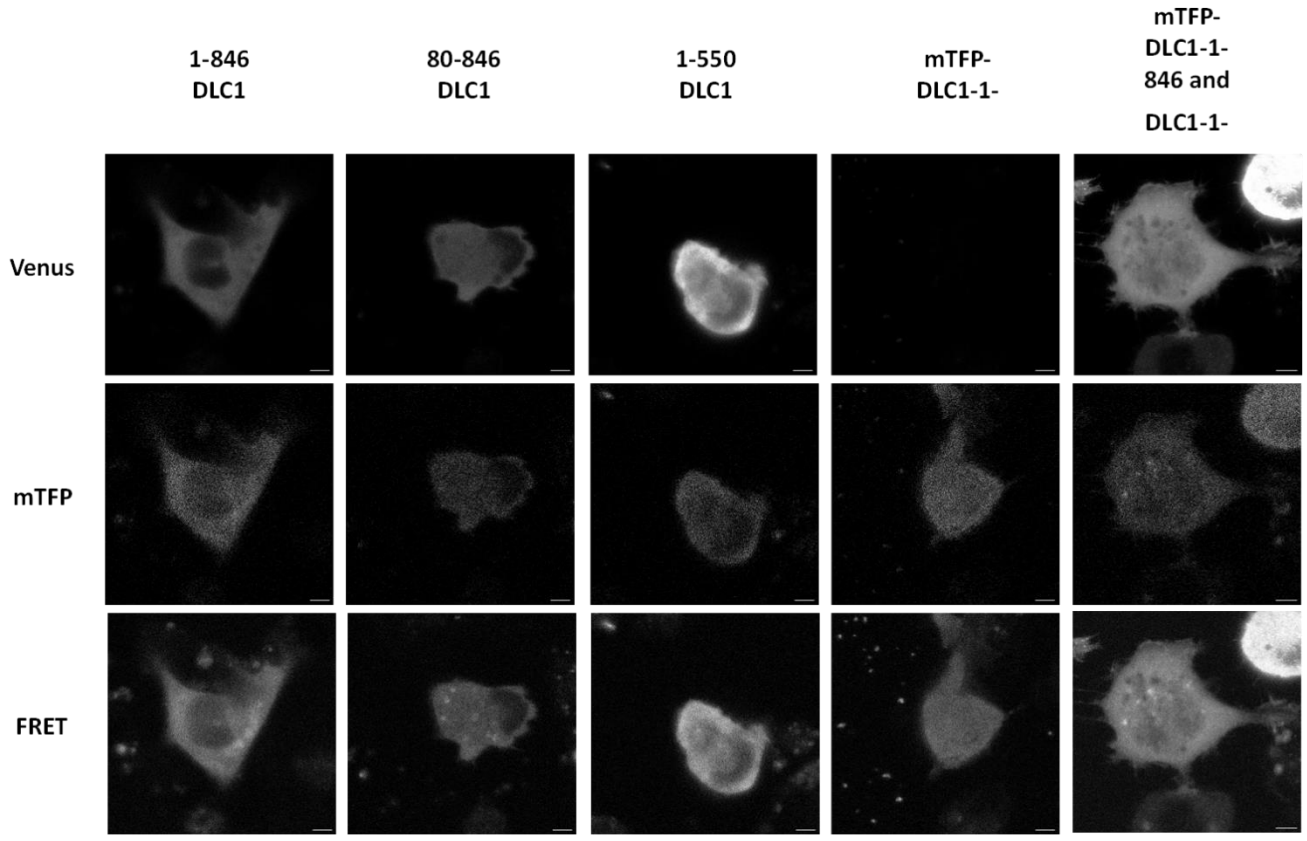

Figure 5.2: Using FRET sensors to assess DLC1 activity. HepG2 cells were transfected with different FRET constructs to assess DLC1 activity. Images were acquired at 40x 1.3NA and analysed using ImageJ plug in pixFRET. Experimental designer was used to create 3 different blocks for imaging. Channels were created for CFP, YFP and FRET, with FRET being excited with CFP (458 nm) and emission in the donor range (YFP). The range for emission for the different channels was taken from the (Pertz et al., 2006) paper to minimize cross talk. Representative images shown from each condition. Scale bar 10μm.

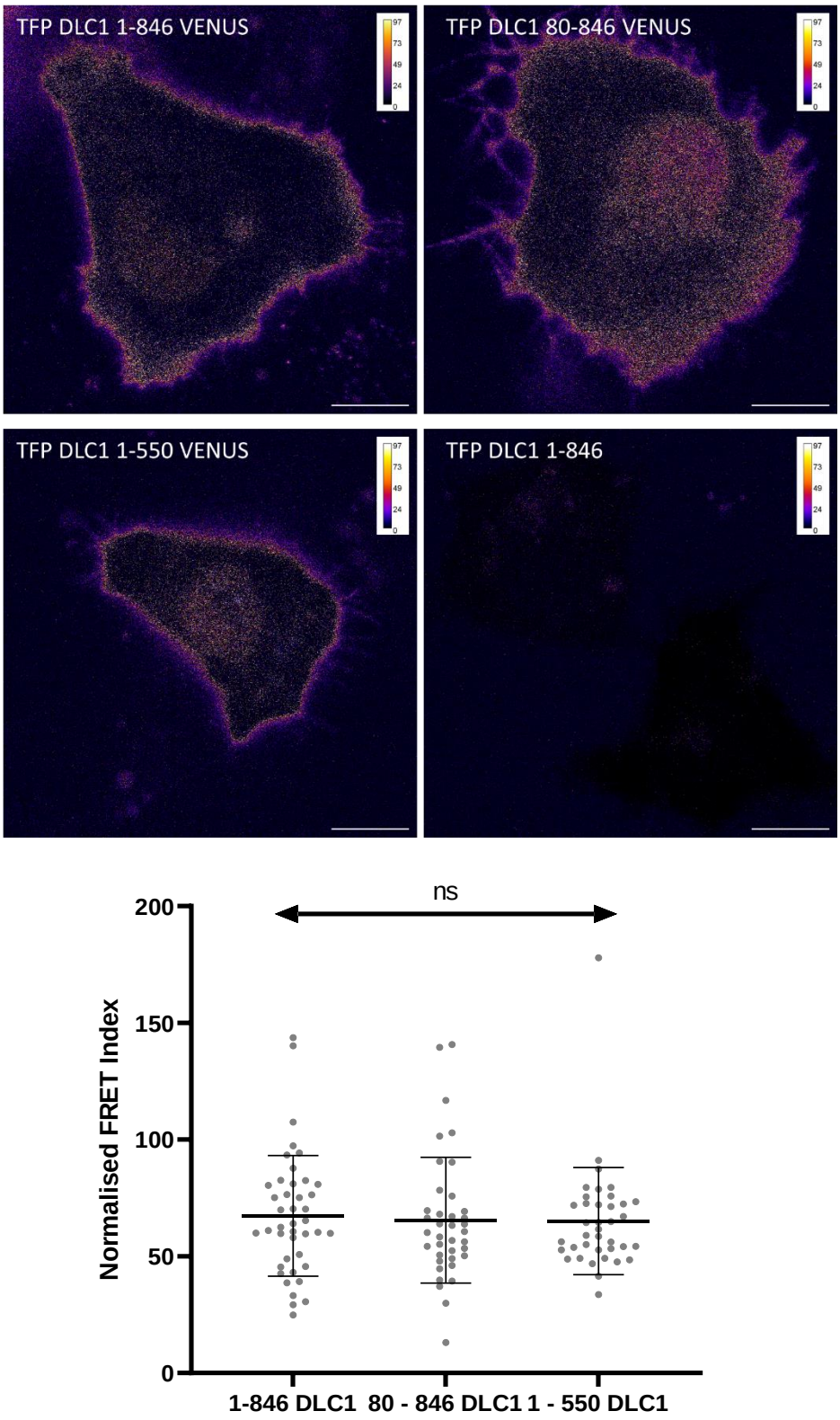

Figure 5.3: Normalised FRET index is unaffected by DLC1 conformation FRET sensors. **A** YFP/CFP ratiometric images showing DLC1 FRET sensor activity. Calibration bar shows intensity **B** Cells were analysed using imageJ plug in pixFRET. There was no significant difference in normalised FRET index between all constructs. N = 3. Scale bar 10µm.

5.3.2 Effect of DLC1 on RhoA activity

To investigate how DLC1 levels affect RhoA dynamics, a RhoA FRET sensor was used (Pertz et al., 2006). Using a RhoA WT sensor aimed to assess the RhoA activity in wild type cells, when DLC1 was overexpressed (mRuby-DLC1) or knocked down by siRNA DLC1. Sensors with functional mutations were also developed with the WT sensor as controls, a positive Q63L sensor and a negative T19N sensor (Pertz et al., 2006). The WT sensor was co-transfected with mRuby-DLC1 to assess how overexpression of DLC1 affected RhoA activity.

First, the WT sensor was transfected into HeLa cells for visualisation and initial optimization. Both YFP and CFP could be detected. To ensure the biosensor was functional, the YFP channel was bleached in a region of interest encompassing one cell, resulting in increased CFP signal, demonstrating that the increase could be measured, and showing FRET (Figure 5.4 B).

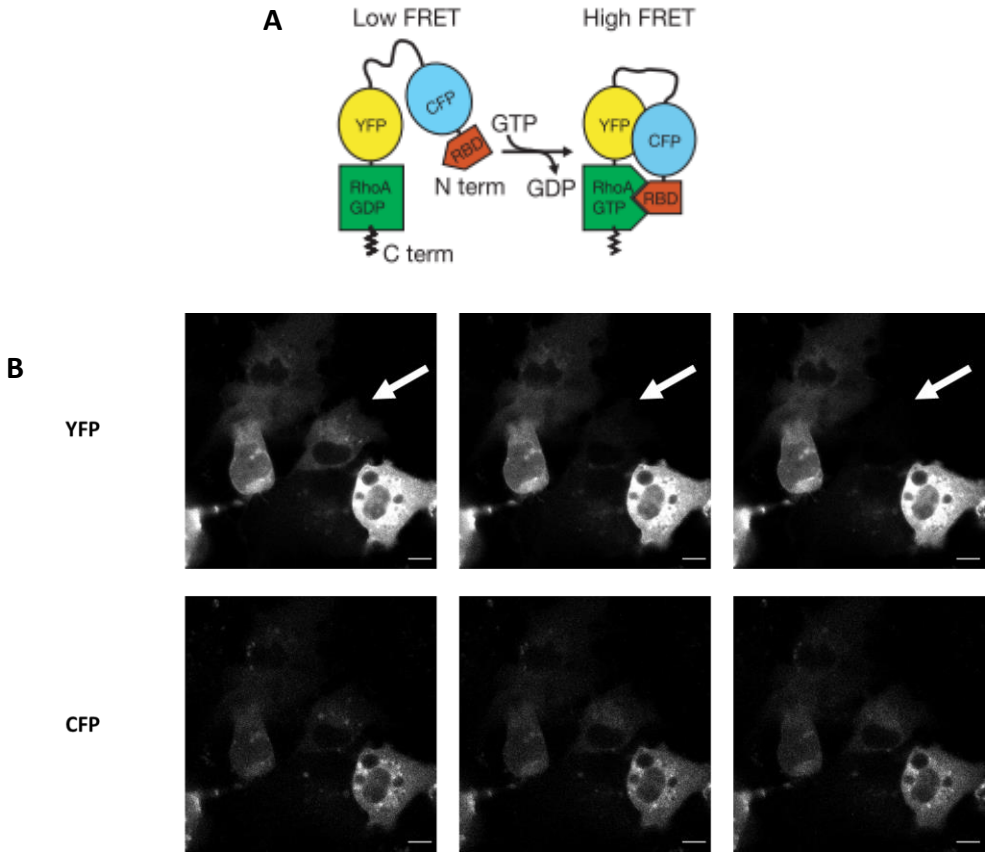

Figure 5.4: Optimisation of RhoA FRET sensor: **A** Illustration of single-chain RhoA FRET sensor. When activated by GTP loading, the RBD binds to Rho, changing the relative orientation of the two fluorophores and increasing FRET. **B** WT RhoA sensor was transiently transfected into HeLa cells. To confirm functionality of the sensor, the YFP channel was bleached resulting in increased signal in the CFP channel. Scale bar 5µm.

The WT RhoA sensor was then compared with a Q63L positive control and T19N negative control. mRuby DLC1 was also co-transfected with the RhoA WT sensor to investigate how overexpression of DLC1 affects RhoA dynamics. The YFP/CFP ratio was calculated to show localisation of RhoA activity (Figure 5.5). The RhoA sensor could be visualised in all conditions, but had reduced intensity in the T19N negative control and mRuby-DLC1 condition, suggesting reduced RhoA activity. The sensor was localised around the edge of the cells for the positive, WT and mRuby DLC1 conditions, whereas was localised to the cytoplasm in the T19N negative condition.

To determine the FRET efficiency, cells were photobleached. At least 16 cells were imaged for each condition, with the CFP and YFP channel acquired. After acquisition of 10 frames, the YFP channel was bleached and the normalized fluorescent intensity of YFP and CFP were calculated. On the point of YFP bleaching, the YFP intensity decreased, and the CFP intensity increased, showing FRET (Figure 5.6). After acquisition of 30 frames, cells were bleached again to measure FRET efficiency. FRET was observed with all RhoA sensors, as the donor intensity increased when the acceptor was bleached.

To calculate FRET, the CFP ratio was calculated (average post bleach intensity/average prebleach intensity) (Figure 5.6). The CFP ratio of mRuby-DLC1 transfected cells were significantly increased (1.45) compared to the RhoA WT sensor (1.28), $P = <0.001$. This was surprising as it is reported that overexpression of DLC1 decreases RhoA activity, and there was less activity in the mRuby-DLC1 YFP/CFP ratiometric image, however here the opposite was observed.

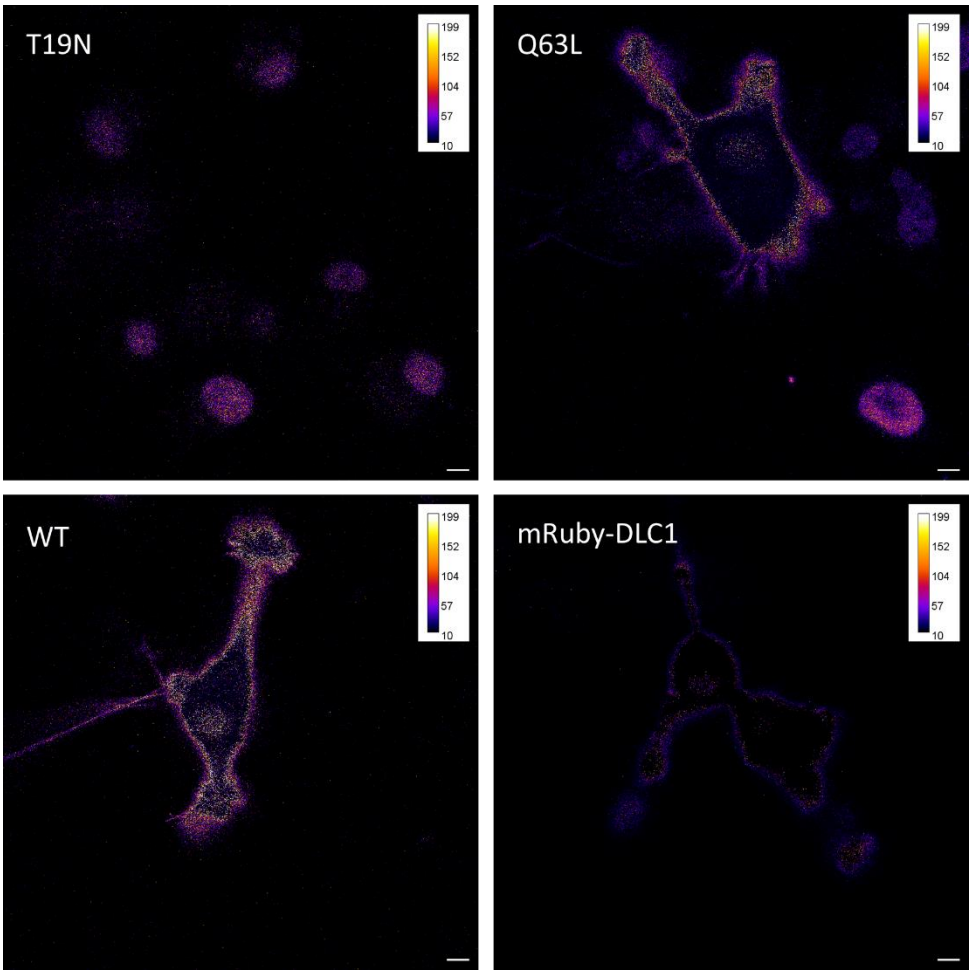

Figure 5.5: YFP/CFP ratiometric images show RhoA activity in U-87 MG cells. YFP/CFP ratiometric images showing RhoA FRET sensor activity. RhoA activity is observed around the cell periphery in WT, Q63L and mRuby-DLC1 conditions. mRuby-DLC1 had decreased levels of RhoA FRET sensor. Calibration bar shows intensity. Scale bar 5µm

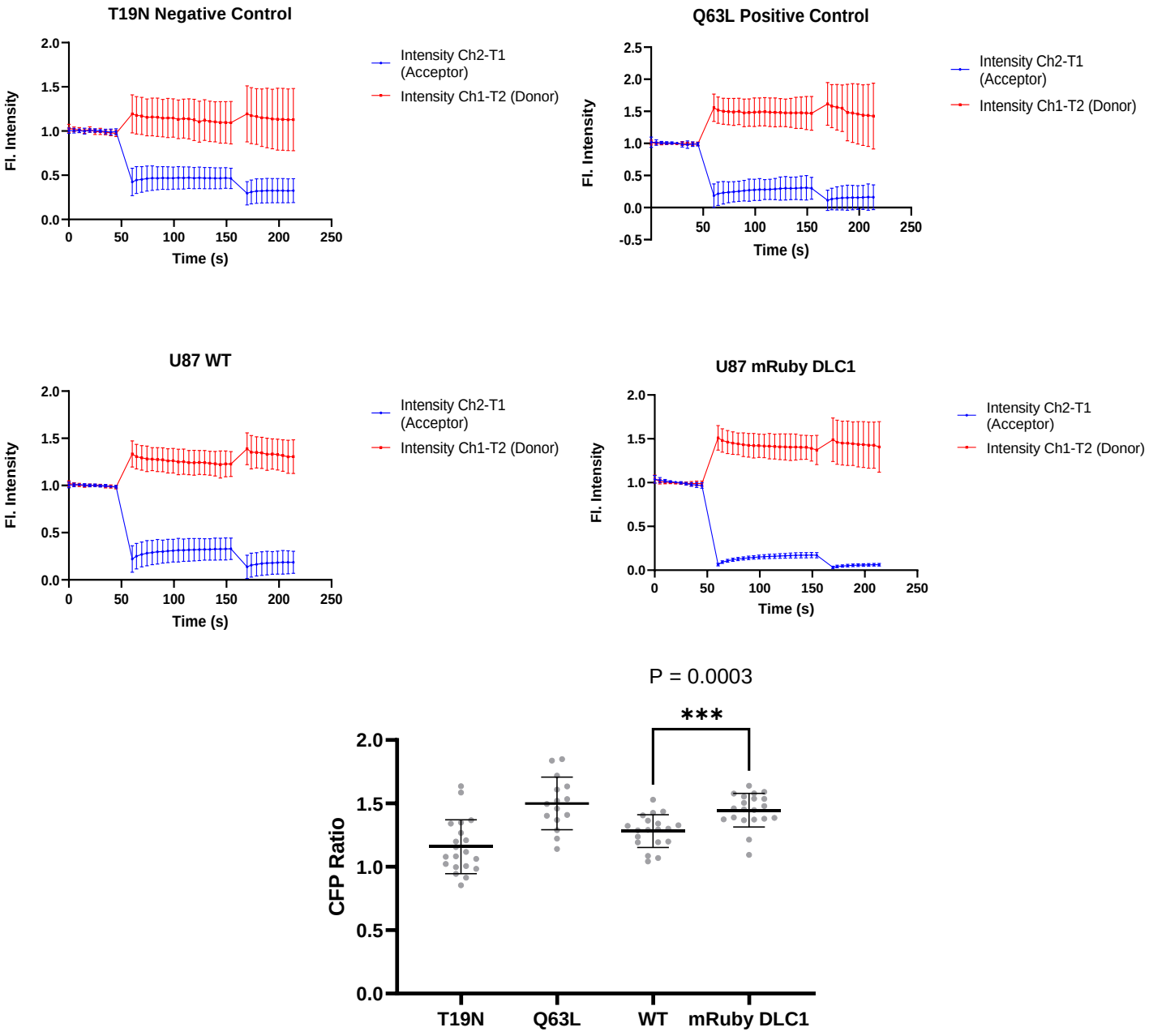

Figure 5.6: mRuby-DLC1 increases RhoA activity. RhoA WT sensor, T19N negative control and Q63L positive control were transiently transfected into U-87 MG cells to investigate RhoA dynamics. mRuby DLC1 was co-transfected with RhoA WT sensor. The YFP channel was bleached after 10 acquisitions, resulting in increased CFP (Donor) intensity. U-87 MG mRuby DLC1 had increased normalized fluorescent intensity compared to RhoA WT. T19N negative control showed a slight increase of intensity. N = 3. The CFP ratio of pre and post bleach intensity was calculated for all conditions. mRuby-DLC1 had a significantly increased CFP ratio compared to RhoA WT, two tailed t test, $t(37) = 3.946$, $p = <0.001$.

The next steps were to investigate how silencing of DLC1 affected RhoA activity. As before the RhoA sensors were transiently transfected into HepG2 cells, including RhoA WT, T19N and 63QL. RhoA WT sensor was also transfected into cells treated with siRNA DLC1 and siRNA scrambled control. YFP/CFP ratio was calculated and RhoA activity was localised in the cytoplasm of siRNA DLC1 conditions, however in the positive control Q63L, WT and siRNA scrambled control RhoA activity was concentrated around the cell periphery (Figure 5.7).

Again, acceptor photobleaching was used to measure FRET efficiency. The YFP and CFP channels were acquired as before, and the YFP channel was bleached. The normalized intensity was calculated for each condition, with >20 cells sampled (Figure 5.8).

The CFP ratio was also calculated for each condition (Figure 5.8). There was no significant difference between the siRNA DLC1 (1.34) and WT condition (1.31), implying that silencing of DLC1 does not increase CFP or FRET. However, there was some variability for the T19N condition.

In conclusion, overexpression of DLC1 increased the CFP ratio, suggesting there was more RhoA activity with increased DLC1, which disputes published reports. Knocking down DLC1 expression (shown in Figure 4.9) using siRNA had no effect on the CFP activity, suggesting that there are other modulators of RhoA activity, or a compensatory mechanism in the cells.

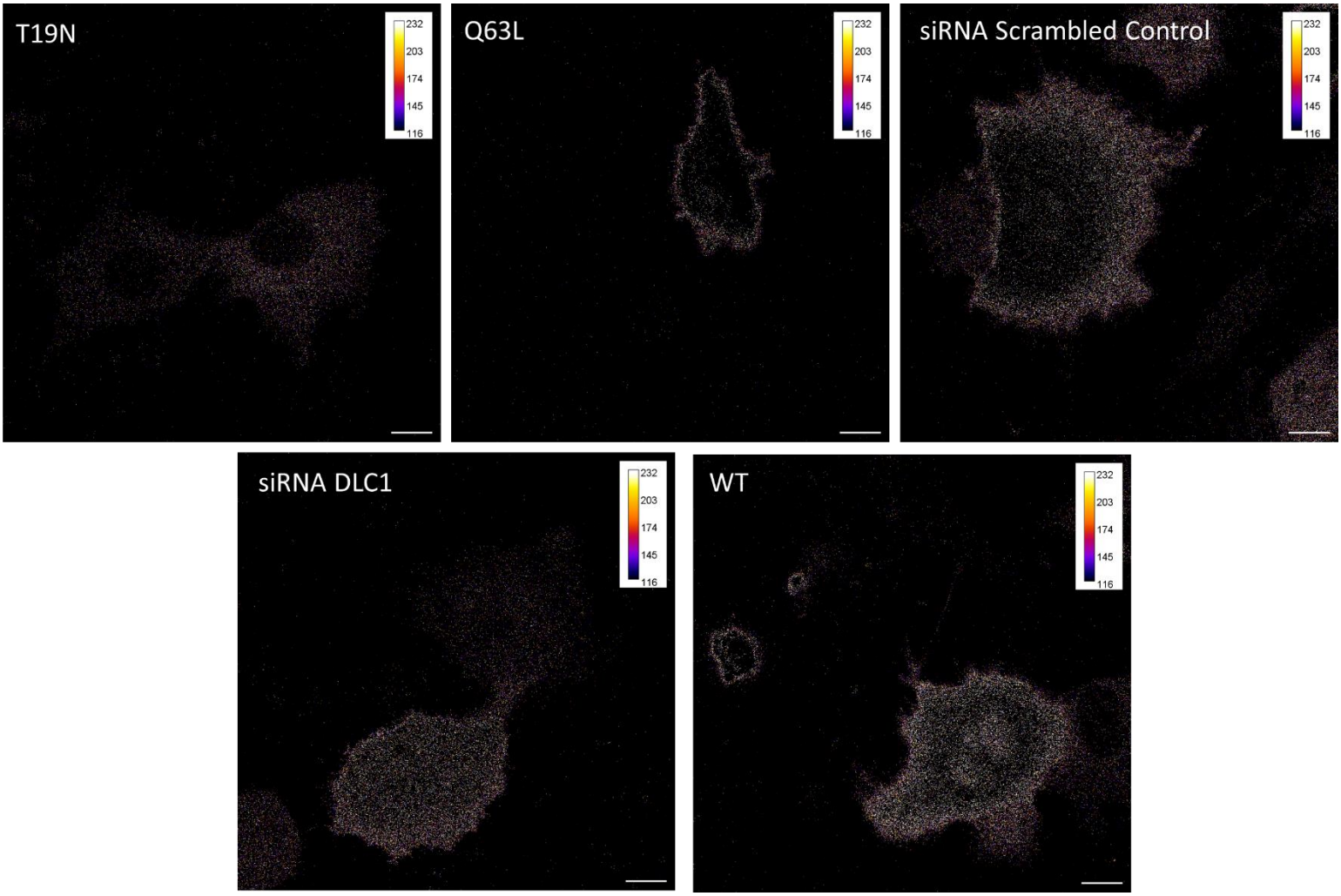

Figure 5.7: YFP/CFP ratiometric images showing RhoA activity in siRNA DLC1 treated cells. YFP/CFP ratiometric images showing RhoA FRET sensor activity in HepG2 cells. RhoA activity is observed throughout the cell cytoplasm in T19N and siRNA DLC1 treated cells. RhoA could be observed around the cell periphery in Q63L positive control cells. Calibration bar shows intensity. Scale bar 5µm.

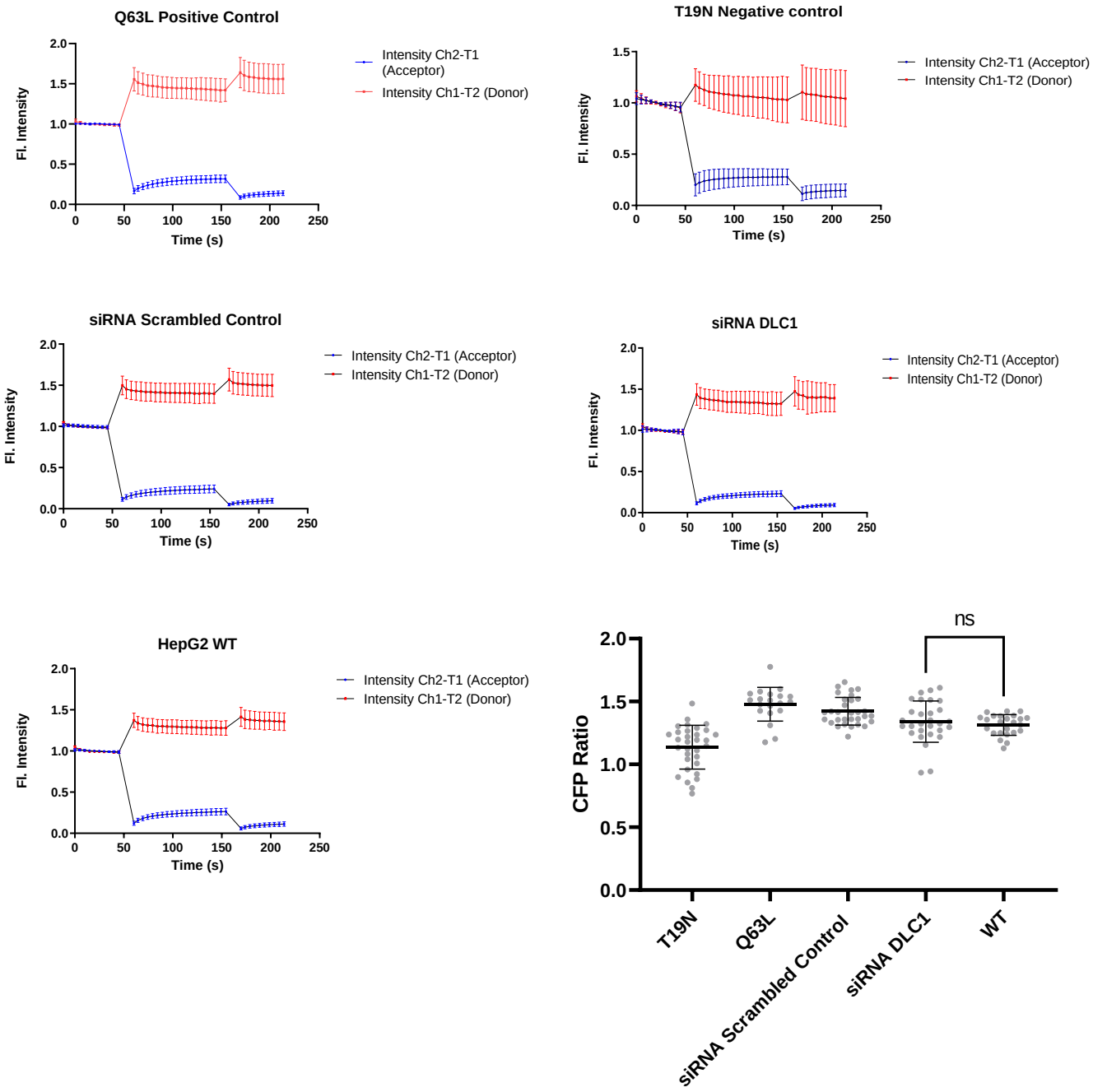

Figure 5.8: siRNA DLC1 does not affect RhoA activity. RhoA WT sensor, T19N negative control and Q63L positive control were transiently transfected into HepG2 cells to investigate the loss of DLC1 on RhoA dynamics. Cells were treated with siRNA DLC1 and scrambled control prior to transfection with RhoA sensors. The YFP channel was bleached after 10 acquisitions, resulting in increased CFP (Donor) intensity. WT, siRNA scrambled control and siRNA DLC1 all showed increased normalized fluorescence. N = 3. CFP ratio was calculated for all conditions for further analysis, however there was no significant differences.

5.4 Discussion

In this chapter the aim was to use different FRET sensors to evaluate DLC1 activity and how DLC1 affects RhoA activity. First, novel DLC1 FRET constructs were used to examine how the different domains affect DLC1 activity. It was expected that if DLC1 was in an active state, the sensor would be in an open conformation, and less FRET would be reported. In contrast, if DLC1 was inactivated the sensor would be closed, with increased FRET. There was no difference between the different FRET constructs, (Full, GAP-deficient and SAM deficient). The FRET index was variable between cells, and further characterisation of the FRET constructs is needed. For example, use of positive and negative controls to allow validation of the novel sensors *in vitro*. The experiments would need to be repeated with an active/inactive mutants to compare the FRET index with positive and negative controls. This could be modification of the sensors to produce a positive control that is consistently folded producing high FRET, and a negative that stays unfolded therefore low FRET. Unfortunately, this could not be carried out within this thesis due to COVID-19 and time constraints.

It is hypothesised that a direct intramolecular interaction between the SAM and RhoGAP domain keeps DLC1 in an autoinhibited state (Joshi et al., 2020, Cao et al., 2012, Kim et al., 2008). This implies that the full sensor (DLC1 1-846) would have had the highest FRET signal as both the SAM and GAP domains are present, leading to inhibition. However, further investigations of the FRET constructs are needed. FRET response is subtle, with a small magnitude of response, therefore it could be beneficial to evaluate FRET measurements subcellularly at focal adhesions, to focus on

the signal area. For future work, quantifying DLC1 activity at different cellular localisations could provide more insight into its dynamics, for example at focal adhesions compared to cytosol.

Another aim was to investigate how DLC1 can affect RhoA activity using a RhoA FRET sensor. It is known that DLC1 can affect several cellular processes controlled by RhoA such as adhesion, migration cell cycle, apoptosis and mechanotransduction (Karlsson et al., 2009). In this work, initially the effect of DLC1 on focal adhesion dynamics and migration was investigated. The next aim was to investigate the effect DLC1 has on RhoA activity itself, upstream of the phenotypic response. First, the RhoA WT sensor and controls (Q63L and T19N) were transfected into the cells to validate that the sensors could be visualised and that FRET could be detected. To ensure FRET efficiency, the acceptor cells were bleached, showing the donor fluorescence increase. This could be seen in all of the sensors, the T19N negative control still showed an increase of FRET, however this was reduced in comparison to the Q63L positive control and WT sensor.

Next, the RhoA WT sensor was co-transfected with mRuby-DLC1, to assess how the overexpression of DLC1 affected RhoA activity. The CFP ratio was significantly increased, suggesting that DLC1 increased RhoA activity. This is conflicting with previous reports that overexpressed DLC1 inhibits cell migration through a RhoA pathway. The hypothesis was that overexpression of DLC1 would decrease RhoA activity as it should inhibit RhoA. This could be due to other activators of RhoA (for example, RhoGEFs), however this would have been observed in the WT condition. Thus, it is more likely that the mRuby-DLC1 transfection caused some bleed through into the CFP channel affecting the ratio. The spectral profiles of fluorescent proteins are very broad, therefore there is overlap of emission spectra between two fluorescent proteins,

where signal from one fluorescent protein can 'bleed' into another channel, creating a false signal. Furthermore, although DLC1 was overexpressed it may not be activated, resulting in no inhibition of RhoA. In the knockdown of DLC1 conditions, as before all transfected cells (Q63L, T19N, WT, siRNA DLC1 and siRNA scrambled control) showed sufficient FRET efficiency. Interestingly knockdown of DLC1 had no significant effect on RhoA activity, suggesting that there could be another mechanism of regulation for RhoA activity. Due to time limitations only initial optimisation of the sensors could be performed, further characterisation of the sensors is needed, for example use of RhoA inhibitors and activators to manipulate RhoA activity and show the effect on sensors. In addition, further controls could be evaluated to understand bleed through, such as a mRuby control. It would also be beneficial to assess the RhoA levels and activity using western blotting and RhoA activity assays, to observe how RhoA is affected by siRNA DLC1 and DLC1 overexpression.

RhoGTPase signalling requires precise co-ordinated action of multiple signalling modules in space and time, using a RhoA FRET biosensor allows observation of real time RhoA activity, and this can be exploited to investigate the relationship between DLC1 and RhoA. In this chapter the expression level of DLC1 was modulated to determine whether this affected RhoA activity, however there are several limitations associated with this approach.

Several biosensors of RhoA regulation have been described, and these FRET-biosensors have played a critical role in the investigation of RhoA signalling dynamics *in vitro* (Nobis et al., 2020). These tools have also become a vital to study *in vivo* protein interactions. These studies have yielded significant insights into the regulation of RhoA in complex 3D disease and model organism

settings. Previous *in vivo* studies using a RhoA FRET sensor have enabled the understanding of RhoA signalling in a range of studies including monitoring live RhoA signalling in neutrophils and the RhoA activity during pancreatic cancer progression and metastasis (Nobis et al., 2017).

Healy et al. previously used RhoA FRET sensors to study DLC1 . In this work, a DLC1-RhoA FRET sensor was stably transduced into cells and demonstrated that DLC1 expression significantly reduced RhoA activity, especially at the leading edge of the cells (Healy et al., 2008). This led to the hypothesis that DLC1 reduces RhoA activity, contributing to the reduced migratory ability of DLC1 expressing cells, and potential to supress invasion and metastasis (Healy et al., 2008). This study was based on the original publication of the RhoA biosensor, and used metamorph software to study the YFP/CFP ratio (Pertz et al., 2006). As previously mentioned, due to time constraints only initial experiments could be performed with the RhoA FRET sensors. A useful follow up experiment would be to assess these sensors subcellularly, and potentially use TIRF microscopy to investigate FRET within focal adhesions.

A more recent study used a RhoA FRET biosensor to investigate how DLC1 affects PKD activation and RhoA regulation. It was hypothesised that Rho activates PKD, which phosphorylates and inactivates the RhoGAP DLC1, to support further Rho activation (Jensch et al., 2018). Active PKD1 showed increased FRET ratio of the RhoA sensor, whereas the inactive PKD1 failed to increase the FRET ratio. These data provided evidence to support a molecular pathway where RhoA activates PKD, which phosphorylates and functionally inactivates DLC1. In this study, the cells were lysed and FRET was measured with a plate reader, not with confocal microscopy as in this chapter, highlighting where there might be key differences. A plate reader would measure global

fluorescence of a well, in contrast to microscopy measuring several cells in one field of view. However, the analysis was similar as the FRET ratio was calculated by dividing the FRET signal by the CFP signal.

Whilst FRET is a powerful tool to measure protein-protein interactions, it can be challenging and have some limitations. In this chapter, two different FRET sensors have been used to answer different biological questions, and although there are a range of FRET sensors available, each measures different factors. One major limitation of FRET is that there is no consensus method, controls and analysis pipeline, which means it can be difficult to compare FRET experiments and interpret the results in the context of the current literature. However there is literature available to avoid the pitfalls (Algar et al., 2019). The FRET experiments have been analysed differently in this chapter according to the available controls. The RhoA FRET sensors had their own positive and negative mutated controls, whereas the DLC1 FRET sensor had single fluorophore chain sensors to use as negative and bleed through control. It was challenging to find open source tools, as most papers had custom scripts for specific FRET sensors or commercial software, and some open source tools require specific controls for quantification. The single chain sensors allowed use of pixFRET ImageJ plug in, which could incorporate bleed through controls to calculate FRET index. For future FRET experiments, it would be beneficial to use a system where FRET controls are considered at the image acquisition stage and incorporated into the software. This would provide a smoother and more robust workflow and image analysis pipeline for FRET experiments.

In conclusion, cancer RhoGTPase signalling pathways cooperate with other signalling platforms, which adds to their complexity, and manipulation of RhoGTPase signalling can lead to diverse

outcomes (Crosas-Molist et al., 2022). Therefore, altering upstream regulators such as GEFs and GAPs may lead to non-discriminant activation of multiple signalling modules. Another consideration is the crosstalk between the Rho GTPases, where affecting one might lead to collateral effects on others, with their own effects (Pertz, 2010). Therefore, it is important to consider that manipulating DLC1 may induce artifacts, and further investigation will be required to ensure its role.

5.5 Conclusions

In summary, this chapter has shown use of FRET sensors to investigate DLC1 activity and the effect of DLC1 on RhoA activity. Unfortunately, full characterisation of FRET sensors could not be completed beyond the initial optimisation. Both sensors require further validation, including improved controls to be able to put changes in FRET index into context.

Chapter 6 : General Discussion

The work in this thesis explored the role of RhoGAP DLC1, a metastatic and tumour suppressor known to play a role in several cancers such as liver, lung and breast (Section 1.8) (Wang et al., 2018, Yuan et al., 2004, Yuan et al., 2003b). Increased invasion is associated with metastatic potential, and as RhoGAP proteins are negative regulators of cell migration, the relationship between DLC1 expression level and the migration and invasive behaviour of cells was investigated. The role of DLC1 was investigated at the site of focal adhesions, and the effect of DLC1 in cell migration was assessed using 2D cell migration and 3D spheroid invasion assays in U-87 MG and HepG2 cells. FRET sensors were utilised to investigate how different structural domains affect DLC1 activity. Finally, the effect of DLC1 on RhoA activity was also measured using a RhoA FRET sensor.

6.1 Investigating the role of DLC1 in focal adhesions dynamics

The first aim of this thesis was to investigate DLC1's role in focal adhesion dynamics. Previous published data has shown that the GAP function of DLC1 is lost when DLC1 cannot localise to focal adhesions (Li et al. 2011). Although DLC1 localises to focal adhesions, a clear mechanism of how the localisation affects activity has not been established. Focal adhesion dynamics were analysed using live TIRF microscopy and evaluated with overexpression of mRuby-DLC1 and GFP-talin. Small changes were observed in focal adhesion dynamics when DLC1 was modulated, which could suggest DLC1 affects focal adhesion turnover. When mRuby-DLC1 was overexpressed, the

rate of assembly was slightly increased compared to GFP-talin only expression. Disassembly of mRuby-DLC1 overexpression focal adhesions was slower compared to GFP-talin. Knockdown of DLC1 had no effect on focal adhesion assembly, however, the speed of disassembly was slower compared to siRNA scrambled control. This could suggest that regulated expression of DLC1 is required for correct focal adhesion disassembly. However, in these experiments GFP-talin was used as a focal adhesion marker, therefore although DLC1 was knocked down the effects could have been masked due to GFP-talin overexpression. The subtle differences in focal adhesion rates when DLC1 and talin are manipulated suggest their involvement in focal adhesion dynamics. This work could provide a foundation for further experiments such as investigating the modulation of DLC1. Investigating dynamics with a neutral marker such as paxillin would provide a clearer picture of how DLC1 affects dynamics. Pairing this with the dynamics of DLC1 mutants could provide a clearer function at focal adhesion level. In addition, investigating the focal adhesion lifetime could also provide details of how DLC1 affects focal adhesion dynamics.

The majority of published studies focus on the mechanosensitive function of focal adhesions, with applications of traction force and atomic force microscopy. Traction force microscopy (TFM) was mainly used to investigate stress on substrates through focal adhesions, components of the focal adhesion and the molecular clutch and mechanical relationships of focal adhesions (Ungai-Salánki et al., 2019, Mishra and Manavathi, 2021). Research using atomic force microscopy (AFM) has allowed real-time assessment of focal adhesion protein dynamics, however this was in response to mechanical stimulus and tension sensitive focal adhesion proteins (Haase et al., 2014, Franz and Müller, 2005, von Bilderling et al., 2017, Mishra and Manavathi, 2021).

Micropatterning can be used to look at focal adhesions, for example, mimicking extra cellular matrix such as fibronectin on surfaces and investigating the effect on focal adhesions (Buskermolen et al., 2020). However, using mechanical and chemical modification as the stimulus, may not reflect physiological focal adhesion properties, such as number and size (Mishra and Manavathi, 2021). In contrast, using TIRF imaging to visualise live DLC1 dynamics has provided quantification of assembly/disassembly rates, giving direct insight into how DLC1 effects focal adhesion dynamics.

A popular tool to study focal adhesion dynamics is using FRET based molecular biosensors, these sensors can be custom made to investigate dynamics, kinase activity, GTPase activity, structural conformational changes and also tension sensing (Sarangi et al., 2017, Morimatsu et al., 2013, Papusheva et al., 2009, Koudelková et al., 2019, Case et al., 2015, Zhang et al., 2016b, Jurchenko and Salaita, 2015). FRET can also be measured at focal adhesion structures, specifically using FRET tension sensors, to measure the arrangement of adhesion molecules and how they respond to traction (Kong et al., 2005). Measuring the FRET of DLC1 at focal adhesions could be an additional technique to provide more specific information about focal adhesion dynamics.

Ultimately, for a comprehensive evaluation of DLC1's role at focal adhesions, further studies would need to be completed. The data presented here, shows an important piece of the picture, however, to date there are limited studies published evaluating specific focal adhesion turnover rates. Therefore, in future work it could be of interest to investigate major focal adhesion protein dynamics, with the inclusion of WT DLC1 and function mutants. This would provide more

information on the function of DLC1 at the focal adhesion complex and put the findings in this thesis into context.

6.2 Modelling invasion

Investigation into migratory, adhesion and invasion phenotype of tumour cells, and understanding the underlying molecular mechanisms is fundamental for the development of novel strategies for clinical diagnosis, prognosis, drug development and treatment approach (Pijuan et al., 2019). Quantification of *in vitro* migration in cancer cell lines using timelapse microscopy can be an important tool to study novel potential therapeutics, and to understand basic principles of molecular metastatic pathways (Pijuan et al., 2019).

Several invasion and migration assays are currently used in the oncology field, with the ability to measure an extensive variety of cell motility parameters, such as wound area, velocity, healing speed, front cell velocity, travelled distance, and invasion rate (Pijuan et al., 2019). These assays allow observation of phenotypic analysis during single cell assays and could provide information about metastatic potential of the type of cancer studied *in vivo* for the understanding of prognosis of the disease (Pijuan et al., 2019).

The current standard methods to assess tumour cell invasion *in vitro* are transwell-based or Boyden chamber assays, or alternatively cells can be seeded on top of an ECM gel, where they form a monolayer then collectively or individually invade into the gel. Another approach is to embed tumour cells into a matrix, as single cells or as a spheroid, this allows cells to invade out of the tumour mass into the surrounding matrix (Vinci et al., 2015, Zimmermann et al., 2013, Brekhman and Neufeld, 2009, Deisboeck et al., 2001, Härmä et al., 2010). Invasion can be

measured in terms of number of invading cells and/or distance travelled from the gel surface (Deisboeck et al., 2001, Vinci et al., 2015).

Many synthetic and animal-derived matrices have been developed for 3D cell culture assays, including mouse sarcoma-derived matrix, Matrigel (Naakka et al., 2019, Nath and Devi, 2016, Vinci et al., 2015, Salo et al., 2015). None of the commercially available matrices have originated from human tumour tissue, therefore they lack the features of human tumour microenvironment, which has significant effects on cancer cell invasion processes (Salo et al., 2015). It has been shown that the protein content of human derived matrix differs significantly from mouse derived, though some proteins such as laminin, type IV collagen, heparan sulphate proteoglycans, nidogen, and epidermal growth factor, are present in both matrices. Additionally, the mouse differs from the human in enzyme contents, with humans having 78 fewer proteases than mice (Naakka et al., 2019). The variability of batches of matrigel could prove problematic in the development of robust invasion assays, so a better alternative may be commercial synthesised hydrogels that are highly reproducible, though these can lack the complexity of matrigel. Matrigel was used in the CIA and spheroid assays, which could explain some of the variability. Another important consideration is the stiffness of the hydrogel, it is important to match the stiffness of the tissue the cell is derived from for true physiological modelling, as different tissues have a different stiffness, though this is a challenge in *in vitro* culture.

Spheroids are considered the main 3D cell culture model in reproducing physiological and biological characteristics of solid tumours and provide an alternative to predict what might occur in *in vivo* models (Lasagna et al., 2022, Costa et al., 2016, Mehta et al., 2012). The capability to

reproduce the *in vivo* 3D tumour environment, including cell heterogeneity, gene expression patterns, cell differentiation, generation of hypoxia, activation of cell signalling pathways, and cell-cell and cell-ECM adhesions are some of the advantages for spheroid use for *in vitro* studies on chemo resistance, migration and invasion and tumour biology such as cancer stem cells, tumorigenicity, hypoxia and tumour metabolism (Pinto et al., 2020). These unique characteristics of the spheroid model also highlight the potential of 3D spheroids to be used as *in vitro* models for screening new anticancer therapeutics (Costa et al., 2016).

There are currently a range of ways to generate spheroids, and each of these have advantages and disadvantages. For example, the hanging drop method, generates a higher quality yield of reproducible uniformly invading spheroids, but can take longer to form and have variability in their end sizes. On the other hand, generating spheroids with the spheroid microplates method provides a large number of compact spheroids, but these can be at a lower quality, therefore lacking consistency and leading to differing behaviour across spheroids (Cisneros Castillo et al., 2016). The spheroids used in this thesis were generated using a microplate, therefore they did vary in size, but did form compact and robust spheroids, suitable for the assays. Using an ultra-low attachment plate or hanging drop could have generated more uniform spheroids and may have reduced variability, however there is no optimal method for the generation of robust and uniform spheroids. In this study, variability was observed between the MSD of spheroids. It is not known whether the variability in MSD was related to how the spheroids were formed or an inherent issue with 3D spheroid formation. In this work, three spheroids were acquired and quantified for each of the conditions. Due to the variability, it would be advantageous to increase

the sample number for each condition to help account for the variability and increase data robustness.

While 3D cultures are more representative of the *in vivo* environment than 2D for differing reasons, 3D cultures come with limitations. 3D cultures are more expensive, harder to replicate, and the assembly can be difficult (Jensen et al., 2022, Antoni et al., 2015, Langhans, 2018, Jensen and Teng, 2020). Furthermore, the large variabilities between 3D models limit their level of standardisation and this threatens and their use as preclinical tools for drug development (Barbosa et al., 2022). Further characterisation and standardisation of 3D cell models are needed before they can be incorporated into routine drug discovery microscopy screening methods.

Another challenge of 3D cultures is quantification. Many microscope techniques have been utilised to study 3D models and despite these imaging techniques steadily improving, imaging still represents a unique challenge for 3D cell culture models (Jensen et al., 2022). 3D model imaging is affected by several issues, namely poor light penetration, light scattering by cells, and high background due to out-of-plane fluorescence (Barbosa et al., 2022, Sirenko et al., 2015). Using lightsheet microscopy to image the spheroids was successful, and although there were problems with sample drift, there was no difficulty in acquiring through the whole sample.

A tool for studying 3D cultures is fluorescence microscopy, fluorescent markers can be used to evaluate viability, DNA presence, and apoptosis, among other parameters (Sirenko et al., 2015). Use of markers can help to overcome challenges such as penetration of dyes, a particular problem in the 3D spheroid model. Live cell imaging of spheroids can be achieved through time-lapse microscopy, a technique which has been used for a variety of studies, notably to study cell

migration and invasion and model metastasis (Conti et al., 2021, Voon et al., 2022, Maruno et al., 2021). In most reported studies, cell migration assays are limited to endpoint assays, however novel *in vitro* time-lapse microscopy approaches provide dynamic data, allowing novel insights into the kinetics of cell behaviour. However, live imaging introduces additional challenges in 3D cultures, such as quantitative analysis and downstream interpretation of motility (Pijuan et al., 2019).

In this thesis, the invasion of DLC1 expressing cells were measured using a spheroid model and live lightsheet microscopy. A revolutionary technique that has made huge advances in the last few years, light sheet microscopy allows fast and gentle imaging of whole spheroids. The cells overexpressing GFP-DLC1 were tracked over time, which provided live measurements of the cell invasion dynamics, such as track speed, mean displacement length and straightness. This allowed establishment of a system to analyse the effect of DLC1 on single cell migration in glioblastoma and liver cancer spheroids.

Live cell imaging can be complex, and lightsheet microscopy produces large data sets so acquisition was limited to 16 hours, though in this time many measurements could be taken. In addition, not only was this type of microscopy able to image through a whole spheroid without optical issues, but this analysis also gave dynamic information about tracks, compared to the usual invasion parameters of distance travelled in a time period in an endpoint assay, for example at 24 hours. Although endpoint assays tend to be analysed after a longer time frame than measured here, it would be possible to extend the assay used here by increasing the intervals between imaging frames from minutes to hours, to ensure data could be captured over an overall

longer time. This would have the advantages of both enabling live imaging by reducing data size, and still maximise the time course length the spheroid could be imaged for. The lightsheet microscope could be altered to support longer imaging. Alternatively, fixed samples could also be imaged on the lightsheet microscope, fixed spheroids would provide exemplar samples for multiangle reconstruction. This could then be applied to live imaging and assessing the effect of DLC1 on the whole reconstructed spheroid could be evaluated over a longer time. There are several adjustments that can be made to the current spheroid assay to improve imaging and to gain insight of DLC1 in 3D invasion.

An additional improvement to the assay could be to use stably transduced cell lines, instead of transient transfection of the spheroids used here, which could increase assay reproducibility. A virally transduced cell line could be produced with overexpressed or knocked down DLC1, and spheroids could be formed with these cells. Transduced cell lines are powerful tools for microscopy, as they reduce the need for manipulation before imaging. In spheroids this also removes the limitation of penetration of dyes or transfection reagents, simplifying the experiment. Furthermore, this would allow the consideration of how spheroid age affects migration and invasion.

6.3 DLC1 and cell migration

One of the aims of this thesis was to investigate the effect of DLC1 in complex environments. While much cell migration research uses 2D models, studies have shown that the presence of 3D extracellular matrix is critical for normal cell behaviour including migration and adhesion (Yamada and Sixt, 2019). Studies comparing cell behaviour in 2D and 3D matrices have revealed

differences in cell morphology, migration, adhesions, and signalling (Hakkinen et al., 2011). 3D models can mimic the ECM environment and can be manipulated to investigate effects on cell behaviour. However, they can differ due to different matrix compositions, highlighting the variability within the 3D migration field (Naakka et al., 2019). Whilst 3D models are more physiologically relevant, 2D models are still desirable due to simplicity and investigation of mechanisms such as adhesion kinetics (Pijuan et al., 2019). 3D cancer cell culture more accurately reflects the complex tumour microenvironment, with cell-cell and cell-matrix interactions, gene expression profiles, drug sensitivity and signalling pathway activity (Naakka et al., 2019, Vinci et al., 2012, Nath and Devi, 2016). Not only do 2D cell cultures fall short with model tumour architecture, but they also cannot mimic mechanical and biochemical signals, and interactions between the cells and ECM (Pampaloni et al., 2007, Barbosa et al., 2022).

2D cell cultures have been used since the early 1900s, playing a vital role in research and can be more advantageous over 3D models due to being more simple, high throughput, standardised and reproducible (Andersen et al., 2015, Karlsson et al., 2012, Barbosa et al., 2022, Jensen et al., 2022, Costa et al., 2016, Ferreira et al., 2018). However 2D cultures have many limitations due to limited representation of the tissue cells *in vitro* (Jensen et al., 2022). Furthermore, cells cultured in monolayers are exposed to surfaces with high stiffness, which can not only alter the cell's behaviour but also influence differentiation, gene expression and drug sensitivity (Barbosa et al., 2022, Ravi et al., 2015).

The difference between 2D and 3D models have been particularly impactful on the cell migration field. Cell migration studies were first researched using classical 2D cell migration, across plastic

and glass surfaces. However studies over the past decade have identified that the mechanisms that control cell motility within 3D microenvironments are varied, some similar and some highly divergent compared to 2D (Caswell and Zech, 2018). It has been observed that in more physiological 3D environments, cells become more flexible and can exhibit a wide variety of migratory modes, including; mesenchymal, lobopodial, amoeboid and collective, and they have the ability to switch between these modes depending on the context (Yamada and Sixt, 2019).

Previous research has investigated the role of DLC1 expression in migration using 2D assays with end point measurements, investigating live dynamics allows insight into the behaviour of the tracks. Here we could assess how overexpression or loss of DLC1 affects track speed and straightness. Although velocity and other live parameters have been reported, no live data has been published on the effect of DLC1 expression on 3D cell invasion tracks. As previously mentioned, the standard for invasion is distance travelled, which is comparable to the mean track displacement or track length in this thesis.

Overexpression of DLC1 reduced track speed and displacement length in 2D and 3D CIA assay whereas the 3D spheroid model showed no detectable differences. This supports the role of DLC1 as a tumour suppressor, as overexpression reduces the speed of cell tracks and the displacement.

When DLC1 was knocked down there was an increased track speed but reduced displacement length in 2D assays implying cells have fast but short tracks. This could suggest a balance of DLC1 is needed and knocking down expression impaired normal cell migration ability. In the 3D spheroid model, knockdown increased track speed and reduced displacement length, similar to the 2D assays. It was hypothesised that loss of DLC1 would increase cell migration, however,

although the cell track speed was increased, the displacement was decreased. The cell model used for knockdown experiments of DLC1 was HepG2 cells, as these cells had a moderate wild-type expression of DLC1. However, HepG2 cells were not as migratory as U-87 MG cells used for overexpression studies. This could explain why there was not much difference in displacement observed in the HepG2 cells as the assay window would be smaller.

Therefore, it could be hypothesised that the mechanisms of action of DLC1 could differ across the 2D and 3D cell models, explaining how overexpression of DLC1 did not have any effect in the 3D spheroid model. There are differences between 3D CIA and spheroid models, whilst the CIA allows visualisation of cells as they interact with a 3D matrix, but still remain close to a glass surface, 3D spheroids demonstrate a greater variety of cell–cell contacts in comparison with the classically used monolayer cell culture, as well as the gas and nutrient gradients characteristic of tumours (Yu and Machesky, 2012, Kutova et al., 2020). While the cells in the CIA assay grow on glass, the cells in a spheroid aggregate together in a microplate, therefore culturing differences such as cell seeding, and growth could also contribute to variations in cell migration.

Furthermore, differences in migration were seen depending on where the cells were located within the spheroid. The cells on the outside of the spheroid were seen to invade more than cells within the spheroid, which was an interesting observation following spheroid image analysis. Differences in migratory behaviour could be masked when observing spheroids as a whole and development of new analysis pipelines to analyse the outer ring of spheroids could provide additional information of DLC1's role in the invasive phenotype.

In this thesis, the spheroids were formed in 24 hours as they were transfected with siRNA or GFP-DLC1 during spheroid formation for better penetration. It would be interesting to see how DLC1 affects the invasion of older spheroids compared to the freshly formed spheroids, which would be achievable with transduced cell lines. Likewise, the use of primary cells would be more representative of *in vivo* environment. However, these are difficult to obtain and may not form spheroids as easily.

Interestingly, the effect of DLC1 on sprouting in angiogenesis has been published, where the level of DLC1 affected the sprouting ability of endothelial cell spheroids (van der Stoel et al., 2020). Overexpression of DLC1 promoted the sprouting ability, and knockdown of DLC1 depleted the sprouting, which could be rescued with DLC1 expression. Sprouts were measured after 16 hours and measured by sprout number. The length of the sprouts was also measured. This report is the only data published investigating DLC1 in spheroid assays. Data generated in this thesis adds to the evidence for DLC1's role in processes associated with cell migration.

6.4 Future perspectives and conclusions

Whilst it is clear that DLC1 has an interesting role within invasion and metastasis, much remains unknown about its mechanism and function. When investigating the role of this protein, an important consideration is the difference in behaviour between 2D and 3D assays. Whilst there is minimal published data describing the role of DLC1 in 2D cell cultures, even less is known about the role of DLC1 in 3D cultures. In this thesis, the role of DLC1 expression in 3D invasion assays was investigated in a spheroid model. Whilst single cells could be tracked, this assay concentrated on a population of cells at low magnification and resolution, to generate the maximum amount

of data on multiple cells, rather than detailed analysis of single cell invasion. For future studies it would be interesting to visualize DLC1 expressing cells invading through matrix at a higher resolution, which could answer questions about how DLC1 affects cell morphology in 3D. Another future perspective would be to investigate the other roles of DLC1, not directly linked to cancer but closely associated. For example, the link between DLC1 and mechanosensing, which could have wider disease implications. Other potential research would be the interaction of DLC1 with other family members, DLC2 and 3.

Whilst DLC1 has some potential as a therapeutic target, further target validation is required. DLC1 is the Rho-GAP gene mutated most frequently in cancer, with 5–8% of tumours in five of the tumour types evaluated having DLC1 missense mutations (Wang et al., 2020). Recently a study has identified the potential of DLC1 as a disease biomarker, as its expression negatively correlated with the clinical characteristics (clinical stage, histologic grade) and positively correlated with the survival of patients with uterine corpus endometrial carcinoma (Wu et al., 2022).

Further characterization is needed to fully understand DLC1's role in cancer progression pathways. The RhoGAP is complex and involved in multiple signalling pathways, therefore it could be concluded that there are likely too many downstream effects to singularly target DLC1. One concern is the biaxial signalling network of Rho GTPases Rac and Rho, their antagonistic relationship can become integrated in coordinated cell behaviour, and the plasticity of cancer cells allow them to use a combined approach in metastasis and invasion (Symons and Segall, 2009).

It is clear that RhoGAPs are involved in every aspect of cancer progression, however the main challenge for targeting them therapeutically is the crosstalk and potential redundancy or compensation between them, and the difficulty to isolate the signalling contribution from each RhoGAP (Kreider-Letterman et al., 2022). Several previous studies contain discrepancies and there is a need to revaluate in more physiological 3D assays to truly understand the impact of RhoGAPs in cancer.

RhoGAPs are considered less attractive therapeutic targets compared to RhoGEFs, however oncogenic RhoGAPs could be targeted with small molecules, although there are no current reported inhibitors (Kreider-Letterman et al., 2022). A more encouraging strategy could be to restore or enhance the activity of tumour suppressor GAPs that are downregulated or inactivated in cancers, such as DLC1. However, for this strategy to be successful it is important to fully understand the mechanisms of RhoGAPs within cancer transformation, and identify interacting partners and define signalling pathways that regulate RhoGAP activation and function (Kreider-Letterman et al., 2022). This will allow for the identification of novel therapeutic strategies to help target cancers.

Chapter 7 : References

ACETO, N., BARDIA, A., MIYAMOTO, D. T., DONALDSON, M. C., WITTNER, B. S., SPENCER, J. A., YU, M., PELY, A., ENGSTROM, A., ZHU, H., BRANNIGAN, B. W., KAPUR, R., STOTT, S. L., SHIODA, T., RAMASWAMY, S., TING, D. T., LIN, C. P., TONER, M., HABER, D. A. & MAHESWARAN, S. 2014. Circulating tumor cell clusters are oligoclonal precursors of breast cancer metastasis. *Cell,* 158**,** 1110-1122.

AL-KOUSSA, H., ATAT, O. E., JAAFAR, L., TASHJIAN, H. & EL-SIBAI, M. 2020. The Role of Rho GTPases in Motility and Invasion of Glioblastoma Cells. *Anal Cell Pathol (Amst),* 2020**,** 9274016.

ALBERTS, A. J., JULIAN LEWIS, MARTIN RAFF, KEITH ROBERTS, AND PETER WALTER 2002. *Molecular Biology of the Cell.,* New York, Garland Science; .

ALEMAN, J. & SKARDAL, A. 2019. A multi-site metastasis-on-a-chip microphysiological system for assessing metastatic preference of cancer cells. *Biotechnol Bioeng,* 116**,** 936-944.

ALGAR, W. R., HILDEBRANDT, N., VOGEL, S. S. & MEDINTZ, I. L. 2019. FRET as a biomolecular research tool — understanding its potential while avoiding pitfalls. *Nature Methods,* 16**,** 815-829.

ANANTHAKRISHNAN, R. & EHRLICHER, A. 2007. The forces behind cell movement. *Int J Biol Sci,* 3**,** 303-17.

ANDERSEN, T., AUK-EMBLEM, P. & DORNISH, M. 2015. 3D Cell Culture in Alginate Hydrogels. *Microarrays (Basel),* 4**,** 133-61.

ANTONI, D., BURCKEL, H., JOSSET, E. & NOEL, G. 2015. Three-Dimensional Cell Culture: A Breakthrough in Vivo. *International Journal of Molecular Sciences,* 16**,** 5517-5527.

BAO-ZHU YUAN, M. J. M., CATHERINE L. KECK, DRAZEN B. ZIMONJIC, SNORRI S. THORGEIRSSON, AND NICHOLAS C. POPESCU1 1998. Cloning, characterization, and chromosomal localization of a gene frequently deleted in human liver cancer (DLC-1) homologous to rat RhoGAP. *Cancer Research,* 58**,** 2196-2199.

BARBOSA, M. A. G., XAVIER, C. P. R., PEREIRA, R. F., PETRIKAITĖ, V. & VASCONCELOS, M. H. 2022. 3D Cell Culture Models as Recapitulators of the Tumor Microenvironment for the Screening of Anti-Cancer Drugs. *Cancers,* 14**,** 190.

BARRAS, D., LORUSSO, G., RÜEGG, C. & WIDMANN, C. 2014. Inhibition of cell migration and invasion mediated by the TAT-RasGAP317-326 peptide requires the DLC1 tumor suppressor. *Oncogene,* 33**,** 5163-72.

BARRAS, D. & WIDMANN, C. 2013. GAP-independent functions of DLC1 in metastasis. *Cancer and Metastasis Reviews,* 33**,** 87-100.

BERGINSKI, M. E. & GOMEZ, S. M. 2013. The Focal Adhesion Analysis Server: a web tool for analyzing focal adhesion dynamics. *F1000Res,* 2**,** 68.

BERGINSKI, M. E., VITRIOL, E. A., HAHN, K. M. & GOMEZ, S. M. 2011. High-Resolution Quantification of Focal Adhesion Spatiotemporal Dynamics in Living Cells. *PLOS ONE,* 6**,** e22025.

BOIX-MONTESINOS, P., SORIANO-TERUEL, P. M., ARMIÑÁN, A., ORZÁEZ, M. & VICENT, M. J. 2021. The past, present, and future of breast cancer models for nanomedicine development. *Advanced drug delivery reviews,* 173**,** 306-330.

BOULTER, E., GARCIA-MATA, R., GUILLUY, C., DUBASH, A., ROSSI, G., BRENNWALD, P. J. & BURRIDGE, K. 2010. Regulation of Rho GTPase crosstalk, degradation and activity by RhoGDI1. *Nat Cell Biol,* 12**,** 477-83.

BRANCATO, V., OLIVEIRA, J. M., CORRELO, V. M., REIS, R. L. & KUNDU, S. C. 2020. Could 3D models of cancer enhance drug screening? *Biomaterials,* 232**,** 119744.

BRAUN, A. C. & OLAYIOYE, M. A. 2015. Rho regulation: DLC proteins in space and time. *Cellular Signalling,* 27**,** 1643-1651.

BREITSPRECHER, D., KOESTLER, S. A., CHIZHOV, I., NEMETHOVA, M., MUELLER, J., GOODE, B. L., SMALL, J. V., ROTTNER, K. & FAIX, J. 2011. Cofilin cooperates with fascin to disassemble filopodial actin filaments. *J Cell Sci,* 124**,** 3305-18.

BREKHMAN, V. & NEUFELD, G. 2009. A novel asymmetric 3D in-vitro assay for the study of tumor cell invasion. *BMC Cancer,* 9**,** 415.

BREMER, C., TUNG, C. H. & WEISSLEDER, R. 2001. In vivo molecular target assessment of matrix metalloproteinase inhibition. *Nat Med,* 7**,** 743-8.

BRUUN, J., KRYEZIU, K., EIDE, P. W., MOOSAVI, S. H., EILERTSEN, I. A., LANGERUD, J., RØSOK, B., TOTLAND, M. Z., BRUNSELL, T. H., PELLINEN, T., SAARELA, J., BERGSLAND, C. H., PALMER, H. G., BRUDVIK, K. W., GUREN, T., DIENSTMANN, R., GUREN, M. G., NESBAKKEN, A., BJØRNBETH, B. A., SVEEN, A. & LOTHE, R. A. 2020. Patient-Derived Organoids from Multiple Colorectal Cancer Liver Metastases Reveal Moderate Intra-patient Pharmacotranscriptomic Heterogeneity. *Clinical Cancer Research,* 26**,** 4107-4119.

BUJKO, M., KOBER, P., RUSETSKA, N., WAKUŁA, M., GORYCA, K., GRECKA, E., MATYJA, E., NESKA, J., MANDAT, T., BONICKI, W. & SIEDLECKI, J. A. 2016. Aberrant DNA methylation of alternative promoter of DLC1 isoform 1 in meningiomas. *Journal of Neuro-Oncology,* 130**,** 473-484.

BURRIDGE, K. & GUILLUY, C. 2016. Focal adhesions, stress fibers and mechanical tension. *Experimental Cell Research,* 343**,** 14-20.

BUSKERMOLEN, A. B. C., RISTORI, T., MOSTERT, D., VAN TURNHOUT, M. C., SHISHVAN, S. S., LOERAKKER, S., KURNIAWAN, N. A., DESHPANDE, V. S. & BOUTEN, C. V. C. 2020. Cellular Contact Guidance Emerges from Gap Avoidance. *Cell Rep Phys Sci,* 1**,** 100055.

BUSSO-LOPES, A. F., MARCHI, F. A., KUASNE, H., SCAPULATEMPO-NETO, C., TRINDADE-FILHO, J. C., DE JESUS, C. M., LOPES, A., GUIMARÃES, G. C. & ROGATTO, S. R. 2015. Genomic profiling of human penile carcinoma predicts worse prognosis and survival. *Cancer Prev Res (Phila),* 8**,** 149-56.

BYRON, A. 2011. Analyzing the anatomy of integrin adhesions. *Sci Signal,* 4**,** jc3.

BYRON, A., MORGAN, M. R. & HUMPHRIES, M. J. 2010. Adhesion signalling complexes. *Curr Biol,* 20**,** R1063-r1067.

CALDERWOOD, D. A., ZENT, R., GRANT, R., REES, D. J., HYNES, R. O. & GINSBERG, M. H. 1999. The Talin head domain binds to integrin beta subunit cytoplasmic tails and regulates integrin activation. *J Biol Chem,* 274**,** 28071-4.

CAMPAGNOLA, P. 2011. Second harmonic generation imaging microscopy: applications to diseases diagnostics. *Anal Chem,* 83**,** 3224-31.

CAMPELLONE, K. G. & WELCH, M. D. 2010. A nucleator arms race: cellular control of actin assembly. *Nat Rev Mol Cell Biol,* 11**,** 237-51.

CAO, X., KANEKO, T., LI, J. S., LIU, A. D., VOSS, C. & LI, S. S. 2015. A phosphorylation switch controls the spatiotemporal activation of Rho GTPases in directional cell migration. *Nat Commun,* 6**,** 7721.

CAO, X., VOSS, C., ZHAO, B., KANEKO, T. & LI, S. S. C. 2012. Differential regulation of the activity of deleted in liver cancer 1 (DLC1) by tensins controls cell migration and transformation. *Proceedings of the National Academy of Sciences,* 109**,** 1455-1460.

CARISEY, A., TSANG, R., GREINER, A. M., NIJENHUIS, N., HEATH, N., NAZGIEWICZ, A., KEMKEMER, R., DERBY, B., SPATZ, J. & BALLESTREM, C. 2013. Vinculin regulates the recruitment and release of core focal adhesion proteins in a force-dependent manner. *Curr Biol,* 23**,** 271-81.

CASE, L. B., BAIRD, M. A., SHTENGEL, G., CAMPBELL, S. L., HESS, H. F., DAVIDSON, M. W. & WATERMAN, C. M. 2015. Molecular mechanism of vinculin activation and nanoscale spatial organization in focal adhesions. *Nat Cell Biol,* 17**,** 880-92.

CASTRO, F., LEITE PEREIRA, C., HELENA MACEDO, M., ALMEIDA, A., JOSÉ SILVEIRA, M., DIAS, S., PATRÍCIA CARDOSO, A., JOSÉ OLIVEIRA, M. & SARMENTO, B. 2021. Advances on colorectal cancer 3D models: The needed translational technology for nanomedicine screening. *Adv Drug Deliv Rev,* 175**,** 113824.

CASTRO, M., GRAU, L., PUERTA, P., GIMENEZ, L., VENDITTI, J., QUADRELLI, S. & SÁNCHEZ-CARBAYO, M. 2010. Multiplexed methylation profiles of tumor suppressor genes and clinical outcome in lung cancer. *Journal of translational medicine,* 8**,** 86-86.

CASWELL, P. T. & ZECH, T. 2018. Actin-Based Cell Protrusion in a 3D Matrix. *Trends Cell Biol,* 28**,** 823-834.

ČERMÁK, V., GANDALOVIČOVÁ, A., MERTA, L., HARANT, K., RÖSEL, D. & BRÁBEK, J. 2020. High-throughput transcriptomic and proteomic profiling of mesenchymal-amoeboid transition in 3D collagen. *Scientific Data,* 7**,** 160.

CHABNER, B. A. & ROBERTS, T. G. 2005. Timeline: Chemotherapy and the war on cancer. *Nature reviews. Cancer,* 5**,** 65-72.

CHAFFER, C. L., SAN JUAN, B. P., LIM, E. & WEINBERG, R. A. 2016. EMT, cell plasticity and metastasis. *Cancer Metastasis Rev,* 35**,** 645-654.

CHAN, L.-K., KO, F. C. F., NG, I. O.-L. & YAM, J. W. P. 2009. Deleted in Liver Cancer 1 (DLC1) Utilizes a Novel Binding Site for Tensin2 PTB Domain Interaction and Is Required for Tumor-Suppressive Function. *PLOS ONE,* 4**,** e5572.

CHEN, B. C., LEGANT, W. R., WANG, K., SHAO, L., MILKIE, D. E., DAVIDSON, M. W., JANETOPOULOS, C., WU, X. S., HAMMER, J. A., 3RD, LIU, Z., ENGLISH, B. P., MIMORI-KIYOSUE, Y., ROMERO, D. P., RITTER, A. T., LIPPINCOTT-SCHWARTZ, J., FRITZ-LAYLIN, L., MULLINS, R. D., MITCHELL, D. M., BEMBENEK, J. N., REYMANN, A. C., BÖHME, R., GRILL, S. W., WANG, J. T., SEYDOUX, G., TULU, U. S., KIEHART, D. P. & BETZIG, E. 2014. Lattice light-sheet microscopy: imaging molecules to embryos at high spatiotemporal resolution. *Science,* 346**,** 1257998.

CHEN, H., DUNCAN, I. C., BOZORGCHAMI, H. & LO, S. H. 2002. Tensin1 and a previously undocumented family member, tensin2, positively regulate cell migration. *Proc Natl Acad Sci U S A,* 99**,** 733-8.

CHEN, W. T., YANG, C. H., WU, C. C., HUANG, Y. C. & CHAI, C. Y. 2013. Aberrant deleted in liver cancer-1 expression is associated with tumor metastasis and poor prognosis in urothelial carcinoma. *Apmis,* 121**,** 1131-8.

CHEUNG, K. J., PADMANABAN, V., SILVESTRI, V., SCHIPPER, K., COHEN, J. D., FAIRCHILD, A. N., GORIN, M. A., VERDONE, J. E., PIENTA, K. J., BADER, J. S. & EWALD, A. J. 2016. Polyclonal breast cancer metastases arise from collective dissemination of keratin 14-expressing tumor cell clusters. *Proc Natl Acad Sci U S A,* 113**,** E854-63.

CHI, D., SINGHAL, H., LI, L., XIAO, T., LIU, W., PUN, M., JESELSOHN, R., HE, H., LIM, E., VADHI, R., RAO, P., LONG, H., GARBER, J. & BROWN, M. 2019. Estrogen receptor signaling is reprogrammed during breast tumorigenesis. *Proc Natl Acad Sci U S A,* 116**,** 11437-11443.

CHI, Q., YIN, T., GREGERSEN, H., DENG, X., FAN, Y., ZHAO, J., LIAO, D. & WANG, G. 2014. Rear actomyosin contractility-driven directional cell migration in three-dimensional matrices: a mechano-chemical coupling mechanism. *J R Soc Interface,* 11**,** 20131072.

CHIBA, S., ENAMI, T., OGAWA, S. & SAKATA-YANAGIMOTO, M. 2015. G17V RHOA: Genetic evidence of GTP-unbound RHOA playing a role in tumorigenesis in T cells. *Small GTPases,* 6**,** 100-3.

CHOI, C. K., VICENTE-MANZANARES, M., ZARENO, J., WHITMORE, L. A., MOGILNER, A. & HORWITZ, A. R. 2008. Actin and alpha-actinin orchestrate the assembly and maturation of nascent adhesions in a myosin II motor-independent manner. *Nat Cell Biol,* 10**,** 1039-50.

CISNEROS CASTILLO, L. R., OANCEA, A.-D., STÜLLEIN, C. & RÉGNIER-VIGOUROUX, A. 2016. Evaluation of Consistency in Spheroid Invasion Assays. *Scientific Reports,* 6**,** 28375.

CITI, S., GUERRERA, D., SPADARO, D. & SHAH, J. 2014. Epithelial junctions and Rho family GTPases: the zonular signalosome. *Small GTPases,* 5**,** e973760.

CLARK, B. J. 2012. The mammalian START domain protein family in lipid transport in health and disease. *J Endocrinol,* 212**,** 257-75.

CLAYTON, N. S. & RIDLEY, A. J. 2020. Targeting Rho GTPase Signaling Networks in Cancer. *Frontiers in Cell and Developmental Biology,* 8.

CONDEELIS, J. & SEGALL, J. E. 2003. Intravital imaging of cell movement in tumours. *Nat Rev Cancer,* 3**,** 921-30.

CONDEELIS, J. & WEISSLEDER, R. 2010. In vivo imaging in cancer. *Cold Spring Harb Perspect Biol,* 2**,** a003848.

CONTI, S., KATO, T., PARK, D., SAHAI, E., TREPAT, X. & LABERNADIE, A. 2021. CAFs and Cancer Cells Co-Migration in 3D Spheroid Invasion Assay. *In:* CAMPBELL, K. & THEVENEAU, E. (eds.) *The Epithelial-to Mesenchymal Transition: Methods and Protocols.* New York, NY: Springer US.

CONWAY, J. R. W., WARREN, S. C. & TIMPSON, P. 2017. Context-dependent intravital imaging of therapeutic response using intramolecular FRET biosensors. *Methods,* 128**,** 78-94.

COOPER, J. A. & SEPT, D. 2008. New insights into mechanism and regulation of actin capping protein. *Int Rev Cell Mol Biol,* 267**,** 183-206.

CORREIA, A. L. & BISSELL, M. J. 2012. The tumor microenvironment is a dominant force in multidrug resistance. *Drug Resistance Updates,* 15**,** 39-49.

COSTA, E. C., MOREIRA, A. F., DE MELO-DIOGO, D., GASPAR, V. M., CARVALHO, M. P. & CORREIA, I. J. 2016. 3D tumor spheroids: an overview on the tools and techniques used for their analysis. *Biotechnology Advances,* 34**,** 1427-1441.

CRITCHLEY, D. R. 2009. Biochemical and structural properties of the integrin-associated cytoskeletal protein talin. *Annu Rev Biophys,* 38**,** 235-54.

CROSAS-MOLIST, E., SAMAIN, R., KOHLHAMMER, L., ORGAZ, J. L., GEORGE, S. L., MAIQUES, O., BARCELO, J. & SANZ-MORENO, V. 2022. Rho GTPase signaling in cancer progression and dissemination. *Physiological Reviews,* 102**,** 455-510.

CZERNICKI, T., ZEGARSKA, J., PACZEK, L., CUKROWSKA, B., GRAJKOWSKA, W., ZAJACZKOWSKA, A., BRUDZEWSKI, K., ULACZYK, J. & MARCHEL, A. 2007. Gene expression profile as a prognostic factor in high-grade gliomas. *Int J Oncol,* 30**,** 55-64.

DE BECO, S., VAIDŽIULYTĖ, K., MANZI, J., DALIER, F., DI FEDERICO, F., CORNILLEAU, G., DAHAN, M. & COPPEY, M. 2018. Optogenetic dissection of Rac1 and Cdc42 gradient shaping. *Nature Communications,* 9**,** 4816.

DE PASCALIS, C. & ETIENNE-MANNEVILLE, S. 2017. Single and collective cell migration: the mechanics of adhesions. *Mol Biol Cell,* 28**,** 1833-1846.

DEISBOECK, T. S., BERENS, M. E., KANSAL, A. R., TORQUATO, S., STEMMER-RACHAMIMOV, A. O. & CHIOCCA, E. A. 2001. Pattern of self-organization in tumour systems: complex growth dynamics in a novel brain tumour spheroid model. *Cell proliferation,* 34**,** 115-134.

DERMARDIROSSIAN, C. & BOKOCH, G. M. 2005. GDIs: central regulatory molecules in Rho GTPase activation. *Trends Cell Biol,* 15**,** 356-63.

DEVREOTES, P. & HORWITZ, A. R. 2015. Signaling networks that regulate cell migration. *Cold Spring Harb Perspect Biol,* 7**,** a005959.

DOYLE, A. D., CARVAJAL, N., JIN, A., MATSUMOTO, K. & YAMADA, K. M. 2015. Local 3D matrix microenvironment regulates cell migration through spatiotemporal dynamics of contractility-dependent adhesions. *Nat Commun,* 6**,** 8720.

DOYLE, A. D., PETRIE, R. J., KUTYS, M. L. & YAMADA, K. M. 2013. Dimensions in cell migration. *Curr Opin Cell Biol,* 25**,** 642-9.

DOYLE, A. D., WANG, F. W., MATSUMOTO, K. & YAMADA, K. M. 2009. One-dimensional topography underlies three-dimensional fibrillar cell migration. *J Cell Biol,* 184**,** 481-90.

DROST, J. & CLEVERS, H. 2018. Organoids in cancer research. *Nature Reviews Cancer,* 18**,** 407-418.

DU, X., QIAN, X., PAPAGEORGE, A., SCHETTER, A. J., VASS, W. C., LIU, X., BRAVERMAN, R., ROBLES, A. I. & LOWY, D. R. 2012. Functional Interaction of Tumor Suppressor DLC1 and Caveolin-1 in Cancer Cells. *Cancer Research,* 72**,** 4405-4416.

DUPONT, S. 2016. Role of YAP/TAZ in cell-matrix adhesion-mediated signalling and mechanotransduction. *Experimental Cell Research,* 343**,** 42-53.

DUPONT, S., MORSUT, L., ARAGONA, M., ENZO, E., GIULITTI, S., CORDENONSI, M., ZANCONATO, F., LE DIGABEL, J., FORCATO, M., BICCIATO, S., ELVASSORE, N. & PICCOLO, S. 2011. Role of YAP/TAZ in mechanotransduction. *Nature,* 474**,** 179-83.

DURKIN, M. E., AVNER, M. R., HUH, C.-G., YUAN, B.-Z., THORGEIRSSON, S. S. & POPESCU, N. C. 2005. DLC-1, a Rho GTPase-activating protein with tumor suppressor function, is essential for embryonic development. *FEBS Letters,* 579**,** 1191-1196.

DURKIN, M. E., YUAN, B.-Z., ZHOU, X., ZIMONJIC, D. B., LOWY, D. R., THORGEIRSSON, S. S. & POPESCU, N. C. 2007a. DLC-1:a Rho GTPase-activating protein and tumour suppressor. *Journal of Cellular and Molecular Medicine,* 11**,** 1185-1207.

DURKIN, M. E., YUAN, B. Z., ZHOU, X., ZIMONJIC, D. B., LOWY, D. R., THORGEIRSSON, S. S. & POPESCU, N. C. 2007b. DLC-1:a Rho GTPase-activating protein and tumour suppressor. *J Cell Mol Med,* 11**,** 1185-207.

DUVAL, K., GROVER, H., HAN, L. H., MOU, Y., PEGORARO, A. F., FREDBERG, J. & CHEN, Z. 2017. Modeling Physiological Events in 2D vs. 3D Cell Culture. *Physiology (Bethesda),* 32**,** 266-277.

EDWARDS, S. C., HOEVENAAR, W. H. M. & COFFELT, S. B. 2021. Emerging immunotherapies for metastasis. *Br J Cancer,* 124**,** 37-48.

EDWARDS, S. J., CARANNANTE, V., KUHNIGK, K., RING, H., TARARUK, T., HALLBÖÖK, F., BLOM, H., ÖNFELT, B. & BRISMAR, H. 2020. High-Resolution Imaging of Tumor Spheroids and Organoids Enabled by Expansion Microscopy. *Frontiers in Molecular Biosciences,* 7.

EGEBLAD, M. & WERB, Z. 2002. New functions for the matrix metalloproteinases in cancer progression. *Nat Rev Cancer,* 2**,** 161-74.

EL-SITT, S. & EL-SIBAI, M. 2013. The STAR of the DLC family. *Journal of Receptors and Signal Transduction,* 33**,** 10-13.

ELOSEGUI-ARTOLA, A., ANDREU, I., BEEDLE, A. E. M., LEZAMIZ, A., UROZ, M., KOSMALSKA, A. J., ORIA, R., KECHAGIA, J. Z., RICO-LASTRES, P., LE ROUX, A.-L., SHANAHAN, C. M., TREPAT, X., NAVAJAS, D., GARCIA-MANYES, S. & ROCA-CUSACHS, P. 2017. Force Triggers YAP Nuclear Entry by Regulating Transport across Nuclear Pores. *Cell,* 171**,** 1397-1410.e14.

ETIENNE-MANNEVILLE, S. 2008. Polarity proteins in migration and invasion. *Oncogene,* 27**,** 6970-80.

ETIENNE-MANNEVILLE, S. & HALL, A. 2002. Rho GTPases in cell biology. *Nature,* 420**,** 629-35.

FAN, H., DEMIRCI, U. & CHEN, P. 2019. Emerging organoid models: leaping forward in cancer research. *Journal of hematology & oncology,* 12**,** 1-10.

FARES, J., FARES, M. Y., KHACHFE, H. H., SALHAB, H. A. & FARES, Y. 2020. Molecular principles of metastasis: a hallmark of cancer revisited. *Signal Transduction and Targeted Therapy,* 5**,** 28.

FEIN, M. R. & EGEBLAD, M. 2013. Caught in the act: revealing the metastatic process by live imaging. *Disease models & mechanisms,* 6**,** 580-593.

FENG, X., LI, C., LIU, W., CHEN, H., ZHOU, W., WANG, L., ZHU, B., YAO, K., JIANG, X. & REN, C. 2013. DLC-1, a candidate tumor suppressor gene, inhibits the proliferation, migration and tumorigenicity of human nasopharyngeal carcinoma cells. *Int J Oncol,* 42**,** 1973-1984.

FERREIRA, L. P., GASPAR, V. M. & MANO, J. F. 2018. Design of spherically structured 3D in vitro tumor models -Advances and prospects. *Acta Biomater,* 75**,** 11-34.

FETAH, K. L., DIPARDO, B. J., KONGADZEM, E. M., TOMLINSON, J. S., ELZAGHEID, A., ELMUSRATI, M., KHADEMHOSSEINI, A. & ASHAMMAKHI, N. 2019. Cancer Modeling-on-a-Chip with Future Artificial Intelligence Integration. *Small,* 15**,** 1901985.

FISHER, K. E., SACHARIDOU, A., STRATMAN, A. N., MAYO, A. M., FISHER, S. B., MAHAN, R. D., DAVIS, M. J. & DAVIS, G. E. 2009. MT1-MMP- and Cdc42-dependent signaling co-regulate cell invasion and tunnel formation in 3D collagen matrices. *J Cell Sci,* 122**,** 4558-69.

FRALEY, S. I., FENG, Y., KRISHNAMURTHY, R., KIM, D. H., CELEDON, A., LONGMORE, G. D. & WIRTZ, D. 2010. A distinctive role for focal adhesion proteins in three-dimensional cell motility. *Nat Cell Biol,* 12**,** 598-604.

FRANTZ, C., STEWART, K. M. & WEAVER, V. M. 2010. The extracellular matrix at a glance. *Journal of Cell Science,* 123**,** 4195-4200.

FRANZ, C. M. & MÜLLER, D. J. 2005. Analyzing focal adhesion structure by atomic force microscopy. *J Cell Sci,* 118**,** 5315-23.

FRIEDL, P. & ALEXANDER, S. 2011. Cancer Invasion and the Microenvironment: Plasticity and Reciprocity. *Cell,* 147**,** 992-1009.

FRIEDL, P. & GILMOUR, D. 2009. Collective cell migration in morphogenesis, regeneration and cancer. *Nat Rev Mol Cell Biol,* 10**,** 445-57.

FRITZ, R. D., LETZELTER, M., REIMANN, A., MARTIN, K., FUSCO, L., RITSMA, L., PONSIOEN, B., FLURI, E., SCHULTE-MERKER, S., VAN RHEENEN, J. & PERTZ, O. 2013. A versatile toolkit to produce sensitive FRET biosensors to visualize signaling in time and space. *Sci Signal,* 6**,** rs12.

FU, H. Y., WU, D. S., ZHOU, H. R. & SHEN, J. Z. 2014. CpG island methylator phenotype and its relationship with prognosis in adult acute leukemia patients. *Hematology,* 19**,** 329-37.

FUKATA, Y., AMANO, M. & KAIBUCHI, K. 2001. Rho-Rho-kinase pathway in smooth muscle contraction and cytoskeletal reorganization of non-muscle cells. *Trends Pharmacol Sci,* 22**,** 32-9.

FULDA, S. 2010. Evasion of apoptosis as a cellular stress response in cancer. *Int J Cell Biol,* 2010**,** 370835.

GAGGIOLI, C., HOOPER, S., HIDALGO-CARCEDO, C., GROSSE, R., MARSHALL, J. F., HARRINGTON, K. & SAHAI, E. 2007. Fibroblast-led collective invasion of carcinoma cells with differing roles for RhoGTPases in leading and following cells. *Nat Cell Biol,* 9**,** 1392-400.

GARCIA-MATA, R., BOULTER, E. & BURRIDGE, K. 2011. The 'invisible hand': regulation of RHO GTPases by RHOGDIs. *Nature Reviews Molecular Cell Biology,* 12**,** 493-504.

GARDEL, M. L., SCHNEIDER, I. C., ARATYN-SCHAUS, Y. & WATERMAN, C. M. 2010. Mechanical Integration of Actin and Adhesion Dynamics in Cell Migration. *Annual Review of Cell and Developmental Biology,* 26**,** 315-333.

GEIGER, B., BERSHADSKY, A., PANKOV, R. & YAMADA, K. M. 2001. Transmembrane crosstalk between the extracellular matrix--cytoskeleton crosstalk. *Nat Rev Mol Cell Biol,* 2**,** 793-805.

GIANNONE, G., MÈGE, R. M. & THOUMINE, O. 2009. Multi-level molecular clutches in motile cell processes. *Trends Cell Biol,* 19**,** 475-86.

GÖKMEN-POLAR, Y., TRUE, J. D., VIETH, E., GU, Y., GU, X., QI, G. D., MOSLEY, A. L. & BADVE, S. S. 2018. Quantitative phosphoproteomic analysis identifies novel functional pathways of tumor suppressor DLC1 in estrogen receptor positive breast cancer. *PLoS One,* 13**,** e0204658.

GOLAN, T., ATIAS, D., STOSSEL, C. & RAITSES-GUREVICH, M. 2021. Patient-derived xenograft models of BRCA-associated pancreatic cancers. *Adv Drug Deliv Rev,* 171**,** 257-265.

GOLDMANN, W. H., GUTTENBERG, Z., KAUFMANN, S., HESS, D., EZZELL, R. M. & ISENBERG, G. 1997. Examining F-actin interaction with intact talin and talin head and tail fragment using static and dynamic light scattering. *Eur J Biochem,* 250**,** 447-50.

GRAZIANI, V., RODRIGUEZ-HERNANDEZ, I., MAIQUES, O. & SANZ-MORENO, V. 2022. The amoeboid state as part of the epithelial-to-mesenchymal transition programme. *Trends in Cell Biology,* 32**,** 228-242.

GREENWALD, E. C., MEHTA, S. & ZHANG, J. 2018. Genetically Encoded Fluorescent Biosensors Illuminate the Spatiotemporal Regulation of Signaling Networks. *Chem Rev,* 118**,** 11707-11794.

GUAN, M., TRIPATHI, V., ZHOU, X. & POPESCU, N. C. 2008. Adenovirus-mediated restoration of expression of the tumor suppressor gene DLC1 inhibits the proliferation and tumorigenicity of aggressive, androgen-independent human prostate cancer cell lines: prospects for gene therapy. *Cancer Gene Therapy,* 15**,** 371-381.

GUAN, M., ZHOU, X., SOULITZIS, N., SPANDIDOS, D. A. & POPESCU, N. C. 2006a. Aberrant methylation and deacetylation of deleted in liver cancer-1 gene in prostate cancer: potential clinical applications. *Clin Cancer Res,* 12**,** 1412-9.

GUAN, M., ZHOU, X., SOULITZIS, N., SPANDIDOS, D. A. & POPESCU, N. C. 2006b. Aberrant methylation and deacetylation of deleted in liver cancer-1 gene in prostate cancer: potential clinical applications. *Clinical cancer research : an official journal of the American Association for Cancer Research,* 12**,** 1412-9.

GUO, J., FENG, X. Q., NIE, S. M., SU, Z., SHI, X., CUI, Z. G., ZHANG, L., LIU, S. G., MENG, F. J. & ZHAO, C. T. 2014. Effect of 5-aza-2'-deoxycytidine combined with trichostatin A on RPMI-8226 cell proliferation, apoptosis and DLC-1 gene expression. *Zhongguo Shi Yan Xue Ye Xue Za Zhi,* 22**,** 357-63.

GUPTA, G. P. & MASSAGUÉ, J. 2006. Cancer metastasis: building a framework. *Cell,* 127**,** 679-95.

HAASE, K., AL-REKABI, Z. & PELLING, A. E. 2014. Chapter Five - Mechanical Cues Direct Focal Adhesion Dynamics. *In:* ENGLER, A. J. & KUMAR, S. (eds.) *Progress in Molecular Biology and Translational Science.* Academic Press.

HADLER-OLSEN, E., WINBERG, J. O. & UHLIN-HANSEN, L. 2013. Matrix metalloproteinases in cancer: their value as diagnostic and prognostic markers and therapeutic targets. *Tumour Biol,* 34**,** 2041-51.

HAEGER, A., WOLF, K., ZEGERS, M. M. & FRIEDL, P. 2015. Collective cell migration: guidance principles and hierarchies. *Trends in Cell Biology,* 25**,** 556-566.

HAGA, H., IRAHARA, C., KOBAYASHI, R., NAKAGAKI, T. & KAWABATA, K. 2005. Collective Movement of Epithelial Cells on a Collagen Gel Substrate. *Biophysical Journal,* 88**,** 2250-2256.

HAGA, R. B. & RIDLEY, A. J. 2016. Rho GTPases: Regulation and roles in cancer cell biology. *Small GTPases,* 7**,** 207-221.

HAINING, A. W. M., RAHIKAINEN, R., CORTES, E., LACHOWSKI, D., RICE, A., VON ESSEN, M., HYTÖNEN, V. P. & DEL RÍO HERNÁNDEZ, A. 2018. Mechanotransduction in talin through the interaction of the R8 domain with DLC1. *PLoS Biol,* 16**,** e2005599.

HAKKINEN, K. M., HARUNAGA, J. S., DOYLE, A. D. & YAMADA, K. M. 2011. Direct comparisons of the morphology, migration, cell adhesions, and actin cytoskeleton of fibroblasts in four different three-dimensional extracellular matrices. *Tissue engineering. Part A,* 17**,** 713-724.

HAMPL, V., MARTIN, C., AIGNER, A., HOEBEL, S., SINGER, S., FRANK, N., SARIKAS, A., EBERT, O., PRYWES, R., GUDERMANN, T. & MUEHLICH, S. 2013. Depletion of the transcriptional coactivators megakaryoblastic leukaemia 1 and 2 abolishes hepatocellular carcinoma xenograft growth by inducing oncogene-induced senescence. *EMBO Mol Med,* 5**,** 1367-82.

HAPACH, L. A., MOSIER, J. A., WANG, W. & REINHART-KING, C. A. 2019. Engineered models to parse apart the metastatic cascade. *npj Precision Oncology,* 3**,** 20.

HÄRMÄ, V., VIRTANEN, J., MÄKELÄ, R., HAPPONEN, A., MPINDI, J.-P., KNUUTTILA, M., KOHONEN, P., LÖTJÖNEN, J., KALLIONIEMI, O. & NEES, M. 2010. A comprehensive panel of three-dimensional

models for studies of prostate cancer growth, invasion and drug responses. *PloS one,* 5**,** e10431-e10431.
HARUNAGA, J. S. & YAMADA, K. M. 2011. Cell-matrix adhesions in 3D. *Matrix Biol,* 30**,** 363-8.
HEALY, K. D., HODGSON, L., KIM, T. Y., SHUTES, A., MADDILETI, S., JULIANO, R. L., HAHN, K. M., HARDEN, T. K., BANG, Y. J. & DER, C. J. 2008. DLC-1 suppresses non-small cell lung cancer growth and invasion by RhoGAP-dependent and independent mechanisms. *Mol Carcinog,* 47**,** 326-37.
HEERING, J., ERLMANN, P. & OLAYIOYE, M. A. 2009a. Simultaneous loss of the DLC1 and PTEN tumor suppressors enhances breast cancer cell migration. *Experimental Cell Research,* 315**,** 2505-2514.
HEERING, J., ERLMANN, P. & OLAYIOYE, M. A. 2009b. Simultaneous loss of the DLC1 and PTEN tumor suppressors enhances breast cancer cell migration. *Exp Cell Res,* 315**,** 2505-14.
HEINRICH, M. A., BANSAL, R., LAMMERS, T., ZHANG, Y. S., MICHEL SCHIFFELERS, R. & PRAKASH, J. 2019. 3D-Bioprinted Mini-Brain: A Glioblastoma Model to Study Cellular Interactions and Therapeutics. *Adv Mater,* 31**,** e1806590.
HEINRICH, M. A., MOSTAFA, A. M. R. H., MORTON, J. P., HAWINKELS, L. J. A. C. & PRAKASH, J. 2021. Translating complexity and heterogeneity of pancreatic tumor: 3D in vitro to in vivo models. *Advanced Drug Delivery Reviews,* 174**,** 265-293.
HICKMAN, J. A., GRAESER, R., DE HOOGT, R., VIDIC, S., BRITO, C., GUTEKUNST, M., VAN DER KUIP, H. & CONSORTIUM, I. P. 2014. Three-dimensional models of cancer for pharmacology and cancer cell biology: Capturing tumor complexity in vitro/ex vivo. *Biotechnology Journal,* 9**,** 1115-1128.
HODGE, R. G. & RIDLEY, A. J. 2016. Regulating Rho GTPases and their regulators. *Nat Rev Mol Cell Biol,* 17**,** 496-510.
HOLEITER, G., BISCHOFF, A., BRAUN, A. C., HUCK, B., ERLMANN, P., SCHMID, S., HERR, R., BRUMMER, T. & OLAYIOYE, M. A. 2012. The RhoGAP protein Deleted in Liver Cancer 3 (DLC3) is essential for adherens junctions integrity. *Oncogenesis,* 1**,** e13-e13.
HOLEITER, G., HEERING, J., ERLMANN, P., SCHMID, S., JÄHNE, R. & OLAYIOYE, M. A. 2008. Deleted in liver cancer 1 controls cell migration through a Dia1-dependent signaling pathway. *Cancer Res,* 68**,** 8743-51.
HORTON, E. R., BYRON, A., ASKARI, J. A., NG, D. H. J., MILLON-FRÉMILLON, A., ROBERTSON, J., KOPER, E. J., PAUL, N. R., WARWOOD, S., KNIGHT, D., HUMPHRIES, J. D. & HUMPHRIES, M. J. 2015. Definition of a consensus integrin adhesome and its dynamics during adhesion complex assembly and disassembly. *Nature Cell Biology,* 17**,** 1577-1587.
HORWITZ, A., DUGGAN, K., BUCK, C., BECKERLE, M. C. & BURRIDGE, K. 1986. Interaction of plasma membrane fibronectin receptor with talin--a transmembrane linkage. *Nature,* 320**,** 531-3.
HORWITZ, R. & WEBB, D. 2003. Cell migration. *Current Biology,* 13**,** R756-R759.
HU, Z., LI, Z., MA, Z. & CURTIS, C. 2020. Multi-cancer analysis of clonality and the timing of systemic spread in paired primary tumors and metastases. *Nature Genetics,* 52**,** 701-708.
HUANG, M., SHEN, A., DING, J. & GENG, M. 2014. Molecularly targeted cancer therapy: some lessons from the past decade. *Trends Pharmacol Sci,* 35**,** 41-50.
HUISKEN, J., SWOGER, J., DEL BENE, F., WITTBRODT, J. & STELZER, E. H. K. 2004. Optical Sectioning Deep Inside Live Embryos by Selective Plane Illumination Microscopy. *Science,* 305**,** 1007-1009.
HUMPHRIES, M. J. & NEWHAM, P. 1998. The structure of cell-adhesion molecules. *Trends Cell Biol,* 8**,** 78-83.
HUNG, W. C., YANG, J. R., YANKASKAS, C. L., WONG, B. S., WU, P. H., PARDO-PASTOR, C., SERRA, S. A., CHIANG, M. J., GU, Z., WIRTZ, D., VALVERDE, M. A., YANG, J. T., ZHANG, J. & KONSTANTOPOULOS, K. 2016. Confinement Sensing and Signal Optimization via Piezo1/PKA and Myosin II Pathways. *Cell Rep,* 15**,** 1430-1441.

HUXLEY, H. E. 1963. ELECTRON MICROSCOPE STUDIES ON THE STRUCTURE OF NATURAL AND SYNTHETIC PROTEIN FILAMENTS FROM STRIATED MUSCLE. *J Mol Biol,* 7**,** 281-308.

HYNES, R. O. 1992. Integrins: versatility, modulation, and signaling in cell adhesion. *Cell,* 69**,** 11-25.

ILINA, O., CAMPANELLO, L., GRITSENKO, P. G., VULLINGS, M., WANG, C., BULT, P., LOSERT, W. & FRIEDL, P. 2018. Intravital microscopy of collective invasion plasticity in breast cancer. *Disease Models & Mechanisms,* 11**,** dmm034330.

ILINA, O. & FRIEDL, P. 2009. Mechanisms of collective cell migration at a glance. *Journal of Cell Science,* 122**,** 3203-3208.

IRESON, C. R., ALAVIJEH, M. S., PALMER, A. M., FOWLER, E. R. & JONES, H. J. 2019. The role of mouse tumour models in the discovery and development of anticancer drugs. *British Journal of Cancer,* 121**,** 101-108.

ISHIGURO, T., OHATA, H., SATO, A., YAMAWAKI, K., ENOMOTO, T. & OKAMOTO, K. 2017. Tumor-derived spheroids: Relevance to cancer stem cells and clinical applications. *Cancer Science,* 108**,** 283-289.

ITOH, R. E., KUROKAWA, K., OHBA, Y., YOSHIZAKI, H., MOCHIZUKI, N. & MATSUDA, M. 2002. Activation of rac and cdc42 video imaged by fluorescent resonance energy transfer-based single-molecule probes in the membrane of living cells. *Mol Cell Biol,* 22**,** 6582-91.

JAFFE, A. B. & HALL, A. 2005. RHO GTPASES: Biochemistry and Biology. *Annual Review of Cell and Developmental Biology,* 21**,** 247-269.

JAIN, R. K., MUNN, L. L. & FUKUMURA, D. 2002. Dissecting tumour pathophysiology using intravital microscopy. *Nat Rev Cancer,* 2**,** 266-76.

JAWHARI, A. U., BUDA, A., JENKINS, M., SHEHZAD, K., SARRAF, C., NODA, M., FARTHING, M. J., PIGNATELLI, M. & ADAMS, J. C. 2003. Fascin, an actin-bundling protein, modulates colonic epithelial cell invasiveness and differentiation in vitro. *Am J Pathol,* 162**,** 69-80.

JENSCH, A., FREY, Y., BITSCHAR, K., WEBER, P., SCHMID, S., HAUSSER, A., OLAYIOYE, M. A. & RADDE, N. E. 2018. The tumor suppressor protein DLC1 maintains protein kinase D activity and Golgi secretory function. *Journal of Biological Chemistry,* 293**,** 14407-14416.

JENSEN, C., SHAY, C. & TENG, Y. 2022. The New Frontier of Three-Dimensional Culture Models to Scale-Up Cancer ResearchCancer research. *In:* GUEST, P. C. (ed.) *Physical Exercise and Natural and Synthetic Products in Health and Disease.* New York, NY: Springer US.

JENSEN, C. & TENG, Y. 2020. Is It Time to Start Transitioning From 2D to 3D Cell Culture? *Frontiers in Molecular Biosciences,* 7.

JI, S., ZHENG, Z., LIU, S., REN, G., GAO, J., ZHANG, Y. & LI, G. 2018. Resveratrol promotes oxidative stress to drive DLC1 mediated cellular senescence in cancer cells. *Exp Cell Res,* 370**,** 292-302.

JOSÉ LUIS, A. & WOLFGANG, H. G. 2016. Cellular mechanotransduction. *AIMS Biophysics,* 3**,** 50-62.

JOSHI, R., QIN, L., CAO, X., ZHONG, S., VOSS, C., MIN, W. & LI, S. S. C. 2020. DLC1 SAM domain-binding peptides inhibit cancer cell growth and migration by inactivating RhoA. *J Biol Chem,* 295**,** 645-656.

JURCHENKO, C. & SALAITA, K. S. 2015. Lighting Up the Force: Investigating Mechanisms of Mechanotransduction Using Fluorescent Tension Probes. *Mol Cell Biol,* 35**,** 2570-82.

KALLURI, R. & WEINBERG, R. A. 2009. The basics of epithelial-mesenchymal transition. *J Clin Invest,* 119**,** 1420-8.

KANCHANAWONG, P., SHTENGEL, G., PASAPERA, A. M., RAMKO, E. B., DAVIDSON, M. W., HESS, H. F. & WATERMAN, C. M. 2010. Nanoscale architecture of integrin-based cell adhesions. *Nature,* 468**,** 580-584.

KANG, Z., XU, F., ZHANG, Q. A., LIN, J., WU, Z., ZHANG, X., LUO, Y., XU, J. & GUAN, M. 2012. Correlation of DLC1 gene methylation with oncogenic PIK3CA mutations in extramammary Paget's disease. *Mod Pathol,* 25**,** 1160-8.

KARLSSON, H., FRYKNÄS, M., LARSSON, R. & NYGREN, P. 2012. Loss of cancer drug activity in colon cancer HCT-116 cells during spheroid formation in a new 3-D spheroid cell culture system. *Exp Cell Res,* 318**,** 1577-85.

KARLSSON, R., PEDERSEN, E. D., WANG, Z. & BRAKEBUSCH, C. 2009. Rho GTPase function in tumorigenesis. *Biochimica et Biophysica Acta (BBA) - Reviews on Cancer,* 1796**,** 91-98.

KAUSHIK, S., RAVI, A., HAMEED, F. M. & LOW, B. C. 2014. Concerted modulation of paxillin dynamics at focal adhesions by Deleted in Liver Cancer-1 and focal adhesion kinase during early cell spreading. *Cytoskeleton (Hoboken),* 71**,** 677-94.

KAWAI, K., KIYOTA, M., SEIKE, J., DEKI, Y. & YAGISAWA, H. 2007. START-GAP3/DLC3 is a GAP for RhoA and Cdc42 and is localized in focal adhesions regulating cell morphology. *Biochemical and Biophysical Research Communications,* 364**,** 783-789.

KESSENBROCK, K., PLAKS, V. & WERB, Z. 2010. Matrix metalloproteinases: regulators of the tumor microenvironment. *Cell,* 141**,** 52-67.

KHALIL, A. A. & FRIEDL, P. 2010. Determinants of leader cells in collective cell migration. *Integrative Biology,* 2**,** 568-574.

KHATIBI, S., RIOS, K. I. & NGUYEN, L. K. 2018. Computational Modeling of the Dynamics of Spatiotemporal Rho GTPase Signaling: A Systematic Review. *In:* RIVERO, F. (ed.) *Rho GTPases: Methods and Protocols.* New York, NY: Springer New York.

KIM, D.-H. & WIRTZ, D. 2013a. Predicting how cells spread and migrate. *Cell Adhesion & Migration,* 7**,** 293-296.

KIM, D. H. & WIRTZ, D. 2011. Recapitulating cancer cell invasion in vitro. *Proceedings of the National Academy of Sciences of the United States of America,* 108**,** 6693-6694.

KIM, D. H. & WIRTZ, D. 2013b. Focal adhesion size uniquely predicts cell migration. *Faseb j,* 27**,** 1351-61.

KIM, T. Y., HEALY, K. D., DER, C. J., SCIAKY, N., BANG, Y. J. & JULIANO, R. L. 2008. Effects of structure of Rho GTPase-activating protein DLC-1 on cell morphology and migration. *J Biol Chem,* 283**,** 32762-70.

KIM, T. Y., JACKSON, S., XIONG, Y., WHITSETT, T. G., LOBELLO, J. R., WEISS, G. J., TRAN, N. L., BANG, Y. J. & DER, C. J. 2013. CRL4A-FBXW5-mediated degradation of DLC1 Rho GTPase-activating protein tumor suppressor promotes non-small cell lung cancer cell growth. *Proc Natl Acad Sci U S A,* 110**,** 16868-73.

KIM, T. Y., LEE, J. W., KIM, H. P., JONG, H. S., KIM, T. Y., JUNG, M. & BANG, Y. J. 2007. DLC-1, a GTPase-activating protein for Rho, is associated with cell proliferation, morphology, and migration in human hepatocellular carcinoma. *Biochem Biophys Res Commun,* 355**,** 72-7.

KIM, T. Y., VIGIL, D., DER, C. J. & JULIANO, R. L. 2009. Role of DLC-1, a tumor suppressor protein with RhoGAP activity, in regulation of the cytoskeleton and cell motility. *Cancer Metastasis Rev,* 28**,** 77-83.

KO, F. C., CHAN, L. K., SZE, K. M., YEUNG, Y. S., TSE, E. Y., LU, P., YU, M. H., NG, I. O. & YAM, J. W. 2013. PKA-induced dimerization of the RhoGAP DLC1 promotes its inhibition of tumorigenesis and metastasis. *Nat Commun,* 4**,** 1618.

KO, F. C., CHAN, L. K., TUNG, E. K., LOWE, S. W., NG, I. O. & YAM, J. W. 2010a. Akt phosphorylation of deleted in liver cancer 1 abrogates its suppression of liver cancer tumorigenesis and metastasis. *Gastroenterology,* 139**,** 1397-407.

KO, F. C., YEUNG, Y. S., WONG, C. M., CHAN, L. K., POON, R. T., NG, I. O. & YAM, J. W. 2010b. Deleted in liver cancer 1 isoforms are distinctly expressed in human tissues, functionally different and under differential transcriptional regulation in hepatocellular carcinoma. *Liver Int,* 30**,** 139-48.

KO, F. C. F. & PING YAM, J. W. 2014. Regulation of deleted in liver cancer 1 tumor suppressor by protein–protein interactions and phosphorylation. *International Journal of Cancer,* 135**,** 264-269.

KOCH, J., MÖNCH, D., MAAß, A., GROMOLL, C., HEHR, T., LEIBOLD, T., SCHLITT, H. J., DAHLKE, M.-H. & RENNER, P. 2021. Three dimensional cultivation increases chemo- and radioresistance of colorectal cancer cell lines. *PLOS ONE,* 16**,** e0244513.

KÖLSCH, V., CHAREST, P. G. & FIRTEL, R. A. 2008. The regulation of cell motility and chemotaxis by phospholipid signaling. *J Cell Sci,* 121**,** 551-9.

KONG, H. J., POLTE, T. R., ALSBERG, E. & MOONEY, D. J. 2005. FRET measurements of cell-traction forces and nano-scale clustering of adhesion ligands varied by substrate stiffness. *Proc Natl Acad Sci U S A,* 102**,** 4300-5.

KOUDELKOVÁ, L., PATAKI, A. C., TOLDE, O., PAVLIK, V., NOBIS, M., GEMPERLE, J., ANDERSON, K., BRÁBEK, J. & ROSEL, D. 2019. Novel FRET-Based Src Biosensor Reveals Mechanisms of Src Activation and Its Dynamics in Focal Adhesions. *Cell Chem Biol,* 26**,** 255-268.e4.

KRAUSE, M. & GAUTREAU, A. 2014. Steering cell migration: lamellipodium dynamics and the regulation of directional persistence. *Nat Rev Mol Cell Biol,* 15**,** 577-90.

KRAYNOV, V. S., CHAMBERLAIN, C., BOKOCH, G. M., SCHWARTZ, M. A., SLABAUGH, S. & HAHN, K. M. 2000. Localized Rac activation dynamics visualized in living cells. *Science,* 290**,** 333-7.

KREIDER-LETTERMAN, G., CARR, N. M. & GARCIA-MATA, R. 2022. Fixing the GAP: The role of RhoGAPs in cancer. *European Journal of Cell Biology,* 101**,** 151209.

KUTOVA, O. M., SENCHA, L. M., POSPELOV, A. D., DOBRYNINA, O. E., BRILKINA, A. A., CHERKASOVA, E. I. & BALALAEVA, I. V. 2020. Comparative Analysis of Cell-Cell Contact Abundance in Ovarian Carcinoma Cells Cultured in Two- and Three-Dimensional In Vitro Models. *Biology (Basel),* 9.

LAHOZ, A. & HALL, A. 2008. DLC1: a significant GAP in the cancer genome. *Genes Dev,* 22**,** 1724-30.

LAI, F. P., SZCZODRAK, M., BLOCK, J., FAIX, J., BREITSPRECHER, D., MANNHERZ, H. G., STRADAL, T. E., DUNN, G. A., SMALL, J. V. & ROTTNER, K. 2008. Arp2/3 complex interactions and actin network turnover in lamellipodia. *Embo j,* 27**,** 982-92.

LÄMMERMANN, T. & SIXT, M. 2009. Mechanical modes of 'amoeboid' cell migration. *Curr Opin Cell Biol,* 21**,** 636-44.

LANGHANS, S. A. 2018. Three-Dimensional in Vitro Cell Culture Models in Drug Discovery and Drug Repositioning. *Frontiers in Pharmacology,* 9.

LASAGNA, M., VENTURA, C., HIELPOS, M. S., MARDIROSIAN, M. N., MARTÍN, G., MIRET, N., RANDI, A., NÚÑEZ, M. & COCCA, C. 2022. Endocrine disruptor chlorpyrifos promotes migration, invasion, and stemness phenotype in 3D cultures of breast cancer cells and induces a wide range of pathways involved in cancer progression. *Environmental Research,* 204**,** 111989.

LAWSON, C. D. & BURRIDGE, K. 2014. The on-off relationship of Rho and Rac during integrin-mediated adhesion and cell migration. *Small GTPases,* 5**,** e27958-e27958.

LE DÉVÉDEC, S. E., YAN, K., DE BONT, H., GHOTRA, V., TRUONG, H., DANEN, E. H., VERBEEK, F. & VAN DE WATER, B. 2010. Systems microscopy approaches to understand cancer cell migration and metastasis. *Cell Mol Life Sci,* 67**,** 3219-40.

LEE, M. H., KUNDU, J. K., CHAE, J. I. & SHIM, J. H. 2019. Targeting ROCK/LIMK/cofilin signaling pathway in cancer. *Arch Pharm Res,* 42**,** 481-491.

LEGERSTEE, K. & HOUTSMULLER, A. B. 2021. A Layered View on Focal Adhesions. *Biology (Basel),* 10.

LELE, T. P., THODETI, C. K., PENDSE, J. & INGBER, D. E. 2008. Investigating complexity of protein-protein interactions in focal adhesions. *Biochem Biophys Res Commun,* 369**,** 929-34.

LEMAY, P., DE MARCO, P., TRAVERSO, M., MERELLO, E., DIONNE-LAPORTE, A., SPIEGELMAN, D., HENRION, É., DIALLO, O., AUDIBERT, F., MICHAUD, J. L., CAMA, A., ROULEAU, G. A., KIBAR, Z. & CAPRA, V. 2019. Whole exome sequencing identifies novel predisposing genes in neural tube defects. *Mol Genet Genomic Med,* 7**,** e00467.

LEUNG, T. H.-Y., CHING, Y.-P., YAM, J. W. P., WONG, C.-M., YAU, T.-O., JIN, D.-Y. & NG, I. O.-L. 2005. Deleted in liver cancer 2 (DLC2) suppresses cell transformation by means of inhibition of RhoA activity. *Proceedings of the National Academy of Sciences,* 102**,** 15207-15212.

LI, G., DU, X., VASS, W. C., PAPAGEORGE, A. G., LOWY, D. R. & QIAN, X. 2011. Full activity of the deleted in liver cancer 1 (DLC1) tumor suppressor depends on an LD-like motif that binds talin and focal adhesion kinase (FAK). *Proceedings of the National Academy of Sciences,* 108**,** 17129-17134.

LI, J., BAO, S., WANG, L. & WANG, R. 2021. CircZKSCAN1 Suppresses Hepatocellular Carcinoma Tumorigenesis by Regulating miR-873-5p/Downregulation of Deleted in Liver Cancer 1. *Dig Dis Sci,* 66**,** 4374-4383.

LIAO, Y.-C. & LO, S. H. 2008. Deleted in liver cancer-1 (DLC-1): a tumor suppressor not just for liver. *The international journal of biochemistry & cell biology,* 40**,** 843-847.

LIAO, Y. C., SI, L., DEVERE WHITE, R. W. & LO, S. H. 2007. The phosphotyrosine-independent interaction of DLC-1 and the SH2 domain of cten regulates focal adhesion localization and growth suppression activity of DLC-1. *J Cell Biol,* 176**,** 43-9.

LIN, R., BAGRODIA, S., CERIONE, R. & MANOR, D. 1997. A novel Cdc42Hs mutant induces cellular transformation. *Curr Biol,* 7**,** 794-7.

LINTZ, M., MUÑOZ, A. & REINHART-KING, C. A. 2017. The Mechanics of Single Cell and Collective Migration of Tumor Cells. *J Biomech Eng,* 139**,** 0210051-9.

LIU, C., LIU, Y., ZHANG, W. & LIU, X. 2017. Screening for potential genes associated with bone overgrowth after mid-shaft femur fracture in a rat model. *Journal of Orthopaedic Surgery and Research,* 12**,** 8.

LIU, H., LIU, Y., SUN, P., LENG, K., XU, Y., MEI, L., HAN, P., ZHANG, B., YAO, K., LI, C., BAI, J. & CUI, B. 2020. Colorectal cancer-derived exosomal miR-106b-3p promotes metastasis by down-regulating DLC-1 expression. *Clin Sci (Lond),* 134**,** 419-434.

LIU, H., SHI, H., HAO, Y., ZHAO, G., YANG, X., WANG, Y., LI, M. & LIU, M. 2012. Effect of FAK, DLC-1 gene expression on OVCAR-3 proliferation. *Mol Biol Rep,* 39**,** 10665-70.

LIU, Y.-J., LE BERRE, M., LAUTENSCHLAEGER, F., MAIURI, P., CALLAN-JONES, A., HEUZÉ, M., TAKAKI, T., VOITURIEZ, R. & PIEL, M. 2015. Confinement and Low Adhesion Induce Fast Amoeboid Migration of Slow Mesenchymal Cells. *Cell,* 160**,** 659-672.

LO, S. H. 2004. Tensin. *The International Journal of Biochemistry & Cell Biology,* 36**,** 31-34.

LOOSLEY, A. J., O'BRIEN, X. M., REICHNER, J. S. & TANG, J. X. 2015. Describing Directional Cell Migration with a Characteristic Directionality Time. *PLOS ONE,* 10**,** e0127425.

LORENTZEN, A., BAMBER, J., SADOK, A., ELSON-SCHWAB, I. & MARSHALL, C. J. 2011. An ezrin-rich, rigid uropod-like structure directs movement of amoeboid blebbing cells. *Journal of Cell Science,* 124**,** 1256-1267.

LOW, J. S., TAO, Q., NG, K. M., GOH, H. K., SHU, X. S., WOO, W. L., AMBINDER, R. F., SRIVASTAVA, G., SHAMAY, M., CHAN, A. T., POPESCU, N. C. & HSIEH, W. S. 2011. A novel isoform of the 8p22 tumor suppressor gene DLC1 suppresses tumor growth and is frequently silenced in multiple common tumors. *Oncogene,* 30**,** 1923-35.

LU, H. & STENZEL, M. H. 2018. Multicellular Tumor Spheroids (MCTS) as a 3D In Vitro Evaluation Tool of Nanoparticles. *Small,* 14**,** 1702858.

LUCA, A. C., MERSCH, S., DEENEN, R., SCHMIDT, S., MESSNER, I., SCHÄFER, K.-L., BALDUS, S. E., HUCKENBECK, W., PIEKORZ, R. P., KNOEFEL, W. T., KRIEG, A. & STOECKLEIN, N. H. 2013. Impact of the 3D Microenvironment on Phenotype, Gene Expression, and EGFR Inhibition of Colorectal Cancer Cell Lines. *PLOS ONE,* 8**,** e59689.

LUKASIK, D., WILCZEK, E., WASIUTYNSKI, A. & GORNICKA, B. 2011. Deleted in liver cancer protein family in human malignancies (Review). *Oncol Lett,* 2**,** 763-768.

MA, X., LIU, C., GAO, C., LI, J., ZHUANG, J., LIU, L., LI, H., WANG, X., ZHANG, X., DONG, S., ZHOU, C. & SUN, C. 2020. circRNA-associated ceRNA network construction reveals the circRNAs involved in the progression and prognosis of breast cancer. *Journal of Cellular Physiology,* 235**,** 3973-3983.

MACHACEK, M., HODGSON, L., WELCH, C., ELLIOTT, H., PERTZ, O., NALBANT, P., ABELL, A., JOHNSON, G. L., HAHN, K. M. & DANUSER, G. 2009. Coordination of Rho GTPase activities during cell protrusion. *Nature,* 461**,** 99-103.

MADDIPATI, R. & STANGER, B. Z. 2015. Pancreatic Cancer Metastases Harbor Evidence of Polyclonality. *Cancer Discov,* 5**,** 1086-97.

MAHLANDT, E. K., ARTS, J. J. G., VAN DER MEER, W. J., VAN DER LINDEN, F. H., TOL, S., VAN BUUL, J. D., GADELLA, T. W. J. & GOEDHART, J. 2021. Visualizing endogenous Rho activity with an improved localization-based, genetically encoded biosensor. *Journal of Cell Science,* 134**,** jcs258823.

MAK, M., SPILL, F., KAMM, R. D. & ZAMAN, M. H. 2016. Single-Cell Migration in Complex Microenvironments: Mechanics and Signaling Dynamics. *J Biomech Eng,* 138**,** 021004.

MALANDRINO, A., KAMM, R. D. & MOEENDARBARY, E. 2018. In Vitro Modeling of Mechanics in Cancer Metastasis. *ACS Biomaterials Science & Engineering,* 4**,** 294-301.

MALET-ENGRA, G., YU, W., OLDANI, A., REY-BARROSO, J., GOV, N. S., SCITA, G. & DUPRÉ, L. 2015. Collective cell motility promotes chemotactic prowess and resistance to chemorepulsion. *Curr Biol,* 25**,** 242-250.

MALLAVARAPU, A. & MITCHISON, T. 1999. Regulated actin cytoskeleton assembly at filopodium tips controls their extension and retraction. *J Cell Biol,* 146**,** 1097-106.

MARTÍN, I., NAVARRO, B., SERRANO, A., VILLAMÓN, E., CALABUIG, M., SOLANO, C., CHAVES, F. J., YAGÜE, N., ORTS, M., AMAT, P., FUENTES, A., SEDA, E., GARCÍA, F., HERNÁNDEZ-BOLUDA, J. C. & TORMO, M. 2020. Impact of clinical features, cytogenetics, genetic mutations, and methylation dynamics of CDKN2B and DLC-1 promoters on treatment response to azacitidine. *Annals of Hematology,* 99**,** 527-537.

MARTINAC, B. 2014. The ion channels to cytoskeleton connection as potential mechanism of mechanosensitivity. *Biochimica et Biophysica Acta (BBA) - Biomembranes,* 1838**,** 682-691.

MARTINO, F., PERESTRELO, A. R., VINARSKÝ, V., PAGLIARI, S. & FORTE, G. 2018. Cellular Mechanotransduction: From Tension to Function. *Front Physiol,* 9**,** 824.

MARUNO, T., FUKUDA, A., GOTO, N., TSUDA, M., IKUTA, K., HIRAMATSU, Y., OGAWA, S., NAKANISHI, Y., YAMAGA, Y., YOSHIOKA, T., TAKAORI, K., UEMOTO, S., SAUR, D., CHIBA, T. & SENO, H. 2021. Visualization of stem cell activity in pancreatic cancer expansion by direct lineage tracing with live imaging. *Elife,* 10.

MASMUDI-MARTÍN, M., ZHU, L., SANCHEZ-NAVARRO, M., PRIEGO, N., CASANOVA-ACEBES, M., RUIZ-RODADO, V., GIRALT, E. & VALIENTE, M. 2021. Brain metastasis models: What should we aim to achieve better treatments? *Advanced Drug Delivery Reviews,* 169**,** 79-99.

MASON, D. E., COLLINS, J. M., DAWAHARE, J. H., NGUYEN, T. D., LIN, Y., VOYTIK-HARBIN, S. L., ZORLUTUNA, P., YODER, M. C. & BOERCKEL, J. D. 2019. YAP and TAZ limit cytoskeletal and focal adhesion maturation to enable persistent cell motility. *J Cell Biol,* 218**,** 1369-1389.

MATSUYAMA, H., PAN, Y., OBA, K., YOSHIHIRO, S., MATSUDA, K., HÄGARTH, L., KUDREN, D., NAITO, K., BERGERHEIM, U. S. & EKMAN, P. 2001. Deletions on chromosome 8p22 may predict disease progression as well as pathological staging in prostate cancer. *Clin Cancer Res,* 7**,** 3139-43.

MATTILA, P. K. & LAPPALAINEN, P. 2008. Filopodia: molecular architecture and cellular functions. *Nat Rev Mol Cell Biol,* 9**,** 446-54.

MAYOR, R. & ETIENNE-MANNEVILLE, S. 2016. The front and rear of collective cell migration. *Nature Reviews Molecular Cell Biology,* 17**,** 97-109.

MAZIVEYI, M. & ALAHARI, S. K. 2017. Cell matrix adhesions in cancer: The proteins that form the glue. *Oncotarget,* 8**,** 48471-48487.

MEDEIROS, N. A., BURNETTE, D. T. & FORSCHER, P. 2006. Myosin II functions in actin-bundle turnover in neuronal growth cones. *Nat Cell Biol,* 8**,** 215-26.

MEHTA, G., HSIAO, A. Y., INGRAM, M., LUKER, G. D. & TAKAYAMA, S. 2012. Opportunities and challenges for use of tumor spheroids as models to test drug delivery and efficacy. *J Control Release,* 164**,** 192-204.

MEHTA, S. & ZHANG, J. 2011. Reporting from the Field: Genetically Encoded Fluorescent Reporters Uncover Signaling Dynamics in Living Biological Systems. *Annual Review of Biochemistry,* 80**,** 375-401.

MELISSARIDOU, S., WIECHEC, E., MAGAN, M., JAIN, M. V., CHUNG, M. K., FARNEBO, L. & ROBERG, K. 2019. The effect of 2D and 3D cell cultures on treatment response, EMT profile and stem cell features in head and neck cancer 11 Medical and Health Sciences 1112 Oncology and Carcinogenesis. *Cancer Cell International,* 19.

MICHALET, X. 2010. Mean square displacement analysis of single-particle trajectories with localization error: Brownian motion in an isotropic medium. *Physical review. E, Statistical, nonlinear, and soft matter physics,* 82**,** 041914-041914.

MICHOD, D., YANG, J.-Y., CHEN, J., BONNY, C. & WIDMANN, C. 2004. A RasGAP-derived cell permeable peptide potently enhances genotoxin-induced cytotoxicity in tumor cells. *Oncogene,* 23**,** 8971-8978.

MILLER, K. D., NOGUEIRA, L., MARIOTTO, A. B., ROWLAND, J. H., YABROFF, K. R., ALFANO, C. M., JEMAL, A., KRAMER, J. L. & SIEGEL, R. L. 2019. Cancer treatment and survivorship statistics, 2019. *CA Cancer J Clin,* 69**,** 363-385.

MISHRA, Y. G. & MANAVATHI, B. 2021. Focal adhesion dynamics in cellular function and disease. *Cellular Signalling,* 85**,** 110046.

MIYAWAKI, A. & NIINO, Y. 2015. Molecular Spies for Bioimaging—Fluorescent Protein-Based Probes. *Molecular Cell,* 58**,** 632-643.

MIYAWAKI, A. & TSIEN, R. Y. 2000. Monitoring protein conformations and interactions by fluorescence resonance energy transfer between mutants of green fluorescent protein. *Methods Enzymol,* 327**,** 472-500.

MORIMATSU, M., MEKHDJIAN, A. H., ADHIKARI, A. S. & DUNN, A. R. 2013. Molecular tension sensors report forces generated by single integrin molecules in living cells. *Nano Lett,* 13**,** 3985-9.

NAAKKA, E., TUOMAINEN, K., WISTRAND, H., PALKAMA, M., SULEYMANOVA, I., AL-SAMADI, A. & SALO, T. 2019. Fully human tumor-based matrix in three-dimensional spheroid invasion assay. *J. Vis. Exp,* 147**,** e59567.

NAGANO, M., HOSHINO, D., KOSHIKAWA, N., AKIZAWA, T. & SEIKI, M. 2012. Turnover of focal adhesions and cancer cell migration. *International journal of cell biology,* 2012**,** 310616-310616.

NAGASAKI, A., KANADA, M. & UYEDA, T. Q. P. 2009. Cell adhesion molecules regulate contractile ring-independent cytokinesis in Dictyostelium discoideum. *Cell Research,* 19**,** 236-246.

NALBANT, P., HODGSON, L., KRAYNOV, V., TOUTCHKINE, A. & HAHN, K. M. 2004. Activation of endogenous Cdc42 visualized in living cells. *Science,* 305**,** 1615-9.

NARDONE, G., OLIVER-DE LA CRUZ, J., VRBSKY, J., MARTINI, C., PRIBYL, J., SKLÁDAL, P., PEŠL, M., CALUORI, G., PAGLIARI, S., MARTINO, F., MACECKOVA, Z., HAJDUCH, M., SANZ-GARCIA, A., PUGNO, N. M., STOKIN, G. B. & FORTE, G. 2017. YAP regulates cell mechanics by controlling focal adhesion assembly. *Nature Communications,* 8**,** 15321.

NATH, S. & DEVI, G. R. 2016. Three-dimensional culture systems in cancer research: Focus on tumor spheroid model. *Pharmacol Ther,* 163**,** 94-108.

NELSON, W. J. 2009. Remodeling epithelial cell organization: transitions between front-rear and apical-basal polarity. *Cold Spring Harb Perspect Biol,* 1**,** a000513.

NEWMAN, D., YOUNG, L., WARING, T., BROWN, L., WOLANSKA, K., MACDONALD, E., ORSZAG, A. C., CASWELL, P., SAKUMA, T., YAMAMOTO, T., MACHESKY, L., MORGAN, M. & ZECH, T. 2021. 3D matrix adhesion composition facilitates nuclear force coupling to drive invasive cell migration. *bioRxiv***,** 2021.05.17.443835.

NIGGLI, V. & ROSSY, J. 2008. Ezrin/radixin/moesin: versatile controllers of signaling molecules and of the cortical cytoskeleton. *Int J Biochem Cell Biol,* 40**,** 344-9.

NOBES, C. D. & HALL, A. 1995. Rho, rac, and cdc42 GTPases regulate the assembly of multimolecular focal complexes associated with actin stress fibers, lamellipodia, and filopodia. *Cell,* 81**,** 53-62.

NOBIS, M., HERRMANN, D., WARREN, S. C., KADIR, S., LEUNG, W., KILLEN, M., MAGENAU, A., STEVENSON, D., LUCAS, M. C., REISCHMANN, N., VENNIN, C., CONWAY, J. R. W., BOULGHOURJIAN, A., ZARATZIAN, A., LAW, A. M., GALLEGO-ORTEGA, D., ORMANDY, C. J., WALTERS, S. N., GREY, S. T., BAILEY, J., CHTANOVA, T., QUINN, J. M. W., BALDOCK, P. A., CROUCHER, P. I., SCHWARZ, J. P., MROWINSKA, A., ZHANG, L., HERZOG, H., MASEDUNSKAS, A., HARDEMAN, E. C., GUNNING, P. W., DEL MONTE-NIETO, G., HARVEY, R. P., SAMUEL, M. S., PAJIC, M., MCGHEE, E. J., JOHNSSON, A. E., SANSOM, O. J., WELCH, H. C. E., MORTON, J. P., STRATHDEE, D., ANDERSON, K. I. & TIMPSON, P. 2017. A RhoA-FRET Biosensor Mouse for Intravital Imaging in Normal Tissue Homeostasis and Disease Contexts. *Cell Rep,* 21**,** 274-288.

NOBIS, M., HERRMANN, D., WARREN, S. C., STRATHDEE, D., COX, T. R., ANDERSON, K. I. & TIMPSON, P. 2020. Shedding new light on RhoA signalling as a drug target in vivo using a novel RhoA-FRET biosensor mouse. *Small GTPases,* 11**,** 240-247.

NUNES, A. S., BARROS, A. S., COSTA, E. C., MOREIRA, A. F. & CORREIA, I. J. 2019. 3D tumor spheroids as in vitro models to mimic in vivo human solid tumors resistance to therapeutic drugs. *Biotechnology and Bioengineering,* 116**,** 206-226.

O'CONNOR, K. & CHEN, M. 2013. Dynamic functions of RhoA in tumor cell migration and invasion. *Small GTPases,* 4**,** 141-7.

O'NEILL, P. R., CASTILLO-BADILLO, J. A., MESHIK, X., KALYANARAMAN, V., MELGAREJO, K. & GAUTAM, N. 2018. Membrane Flow Drives an Adhesion-Independent Amoeboid Cell Migration Mode. *Dev Cell,* 46**,** 9-22.e4.

OKAYAMA, H., SCHETTER, A. J., ISHIGAME, T., ROBLES, A. I., KOHNO, T., YOKOTA, J., TAKENOSHITA, S. & HARRIS, C. C. 2014. The expression of four genes as a prognostic classifier for stage I lung adenocarcinoma in 12 independent cohorts. *Cancer Epidemiol Biomarkers Prev,* 23**,** 2884-94.

OLEKSIUK, O., ABBA, M., TEZCAN, K. C., SCHAUFLER, W., BESTVATER, F., PATIL, N., BIRK, U., HAFNER, M., ALTEVOGT, P., CREMER, C. & ALLGAYER, H. 2015. Single-Molecule Localization Microscopy allows for the analysis of cancer metastasis-specific miRNA distribution on the nanoscale. *Oncotarget,* 6**,** 44745-57.

OLOFSSON, K., CARANNANTE, V., TAKAI, M., ÖNFELT, B. & WIKLUND, M. 2021. Single cell organization and cell cycle characterization of DNA stained multicellular tumor spheroids. *Scientific Reports,* 11**,** 17076.

OMELCHENKO, T., VASILIEV, J. M., GELFAND, I. M., FEDER, H. H. & BONDER, E. M. 2003. Rho-dependent formation of epithelial “leader” cells during wound healing. *Proceedings of the National Academy of Sciences,* 100**,** 10788-10793.

PAJIC, M., HERRMANN, D., VENNIN, C., CONWAY, J. R., CHIN, V. T., JOHNSSON, A. K., WELCH, H. C. & TIMPSON, P. 2015. The dynamics of Rho GTPase signaling and implications for targeting cancer and the tumor microenvironment. *Small GTPases,* 6**,** 123-33.

PALUCH, E. K., ASPALTER, I. M. & SIXT, M. 2016. Focal Adhesion–Independent Cell Migration. *Annual Review of Cell and Developmental Biology,* 32**,** 469-490.

PALUCH, E. K. & RAZ, E. 2013. The role and regulation of blebs in cell migration. *Curr Opin Cell Biol,* 25**,** 582-90.

PAMPALONI, F., CHANG, B.-J. & STELZER, E. H. K. 2015. Light sheet-based fluorescence microscopy (LSFM) for the quantitative imaging of cells and tissues. *Cell and Tissue Research,* 360**,** 129-141.

PAMPALONI, F., REYNAUD, E. G. & STELZER, E. H. 2007. The third dimension bridges the gap between cell culture and live tissue. *Nat Rev Mol Cell Biol,* 8**,** 839-45.

PAPUSHEVA, E., DE QUEIROZ, F. M., DALOUS, J., HAN, Y., ESPOSITO, A., JARES-ERIJMANXA, E. A., JOVIN, T. M. & BUNT, G. 2009. Dynamic conformational changes in the FERM domain of FAK are involved in focal-adhesion behavior during cell spreading and motility. *Journal of Cell Science,* 122**,** 656-666.

PARDOLL, D. M. 2012. The blockade of immune checkpoints in cancer immunotherapy. *Nat Rev Cancer,* 12**,** 252-64.

PARRI, M. & CHIARUGI, P. 2010. Rac and Rho GTPases in cancer cell motility control. *Cell Communication and Signaling,* 8**,** 23.

PARSLOW, A., CARDONA, A. & BRYSON-RICHARDSON, R. J. 2014. Sample drift correction following 4D confocal time-lapse imaging. *J Vis Exp*.

PATSIALOU, A., BRAVO-CORDERO, J. J., WANG, Y., ENTENBERG, D., LIU, H., CLARKE, M. & CONDEELIS, J. S. 2013. Intravital multiphoton imaging reveals multicellular streaming as a crucial component of in vivo cell migration in human breast tumors. *Intravital,* 2**,** e25294.

PAUL, C. D., MISTRIOTIS, P. & KONSTANTOPOULOS, K. 2017. Cancer cell motility: lessons from migration in confined spaces. *Nat Rev Cancer,* 17**,** 131-140.

PEARSON, G. W. 2019. Control of Invasion by Epithelial-to-Mesenchymal Transition Programs during Metastasis. *Journal of Clinical Medicine,* 8**,** 646.

PELLEGRIN, S. & MELLOR, H. 2007. Actin stress fibres. *J Cell Sci,* 120**,** 3491-9.

PENG, H., LONG, F., WU, Z., CHU, Y., LI, J., KUAI, R., ZHANG, J., KANG, Z., ZHANG, X. & GUAN, M. 2013. Downregulation of DLC-1 gene by promoter methylation during primary colorectal cancer progression. *Biomed Res Int,* 2013**,** 181384.

PERTZ, O. 2010. Spatio-temporal Rho GTPase signaling – where are we now? *Journal of Cell Science,* 123**,** 1841-1850.

PERTZ, O. & HAHN, K. M. 2004. Designing biosensors for Rho family proteins — deciphering the dynamics of Rho family GTPase activation in living cells. *Journal of Cell Science,* 117**,** 1313-1318.

PERTZ, O., HODGSON, L., KLEMKE, R. L. & HAHN, K. M. 2006. Spatiotemporal dynamics of RhoA activity in migrating cells. *Nature,* 440**,** 1069-1072.

PETRIE, R. J., GAVARA, N., CHADWICK, R. S. & YAMADA, K. M. 2012. Nonpolarized signaling reveals two distinct modes of 3D cell migration. *J Cell Biol,* 197**,** 439-55.

PETRIE, R. J. & YAMADA, K. M. 2012. At the leading edge of three-dimensional cell migration. *Journal of cell science,* 125**,** 5917-5926.

PIJUAN, J., BARCELÓ, C., MORENO, D. F., MAIQUES, O., SISÓ, P., MARTI, R. M., MACIÀ, A. & PANOSA, A. 2019. In vitro Cell Migration, Invasion, and Adhesion Assays: From Cell Imaging to Data Analysis. *Frontiers in Cell and Developmental Biology,* 7.

PINTO, B., HENRIQUES, A. C., SILVA, P. M. A. & BOUSBAA, H. 2020. Three-Dimensional Spheroids as In Vitro Preclinical Models for Cancer Research. *Pharmaceutics,* 12.

PLUQUET, O., POURTIER, A. & ABBADIE, C. 2015. The unfolded protein response and cellular senescence. A review in the theme: cellular mechanisms of endoplasmic reticulum stress signaling in health and disease. *Am J Physiol Cell Physiol,* 308**,** C415-25.

POLLARD, T. D. 2016. Actin and Actin-Binding Proteins. *Cold Spring Harb Perspect Biol,* 8.

POLLARD, T. D. & BORISY, G. G. 2003. Cellular motility driven by assembly and disassembly of actin filaments. *Cell,* 112**,** 453-65.

POPESCU, N. C. & GOODISON, S. 2014. Deleted in liver cancer-1 (DLC1): an emerging metastasis suppressor gene. *Mol Diagn Ther,* 18**,** 293-302.

PORTER, A. P., PAPAIOANNOU, A. & MALLIRI, A. 2016. Deregulation of Rho GTPases in cancer. *Small GTPases,* 7**,** 123-38.

POZZI, S., SCOMPARIN, A., ISRAELI DANGOOR, S., RODRIGUEZ AJAMIL, D., OFEK, P., NEUFELD, L., KRIVITSKY, A., VASKOVICH-KOUBI, D., KLEINER, R., DEY, P., KOSHROVSKI-MICHAEL, S., REISMAN, N. & SATCHI-FAINARO, R. 2021. Meet me halfway: Are in vitro 3D cancer models on the way to replace in vivo models for nanomedicine development? *Adv Drug Deliv Rev,* 175**,** 113760.

PRENDERGAST, G. C., KHOSRAVI-FAR, R., SOLSKI, P. A., KURZAWA, H., LEBOWITZ, P. F. & DER, C. J. 1995. Critical role of Rho in cell transformation by oncogenic Ras. *Oncogene,* 10**,** 2289-96.

PRESCHER, J. A. & CONTAG, C. H. 2010. Guided by the light: visualizing biomolecular processes in living animals with bioluminescence. *Curr Opin Chem Biol,* 14**,** 80-9.

PRIEGO, N., ZHU, L., MONTEIRO, C., MULDERS, M., WASILEWSKI, D., BINDEMAN, W., DOGLIO, L., MARTÍNEZ, L., MARTÍNEZ-SAEZ, E., RAMÓN Y CAJAL, S., MEGÍAS, D., HERNÁNDEZ-ENCINAS, E., BLANCO-APARICIO, C., MARTÍNEZ, L., ZARZUELA, E., MUÑOZ, J., FUSTERO-TORRE, C., PIÑEIRO-YÁÑEZ, E., HERNÁNDEZ-LAÍN, A., BERTERO, L., POLI, V., SANCHEZ-MARTINEZ, M., MENENDEZ, J. A., SOFFIETTI, R., BOSCH-BARRERA, J. & VALIENTE, M. 2018. STAT3 labels a subpopulation of reactive astrocytes required for brain metastasis. *Nature Medicine,* 24**,** 1024-1035.

PROVENZANO, P. P., ELICEIRI, K. W., CAMPBELL, J. M., INMAN, D. R., WHITE, J. G. & KEELY, P. J. 2006. Collagen reorganization at the tumor-stromal interface facilitates local invasion. *BMC Medicine,* 4**,** 38.

QADI, S. A., HASSAN, M. A., SHEIKH, R. A., BAOTHMAN, O. A., ZAMZAMI, M. A., CHOUDHRY, H., AL-MALKI, A. L., ALBUKHARI, A. & ALHOSIN, M. 2019. Thymoquinone-Induced Reactivation of Tumor Suppressor Genes in Cancer Cells Involves Epigenetic Mechanisms. *Epigenetics Insights,* 12**,** 2516865719839011.

QIAN, X., LI, G., ASMUSSEN, H. K., ASNAGHI, L., VASS, W. C., BRAVERMAN, R., YAMADA, K. M., POPESCU, N. C., PAPAGEORGE, A. G. & LOWY, D. R. 2007. Oncogenic inhibition by a deleted in liver cancer gene requires cooperation between tensin binding and Rho-specific GTPase-activating protein activities. *Proc Natl Acad Sci U S A,* 104**,** 9012-7.

QIAO, B. J. 2005. The many faces of SAM. *Science Signalling,* 286.

QIN, Y., CHU, B., GONG, W., WANG, J., TANG, Z., SHEN, J. & QUAN, Z. 2014. Inhibitory effects of deleted in liver cancer 1 gene on gallbladder cancer growth through induction of cell cycle arrest and apoptosis. *J Gastroenterol Hepatol,* 29**,** 964-72.

QUAIL, D. F. & JOYCE, J. A. 2013. Microenvironmental regulation of tumor progression and metastasis. *Nature Medicine,* 19**,** 1423-1437.

RAFTOPOULOU, M. & HALL, A. 2004. Cell migration: Rho GTPases lead the way. *Developmental Biology,* 265**,** 23-32.

RAHIKAINEN, R., VON ESSEN, M., SCHAEFER, M., QI, L., AZIZI, L., KELLY, C., IHALAINEN, T. O., WEHRLE-HALLER, B., BASTMEYER, M., HUANG, C. & HYTÖNEN, V. P. 2017. Mechanical stability of talin rod controls cell migration and substrate sensing. *Scientific Reports,* 7**,** 3571.

RAHMANI, M., TALEBI, M., HAGH, M. F., FEIZI, A. A. H. & SOLALI, S. 2018. Aberrant DNA methylation of key genes and Acute Lymphoblastic Leukemia. *Biomed Pharmacother,* 97**,** 1493-1500.

RAVI, M., PARAMESH, V., KAVIYA, S. R., ANURADHA, E. & SOLOMON, F. D. 2015. 3D cell culture systems: advantages and applications. *J Cell Physiol,* 230**,** 16-26.

REN, G. & LI, G. 2021. Tumor suppressor gene DLC1: Its modifications, interactive molecules, and potential prospects for clinical cancer application. *International Journal of Biological Macromolecules,* 182**,** 264-275.

RENKAWITZ, J., KOPF, A., STOPP, J., DE VRIES, I., DRISCOLL, M. K., MERRIN, J., HAUSCHILD, R., WELF, E. S., DANUSER, G., FIOLKA, R. & SIXT, M. 2019. Nuclear positioning facilitates amoeboid migration along the path of least resistance. *Nature,* 568**,** 546-550.

RIDLEY, A. J. 2011. Life at the leading edge. *Cell,* 145**,** 1012-22.

RIDLEY, A. J. 2015. Rho GTPase signalling in cell migration. *Current Opinion in Cell Biology,* 36**,** 103-112.

RIDLEY, A. J., SCHWARTZ, M. A., BURRIDGE, K., FIRTEL, R. A., GINSBERG, M. H., BORISY, G., PARSONS, J. T. & HORWITZ, A. R. 2003. Cell migration: integrating signals from front to back. *Science,* 302**,** 1704-9.

RIEDL, A., SCHLEDERER, M., PUDELKO, K., STADLER, M., WALTER, S., UNTERLEUTHNER, D., UNGER, C., KRAMER, N., HENGSTSCHLÄGER, M., KENNER, L., PFEIFFER, D., KRUPITZA, G. & DOLZNIG, H. 2017. Comparison of cancer cells in 2D vs 3D culture reveals differences in AKT-mTOR-S6K signaling and drug responses. *Journal of Cell Science,* 130**,** 203-218.

RIENTO, K. & RIDLEY, A. J. 2003. Rocks: multifunctional kinases in cell behaviour. *Nat Rev Mol Cell Biol,* 4**,** 446-56.

RISS, T. & TRASK, O. J. 2021. Factors to consider when interrogating 3D culture models with plate readers or automated microscopes. *In Vitro Cellular & Developmental Biology - Animal,* 57**,** 238-256.

RITCH, S. J., BRANDHAGEN, B. N., GOYENECHE, A. A. & TELLERIA, C. M. 2019. Advanced assessment of migration and invasion of cancer cells in response to mifepristone therapy using double fluorescence cytochemical labeling. *BMC Cancer,* 19**,** 376.

RIZWAN, A., BULTE, C., KALAICHELVAN, A., CHENG, M., KRISHNAMACHARY, B., BHUJWALLA, Z. M., JIANG, L. & GLUNDE, K. 2015. Metastatic breast cancer cells in lymph nodes increase nodal collagen density. *Sci Rep,* 5**,** 10002.

ROBINSON, D. R., WU, Y.-M., LONIGRO, R. J., VATS, P., COBAIN, E., EVERETT, J., CAO, X., RABBAN, E., KUMAR-SINHA, C., RAYMOND, V., SCHUETZE, S., ALVA, A., SIDDIQUI, J., CHUGH, R., WORDEN, F., ZALUPSKI, M. M., INNIS, J., MODY, R. J., TOMLINS, S. A., LUCAS, D., BAKER, L. H., RAMNATH, N., SCHOTT, A. F., HAYES, D. F., VIJAI, J., OFFIT, K., STOFFEL, E. M., ROBERTS, J. S., SMITH, D. C., KUNJU, L. P., TALPAZ, M., CIEŚLIK, M. & CHINNAIYAN, A. M. 2017. Integrative clinical genomics of metastatic cancer. *Nature,* 548**,** 297-303.

RODRIGUES, T., KUNDU, B., SILVA-CORREIA, J., KUNDU, S. C., OLIVEIRA, J. M., REIS, R. L. & CORRELO, V. M. 2018. Emerging tumor spheroids technologies for 3D in vitro cancer modeling. *Pharmacology & Therapeutics,* 184**,** 201-211.

ROHIWAL (ed.) 2020. *Consensus protocols for animal experimentation and nanomedicine trials at clinical stage in breast cancer.*

: Elsevier; Theranostics: .

ROMERO, S., LE CLAINCHE, C., DIDRY, D., EGILE, C., PANTALONI, D. & CARLIER, M. F. 2004. Formin is a processive motor that requires profilin to accelerate actin assembly and associated ATP hydrolysis. *Cell,* 119**,** 419-29.

ROTHENBERG, K. E., SCOTT, D. W., CHRISTOFOROU, N. & HOFFMAN, B. D. 2018. Vinculin Force-Sensitive Dynamics at Focal Adhesions Enable Effective Directed Cell Migration. *Biophys J,* 114**,** 1680-1694.

ROTTNER, K., HÄNISCH, J. & CAMPELLONE, K. G. 2010. WASH, WHAMM and JMY: regulation of Arp2/3 complex and beyond. *Trends Cell Biol,* 20**,** 650-61.

SABBIR, M. G., WIGLE, N., LOEWEN, S., GU, Y., BUSE, C., HICKS, G. G. & MOWAT, M. R. 2010. Identification and characterization of Dlc1 isoforms in the mouse and study of the biological function of a single gene trapped isoform. *BMC Biol,* 8**,** 17.

SAHAI, E. & MARSHALL, C. J. 2002. RHO–GTPases and cancer. *Nature Reviews Cancer,* 2**,** 133-142.

SALO, T., SUTINEN, M., HOQUE APU, E., SUNDQUIST, E., CERVIGNE, N. K., DE OLIVEIRA, C. E., AKRAM, S. U., OHLMEIER, S., SUOMI, F., EKLUND, L., JUUSELA, P., ÅSTRÖM, P., BITU, C. C., SANTALA, M., SAVOLAINEN, K., KORVALA, J., PAES LEME, A. F. & COLETTA, R. D. 2015. A novel human leiomyoma tissue derived matrix for cell culture studies. *BMC Cancer,* 15**,** 981.

SÁNCHEZ-MARTÍN, D., OTSUKA, A., KABASHIMA, K., HA, T., WANG, D., QIAN, X., LOWY, D. R. & TOSATO, G. 2018. Effects of DLC1 Deficiency on Endothelial Cell Contact Growth Inhibition and Angiosarcoma Progression. *J Natl Cancer Inst,* 110**,** 390-399.

SANZ-MORENO, V., GADEA, G., AHN, J., PATERSON, H., MARRA, P., PINNER, S., SAHAI, E. & MARSHALL, C. J. 2008. Rac activation and inactivation control plasticity of tumor cell movement. *Cell,* 135**,** 510-23.

SARANGI, B. R., GUPTA, M., DOSS, B. L., TISSOT, N., LAM, F., MÈGE, R.-M., BORGHI, N. & LADOUX, B. 2017. Coordination between Intra- and Extracellular Forces Regulates Focal Adhesion Dynamics. *Nano letters,* 17**,** 399-406.

SAXTON, M. J. & JACOBSON, K. 1997. SINGLE-PARTICLE TRACKING:Applications to Membrane Dynamics. *Annual Review of Biophysics and Biomolecular Structure,* 26**,** 373-399.

SCARPA, E. & MAYOR, R. 2016. Collective cell migration in development. *J Cell Biol,* 212**,** 143-55.

SCHAKS, M., GIANNONE, G. & ROTTNER, K. 2019. Actin dynamics in cell migration. *Essays Biochem,* 63**,** 483-495.

SCHILLER, H. B. & FÄSSLER, R. 2013. Mechanosensitivity and compositional dynamics of cell-matrix adhesions. *EMBO Rep,* 14**,** 509-19.

SCHILLER, H. B., FRIEDEL, C. C., BOULEGUE, C. & FÄSSLER, R. 2011. Quantitative proteomics of the integrin adhesome show a myosin II-dependent recruitment of LIM domain proteins. *EMBO Rep,* 12**,** 259-66.

SCHOLZ, R. P., GUSTAFSSON, J. O., HOFFMANN, P., JAISWAL, M., AHMADIAN, M. R., EISLER, S. A., ERLMANN, P., SCHMID, S., HAUSSER, A. & OLAYIOYE, M. A. 2011. The tumor suppressor protein DLC1 is regulated by PKD-mediated GAP domain phosphorylation. *Exp Cell Res,* 317**,** 496-503.

SCHOLZ RP, R. J., THEIL A, ERLMANN P, HOLEITER G, JÄHNE R, SCHMID S, HAUSSER A, OLAYIOYE MA. 2009. DLC1 interacts with 14-3-3 proteins to inhibit RhoGAP activity and block nucleocytoplasmic shuttling. *Journal of Cell Science,* 122**,** 92-102.

SEKIMATA, M., KABUYAMA, Y., EMORI, Y. & HOMMA, Y. 1999. Morphological Changes and Detachment of Adherent Cells Induced by p122, a GTPase-activating Protein for Rho *. *Journal of Biological Chemistry,* 274**,** 17757-17762.

SENG, T. J., LOW, J. S., LI, H., CUI, Y., GOH, H. K., WONG, M. L., SRIVASTAVA, G., SIDRANSKY, D., CALIFANO, J., STEENBERGEN, R. D., RHA, S. Y., TAN, J., HSIEH, W. S., AMBINDER, R. F., LIN, X., CHAN, A. T. & TAO, Q. 2007. The major 8p22 tumor suppressor DLC1 is frequently silenced by methylation in both endemic and sporadic nasopharyngeal, esophageal, and cervical carcinomas, and inhibits tumor cell colony formation. *Oncogene,* 26**,** 934-44.

SERRA, D., MAYR, U., BONI, A., LUKONIN, I., REMPFLER, M., CHALLET MEYLAN, L., STADLER, M. B., STRNAD, P., PAPASAIKAS, P., VISCHI, D., WALDT, A., ROMA, G. & LIBERALI, P. 2019. Self-organization and symmetry breaking in intestinal organoid development. *Nature,* 569**,** 66-72.

SEYFRIED, T. N., FLORES, R. E., POFF, A. M. & D'AGOSTINO, D. P. 2014. Cancer as a metabolic disease: implications for novel therapeutics. *Carcinogenesis,* 35**,** 515-27.

SHAMS, H., HOFFMAN, B. D. & MOFRAD, M. R. K. 2018. The "Stressful" Life of Cell Adhesion Molecules: On the Mechanosensitivity of Integrin Adhesome. *J Biomech Eng,* 140.

SHELLARD, A. & MAYOR, R. 2019. Supracellular migration – beyond collective cell migration. *Journal of Cell Science,* 132.

SHEMESH, T., GEIGER, B., BERSHADSKY, A. D. & KOZLOV, M. M. 2005. Focal adhesions as mechanosensors: A physical mechanism. *Proceedings of the National Academy of Sciences of the United States of America,* 102**,** 12383-12388.

SHIH, Y. P., TAKADA, Y. & LO, S. H. 2012. Silencing of DLC1 upregulates PAI-1 expression and reduces migration in normal prostate cells. *Mol Cancer Res,* 10**,** 34-9.

SHUMAN MOSS, L. A., JENSEN-TAUBMAN, S. & STETLER-STEVENSON, W. G. 2012. Matrix metalloproteinases: changing roles in tumor progression and metastasis. *Am J Pathol,* 181**,** 1895-9.

SINGH, D., BHARTI, A., BISWAS, D., TEWARI, M., KAR, A. G., ANSARI, M. A., SINGH, S. & NARAYAN, G. 2022. Frequent Downregulation and Promoter Hypermethylation of DLC1: Relationship with Clinical Outcome in Gallbladder Cancer. *J Gastrointest Cancer,* 53**,** 237-244.

SIRENKO, O., MITLO, T., HESLEY, J., LUKE, S., OWENS, W. & CROMWELL, E. F. 2015. High-content assays for characterizing the viability and morphology of 3D cancer spheroid cultures. *Assay and drug development technologies,* 13**,** 402-414.

SJOESTROEM, C., KHOSRAVI, S., CHENG, Y., SAFAEE ARDEKANI, G., MARTINKA, M. & LI, G. 2014. DLC1 expression is reduced in human cutaneous melanoma and correlates with patient survival. *Mod Pathol,* 27**,** 1203-11.

SMALL, J. V. & CELIS, J. E. 1978. Filament arrangements in negatively stained cultured cells: the organization of actin. *Cytobiologie,* 16**,** 308-25.

SMILENOV, L. B., MIKHAILOV, A., PELHAM, R. J., MARCANTONIO, E. E. & GUNDERSEN, G. G. 1999. Focal adhesion motility revealed in stationary fibroblasts. *Science,* 286**,** 1172-4.

SONG, L. J., LIU, Q., MENG, X. R., LI SH, L., WANG, L. X., FAN, Q. X. & XUAN, X. Y. 2016. DLC-1 is an independent prognostic marker and potential therapeutic target in hepatocellular cancer. *Diagn Pathol,* 11**,** 19.

SONG, Y. F., XU, R., ZHANG, X. H., CHEN, B. B., CHEN, Q., CHEN, Y. M. & XIE, Y. 2006. High-frequency promoter hypermethylation of the deleted in liver cancer-1 gene in multiple myeloma. *Journal of clinical pathology,* 59**,** 947-951.

SONNENSCHEIN, C. & SOTO, A. M. 2016. Carcinogenesis explained within the context of a theory of organisms. *Prog Biophys Mol Biol,* 122**,** 70-76.

STEVE GOODISON, J. Y., DEREK SLOAN, RYUNG KIM, CHENG LI, NICHOLAS C. POPESCU, AND VIRGINIA URQUIDI 2005. The RhoGAP Protein DLC-1 Functions as a Metastasis Suppressor in Breast Cancer Cells. *Cancer Research,* 65**,** 6042-6053.

STOCK, J. & PAULI, A. 2021. Self-organized cell migration across scales – from single cell movement to tissue formation. *Development,* 148**,** dev191767.

STYLIANOU, A., GKRETSI, V., LOUCA, M., ZACHARIA, L. C. & STYLIANOPOULOS, T. 2019. Collagen content and extracellular matrix cause cytoskeletal remodelling in pancreatic fibroblasts. *J R Soc Interface,* 16**,** 20190226.

SU, Y., LIN, L., ZHANG, J., JIANG, Y., PAN, C., SUN, L., DUAN, J. & LIAO, W. 2015. Low expression of DLC1 is predictive of poor therapeutic efficiency of fluoropyrimidine and oxaliplatin as adjuvant chemotherapy in gastric cancer. *Mol Med Rep,* 12**,** 5771-9.

SUHAIL, Y., CAIN, M. P., VANAJA, K., KURYWCHAK, P. A., LEVCHENKO, A., KALLURI, R. & KSHITIZ 2019. Systems Biology of Cancer Metastasis. *Cell Systems,* 9**,** 109-127.

SUN, L., SUN, J. & SONG, J. D. 2019. High expression of DLC family proteins predicts better prognosis and inhibits tumor progression in NSCLC. *Mol Med Rep,* 19**,** 4881-4889.
SVENSMARK, J. H. & BRAKEBUSCH, C. 2019. Rho GTPases in cancer: friend or foe? *Oncogene,* 38**,** 7447-7456.
SVITKINA, T. 2018. The Actin Cytoskeleton and Actin-Based Motility. *Cold Spring Harb Perspect Biol,* 10.
SVITKINA, T. M. & BORISY, G. G. 1999. Arp2/3 complex and actin depolymerizing factor/cofilin in dendritic organization and treadmilling of actin filament array in lamellipodia. *J Cell Biol,* 145**,** 1009-26.
SVITKINA, T. M., BULANOVA, E. A., CHAGA, O. Y., VIGNJEVIC, D. M., KOJIMA, S., VASILIEV, J. M. & BORISY, G. G. 2003. Mechanism of filopodia initiation by reorganization of a dendritic network. *J Cell Biol,* 160**,** 409-21.
SVITKINA, T. M., VERKHOVSKY, A. B., MCQUADE, K. M. & BORISY, G. G. 1997. Analysis of the actin-myosin II system in fish epidermal keratocytes: mechanism of cell body translocation. *J Cell Biol,* 139**,** 397-415.
SYMONS, M. & SEGALL, J. E. 2009. Rac and Rho driving tumor invasion: who's at the wheel? *Genome Biology,* 10**,** 213.
TAKAOKA, M., ITO, S., MIKI, Y. & NAKANISHI, A. 2017. FKBP51 regulates cell motility and invasion via RhoA signaling. *Cancer Sci,* 108**,** 380-389.
TARANTINO, N., TINEVEZ, J.-Y., CROWELL, E. F., BOISSON, B., HENRIQUES, R., MHLANGA, M., AGOU, F., ISRAËL, A. & LAPLANTINE, E. 2014. TNF and IL-1 exhibit distinct ubiquitin requirements for inducing NEMO–IKK supramolecular structures. *Journal of Cell Biology,* 204**,** 231-245.
TE BOEKHORST, V., PREZIOSI, L. & FRIEDL, P. 2016. Plasticity of Cell Migration In Vivo and In Silico. *Annual Review of Cell and Developmental Biology,* 32**,** 491-526.
THEVENEAU, E., MARCHANT, L., KURIYAMA, S., GULL, M., MOEPPS, B., PARSONS, M. & MAYOR, R. 2010. Collective chemotaxis requires contact-dependent cell polarity. *Dev Cell,* 19**,** 39-53.
THIJSSEN-VAN LOOSDREGT, I. 2020. *Modes of cell migration* [Online]. CytoSMART. Available: https://cytosmart.com/resources/modes-of-cell-migration [Accessed 07 June 2022 2022].
TOKSOZ, D. & MERDEK, K. D. 2002. The Rho small GTPase: functions in health and disease. *Histol Histopathol,* 17**,** 915-27.
TRIPATHI, B. K., GRANT, T., QIAN, X., ZHOU, M., MERTINS, P., WANG, D., PAPAGEORGE, A. G., TARASOV, S. G., HUNTER, K. W., CARR, S. A. & LOWY, D. R. 2017. Receptor tyrosine kinase activation of RhoA is mediated by AKT phosphorylation of DLC1. *J Cell Biol,* 216**,** 4255-4270.
TRIPATHI, B. K., QIAN, X., MERTINS, P., WANG, D., PAPAGEORGE, A. G., CARR, S. A. & LOWY, D. R. 2014a. CDK5 is a major regulator of the tumor suppressor DLC1. *Journal of Cell Biology,* 207**,** 627-642.
TRIPATHI, B. K., QIAN, X., MERTINS, P., WANG, D., PAPAGEORGE, A. G., CARR, S. A. & LOWY, D. R. 2014b. CDK5 is a major regulator of the tumor suppressor DLC1. *J Cell Biol,* 207**,** 627-42.
TSAI, J. H. & YANG, J. 2013. Epithelial-mesenchymal plasticity in carcinoma metastasis. *Genes Dev,* 27**,** 2192-206.
UEDA, T., TAKEYAMA, Y., OHMORI, T., OHYANAGI, H., SAITOH, Y. & TAKAI, Y. 1991. Purification and characterization from rat liver cytosol of a GDP dissociation inhibitor (GDI) for liver 24K G, a ras p21-like GTP-binding protein, with properties similar to those of smg p25A GDI. *Biochemistry,* 30**,** 909-917.
ULLMANNOVA-BENSON, V., GUAN, M., ZHOU, X., TRIPATHI, V., YANG, X. Y., ZIMONJIC, D. B. & POPESCU, N. C. 2009. DLC1 tumor suppressor gene inhibits migration and invasion of multiple myeloma cells through RhoA GTPase pathway. *Leukemia,* 23**,** 383-390.
UNGAI-SALÁNKI, R., PETER, B., GERECSEI, T., ORGOVAN, N., HORVATH, R. & SZABÓ, B. 2019. A practical review on the measurement tools for cellular adhesion force. *Advances in Colloid and Interface Science,* 269**,** 309-333.

UNNERSJÖ-JESS, D., SCOTT, L., BLOM, H. & BRISMAR, H. 2016. Super-resolution stimulated emission depletion imaging of slit diaphragm proteins in optically cleared kidney tissue. *Kidney Int,* 89**,** 243-7.

VALASTYAN, S. & WEINBERG, R. A. 2011. Tumor metastasis: molecular insights and evolving paradigms. *Cell,* 147**,** 275-92.

VAN DEN BERG, M. C. W., MACCARTHY-MORROGH, L., CARTER, D., MORRIS, J., RIBEIRO BRAVO, I., FENG, Y. & MARTIN, P. 2019. Proteolytic and Opportunistic Breaching of the Basement Membrane Zone by Immune Cells during Tumor Initiation. *Cell reports,* 27**,** 2837-2846.e4.

VAN DER STOEL, M., SCHIMMEL, L., NAWAZ, K., VAN STALBORCH, A. M., DE HAAN, A., KLAUS-BERGMANN, A., VALENT, E. T., KOENIS, D. S., VAN NIEUW AMERONGEN, G. P., DE VRIES, C. J., DE WAARD, V., GLOERICH, M., VAN BUUL, J. D. & HUVENEERS, S. 2020. DLC1 is a direct target of activated YAP/TAZ that drives collective migration and sprouting angiogenesis. *J Cell Sci,* 133.

VAN ROOSMALEN, W., LE DÉVÉDEC, S. E., GOLANI, O., SMID, M., PULYAKHINA, I., TIMMERMANS, A. M., LOOK, M. P., ZI, D., PONT, C., DE GRAAUW, M., NAFFAR-ABU-AMARA, S., KIRSANOVA, C., RUSTICI, G., HOEN, P. A. C. T., MARTENS, J. W. M., FOEKENS, J. A., GEIGER, B. & VAN DE WATER, B. 2015. Tumor cell migration screen identifies SRPK1 as breast cancer metastasis determinant. *The Journal of Clinical Investigation,* 125**,** 1648-1664.

VAUGHAN, R. B. & TRINKAUS, J. P. 1966. Movements of epithelial cell sheets in vitro. *J Cell Sci,* 1**,** 407-13.

VERMA, R., AGARWAL, A. K., SAKHUJA, P. & SHARMA, P. C. 2019. Microsatellite instability in mismatch repair and tumor suppressor genes and their expression profiling provide important targets for the development of biomarkers in gastric cancer. *Gene,* 710**,** 48-58.

VICENTE-MANZANARES, M., CHOI, C. K. & HORWITZ, A. R. 2009. Integrins in cell migration – the actin connection. *Journal of Cell Science,* 122**,** 199-206.

VICENTE-MANZANARES, M., WEBB, D. J. & HORWITZ, A. R. 2005. Cell migration at a glance. *Journal of Cell Science,* 118**,** 4917-4919.

VIGNJEVIC, D., KOJIMA, S., ARATYN, Y., DANCIU, O., SVITKINA, T. & BORISY, G. G. 2006. Role of fascin in filopodial protrusion. *J Cell Biol,* 174**,** 863-75.

VIGNJEVIC, D. & MONTAGNAC, G. 2008. Reorganisation of the dendritic actin network during cancer cell migration and invasion. *Semin Cancer Biol,* 18**,** 12-22.

VINCI, M., BOX, C. & ECCLES, S. A. 2015. Three-Dimensional (3D) Tumor Spheroid Invasion Assay. *JoVE***,** e52686.

VINCI, M., GOWAN, S., BOXALL, F., PATTERSON, L., ZIMMERMANN, M., COURT, W., LOMAS, C., MENDIOLA, M., HARDISSON, D. & ECCLES, S. A. 2012. Advances in establishment and analysis of three-dimensional tumor spheroid-based functional assays for target validation and drug evaluation. *BMC Biol,* 10**,** 29.

VOIE, A. H., BURNS, D. H. & SPELMAN, F. A. 1993. Orthogonal-plane fluorescence optical sectioning: Three-dimensional imaging of macroscopic biological specimens. *Journal of Microscopy,* 170**,** 229-236.

VON BILDERLING, C., CALDAROLA, M., MASIP, M. E., BRAGAS, A. V. & PIETRASANTA, L. I. 2017. Monitoring in real-time focal adhesion protein dynamics in response to a discrete mechanical stimulus. *Rev Sci Instrum,* 88**,** 013703.

VOON, Y. C., OMAR, I. S., WU, M.-H., SAID, N. A. B. M. & CHUNG, I. 2022. Cancer-associated fibroblasts as cellular vehicles in endometrial cancer cell migration. *Oncol Lett,* 23**,** 3.

WALCOTT, S., KIM, D. H., WIRTZ, D. & SUN, S. X. 2011. Nucleation and decay initiation are the stiffness-sensitive phases of focal adhesion maturation. *Biophys J,* 101**,** 2919-28.

WANG, C., WANG, J., LIU, H. & FU, Z. 2014. Tumor suppressor DLC-1 induces apoptosis and inhibits the growth and invasion of colon cancer cells through the Wnt/beta-catenin signaling pathway. *Oncol Rep,* 31**,** 2270-8.

WANG, D., QIAN, X., RAJARAM, M., DURKIN, M. E. & LOWY, D. R. 2016. DLC1 is the principal biologically-relevant down-regulated DLC family member in several cancers. *Oncotarget,* 7**,** 45144-45157.

WANG, D., QIAN, X., SANCHEZ-SOLANA, B., TRIPATHI, B. K., DURKIN, M. E. & LOWY, D. R. 2020. Cancer-Associated Point Mutations in the DLC1 Tumor Suppressor and Other Rho-GAPs Occur Frequently and Are Associated with Decreased Function. *Cancer Research,* 80**,** 3568-3579.

WANG, Y., XU, X., MAGLIC, D., DILL, M. T., MOJUMDAR, K., NG, P. K., JEONG, K. J., TSANG, Y. H., MORENO, D., BHAVANA, V. H., PENG, X., GE, Z., CHEN, H., LI, J., CHEN, Z., ZHANG, H., HAN, L., DU, D., CREIGHTON, C. J., MILLS, G. B., CAMARGO, F. & LIANG, H. 2018. Comprehensive Molecular Characterization of the Hippo Signaling Pathway in Cancer. *Cell Rep,* 25**,** 1304-1317.e5.

WANG, Y. L. 1985. Exchange of actin subunits at the leading edge of living fibroblasts: possible role of treadmilling. *J Cell Biol,* 101**,** 597-602.

WEBB, D. J., DONAIS, K., WHITMORE, L. A., THOMAS, S. M., TURNER, C. E., PARSONS, J. T. & HORWITZ, A. F. 2004. FAK-Src signalling through paxillin, ERK and MLCK regulates adhesion disassembly. *Nat Cell Biol,* 6**,** 154-61.

WEBB, D. J., PARSONS, J. T. & HORWITZ, A. F. 2002. Adhesion assembly, disassembly and turnover in migrating cells – over and over and over again. *Nature Cell Biology,* 4**,** E97-E100.

WEBB, Z., AND HORWITZ 2005. *Cell Migration An Overview,* Totowa, NJ, Humana Press Inc.

WEIJER, C. J. 2009. Collective cell migration in development. *J Cell Sci,* 122**,** 3215-23.

WELCH, D. R. 2006. Do we need to redefine a cancer metastasis and staging definitions? *Breast Dis,* 26**,** 3-12.

WERTHEIMER, E., GUTIERREZ-UZQUIZA, A., ROSEMBLIT, C., LOPEZ-HABER, C., SOSA, M. S. & KAZANIETZ, M. G. 2012. Rac signaling in breast cancer: a tale of GEFs and GAPs. *Cell Signal,* 24**,** 353-362.

WILKINSON, S., PATERSON, H. F. & MARSHALL, C. J. 2005. Cdc42–MRCK and Rho–ROCK signalling cooperate in myosin phosphorylation and cell invasion. *Nature Cell Biology,* 7**,** 255-261.

WOLF, K., ALEXANDER, S., SCHACHT, V., COUSSENS, L. M., VON ANDRIAN, U. H., VAN RHEENEN, J., DERYUGINA, E. & FRIEDL, P. 2009. Collagen-based cell migration models in vitro and in vivo. *Semin Cell Dev Biol,* 20**,** 931-41.

WOLF, K. & FRIEDL, P. 2011. Extracellular matrix determinants of proteolytic and non-proteolytic cell migration. *Trends Cell Biol,* 21**,** 736-44.

WOLF, K., TE LINDERT, M., KRAUSE, M., ALEXANDER, S., TE RIET, J., WILLIS, A. L., HOFFMAN, R. M., FIGDOR, C. G., WEISS, S. J. & FRIEDL, P. 2013. Physical limits of cell migration: control by ECM space and nuclear deformation and tuning by proteolysis and traction force. *J Cell Biol,* 201**,** 1069-84.

WOLFENSON, H., LUBELSKI, A., REGEV, T., KLAFTER, J., HENIS, Y. I. & GEIGER, B. 2009. A role for the juxtamembrane cytoplasm in the molecular dynamics of focal adhesions. *PLoS One,* 4**,** e4304.

WOLOSZ, D., WALCZAK, A., WILCZYNSKI, G. M., SZPARECKI, G., WILCZEK, E. & GORNICKA, B. 2014. Deleted in liver cancer 1 expression and localization in hepatocellular carcinoma tissue sections. *Oncol Lett,* 8**,** 785-788.

WONG, C. M., YAM, J. W., CHING, Y. P., YAU, T. O., LEUNG, T. H., JIN, D. Y. & NG, I. O. 2005. Rho GTPase-activating protein deleted in liver cancer suppresses cell proliferation and invasion in hepatocellular carcinoma. *Cancer Res,* 65**,** 8861-8.

WOODRUM, D. T., RICH, S. A. & POLLARD, T. D. 1975. Evidence for biased bidirectional polymerization of actin filaments using heavy meromyosin prepared by an improved method. *J Cell Biol,* 67**,** 231-7.

WU, H. T., XIE, C. R., LV, J., QI, H. Q., WANG, F., ZHANG, S., FANG, Q. L., WANG, F. Q., LU, Y. Y. & YIN, Z. Y. 2018. The tumor suppressor DLC1 inhibits cancer progression and oncogenic autophagy in hepatocellular carcinoma. *Lab Invest,* 98**,** 1014-1024.

WU, J. S., JIANG, J., CHEN, B. J., WANG, K., TANG, Y. L. & LIANG, X. H. 2021a. Plasticity of cancer cell invasion: Patterns and mechanisms. *Transl Oncol,* 14**,** 100899.

WU, P.-P., ZOU, J.-H., TANG, R.-N., YAO, Y. & YOU, C.-Z. 2011. Detection and Clinical Significance of DLC1 Gene Methylation in Serum DNA from Colorectal Cancer Patients. *Chinese journal of cancer research = Chung-kuo yen cheng yen chiu,* 23**,** 283-287.

WU, P. P., JIN, Y. L., SHANG, Y. F., JIN, Z., WU, P. & HUANG, P. L. 2009. Restoration of DLC1 gene inhibits proliferation and migration of human colon cancer HT29 cells. *Ann Clin Lab Sci,* 39**,** 263-9.

WU, P. P., ZHU, H. Y., SUN, X. F., CHEN, L. X., ZHOU, Q. & CHEN, J. 2015. MicroRNA-141 regulates the tumour suppressor DLC1 in colorectal cancer. *Neoplasma,* 62**,** 705-12.

WU, Y., ZANOTELLI, M. R., ZHANG, J. & REINHART-KING, C. A. 2021b. Matrix-driven changes in metabolism support cytoskeletal activity to promote cell migration. *Biophysical Journal,* 120**,** 1705-1717.

WU, Y., ZHENG, L.-E., CHEN, S., LV, C. & HUANG, Y. 2022. DLC1 Is a Prognosis-Related Biomarker Correlated With Tumor Microenvironment Remodeling in Endometrial Carcinoma. *Frontiers in Oncology,* 12.

XUE, W., KRASNITZ, A., LUCITO, R., SORDELLA, R., VANAELST, L., CORDON-CARDO, C., SINGER, S., KUEHNEL, F., WIGLER, M., POWERS, S., ZENDER, L. & LOWE, S. W. 2008. DLC1 is a chromosome 8p tumor suppressor whose loss promotes hepatocellular carcinoma. *Genes Dev,* 22**,** 1439-44.

XUE, Y. Z., WU, T. L., WU, Y. M., SHENG, Y. Y., WEI, Z. Q., LU, Y. F., YU, L. H., LI, J. P. & LI, Z. S. 2013. DLC-1 is a candidate biomarker methylated and down-regulated in pancreatic ductal adenocarcinoma. *Tumour Biol,* 34**,** 2857-61.

YAM, J. W., KO, F. C., CHAN, C. Y., JIN, D. Y. & NG, I. O. 2006. Interaction of deleted in liver cancer 1 with tensin2 in caveolae and implications in tumor suppression. *Cancer Res,* 66**,** 8367-72.

YAM, J. W. P., TSE, E. Y. T. & NG, I. O.-L. 2009. Role and significance of focal adhesion proteins in hepatocellular carcinoma. *Journal of Gastroenterology and Hepatology,* 24**,** 520-530.

YAMADA, K. M. & CUKIERMAN, E. 2007. Modeling Tissue Morphogenesis and Cancer in 3D. *Cell,* 130**,** 601-610.

YAMADA, K. M. & SIXT, M. 2019. Mechanisms of 3D cell migration. *Nature Reviews Molecular Cell Biology,* 20**,** 738-752.

YAMAZAKI, D., KURISU, S. & TAKENAWA, T. 2009. Involvement of Rac and Rho signaling in cancer cell motility in 3D substrates. *Oncogene,* 28**,** 1570-1583.

YANG, B., ZHU, W., ZHENG, Z., CHAI, R., JI, S., REN, G., LIU, T., LIU, Z., SONG, T., LI, F., LIU, S. & LI, G. 2017. Fluctuation of ROS regulates proliferation and mediates inhibition of migration by reducing the interaction between DLC1 and CAV-1 in breast cancer cells. *In Vitro Cell Dev Biol Anim,* 53**,** 354-362.

YANG, C., CZECH, L., GERBOTH, S., KOJIMA, S.-I., SCITA, G. & SVITKINA, T. 2007. Novel Roles of Formin mDia2 in Lamellipodia and Filopodia Formation in Motile Cells. *PLOS Biology,* 5**,** e317.

YANG, J., ANTIN, P., BERX, G., BLANPAIN, C., BRABLETZ, T., BRONNER, M., CAMPBELL, K., CANO, A., CASANOVA, J., CHRISTOFORI, G., DEDHAR, S., DERYNCK, R., FORD, H. L., FUXE, J., GARCÍA DE HERREROS, A., GOODALL, G. J., HADJANTONAKIS, A.-K., HUANG, R. Y. J., KALCHEIM, C., KALLURI, R., KANG, Y., KHEW-GOODALL, Y., LEVINE, H., LIU, J., LONGMORE, G. D., MANI, S. A., MASSAGUÉ, J., MAYOR, R., MCCLAY, D., MOSTOV, K. E., NEWGREEN, D. F., NIETO, M. A., PUISIEUX, A., RUNYAN, R., SAVAGNER, P., STANGER, B., STEMMLER, M. P., TAKAHASHI, Y., TAKEICHI, M., THEVENEAU, E., THIERY, J. P., THOMPSON, E. W., WEINBERG, R. A., WILLIAMS, E. D., XING, J., ZHOU, B. P., SHENG, G. & ON BEHALF OF THE, E. M. T. I. A. 2020. Guidelines and definitions for research on epithelial–mesenchymal transition. *Nature Reviews Molecular Cell Biology,* 21**,** 341-352.

YANG, Q., ZHANG, X. F., POLLARD, T. D. & FORSCHER, P. 2012. Arp2/3 complex-dependent actin networks constrain myosin II function in driving retrograde actin flow. *J Cell Biol,* 197**,** 939-56.

YANG, X., POPESCU, N. C. & ZIMONJIC, D. B. 2011. DLC1 interaction with S100A10 mediates inhibition of in vitro cell invasion and tumorigenicity of lung cancer cells through a RhoGAP-independent mechanism. *Cancer Res,* 71**,** 2916-25.

YANG, X. Y., GUAN, M., VIGIL, D., DER, C. J., LOWY, D. R. & POPESCU, N. C. 2009. p120Ras-GAP binds the DLC1 Rho-GAP tumor suppressor protein and inhibits its RhoA GTPase and growth-suppressing activities. *Oncogene,* 28**,** 1401-9.

YIN, X.-L., PANG, J. C.-S. & NG, H.-K. 2002. Identification of a region of homozygous deletion on 8p22–23.1 in medulloblastoma. *Oncogene,* 21**,** 1461-1468.

YU, X. & MACHESKY, L. M. 2012. Cells assemble invadopodia-like structures and invade into matrigel in a matrix metalloprotease dependent manner in the circular invasion assay. *PLoS One,* 7**,** e30605.

YUAN, B.-Z., JEFFERSON, A. M., BALDWIN, K. T., THORGEIRSSON, S. S., POPESCU, N. C. & REYNOLDS, S. H. 2004. DLC-1 operates as a tumor suppressor gene in human non-small cell lung carcinomas. *Oncogene,* 23**,** 1405-1411.

YUAN, B.-Z., ZHOU, X., DURKIN, M. E., ZIMONJIC, D. B., GUMUNDSDOTTIR, K., EYFJORD, J. E., THORGEIRSSON, S. S. & POPESCU, N. C. 2003a. DLC-1 gene inhibits human breast cancer cell growth and in vivo tumorigenicity. *Oncogene,* 22**,** 445-450.

YUAN, B. Z., JEFFERSON, A. M., MILLECCHIA, L., POPESCU, N. C. & REYNOLDS, S. H. 2007. Morphological changes and nuclear translocation of DLC1 tumor suppressor protein precede apoptosis in human non-small cell lung carcinoma cells. *Exp Cell Res,* 313**,** 3868-80.

YUAN, B. Z., ZHOU, X., DURKIN, M. E., ZIMONJIC, D. B., GUMUNDSDOTTIR, K., EYFJORD, J. E., THORGEIRSSON, S. S. & POPESCU, N. C. 2003b. DLC-1 gene inhibits human breast cancer cell growth and in vivo tumorigenicity. *Oncogene,* 22**,** 445-50.

ZACHARCHENKO, T., QIAN, X., GOULT, B. T., JETHWA, D., ALMEIDA, T. B., BALLESTREM, C., CRITCHLEY, D. R., LOWY, D. R. & BARSUKOV, I. L. 2016. LD Motif Recognition by Talin: Structure of the Talin-DLC1 Complex. *Structure (London, England : 1993),* 24**,** 1130-1141.

ZAIDEL-BAR, R., ITZKOVITZ, S., MA'AYAN, A., IYENGAR, R. & GEIGER, B. 2007. Functional atlas of the integrin adhesome. *Nat Cell Biol,* 9**,** 858-67.

ZAMIR, E., KATZ, B. Z., AOTA, S., YAMADA, K. M., GEIGER, B. & KAM, Z. 1999. Molecular diversity of cell-matrix adhesions. *J Cell Sci,* 112 (Pt 11)**,** 1655-69.

ZANCONATO, F., CORDENONSI, M. & PICCOLO, S. 2016. YAP/TAZ at the Roots of Cancer. *Cancer Cell,* 29**,** 783-803.

ZANCONATO, F., CORDENONSI, M. & PICCOLO, S. 2019. YAP and TAZ: a signalling hub of the tumour microenvironment. *Nature Reviews Cancer,* 19**,** 454-464.

ZEHIR, A., BENAYED, R., SHAH, R. H., SYED, A., MIDDHA, S., KIM, H. R., SRINIVASAN, P., GAO, J., CHAKRAVARTY, D., DEVLIN, S. M., HELLMANN, M. D., BARRON, D. A., SCHRAM, A. M., HAMEED, M., DOGAN, S., ROSS, D. S., HECHTMAN, J. F., DELAIR, D. F., YAO, J., MANDELKER, D. L., CHENG, D. T., CHANDRAMOHAN, R., MOHANTY, A. S., PTASHKIN, R. N., JAYAKUMARAN, G., PRASAD, M., SYED, M. H., REMA, A. B., LIU, Z. Y., NAFA, K., BORSU, L., SADOWSKA, J., CASANOVA, J., BACARES, R., KIECKA, I. J., RAZUMOVA, A., SON, J. B., STEWART, L., BALDI, T., MULLANEY, K. A., AL-AHMADIE, H., VAKIANI, E., ABESHOUSE, A. A., PENSON, A. V., JONSSON, P., CAMACHO, N., CHANG, M. T., WON, H. H., GROSS, B. E., KUNDRA, R., HEINS, Z. J., CHEN, H.-W., PHILLIPS, S., ZHANG, H., WANG, J., OCHOA, A., WILLS, J., EUBANK, M., THOMAS, S. B., GARDOS, S. M., REALES, D. N., GALLE, J., DURANY, R., CAMBRIA, R., ABIDA, W., CERCEK, A., FELDMAN, D. R., GOUNDER, M. M., HAKIMI, A. A., HARDING, J. J., IYER, G., JANJIGIAN, Y. Y., JORDAN, E. J., KELLY, C. M., LOWERY, M. A., MORRIS, L. G. T., OMURO, A. M., RAJ, N., RAZAVI, P., SHOUSHTARI, A. N., SHUKLA, N., SOUMERAI, T. E., VARGHESE, A. M., YAEGER, R., COLEMAN, J., BOCHNER, B., RIELY, G. J., SALTZ, L. B., SCHER, H. I., SABBATINI, P. J., ROBSON, M. E., KLIMSTRA, D. S., TAYLOR, B. S., BASELGA, J., SCHULTZ, N.,

HYMAN, D. M., ARCILA, M. E., SOLIT, D. B., LADANYI, M. & BERGER, M. F. 2017. Mutational landscape of metastatic cancer revealed from prospective clinical sequencing of 10,000 patients. *Nature Medicine,* 23**,** 703-713.

ZHANG, D., SUN, M. B., LEE, J., ABDEEN, A. A. & KILIAN, K. A. 2016a. Cell shape and the presentation of adhesion ligands guide smooth muscle myogenesis. *Journal of Biomedical Materials Research Part A,* 104**,** 1212-1220.

ZHANG, G. J., LI, J. S., ZHOU, H., XIAO, H. X., LI, Y. & ZHOU, T. 2015. MicroRNA-106b promotes colorectal cancer cell migration and invasion by directly targeting DLC1. *J Exp Clin Cancer Res,* 34**,** 73.

ZHANG, L., CAO, H., HE, T., YANG, J., TAO, H., WANG, Y. & HU, Q. 2018. Overexpression of PRDM13 inhibits glioma cells via Rho and GTP enzyme activation protein. *Int J Mol Med,* 42**,** 966-974.

ZHANG, L., ZHANG, Y., ZHU, H., SUN, X., WANG, X., WU, P. & XU, X. 2019. Overexpression of miR-301a-3p promotes colorectal cancer cell proliferation and metastasis by targeting deleted in liver cancer-1 and runt-related transcription factor 3. *J Cell Biochem,* 120**,** 6078-6089.

ZHANG, S., TANG, Q., XU, F., XUE, Y., ZHEN, Z., DENG, Y., LIU, M., CHEN, J., LIU, S., QIU, M., LIAO, Z., LI, Z., LUO, D., SHI, F., ZHENG, Y. & BI, F. 2009. RhoA regulates G1-S progression of gastric cancer cells by modulation of multiple INK4 family tumor suppressors. *Mol Cancer Res,* 7**,** 570-80.

ZHANG, X., JIANG, F., LI, P., LI, C., MA, Q., NICOSIA, S. V. & BAI, W. 2005. Growth suppression of ovarian cancer xenografts in nude mice by vitamin D analogue EB1089. *Clin Cancer Res,* 11**,** 323-8.

ZHANG, Y. & LI, G. 2020. A tumor suppressor DLC1: The functions and signal pathways. *Journal of Cellular Physiology,* 235**,** 4999-5007.

ZHANG, Y., LI, S. & ZHAO, Z. 2016b. Using Nanoliposomes To Construct a FRET-Based Ratiometric Fluorescent Probe for Sensing Intracellular pH Values. *Anal Chem,* 88**,** 12380-12385.

ZHONG, D., ZHANG, J., YANG, S., SOH, U. J., BUSCHDORF, J. P., ZHOU, Y. T., YANG, D. & LOW, B. C. 2009. The SAM domain of the RhoGAP DLC1 binds EF1A1 to regulate cell migration. *J Cell Sci,* 122**,** 414-24.

ZHOU, X., JIAO, D., DOU, M., ZHANG, W., LV, L., CHEN, J., LI, L., WANG, L. & HAN, X. 2020. Curcumin inhibits the growth of triple-negative breast cancer cells by silencing EZH2 and restoring DLC1 expression. *J Cell Mol Med,* 24**,** 10648-10662.

ZHOU, X., THORGEIRSSON, S. S. & POPESCU, N. C. 2004. Restoration of DLC-1 gene expression induces apoptosis and inhibits both cell growth and tumorigenicity in human hepatocellular carcinoma cells. *Oncogene,* 23**,** 1308-13.

ZHOU, X., YANG, X.-Y. & POPESCU, N. C. 2012. Preclinical evaluation of combined antineoplastic effect of DLC1 tumor suppressor protein and suberoylanilide hydroxamic acid on prostate cancer cells. *Biochemical and Biophysical Research Communications,* 420**,** 325-330.

ZHOU, X., ZIMONJIC, D. B., PARK, S. W., YANG, X. Y., DURKIN, M. E. & POPESCU, N. C. 2008. DLC1 suppresses distant dissemination of human hepatocellular carcinoma cells in nude mice through reduction of RhoA GTPase activity, actin cytoskeletal disruption and down-regulation of genes involved in metastasis. *Int J Oncol,* 32**,** 1285-91.

ZHU, W., MA, L., YANG, B., ZHENG, Z., CHAI, R., LIU, T., LIU, Z., SONG, T., LI, F. & LI, G. 2016. Flavone inhibits migration through DLC1/RhoA pathway by decreasing ROS generation in breast cancer cells. *In Vitro Cellular & Developmental Biology - Animal,* 52**,** 589-597.

ZIMMERMANN, M., BOX, C. & ECCLES, S. A. 2013. Two-dimensional vs. three-dimensional in vitro tumor migration and invasion assays. *Methods Mol Biol,* 986**,** 227-52.

Supplementary Data

DLC1 sequence

> VIRT-34582:5'3' Frame 3, start_pos=106

MCRKKPDTMILTQIEAKEACDWLRATGFPQYAQLYEDFLFPIDISLVKRE

HDFLDRDAIEALCRRLNTLNKCAVMKLEISPHRKRSDDSDEDEPCAISGK

WTFQRDSKRWSRLEEFDVFSPKQDLVPGSPDDSHPKDGPSPGGTLMDLSE

RQEVSSVRSLSSTGSLPSHAPPSEDAATPRTNSVISVCSSSNLAGNDDSF

GSLPSPKELSSFSFSMKGHEKTAKSKTRSLLKRMESLKLKSSHHSKHKAP

SKLGLIISGPILQEGMDEEKLKQLNCVEISALNGNRINVPMVRKRSVSNS

TQTSSSSSQSETSSAVSTPSPVTRTRSLSACNKRVGMYLEGFDPFNQSTF

NNVVEQNFKNRESYPEDTVFYIPEDHKPGTFPKALTNGSFSPSGNNGSVN

WRTGSFHGPGHISLRRENSSDSPKELKRRNSSSSMSSRLSIYDNVPGSIL

YSSSGDLADLENEDIFPELDDILYHVKGMQRIVNQWSEKFSDEGDSDSAL

DSVSPCPSSPKQIHLDVDNDRTTPSDLDSTGNSLNEPEEPSEIPERRDSG

VGASLTRSNRHRLRWHSFQSSHRPSLNSVSLQINCQSVAQMNLLQKYSLL

KLTALLEKYTPSNKHGFSWAVPKFMKRIKVPDYKDRSVFGVPLTVNVQRT

GQPLPQSIQQAMRYLRNHCLDQVGLFRKSGVKSRIQALRQMNEGAIDCVN

YEGQSAYDVADMLKQYFRDLPEPLMTNKLSETFLQIYQYVPKDQRLQAIK

AAIMLLPDENREVLQTLLYFLSDVTAAVKENQMTPTNLAVCLAPSLFHLN

TLKRENSSPRVMQRKQSLGKPDQKDLNENLAATQGLAHMIAECKKLFQVP

EEMSRCRNSYTEQELKPLTLEALGHLGNDDSADYQHFLQDCVDGLFKEVK

EKFKGWVSYSTSEQAELSYKKVSEGPPLRLWRSVIEVPAVPEEILKRLLK

EQHLWDVDLLDSKVIEILDSQTEIYQYVQNSMAPHPARDYVVLRTWRTNL

PKGACALLLTSVDHDRAPVVGVRVNVLLSRYLIEPCGPGKSKLTYMCRVD

LRGHMPEWYTKSFGHLCAAEVVKIRDSFSNQNTETKDTKSR

mRuby-DLC1 sequencing

```
NM_006094 5'3'       ------------------------------MCRKKPDTMILTQIEAKEACDWLRATGFPQY
mRuby DLC1 :5'3'     MFVXQXRXAVAKFAGLGGGMDELYKRSRAMCRKKPDTMILTQIEAKEACDWLRATGFPQY
                                                   ********************************

NM_006094  5'3'      AQLYEDFLFPIDISLVKREHDFLDRDAIEALCRRLNTLNKCAVMKLEISPHRKRSDDSDE
mRuby DLC1 :5'3'     AQLYEDFLFPIDISLVKREHDFLDRDAIEALCRRLNTLNKCAVMKLEISPHRKRSDDSDE
                     ************************************************************

NM_006094  5'3'      DEPCAISGKWTFQRDSKRWSRLEEFDVFSPKQDLVPGSPDDSHPKDGPSPGGTLMDLSER
mRuby DLC1 :5'3'     DEPCAISGKWTFQRDSKRWSRLEEFDVFSPKQDLVPGSPDDSHPKDGPSPGGTLMDLSER
                     ************************************************************

NM_006094  5'3'      QEVSSVRSLSSTGSLPSHAPPSEDAATPRTNSVISVCSSSNLAGNDDSFGSLPSPKELSS
mRuby DLC1 :5'3'     QEVSSVRSLSSTGSLPSHAPPSEDAATPRTNSVISVCSSSNLAGNDDSFGSLPSPKELSS
                     ************************************************************

NM_006094  5'3'      FSFSMKGHEKTAKSKTRSLLKRMESLKLKSSHHSKHKAPSKLGLIISGPILQEGMDEEKL
mRuby DLC1 :5'3'     FSFSMKGHEKTAKSKTRSLLKRMESLKLKSSHHSKHKAPSKLGLIISGPILQEGMDEEKL
                     ************************************************************

NM_006094  5'3'      KQLNCVEISALNGNRINVPMVRKRSVSNSTQTSSSSSQSETSSAVSTPSPVTRTRSLSAC
mRuby DLC1 :5'3'     KQLNCVEISALNGNRINVPMVRKRSVSNSTQTSSSSSQSETSSAVSTPSPVXRTRNLSAC
                     ************************************************** ***.****

NM_006094  5'3'      NKRVGMYLEGFDPFNQSTFNNVVEQNFKNRESYPEDTVFYIPEDHKPGTFPKALTNGSFS
mRuby DLC1 :5'3'     NKRVGMYLXGFXPFNQSTFNNVVXQ----------------------------------
                     ******** ** *********** *
```

GFP-Talin Sequencing

```
CLUSTAL multiple sequence alignment by MUSCLE (3.8)


GFP Talin 5'3'            LSTQSALSKDPNEKRDHMXXLEFVTAAGITLGMDELYKSGLRSRAQASFEFAEAATMVAL
sp|Q9Y490|TLN1_HUMAN      ------------------------------------------------------------MVAL
                                                                                     ****

GFP Talin  5'3'           SLKISIGNVVKTMQFEPSTMVYDACRMIRERIPEALAGPPNDFGLFLSDDDPKKGIWLEA
sp|Q9Y490|TLN1_HUMAN      SLKISIGNVVKTMQFEPSTMVYDACRIIRERIPEAPAGPPSDFGLFLSDDDPKKGIWLEA
                          **************************:******** ****.******************

GFP Talin 5'3'            GKALDYYMLRNGDTMEYRKKQRPLKIRMLDGTVKTIMVDDSKTVTDMLMTICARIGITNH
sp|Q9Y490|TLN1_HUMAN      GKALDYYMLRNGDTMEYRKKQRPLKIRMLDGTVKTIMVDDSKTVTDMLMTICARIGITNH
                          ************************************************************

GFP Talin 5'3'            DEYSLVRELMEEKKDEGTGTLRKDKTLLRDEKKMEKLKQKLHTDDELNWLDHGRTLREQG
sp|Q9Y490|TLN1_HUMAN      DEYSLVRELMEEKKEEITGTLRKDKTLLRDEKKMEKLKQKLHTDDELNWLDHGRTLREQG
                          **************:* ****************************************

GFP Talin 5'3'            VEEHETLLLRRKFFYSDQNVDSRDPVQLNLLYVQARDDILNGSHPVSFDKACEFAGFQCQ
sp|Q9Y490|TLN1_HUMAN      VEEHETLLLRRKFFYSDQNVDSRDPVQLNLLYVQARDDILNGSHPVSFDKACEFAGFQCQ
                          ************************************************************

GFP Talin 5'3'            IQFGPHNEQKHKAGFLDLKDFLPKEYVKQKGXA--------------------------
sp|Q9Y490|TLN1_HUMAN      IQFGPHNEQKHKAGFLDLKDFLPKEYVKQKGERKIFQAHKNCGQMSEIEAKVRYVKLARS
                          ******************************
```

DLC1 FRET Sensors

TFP-DLC1(1-846)-Venus

MAHHHH HHGSGEQKLI SEEDLGSGSG SVSKGEETTM GVIKPDMKIK

LKMEGNVNGH AFVIEGEGEG KPYDGTNTIN LEVKEGAPLP FSYDILTTAF

AYGNRAFTKY PDDIPNYFKQ SFPEGYSWER TMTFEDKGIV KVKSDISMEE

DSFIYEIHLK GENFPPNGPV MQKKTTGWDA STERMYVRDG VLKGDVKHKL

LLEGGGHHRV DFKTIYRAKK AVKLPDYHFV DHRIEILNHD KDYNKVTVYE

SAVARNSTDG MDELYKSG

MCRKKPDTMILTQIEAKEACDWLRATGFPQYAQLYEDFLFPIDI

SLVKREHDFLDRDAIEALCRRLNTLNKCAVMKLEISPHRKRSDDSDEDEPCAISGKWT

FQRDSKRWSRLEEFDVFSPKQDLVPGSP**D**DSHPKDGPSPGGTLMDLSERQEVSSVRSL

SSTGSLPSHAPPSEDAATPRTNSVISVCSSSNLAGNDDSFGSLPSPKELSSFSFSMKG

HEKTAKSKTRSLLKRMESLKLKSSHHSKHKAPSKLGLIISGPILQEGMDEEKLKQLNC

VEISALNGNRINVPMVRKRSVSNSTQTSSSSSQSETSSAVSTPSPVTRTRSLS**A**CNKR

VGMYLEGFDPFNQSTFNNVVEQNFKNRESYPEDTVFYIPEDHKPGTFPKALTNGSFSP

SGNNGSVNWRTGSFHGPGHISLRRENSSDSPKELKRRNSSSSM**S**SRLSIYDNVPGSIL

YSSSGDLADLENEDIFPELDDILYHVKGMQRIVNQWSEKFSDEGDSDSALDSVSPCPS

SPKQIHLDVDNDRTTPSDLDSTGNSLNEPEEPSEIPERRDSGVGASLTRSNRHRLRWH

SFQSSHRP**S**LNSVSLQINCQSVAQMNLLQKYSLLKLTALLEKYTP**S**NKHGFSWAVPKF

MKRIKVPDYKDR**S**VFGVPLTVNVQRTGQPLPQSIQQAMRYLRNHCLDQVGLFRKSGVK

SRIQALRQMNEGAIDCVNYEGQSAYDVADMLKQYFRDLPEPLMTNKLSETFLQIYQYV

PKDQRLQAIKAAIMLLPDENREVLQTLLYFLSDVTAAVKENQMTPTNLAVCLAPSLFH

LNTLKRENSSPRVMQRKQSLGKPDQKDLNENLAATQGLAHMIAECKK**L**

AAAM VSKGEELFTG VVPILVELDG DVNGHKFSVS GEGEGDATYG

KLTLKLICTT GKLPVPWPTL VTTLGYGLQC FARYPDHMKQ HDFFKSAMPE

GYVQERTIFF KDDGNYKTRA EVKFEGDTLV NRIELKGIDF KEDGNILGHK

LEYNYNSHNV YITADKQKNG IKANFKIRHN IEDGGVQLAD HYQQNTPIGD

GPVLLPDNHY LSYQSALSKD PNEKRDHMVL LEFVTAAGIT LGMDELYKGT

DILQKKLEEL ELDE*DI**

TFP-DLC1(80-846)-Venus

MAHHHH HHGSGEQKLI SEEDLGSGSG SVSKGEETTM GVIKPDMKIK

LKMEGNVNGH AFVIEGEGEG KPYDGTNTIN LEVKEGAPLP FSYDILTTAF

AYGNRAFTKY PDDIPNYFKQ SFPEGYSWER TMTFEDKGIV KVKSDISMEE

DSFIYEIHLK GENFPPNGPV MQKKTTGWDA STERMYVRDG VLKGDVKHKL

LLEGGGHHRV DFKTIYRAKK AVKLPDYHFV DHRIEILNHD KDYNKVTVYE

SAVARNSTDG MDELYKSG

SPHRKRSDDSDEDEPCAISGKWT

FQRDSKRWSRLEEFDVFSPKQDLVPGSPDDSHPKDGPSPGGTLMDLSERQEVSSVRSL

SSTGSLPSHAPPSEDAATPRTNSVISVCSSSNLAGNDDSFGSLPSPKELSSFSFSMKG

HEKTAKSKTRSLLKRMESLKLKSSHHSKHKAPSKLGLIISGPILQEGMDEEKLKQLNC

VEISALNGNRINVPMVRKRSVSNSTQTSSSSSQSETSSAVSTPSPVTRTRSLSACNKR

VGMYLEGFDPFNQSTFNNVVEQNFKNRESYPEDTVFYIPEDHKPGTFPKALTNGSFSP

SGNNGSVNWRTGSFHGPGHISLRRENSSDSPKELKRRNSSSSMSSRLSIYDNVPGSIL

YSSSGDLADLENEDIFPELDDILYHVKGMQRIVNQWSEKFSDEGDSDSALDSVSPCPS

SPKQIHLDVDNDRTTPSDLDSTGNSLNEPEEPSEIPERRDS**G**VGASLTRSNRHRLRWH

SFQSSHRPSLNSVSLQINCQSVAQMNLLQKYSLLKLTALLEKYTPSNKHGFSWAVPKF

MKRIKVPDYKDR**S**VFGVPLTVNVQRTGQPLPQSIQQAMRYLRNHCLDQVGLFRKSGVK

SRIQALRQMNEGAIDCVNYEGQSAYDVADMLKQYFRDLPEPLMTNKLSETFLQIYQYV

PKDQRLQAIKAAIMLLPDENREVLQTLLYFLSDVTAAVKENQMTPTNLAVCLAPSLFH

LNTLKRENSSPRVMQRKQSLGKPDQKDLNENLAATQGLAHMIAECKKL

AAAM VSKGEELFTG VVPILVELDG DVNGHKFSVS GEGEGDATYG

KLTLKLICTT GKLPVPWPTL VTTLGYGLQC FARYPDHMKQ HDFFKSAMPE

GYVQERTIFF KDDGNYKTRA EVKFEGDTLV NRIELKGIDF KEDGNILGHK

LEYNYNSHNV YITADKQKNG IKANFKIRHN IEDGGVQLAD HYQQNTPIGD

GPVLLPDNHY LSYQSALSKD PNEKRDHMVL LEFVTAAGIT LGMDELYKGT

DILQKKLEEL ELDE*DI**

TFP-DLC1(1-550)-Venus

MAHHHH HHGSGEQKLI SEEDLGSGSG SVSKGEETTM GVIKPDMKIK

LKMEGNVNGH AFVIEGEGEG KPYDGTNTIN LEVKEGAPLP FSYDILTTAF

AYGNRAFTKY PDDIPNYFKQ SFPEGYSWER TMTFEDKGIV KVKSDISMEE

DSFIYEIHLK GENFPPNGPV MQKKTTGWDA STERMYVRDG VLKGDVKHKL

LLEGGGHHRV DFKTIYRAKK AVKLPDYHFV DHRIEILNHD KDYNKVTVYE

SAVARNSTDG MDELYKSG

MCRKKPDTMILTQIEAKEACDWLRATGFPQYAQLYEDFLFPIDI

SLVKREHDFLDRDAIEALCRRLNTLNKCAVMKLEIS**S**PHRKRSDDSDEDEPCAISGKWT

FQRDSKRWSRLEEFDVFSPKQDLVPGSPDDSHPKDGPSPGGTLMDLSERQEVSSVRSL

SSTGSLPSHAPPSEDAATPRTNSVISVCSSSNLAGNDDSFGSLPSPKELSSFSFSMKG

HEKTAKSKTRSLLKRMESLKLKSSHHSKHKAPSKLGLIISGPILQEGMDEEKLKQLNC

VEISALNGNRINVPMVRKRSVSNSTQTSSSSSQSETSSAVSTPSPVTRTRSLSACNKR

VGMYLEGFDPFNQSTFNNVVEQNFKNRESYPEDTVFYIPEDHKPGTFPKALTNGSFSP

SGNNGSVNWRTGSFHGPGHISLRRENSSDSPKELKRRNSSSSMSSRLSIYDNVPGSIL

YSSSGDLADLENEDIFPELDDILYHVKGMQRIVNQWSEKFSDEGDSDSALDSVSPCPS

SPKQIHLDVDNDRTTPSDLDSTGNSLNEPEEPSEIPERRDS**G**

AAAM VSKGEELFTG VVPILVELDG DVNGHKFSVS GEGEGDATYG

KLTLKLICTT GKLPVPWPTL VTTLGYGLQC FARYPDHMKQ HDFFKSAMPE

GYVQERTIFF KDDGNYKTRA EVKFEGDTLV NRIELKGIDF KEDGNILGHK

LEYNYNSHNV YITADKQKNG IKANFKIRHN IEDGGVQLAD HYQQNTPIGD

GPVLLPDNHY LSYQSALSKD PNEKRDHMVL LEFVTAAGIT LGMDELYKGT

DILQKKLEEL ELDE*DI**

TFP-DLC1(1-846)

MAHHHH HHGSGEQKLI SEEDLGSGSG SVSKGEETTM GVIKPDMKIK

LKMEGNVNGH AFVIEGEGEG KPYDGTNTIN LEVKEGAPLP FSYDILTTAF

AYGNRAFTKY PDDIPNYFKQ SFPEGYSWER TMTFEDKGIV KVKSDISMEE

DSFIYEIHLK GENFPPNGPV MQKKTTGWDA STERMYVRDG VLKGDVKHKL

LLEGGGHHRV DFKTIYRAKK AVKLPDYHFV DHRIEILNHD KDYNKVTVYE

SAVARNSTDG MDELYKSG

MCRKKPDTMILTQIEAKEACDWLRATGFPQYAQLYEDFLFPIDI

SLVKREHDFLDRDAIEALCRRLNTLNKCAVMKLEISPHRKRSDDSDEDEPCAISGKWT

FQRDSKRWSRLEEFDVFSPKQDLVPGSPDDSHPKDGPSPGGTLMDLSERQEVSSVRSL

SSTGSLPSHAPPSEDAATPRTNSVISVCSSSNLAGNDDSFGSLPSPKELSSFSFSMKG

HEKTAKSKTRSLLKRMESLKLKSSHHSKHKAPSKLGLIISGPILQEGMDEEKLKQLNC

VEISALNGNRINVPMVRKRSVSNSTQTSSSSSQSETSSAVSTPSPVTRTRSLSACNKR

VGMYLEGFDPFNQSTFNNVVEQNFKNRESYPEDTVFYIPEDHKPGTFPKALTNGSFSP

SGNNGSVNWRTGSFHGPGHISLRRENSSDSPKELKRRNSSSSMSSRLSIYDNVPGSIL

YSSSGDLADLENEDIFPELDDILYHVKGMQRIVNQWSEKFSDEGDSDSALDSVSPCPS

SPKQIHLDVDNDRTTPSDLDSTGNSLNEPEEPSEIPERRDSGVGASLTRSNRHRLRWH

SFQSSHRPSLNSVSLQINCQSVAQMNLLQKYSLLKLTALLEKYTPSNKHGFSWAVPKF

MKRIKVPDYKDRSVFGVPLTVNVQRTGQPLPQSIQQAMRYLRNHCLDQVGLFRKSGVK

SRIQALRQMNEGAIDCVNYEGQSAYDVADMLKQYFRDLPEPLMTNKLSETFLQIYQYV

PKDQRLQAIKAAIMLLPDENREVLQTLLYFLSDVTAAVKENQMTPTNLAVCLAPSLFH

LNTLKRENSSPRVMQRKQSLGKPDQKDLNENLAATQGLAHMIAECKKLGTDILQKKLEEL ELDE*DI**

DLC1(1-846)-Venus

MAHHHH HHGSGEQKLI SEEDLGSGSG

MCRKKPDTMILTQIEAKEACDWLRATGFPQYAQLYEDFLFPIDI

SLVKREHDFLDRDAIEALCRRLNTLNKCAVMKLEISPHRKRSDDSDEDEPCAISGKWT

FQRDSKRWSRLEEFDVFSPKQDLVPGSP**D**DSHPKDGPSPGGTLMDLSERQEVSSVRSL

SSTGSLPSHAPPSEDAATPRTNSVISVCSSSNLAGNDDSFGSLPSPKELSSFSFSMKG

HEKTAKSKTRSLLKRMESLKLKSSHHSKHKAPSKLGLIISGPILQEGMDEEKLKQLNC

VEISALNGNRINVPMVRKRSVSNSTQTSSSSSQSETSSAVSTPSPVTRTRSLS**A**CNKR

VGMYLEGFDPFNQSTFNNVVEQNFKNRESYPEDTVFYIPEDHKPGTFPKALTNGSFSP

SGNNGSVNWRTGSFHGPGHISLRRENSSDSPKELKRRNSSSSM**S**SRLSIYDNVPGSIL

YSSSGDLADLENEDIFPELDDILYHVKGMQRIVNQWSEKFSDEGDSDSALDSVSPCPS

SPKQIHLDVDNDRTTPSDLDSTGNSLNEPEEPSEIPERRDSGVGASLTRSNRHRLRWH

SFQSSHRP**S**LNSVSLQINCQSVAQMNLLQKYSLLKLTALLEKYTP**S**NKHGFSWAVPKF

MKRIKVPDYKDR**S**VFGVPLTVNVQRTGQPLPQSIQQAMRYLRNHCLDQVGLFRKSGVK

SRIQALRQMNEGAIDCVNYEGQSAYDVADMLKQYFRDLPEPLMTNKLSETFLQIYQYV

PKDQRLQAIKAAIMLLPDENREVLQTLLYFLSDVTAAVKENQMTPTNLAVCLAPSLFH

LNTLKRENSSPRVMQRKQSLGKPDQKDLNENLAATQGLAHMIAECKK**L**

AAAM VSKGEELFTG VVPILVELDG DVNGHKFSVS GEGEGDATYG

KLTLKLICTT GKLPVPWPTL VTTLGYGLQC FARYPDHMKQ HDFFKSAMPE

GYVQERTIFF KDDGNYKTRA EVKFEGDTLV NRIELKGIDF KEDGNILGHK

LEYNYNSHNV YITADKQKNG IKANFKIRHN IEDGGVQLAD HYQQNTPIGD

GPVLLPDNHY LSYQSALSKD PNEKRDHMVL LEFVTAAGIT LGMDELYKGT

DILQKKLEEL ELDE*DI**